

**Thermodynamic and Mathematical Relationships for Predicting Cocrystal Stability and Controlling
Dissolution – Supersaturation – Precipitation Behavior**

by

Katie L. Cavanagh

A dissertation submitted in partial fulfillment
of the requirements for the degree of
Doctor of Philosophy
(Pharmaceutical Sciences)
in the University of Michigan
2020

Doctoral Committee:

Professor Naír Rodríguez-Hornedo, Chair
Research Professor Gregory E. Amidon
Professor Adam J. Matzger
Associate Professor Anna Schwendeman

Katie L. Cavanagh

kcavanag@umich.edu

ORCID iD: 0000-0002-8973-2907

© Katie L. Cavanagh 2020

ACKNOWLEDGEMENTS

I would gratefully like to acknowledge all of the individuals who have supported and encouraged me in preparing for and attending graduate school.

First, I would like to express my sincerest gratitude to my advisor, Dr. Naír Rodríguez-Hornedo, for her mentorship during the past five years. Her training has allowed me to develop in independence, confidence, and critical thinking, and her enthusiasm for science and creative ideation will continue to inspire me for the rest of my career. I am also deeply appreciative of her compassion for the underrepresented and for her willingness to challenge inequity. Besides her pursuit of technically sound research, her example in both advocating for others and navigating the unique challenges of being a woman in science have been invaluable to me.

I would also like to thank my dissertation committee members: Professors Gregory E. Amidon, Adam J. Matzger, and Anna Schwendeman. I am appreciative of their critical review and helpful suggestions to improve the strength and translational value of my work. In addition, I am specifically grateful for Dr. Amidon's example in participating in professional service, Dr. Matzger's collaboration and welcome into his laboratory, and Dr. Schwendeman's mentorship in teaching and managing a classroom.

I also acknowledge the mentorship and training that I received prior to attending graduate school. I am grateful to my former internship mentors at Eli Lilly and Company, including Lee Burns, Mehuli Kulkarni, Shobha Bhattachar, David Bender, and Dr. Matthew Yates, and to my undergraduate research advisor at Purdue University, Dr. Tonglei Li. Thank you for your interest in me even when I did not have any laboratory experience, and for keeping up with my

achievements in graduate school. I would not have had the courage to apply for graduate school without your advice and recommendation.

Next, I fondly acknowledge the support and collaboration of my colleagues in the Rodríguez lab, most notably including Dr. Yitian Chen, Tatiane Cogo Machado, Dr. Yaohui Huang, Oisín Kavanagh, Dr. Gislaine Kuminek, and Dr. Nicholas Waltz. It has been my pleasure to work alongside each of you, and I have been incredibly blessed by your flexibility, generosity, strong ethics, and friendship. I also acknowledge the direct contributions of Professor M. Fátima M. da Piedade, Jennifer Diaz-Espinosa, Dr. Gislaine Kuminek, Dr. Chinmay Maheshwari, Professor Adam J. Matzger, and Professor Gus R. Rosania to my dissertation work; thank you for your collaboration. I would like to more specifically thank Gis Kuminek, who has been an incredibly patient and available mentor and friend.

This research was made possible by the support of multiple funding sources and College of Pharmacy staff. I am grateful for financial support from the Upjohn Award from the College of Pharmacy at the University of Michigan, the National Institute of General Medical Sciences of the National Institutes of Health under Award Number R01GM107146, the Warner-Lambert Parke-Davis Fellowship, and the Graduate Student Instructor program within the College of Pharmacy at the University of Michigan. I am also thankful for the support of Nicole Crandall, Dr. Cherie Dotson, Dean Vicki Ellingrod, Pat Greeley, Patrina Hardy, L.D. Hieber, Antoinette Hopper, Kylee Pulver, Brian Vanderziel, and Carrie Vaquera, as well as the IT and custodial staffs.

Finally, I want to thank all my friends and family for all of their support, encouragement, and prayer. To my closest friends – Joanne Beckwith, Jennifer Diaz-Espinosa, Mery Vet George de la Rosa, Beth Kuhl, Rebecca Miller, Sarah Owen, Angela Schurman, Brian R. Thompson, and

Hannah Wheaton – thank you for caring for me well. I have appreciated the coffee and meals we have shared, the hiking and yoga we have done, the mail you have sent, and, most importantly, your willingness to listen and unwavering belief in my abilities. And finally, thank you to my family, especially to my aunt Lee Ann Wilbur, my cousin Lindsey Morgan, and my parents, Paul and Leah Cavanagh, to whom this work is dedicated. Thank you for teaching me the joy of learning and of hard work, for always giving me the freedom and support to choose my own pursuits, and for loving me unconditionally.

TABLE OF CONTENTS

ACKNOWLEDGEMENTS	ii
LIST OF TABLES	ix
LIST OF FIGURES	xi
ABSTRACT.....	xix
CHAPTER 1 Introduction	1
Cocrystal Formation and Design	3
Cocrystal Screening and Synthesis	6
Cocrystal Eutectic Point and K_{eu}	9
Cocrystal Solubility and Transition Points.....	13
Mathematical Forms of Cocrystal Solubility and Stability	13
General Solubility Expressions	18
Applications.....	20
Using Solubility Advantage Diagrams to Control Dissolution – Supersaturation – Precipitation Behavior	26
Cocrystal Solubility Advantage – Drug Solubilization Power (SA – SP) Diagrams	28
Physiologically Relevant Surfactants	32
Synthetic Additives.....	34
Effect of pH on Cocrystal Dissolution	35
Statement of Dissertation Research.....	39
References	43
CHAPTER 2 Understanding the Differences between Cocrystal and Salt Aqueous Solubilities.....	49
Introduction	49
Materials and Methods	50
Materials	50
Cocrystal and Salt Constituents	50

Solvents and Buffer Components	51
Methods	51
Buffer Preparation	51
Cocrystal and Salt Synthesis.....	52
Drug Solubility Measurement	52
Cocrystal and Salt Solubility Measurements.....	52
X-ray Powder Diffraction (XRPD).....	53
Thermal Analysis.....	54
High Performance Liquid Chromatography (HPLC)	54
Results and Discussion	54
Solubility-pH Dependence and Supersaturation Index	54
Relationships between Solubility, pK _a , and pH.....	58
Solubility Product, K _{sp}	60
pH _{max} of Cocrystals and Salts	65
Conclusions	70
Acknowledgements.....	70
References	71
CHAPTER 3 Cocrystal Solubility Advantage and Dose/Solubility Ratio Diagrams: A Mechanistic Approach to Selecting Additives and Controlling Dissolution – Supersaturation – Precipitation Behavior	75
Introduction	75
Theoretical	78
Materials and Methods	82
Materials	82
Cocrystal Synthesis.....	83
Media Preparation.....	83
Eutectic Concentrations.....	84
Eutectic Constant, Cocrystal Solubility, and Solubility Product.....	84
Cocrystal and Drug Powder Dissolution	85
High Performance Liquid Chromatography (HPLC)	86
X-ray Powder Diffraction (XRPD).....	86
Thermal Analysis.....	86
Inverted Light Microscopy	86

Results and Discussion	87
Aqueous Cocrystal Solubility and Stability.....	87
Using Solubilizing Additives to Decrease Unnecessarily High Cocrystal Solubility Advantage (SA).....	90
Modulation of Cocrystal Solubility Advantage (SA) and Critical Supersaturation	92
Effect of Cocrystal Solubility Advantage (SA) and Additive Selection on Dissolution – Supersaturation – Precipitation (DSP) Behavior.....	97
Influence of Additive on Drug Nucleation	103
Drug Dose/Solubility – Limited Supersaturation	105
A Simple, Rational Approach to Control Dissolution – Supersaturation – Precipitation Behavior.....	113
Conclusions	116
Acknowledgements	117
References	118
Appendix 3A	122
Effect of Coformer Impurity on Cocrystal Solubility and SA.....	122
Appendix 3B	124
Eutectic Concentration Measurements in the Presence of Additives	124
Speciation and SA in Micellar Solutions Derivation.....	125
References	127
Appendix 3C	128
CHAPTER 4 Novel Posaconazole Cocrystals with Potential to Overcome Clinical Challenges	133
Introduction	133
Materials and Methods	136
Materials	136
Cocrystal Synthesis.....	136
Phase Purity and Cocrystal Stoichiometry	137
Synchrotron X-ray Diffraction (SXR)	138
Powder X-ray Diffraction (PXRD).....	138
Differential Scanning Calorimetry (DSC).....	138
Raman Spectroscopy	138
High-Performance Liquid Chromatography (HPLC).....	139
Dissolution and Solubility Media Preparation.....	139

Eutectic Concentrations	140
Cocrystal and Drug Powder Dissolution	140
Dissolution and Precipitation Pathways	140
Results and Discussion	141
Characterization of PSZ-4HBA Cocrystal	141
Cocrystal Eutectic Constant K_{eu} , Solubility, and Solubility Advantage (SA).....	145
Cocrystal Solubility and Dissolution with Excess Coformer	155
Conclusions	160
Acknowledgements.....	161
References	162
Appendix 4A	166
Single Crystals of PSZ-4HBA.....	166
PSZ-4HBA Stoichiometry Determination by HPLC.....	167
Appendix 4B	168
Derivation of 2:3 PSZ-4ABA Cocrystal Solubility as a Function of pH	168
Derivation of 2:3 and 1:2 PSZ-4HBA Cocrystal Solubility as a Function of pH	171
Solubility Calculations for 1:2 PSZ-4HBA versus 2:3 PSZ-4HBA	173
Appendix 4C	176
Photomicrographs of Cocrystal Dissolution.....	176
Reference	177
CHAPTER 5 Conclusions and Future Directions.....	178
References	183

LIST OF TABLES

Table 1.1. Ionization (δ_I) and solubilization (δ_S) terms used to calculate cocrystal solubility according to Equations 1.9, 1.10, and 1.12. The expressions for cocrystal solubilities were previously derived and experimentally confirmed. ^a	15
Table 1.2. Equilibrium expressions and constants of drug or coformer cocrystal components that are nonionizable, acidic, basic, amphoteric, or zwitterionic. Equilibrium constant equations can be used with knowledge of system mass balance to derive δ_I and δ_S equations. Subscripts m and aq refer to the micellar and aqueous pseudophases, respectively.	16
Table 1.3. S^* Deviations Due to Coformer Solubilization	26
Table 1.4. Values to Predict Cocrystal and Drug Solubility – pH Profiles. ¹⁰	37
Table 2.1. pK_a Values of Cocrystal and Salt Constituents.	50
Table 2.2. Solubility Product K_{sp} , Intrinsic Solubility (S_0), and Solubility Advantage $SA = S_0, CC$ or $S_0, SaltS_0, LTG$ of LTG Cocrystals and Salts.	62
Table 2.3. Cocrystal and Salt pK_{sp}	64
Table 2.4. pH_{max}^a for LTG Cocrystals and Salts.	67
Table 3.1. Aqueous Cocrystal Solubility and Stability.	88
Table 3.2. Cocrystal Solubility, Eutectic Constant K_{eu} , and Solubility Advantage (SA).	92
Table 3.3. Cocrystal Dissolution Parameters in Different Media. ^a	100
Table 3.4. Time to Nucleation during Dissolution Varies with Different Additives.	104
Table 3.5. How drug solubilization power (SP_D), cocrystal solubility advantage (SA), drug dose/solubility ratio (D_{0D}), and cocrystal dose/solubility ratio (D_{0CC}) influence solubility, dissolution, supersaturation, and absorption.	107
Table 3.6. Calculated drug solubilization power (SP_D), cocrystal solubility advantage (SA), drug dose/solubility ratio (D_{0D}), and cocrystal dose/solubility ratio (D_{0CC}) in different media.	109
Table 3A.1. Effect of Coformer Impurity on Cocrystal Solubility and SA for Different Doses.	123
Table 3B.1. Selected Solubilizing	124
Table 3B.2. Drug and Coformer Eutectic Concentrations to Calculate Cocrystal Solubility and Eutectic Constant K_{eu}	125
Table 3B.3. Drug Solubilization Constants and Associated Solubility and Stability Parameters.	127

Table 3C.1. Dissolution Parameters for DNZ-VAN and DNZ in Different Media.....	129
Table 3C.2. Percent Cocrystal Dissolved during Dissolution Studies. ^a	131
Table 4.1. Chemical Structures and pK _a Values of Drug and Coformers.....	135
Table 4.2. Component Eutectic Concentrations and Calculated Cocrystal Solubility Values in Blank and Biorelevant Media.	147
Table 4.3. Cocrystal Solubility, Solubility Advantage (SA), and Dose/solubility Ratio (D ₀) Values.	150
Table 4.4. K _{sp} , pK _{sp} , pH _{max} , and S _{cocrystal} at pH _{max} Values for Posaconazole Cocrystals.	152
Table 4.5. Ionization Terms (δ _i) for Posaconazole Drug and Coformers to Predict Cocrystal and Drug Solubilities according to Equations 4.12, 4.13, and 4.15.	154
Table 4.6. Cocrystal Dissolution Parameters with and without Excess Coformer.	158
Table 4A.1. Unit cell dimensions of 1:2 PSZ-4HBA cocrystal.	166
Table 4B.1. Cocrystal Solubility and Solubility Advantage (SA) values	174
Table 4B.2. K _{sp} , pK _{sp} , pH _{max} , and S _{cocrystal} at pH _{max} Values for 1:2 and 2:3 PSZ-4HBA.....	174

LIST OF FIGURES

- Figure 1.1.** Cocrystal solubility and stability vary with solution conditions such as (a) pH, (b) drug solubilizing agents, and (c) excess coformer concentration. The intersection of the cocrystal and drug solubility curves represents a transition point, where $S_{\text{cocrystal}} = S_{\text{drug}}$. Cocrystal is stable when $S_{\text{cocrystal}} < S_{\text{drug}}$, and has solubility advantage when $S_{\text{cocrystal}} > S_{\text{drug}}$. Changing solution conditions can be used to fine-tune relative cocrystal stability.³..... 2
- Figure 1.2.** Multicomponent crystalline forms that can be used to alter the physicochemical properties of an active pharmaceutical ingredient (API) or drug without changing molecular structure.¹² 4
- Figure 1.3.** Common supramolecular synthons formed with hydrogen bonds between carboxylic acids, amides, pyridines, and other aromatic nitrogens.^{3, 18-20} 5
- Figure 1.4.** A correlation is observed between cocrystal solubility advantage ($S_{\text{cocrystal}} / S_{\text{drug}}$) and the ratio of coformer to drug solubilities ($S_{\text{coformer}} / S_{\text{drug}}$). $S_{\text{coformer}} / S_{\text{drug}} > \sim 10$ relates to $S_{\text{cocrystal}} / S_{\text{drug}} = 1$. Final pH values from equilibrium solubility measurements at 25°C are shown as numbers by data points.³ 6
- Figure 1.5.** Phase solubility diagram defining regions where cocrystal can form or dissolve. Solubility of drug A is indicated with dashed blue line, solubility of coformer B is indicated with solid green line, and solubility of cocrystal AB is indicated with red curve. Nonstoichiometric cocrystal solubility decreases with increasing coformer concentration ($[B]_T$). Subscript T represents total analytical concentrations. Region I represents supersaturation with respect to drug, where the cocrystal can convert to drug. Region II represents supersaturation with respect to cocrystal and drug, where both forms can precipitate. Region III represents undersaturation, where cocrystal, drug, and coformer may dissolve. Region IV represents supersaturation with respect to cocrystal, but undersaturation with respect to drug. Pink arrows represent a possible cocrystal formation pathway, whereby drug in saturated coformer solution may dissolve above nonstoichiometric cocrystal solubility and convert to precipitate pure cocrystal. This method of cocrystal synthesis is known as reaction crystallization method (RCM).^{3, 37, 38} 8
- Figure 1.6.** Schematic phase solubility diagram indicating the eutectic points (*) where cocrystal and drug solid phases are in equilibrium with solution.¹¹ C_{eu} represents the eutectic concentrations of drug and coformer. The circles represent stoichiometric cocrystal solubilities. Two different cocrystals are considered based on their stability with respect to drug under stoichiometric conditions: a stable cocrystal (cocrystal 1), and a metastable cocrystal (cocrystal 2) where the cocrystal generates supersaturation with respect to drug. Drug solubility (S_{drug}) is indicated and is much lower than the solubility of the coformer, which is not shown. The dashed line illustrates stoichiometric concentrations of cocrystal components, which congruent dissolution would follow.³ 11

Figure 1.7. Predicted and experimental eutectic constant K_{eu} and solubility advantage ($SA = S_{cocrysal} / S_{drug}$) values for 1:1 NVP–MLE (solid line) and 2:1 NVP–SAC and NVP–SLC cocrystals (dashed line). K_{eu} is a key indicator of SA, and K_{eu} dependence on pH reveals the cocrystal pH_{max} . At pH_{max} , $K_{eu} = 1$ for 1:1 cocrystals and $K_{eu} = 0.5$ for 2:1 cocrystals. Symbols represent experimental values. The numbers next to data points indicate pH at eutectic point or equilibrium pH. Predicted lines were calculated according to Equation 1.7 (shown for 1:1 and 2:2 cocrystals on plot).⁴³ 12

Figure 1.8. A single eutectic point measurement can be used to obtain important cocrystal parameters, transition points, and diagrams. General equations refer to a cocrystal of stoichiometry $y:z$ 13

Figure 1.9. Cocrystal solubility is determined by the total analytical concentrations of its molecular constituents in solution. This diagram shows cocrystal-solution phase interactions for a cocrystal RHA composed of nonionizable drug (R) and acidic cofomer (HA), as well as the associated equilibria common to pharmaceutical dosage forms, including dissociation, complexation, ionization, and solubilization. K_{sp} represents the cocrystal solubility product, K_a is the ionization constant, K_c is the complexation constant, and K_s^{HA} and K_s^R are the solubilization constants for HA and R, respectively.^{3, 48} 17

Figure 1.10. Schematic illustration of the equilibria between the cocrystal solid phase and its components in the aqueous and micellar solution pseudophases. This scheme represents preferential micellar solubilization of the drug component, which leads to excess cofomer in the aqueous phase and stabilization of the cocrystal in the aqueous phase.^{44, 48} 19

Figure 1.11. Solubility-pH profiles for (a) 1:1 HAHX cocrystal composed of two acidic components was calculated using $SHAHX, T = K_{sp1} + K_{a1HA}[H+] + K_{a1HX}[H+]$, (b) 1:1 RHA cocrystal composed of nonionizable drug and acidic cofomer was calculated using Equation 1.17, (c) 2:1 R_2HAB cocrystal composed of nonionizable drug and amphoteric cofomer was calculated using $SR_2HAB, T = 3K_{sp41} + K_{a1HAB}[H+] + [H+]K_{a2H2AB} +$, and (d) 1:1 BH_2A and 2:1 B_2HA cocrystals composed of basic drug and diprotic and monoprotic acidic cofomers was calculated using $SBH_2A, T = K_{sp} + [H+]K_{a1B1} + K_{a1H2AH} + K_{a1H2AKa2HA} - [H+]^2$ and 21

Figure 1.12. Solubilities and transition points of (a) 1:1 carbamazepine-saccharin (CBZ–SAC) and (b) 2:1 carbamazepine-4-aminobenzoic acid-hydrate (CBZ-4ABA–HYD) with carbamazepine dihydrate (CBZD) induced by sodium lauryl sulfate (SLS) preferential solubilization of CBZ.⁴⁴ Transition points are characterized by a solubility (S^*) and a solubilizing agent concentration (CSC) (dashed lines). S^* and CSC vary with cocrystal aqueous solubility and stoichiometry. Symbols represent experimentally measured cocrystal (\circ) and drug (Δ) solubility values. Predicted drug and cocrystal solubilities (solid lines) were calculated according to Equation 1.17 and $SR_2HAB, T = 3K_{sp41} + K_{sRM21} + [H+]K_{aH2AB} + K_{aHAB}[H+] + K_{sHAB}[M]$, with previously reported values.^{44, 60} 23

Figure 1.13. Transition points S^* and critical stabilization concentration (CSC) for a cocrystal (red line) and its constituent drug (blue line) in the presence of two different solubilizing agents, a and b. S^* is a constant for a given cocrystal, but CSC varies with the extent of drug solubilization by a particular solubilizing agent. For this case, drug is solubilized to a greater extent by a than by b, and thus $CSC_a < CSC_b$. The curves were generated from Equations 1.23

and 1.24 with parameter values $S_{D, aq} = 0.5 \text{ mM}$, $S_{CC, aq} = 2.4 \text{ mM}$ ($K_{sp} = 5.76 \text{ mM}^2$), and $K_s^D = 1.5 \text{ mM}^{-1}$ and 0.5 mM^{-1} for solubilizing agents a and b, respectively.⁶⁰ 24

Figure 1.14. C_{max} is a kinetic parameter determined by the rates of cocrystal dissolution and drug precipitation. C_{max} is not proportional to cocrystal solubility advantage (SA), as the relation between dissolution and precipitation rates change with SA. For highly soluble cocrystals, C_{max} will decrease and may elude detection as precipitation rates become much higher than dissolution.³ 27

Figure 1.15. Cocrystal solubility advantage over drug ($SA = S_{cocrystal} / S_{drug}$) predictably decreases with increasing drug solubilization power ($SP_{drug} = S_{drug, T} / S_{drug, aq}$). Solid lines represent 1:1 cocrystals with $SA_{aq} = 2, 10, \text{ and } 100$. The dashed line indicates transition point $SA = 1$, and its intersection with solid cocrystal SA lines represents where $S_{cocrystal} = S_{drug}$ ($SP_{drug} = 4, 100, \text{ and } 10,000$ for the corresponding cocrystals). Solubilizing additives and their concentrations can be rationally selected to promote sustained supersaturation by dialing SP_{drug} and corresponding SA to maximum theoretical supersaturations within the metastable zone width.³ 30

Figure 1.16. The log-linear dependence of cocrystal solubility advantage (SA) on drug solubilization power (SP_D) for 1:1 IND-SAC cocrystal at pH 2.1 and 5.0. Lines are predicted from Equation 1.39 $SA_{aq} = 25$ at pH 2.1 and $SA_{aq} = 220$ at pH 5.0. Symbols represent values calculated from experimental drug and cofomer eutectic concentrations in aqueous and surfactant media at 25°C. Dashed arrows represent media used to conduct dissolution studies at pH 2.1. Error bars (within the points) represent standard deviations.^{63, 64} 32

Figure 1.17. Influence of aqueous (blue diamond) and biorelevant medium FeSSIF (red square) on the (a) concentration – time and (b) supersaturation – time profiles of 1:1 indomethacin - saccharin (IND-SAC) cocrystal at 25°C. Cocrystal solubility advantage (SA) was modulated from 220 in blank buffer to approximately 57 in FeSSIF.^{3, 64} 33

Figure 1.18. Influence of SA, $S_{cocrystal}$, and S_{drug} , on the concentration – time profiles of (a) 1:1 indomethacin – saccharin (IND-SAC) cocrystal and (b) indomethacin drug, and (c) the supersaturation – time profile of IND-SAC. SA was modulated from 25 to 2 by increasing surfactant concentration.⁶³ 34

Figure 1.19. Influence of additive selection on the concentration – time profiles of (a) 1:1 indomethacin – saccharin (IND-SAC) cocrystal and (b) indomethacin drug, and (c) the supersaturation – time profile of IND-SAC. SA was tailored to 11 – 13 with three different surfactants.⁶³ 35

Figure 1.20. (a) Aqueous solubility and (b) aqueous solubility advantage (SA) of 1:1 ketoconazole cocrystals and drug. Solubility – pH curves for ketoconazole – fumaric acid (KTZ-FUM), ketoconazole – succinic acid (KTZ-SUC), and ketoconazole – adipic acid (KTZ-ADP) were predicted according to Equation 1.40 and values in Table 1.4. SA lines were predicted from the ratio of Equation 1.40 to Equation 1.41. Symbols represent experimental solubility values. pH values represent equilibrium pH. Standard errors are less than 7% and within points.¹⁰ 36

Figure 1.21. Cocrystal σ_{max} and $AUC_{cocrystal/drug}$ related to cocrystal solubility advantage ($SA = S_{cocrystal} / S_{drug}$). Letters A, S, and F represent ketoconazole – adipic acid cocrystal, ketoconazole succinic acid cocrystal, and ketoconazole – fumaric acid cocrystal, respectively. pH 5.0

represents FeSSIF and blank FeSSIF media, and pH 6.5 represents FaSSIF and blank FaSSIF media. Error bars (some within points) represent standard error.¹⁰ 38

Figure 1.22. Interfacial pH of ketoconazole (KTZ), ketoconazole – adipic acid cocrystal (KTZ-ADP), ketoconazole – fumaric acid cocrystal (KTZ-FUM), and ketoconazole – succinic acid cocrystal (KTZ-SUC) as a function of bulk pH.⁶⁵ 39

Figure 2.1. Solubility-pH dependence of drug, cocrystals, and salt of LTG. Solubility values for cocrystals and salt were determined under equilibrium conditions and calculated from Equations 2.1 and 2.2. Some of the solubility values are above LTG solubility and are useful as indicators of supersaturation. Solubility curves were generated using Equations 2.4-2.7, and previously published results for LTG-PB are included for comparison. Dashed lines represent supersaturated conditions with respect to LTG.¹ pH values represent equilibrium pH. Standard deviation of data points is less than 5%. Portions of data courtesy of Dr. Chinmay Maheshwari. 55

Figure 2.2. Supersaturation Index ($SA = S_{CC}/S_D$) is the ratio of salt or cocrystal solubility to parent drug. $SA = 1$ represents equal drug and salt or cocrystal solubility and corresponds to pH_{max} . LTG-NCT·H₂O is more soluble than drug ($SA = 1.2$ to 18). LTG-SAC salt is less soluble than drug a $pH < pH_{max} = 5.0$, and LTG-PB cocrystal is less soluble than LTG ($SA < 1$) below $pH_{max} 9.0$. Experimental measurements at pH 4.0 to 4.3 show that SA for NCT cocrystal is 2.8, for SAC salt is 0.16, and for PB cocrystal is 0.03, demonstrating the range of behavior among these solid phase. Salt SA exhibits a fast increase with pH than cocrystal SA. Supersaturation index curves were generated by dividing Equations 2.5-2.7 by Equation 2.4.... 56

Figure 2.3. Cocrystal/salt pH_{max} dependence on pK_{sp} for basic drug with $pK_a = 5.71$ and acidic cofomer/counterion pK_a 1 to 4. Plots were generated using Equations 2.18 and 2.19 and $S_{0,D} = 6.6 \times 10^{-4}$ M. Cocrystals show lower pH_{max} values with higher sensitivity to cofomer pK_a than salts. For both cocrystals and salts, pH_{max} increases with pK_{sp} 68

Figure 2.4. Cocrystal/salt pH_{max} dependence on pK_{sp} for basic drugs according to Equations 2.18 and 2.19 with pK_a 4 to 6, acidic cofomer/counterion $pK_a = 2.0$, and $S_{0,D} = 6.6 \times 10^{-4}$ M. Cocrystal pH_{max} values are lower than salt across the plotted pK_{sp} range. pH_{max} increases with pK_{sp} for both cocrystals and salts. Changes in salt pH_{max} with drug pK_a are larger than for cocrystals. Changes in cocrystal pH_{max} decrease with increasing K_{sp} 69

Figure 3.1. Danazol (DNZ) and vanillin (VAN) eutectic concentrations in both the presence and absence of different additives. $[DNZ]_{eu}$ is the drug solubility under the solution conditions studied. Numbers above bars represent K_{eu} values calculated from Equation 3.9. Initial pH was 6.5 and equilibrium pH values were 6.28 – 6.51 for all media except FeSSIF, which had an initial pH 5.0 and an equilibrium pH 4.95. pH values for each media are reported in Table 3.2. Error bars represent standard deviations. 90

Figure 3.2. Predicted relationship between cocrystal solubility advantage (SA) and eutectic constant K_{eu} for 1:1 danazol – vanillin cocrystal (CC) and danazol drug (D). Symbols represent values calculated from experimental danazol (DNZ) and vanillin (VAN) eutectic concentrations (Figure 3.1 and Appendix 3B). Error bars (within the points) represent standard deviations. 91

Figure 3.3. Cocrystal SA – SP diagram shows the linear dependence of log cocrystal solubility advantage (SA) on log drug solubilization power (SP_D) predicted from Equation 3.4. Symbols represent SA and SP_D values calculated from experimental measurements of drug (danazol) and

coformer (vanillin) eutectic concentrations (Appendix 3B). 0.5% TPGS SP_D and SA_T values were estimated from $S_{D,T} = 0.17$ mM reported by Childs et. al., $S_{D,aq}$ and SA_{aq} in Table 3.1, and Equation 3.3. Transition point $SA_T = 1$ shows where cocrystal and drug solubilities are equal and above which the cocrystal generates supersaturation with respect to the drug. Error bars (within the points) represent standard deviations of SA and SP_D 93

Figure 3.4. Predicted drug and cocrystal solubilities as a function of micellar surfactant concentrations showing total, micellar, and aqueous (free) drug contributions to solubility, represented by $[D]$. The following parameter values were used: $S_{D,aq} = 0.0009$ mM, $K_s(DNZ,TPGS) = 50$ mM⁻¹, and $K_{sp} = 0.03$ mM². (a) Drug solubility was calculated according to $S_{drug,T} = S_{drug,aq}(1 + K_sM)$ and (b) cocrystal solubility was calculated according to $S_{cocrystal,T} = K_{sp}(1 + K_sM)$ and $[D]_{aqueous} = K_{sp}S_{cocrystal,T}$. $[D]_{micellar}$ was calculated from the difference of $[D]_{total} - [D]_{aq}$. K_s values for other surfactants are reported in Appendix 3B. 96

Figure 3.5. How free drug concentrations change with increasing surfactant micellar solubilization of drug. Green lines indicate surfactant concentrations of TPGS and biorelevant media used in this work. Aqueous cocrystal solubility was calculated from $[D]_{aqueous} = K_{sp}S_{cocrystal,T}$. $[D]_{micellar}$ was calculated from the difference of $[D]_{total} - [D]_{aq}$. The following parameter values were used: $S_{D,aq} = 0.0009$ mM, $K_s(DNZ,TPGS) = 50$ mM⁻¹, $K_s(DNZ,FaSSIF/FeSSIF) = 3$ mM⁻¹, and $K_{sp} = 0.03$ mM². 97

Figure 3.6. Concentration – time and supersaturation – time profiles of cocrystal DNZ-VAN (colored profiles) and drug DNZ (gray profiles) in surfactant media at 37°C with decreasing solubility advantage (SA_T): (a) FaSSIF, (b) FeSSIF, (c) 0.5 FaSSIF + 0.5% TPGS + 1% HPC, (d) FaSSIF + 0.25% Soluplus, (e) FaSSIF + 1% TPGS + 2% HPC, (f) FaSSIF + 1% TPGS, and (g) FaSSIF + 2.5% Soluplus. Different additives and concentrations corresponding to different cocrystal SA_T were selected to study their influence on dissolution – supersaturation – precipitation behavior. Dissolution in Figure (c) was conducted by Childs et. al, labeled as 1% TPGS + 2% HPC but described in their Methods and Results sections as the final solution being half concentrated.²⁴ $SA_T = 13.4$ for 0.5% TPGS was used to analyze this dissolution since HPC does not solubilize the drug and drug solubilization by FaSSIF <<< drug solubilization by TPGS. Supersaturation values are calculated as $\sigma = ([DNZ] / S_{DNZ})$, according to solubility values in Appendix 3B. Percentages represent cumulative percent cocrystal dissolved at 2, 30, and 120 minutes relative to the initial cocrystal mass added and calculated according to Equation 13. Percentages increase even as $[DNZ]$ decreases when drug precipitation begins to outcompete cocrystal dissolution. Values above 100% are due to experimental error. Percentage component dissolved plots are shown in Figure S1 and selected values in Table S5. Error bars represent standard deviations. 99

Figure 3.7. Cocrystal dissolution in surfactant media shows the effect of modulating cocrystal solubility advantage (SA_T) with the same additives of FaSSIF, FeSSIF, and Soluplus in (a), (c), and (e), and the effect of targeting similar SA_T 10.9 – 13.4 with different surfactants and precipitation and growth inhibitors in (b), (d), and (f). Concentration – time profiles are shown in (a) and (b) compared to dose concentration (C_{dose}) of 2.37 mM. Dissolution in 0.5 FaSSIF + 0.5% TPGS + 1% HPC was performed by Childs et. al. (reported with a label of 1% TPGS + 2% HPC, but described in the Methods and Results with final surfactant concentrations as presented here) with a C_{dose} of 2.0 mM. Supersaturation – time profiles are shown in (c) and (d). Percentage cocrystal dissolved values shown in (e) and (f) were calculated from Equation 13 as previously described. Values over 100 are due to experimental error. Percentage component

dissolved plots are shown in Figure S1 and selected values in Table S5. Percentage cocrystal dissolved was not reported by Childs et. al.²⁴ $SA_T = 13.4$ for 0.5% TPGS was used to analyze this dissolution since HPC does not solubilize the drug and drug solubilization by FaSSIF <<< drug solubilization by TPGS. Percentage component dissolved plots and selected values in Appendix 3C. Error bars represent standard deviations. 101

Figure 3.8. Photomicrographs of danazol – vanillin cocrystal (DNZ-VAN) dissolution aliquots at 120 minutes showing the cocrystal induced drug crystallization in the presence of drug solubilizer (1% TPGS) with and without growth inhibitor (2% HPC). DNZ crystals grow as elongated or isomorphous shapes depending on the additive. The addition of HPC sustains supersaturation and slows DNZ crystal growth rate along the elongated crystal axis (fastest growth axis). Nucleation is observed to occur on the surface of the dissolving cocrystal and in the bulk solution. Darker regions represent original sites of surface nucleation before cocrystal completely dissolved. Photomicrographs in other dissolution media and time points are presented in Appendix 3C..... 104

Figure 3.9. Schematic cocrystal solubility advantage (SA) and drug dose/solubility ratio (D_{0D}) diagram shows how the parameters predictably decrease with log-log linear dependence on drug solubilization power (SP_D) according to Equations 3.4 and 3.8. In tandem, SA and D_{0D} represent maximum theoretical supersaturation that a cocrystal can generate as a function of cocrystal solubility (S_{CC}) or the dose concentration (C_{dose}). $SA < D_{0D}$ represents solubility-limited supersaturation, while $SA > D_{0D}$ represents dose-limited saturation or supersaturation. SA and/or D_{0D} can be predictably decreased within the metastable zone by rational additive selection in order to promote sustained supersaturation. 111

Figure 3.10. Cocrystal SA – SP and drug D_{0D} – SP diagram shows the log-log linear dependence of cocrystal solubility advantage (SA) and drug dose/solubility ratio (D_{0D}) on drug solubilization power (SP_D), predicted from Equations 3.4 and 3.8, respectively. SA_T should be modulated with cognizance of D_{0D} to avoid inadvertently dose-limiting supersaturation. Symbols represent SA, D_{0D} , and SP_D values calculated from experimental measurements of drug (danazol) and cofomer (vanillin) eutectic concentrations (Appendix 3B), and $C_{dose} = 2.37$ mM (molar equivalent of 200 mg dose in 250 mL luminal volume). 0.5% TPGS D_{0D} was calculated from $C_{dose} = 2.0$ mM. Transition point $SA_T = 1$ shows where cocrystal and drug solubilities are equal and above which the cocrystal generates supersaturation with respect to the drug. Below $D_{0D,T} = 1$, supersaturating drug delivery systems such as cocrystals are unable to generate bulk supersaturation at the given dose. $D_{0CC,T} = 1$ shows where $SA_T = D_{0D,T}$ and below which bulk supersaturation is generated but is dose-limited. Error bars (within the points) represent standard deviations of SA, D_{0D} , and SP_D 112

Figure 3.11. Comparison of drug dose/solubility ratio ($D_{0D,T} = C_{dose} / S_{drug}$), cocrystal solubility advantage ($SA_T = S_{cocrystal} / S_{drug}$), cocrystal dose/solubility ratio ($D_{0CC,T} = C_{dose} / S_{cocrystal}$), maximum supersaturation ($\sigma_{max} = [drug] / S_{drug}$), and relative area under the curve (RAUC = $AUC_{cocrystal} / AUC_{drug}$) during *in vitro* dissolution experiments. Dissolution in 0.5 FaSSIF + 0.5% TPGS + 1% HPC was performed by Childs et. al.²⁴ SA_T , $D_{0D,T}$, and $D_{0CC,T}$ are important thermodynamic parameters to assess the maximum theoretical supersaturation that a cocrystal may generate, and can be predictably modulated below critical supersaturation. Precipitation and growth inhibitors play an important role in sustaining supersaturation and increasing RAUC. Error bars represent standard deviations of SA_T and $D_{0D,T}$. σ_{max} and RAUC error are shown in Table 3.3. 114

Figure 3.12. Summary of properties and relationships to characterize and formulate pharmaceutical cocrystals. Cocrystal solubility, thermodynamic parameters, transition points, equilibrium constants, and SA – SP and D_{0D} – SP diagrams can be determined or predicted from a single eutectic point measurement. The eutectic point is measured at saturation with both cocrystal and drug solid phases. The cocrystal conversion risk is assessed and modulated by additive selection at SA and D_{0D} below critical supersaturation, to control cocrystal dissolution – supersaturation – precipitation behavior. Drug and coformer stoichiometric coefficients are represented by y and z , respectively. 116

Figure 3A.1. Increasing coformer impurity decreases nonstoichiometric cocrystal solubility and SA. Line was calculated according to $K_{sp} = (2.6 \pm 0.1) \times 10^{-8} M^2$ 122

Figure 3C.1. Percentage DNZ and VAN dissolved during DNZ-VAN cocrystal dissolution in (a) FaSSIF, (b) FeSSIF, (c) FaSSIF + 1% TPGS, (d) FaSSIF + 1% TPGS + 2% HPC, (e) FaSSIF + 0.25% Soluplus, and (f) FaSSIF + 2.5% Soluplus at 37°C. Percent dissolved was calculated from the ratio of measured DNZ or VAN in solution to the theoretical concentration from the initial mass added ($100 \times [\text{DNZ or VAN}] \text{ dissolved} / [\text{DNZ or VAN}] \text{ total added}$ from the cocrystal. Error bars represent standard deviations. 130

Figure 3C.2. Photomicrographs of DNZ-VAN dissolution aliquots at different time points (x -axis) show dissolution – supersaturation – precipitation (DSP) behavior in the presence of different additives (y -axis). Scale bar represents 50 μm . ^a Photo of 20 minute aliquot. 132

Figure 4.1. Powder X-ray diffraction (PXRD) patterns of cocrystal (PSZ-4HBA), drug (PSZ), and coformer (4HBA). PXRD pattern of 2:3 PSZ-4HBA obtained from reaction crystallization method (RCM) does not match the calculated pattern simulated by Mercury for the synchrotron X-ray diffraction (SXR) data. Cocrystal PXRD courtesy of Prof. Adam Matzger. SXR was calculated from single crystal analysis courtesy of Dr. Dongzhou Zhang and Prof. M. Fátima M. da Piedade. 142

Figure 4.2. Raman spectra of cocrystals (PSZ-4HBA), drug (PSZ), and coformer (4HBA) show unique chemical fingerprints. The spectra displayed are the averages of large area scans. Courtesy of Jennifer Diaz-Espinosa. 143

Figure 4.3. Raman spectra of 1:2 PSZ-4HBA single crystal and 2:3 PSZ-4HBA powder from reaction crystallization method (RCM). The spectra are shown as average and standard deviation obtained from single point scans. Courtesy of Jennifer Diaz-Espinosa. 144

Figure 4.4. Differential scanning calorimetry (DSC) thermograms of cocrystal (PSZ-4HBA), drug (PSZ), and coformer (4HBA). 145

Figure 4.5. Drug and coformer eutectic concentrations in blank and biorelevant media. Figure (a) shows posaconazole – 4-aminobenzoic acid (PSZ-4ABA) cocrystal and (b) shows posaconazole – 4-hydroxybenzoic acid (PSZ-4HBA) cocrystal. Eutectic constant K_{eu} values are above bars and were calculated according to Equation 4.1. PSZ and 4ABA eutectic concentrations in FaSSIF and FeSSIF has been previously reported and are included here for comparison.⁶ Error bars represent standard deviations. PSZ-4ABA data courtesy of Dr. Gislaine Kuminek. 146

Figure 4.6. Predicted relationship between eutectic constant K_{eu} and cocrystal solubility advantage (SA) for 2:3 posaconazole – 4-aminobenzoic acid (PSZ-4ABA) cocrystal and 2:3

posaconazole – 4-hydroxybenzoic acid (PSZ-4HBA) cocrystal. K_{eu} value of 1.5 indicates pH_{max} for a 2:3 cocrystal. Symbols represent values calculated from experimental measurements. Numbers next to symbols represent equilibrium pH. Line predicted from Equation 4.4. Error bars represent standard deviations. PSZ-4ABA data courtesy of Dr. Gislaine Kuminek..... 149

Figure 4.7. Solubility – pH dependence of basic drug posaconazole (PSZ), 2:3 posaconazole – 4-aminobenzoic acid cocrystal (PSZ-4ABA), and 2:3 posaconazole – 4-hydroxybenzoic acid cocrystal (PSZ-4HBA). Lines predicted according to Equations 4.12, 4.13, and 4.15, values in Tables 4.1 and 4.4, and $S_{PSZ,0} = 1.2 \times 10^{-4}$ mM. Experimental values are in Tables 4.2 and 4.3. Error bars represent standard deviations. PSZ-4ABA data courtesy of Dr. Gislaine Kuminek. 153

Figure 4.8. Cocrystal concentration – time and percentage cocrystal dissolved profiles in FeSSIF with and without excess coformer. SA was predictably modulated from 48 to 5.6 with the addition of 5.8 mM 4ABA. Drug precipitation resulted in incongruent saturation, and the additional coformer further decreased SA to 27.5 and 5.3 by 180 minutes. Cocrystal sustained supersaturation and performed better than the drug with and without excess coformer, but lack of concentration spike and precipitation with excess coformer at SA = 5.6 corresponded to a lower sustained supersaturation level and lower percentage cocrystal dissolved. Cocrystal and drug dissolution in FeSSIF have been previously reported and are included here for comparison.⁶ Error bars represent standard deviations. 157

Figure 4.9. Component concentrations during PSZ-4ABA cocrystal dissolution in FeSSIF (a) with and (b) without 5.8 mM excess coformer. Incongruent dissolution was observed after 5 minutes in FeSSIF, but component dissolution was much closer to a stoichiometric ratio in FeSSIF + 5.8 mM 4ABA. Congruent [4BA] line was calculated as $1.5 \times [PSZ]$. Error bars represent standard deviations (within points for [PSZ] and [4ABA] in FeSSIF). 159

Figure 4.10. Phase solubility diagram for PSZ-4ABA in FeSSIF. Stoichiometric cocrystal solubility corresponds to SA = 48, and nonstoichiometric cocrystal solubility can be predictably modulated according to the K_{sp} (Equation 4.10). Excess of 5.5 mM 4ABA was predicted to correspond to SA = 6. Connected points show drug and coformer concentrations during dissolution with and without excess 4ABA. 160

Figure 4A.1. Molecular interactions in the structure of PSZ-4HBA cocrystal. Figure was prepared using Mercury Version 4.3.1. 166

Figure 4A.2. Photos and photomicrograph of single crystal growth. 167

Figure 4A.3. 2:3 stoichiometry is indicated by completely dissolving pure PSZ-4HBA cocrystal synthesized by reaction crystallization method (RCM) and analyzing the concentration ratios by HPLC. 168

Figure 4B.1. PSZ-4HBA has similar solubility – pH dependence when calculated as a 1:2 and as a 2:3 cocrystal. 175

Figure 4C.1. Photomicrographs of cocrystal dissolution aliquots in FeSSIF + 5.8 mM 4ABA. With the addition of excess coformer, cocrystal did not form agglomerates as previously observed during dissolution in FeSSIF. 176

Figure 4C.2. Microscopy images of the transformation of PSZ-4ABA to PSZ during dissolution in FaSSIF and FeSSIF as reported by Kuminek et. al.¹ 177

ABSTRACT

Although pharmaceutical cocrystals have emerged as a useful strategy for enhancing the solubility, dissolution, and oral bioavailability of poorly water-soluble drugs, their development has thus far been marked by a lack of critical understanding of their solution behavior and the underlying solution interactions that govern drug supersaturation and exposure. This has led to empirical, time-consuming approaches with inadequate methods to control cocrystal behavior, leaving cocrystals as appearing overly risky and a largely untapped drug development strategy.

However, changes in cocrystal solubility and thermodynamic stability have been shown to be readily predictable as a function of changing solution conditions. The purpose of this research is (1) to develop a quantitative, mechanistic-based approach through which known relationships between cocrystal solubility advantage ($SA = S_{\text{cocrystal}} / S_{\text{drug}}$) and solution conditions such as pH, surfactant concentration, or excess coformer concentration can be used to fine-tune cocrystal inherent supersaturation, and (2) to modulate nucleation by selecting additives that will exhibit thermodynamic and kinetic control over the dissolution-supersaturation-precipitation (DSP) behavior of cocrystal systems.

The effects of changing solution conditions on SA and corresponding DSP behavior were studied for cocrystals of three different poorly water-soluble drugs: lamotrigine, danazol, and posaconazole. Cocrystals with highly soluble cofomers were found to have SA values orders of magnitude higher than parent drug in aqueous conditions, which left them at high risk for rapid solution-mediated conversion during previously reported *in vitro* and *in vivo* dissolution studies. For cocrystals with ionizable components, aqueous solubility was found to predictably change

with pH, with some cocrystals exhibiting a transition point pH_{max} at which cocrystal and drug solubilities were equal and above or below which their relative stabilities were inverted.

Cocrystal SA was found to predictably decrease in the presence of additives with increasing drug solubilization power ($\text{SP}_D = S_{\text{drug,T}} / S_{\text{drug,aq}}$). The SA - SP relationship provided a mechanistic basis to fine-tune SA (thermodynamic supersaturation limit) below critical supersaturation (kinetic supersaturation limit) which, combined with precipitation and growth inhibitors, promoted sustained supersaturation. Drug dose/solubility ratio ($D_{0(D)} = C_{\text{dose}} / S_{\text{drug}}$) was found to be an important parameter to define the potential fraction dose dissolved by the cocrystal as well as the risk of dose-limited supersaturation or undersaturation if SA was dialed too low. Finally, excess coformer concentration was also shown to predictably modulate cocrystal SA according to the solubility product K_{sp} , which allowed the cocrystal to sustain supersaturation and maintain a quasi-equilibrium at concentrations near the eutectic point.

Design of cocrystal delivery systems that can generate both thermodynamically possible and kinetically sustainable supersaturation in the gastrointestinal tract is essential for cocrystals to be a viable strategy to enhance the oral bioavailability of poorly soluble drugs. Although cocrystals may appear to be risky due to their vulnerability to conversion to less soluble forms, their development can be successfully streamlined through rational, mechanistic approaches that are cognizant of solubility transition points and utilize both the thermodynamic and kinetic control of additives on DSP behavior.

CHAPTER 1

Introduction

Orally administered drug products may be the most preferred dosage forms, but their successful delivery remains challenged by dissolution- and solubility-limited absorption in the gastrointestinal tract. Solubility and permeability have been defined by the Biopharmaceutics Classification System (BCS) as the primary factors that influence oral drug absorption.¹ BCS Class II drugs are categorized as having low solubility and high permeability, where drug dissolution is the rate-limiting step to absorption and the drug dose/solubility ratio ($D_0 = \text{dose concentration} / S_{\text{drug}}$) is greater than 1.² For these drugs, development efforts to improve both dissolution and solubility must be made in order to successfully dissolve the drug dose and achieve efficacious drug concentration levels *in vivo*.

Supersaturating drug delivery systems such as cocrystals, salts, and amorphous forms have been shown to enhance the solubility of crystalline drug, which can lead to increases in drug dissolution rate, exposure, and oral bioavailability.³⁻⁸ Cocrystals in particular have recently gained a lot of pharmaceutical interest in this area. Cocrystals are defined as multicomponent solid forms composed of two or more neutral molecular components in a single homogenous crystalline phase with well-defined stoichiometry. When a poorly-soluble parent drug is cocrystallized with a highly soluble, generally regarded as safe, typically inert coformer, pharmaceutical cocrystals have been shown to impart solubility advantage orders of magnitude higher than parent drug.^{3, 9-11}

As shown in Figure 1.1, one of the most important properties of cocrystals is the ability to fine-tune their solubility and solubility advantage ($SA = S_{CC} / S_D$) as a function of solution conditions, such as pH, solubilizing agent concentration, and nonstoichiometric coformer concentration. This unique property of cocrystals gives them the development advantage of being versatile and tailorable to a wide range of solution conditions.

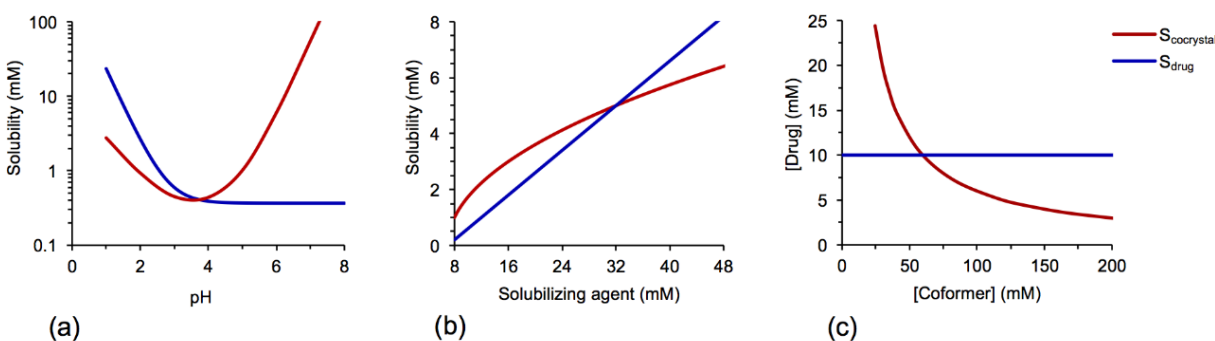


Figure 1.1. Cocrystal solubility and stability vary with solution conditions such as (a) pH, (b) drug solubilizing agents, and (c) excess coformer concentration. The intersection of the cocrystal and drug solubility curves represents a transition point, where $S_{cocrystal} = S_{drug}$. Cocrystal is stable when $S_{cocrystal} < S_{drug}$, and has solubility advantage when $S_{cocrystal} > S_{drug}$. Changing solution conditions can be used to fine-tune relative cocrystal stability.³

Despite the increased interest in cocrystals due to these unique properties, their development has thus far been marked by a lack of critical understanding of their solution behavior and the underlying solution interactions that govern drug supersaturation and exposure. This has led to empirical, time-consuming approaches with inadequate methods to control dissolution – supersaturation – precipitation (DSP) behavior of cocrystal systems. Such studies have stereotyped highly soluble cocrystals as risky to develop, owing to their vulnerability to rapidly undergo solution-mediated transformation to their more thermodynamically stable parent drug forms and essentially negating their solubility advantage.

The purpose of this chapter is to introduce the well-recognized concepts of cocrystal formation, synthesis, solubility, and dissolution that relate to their ability to generate supersaturation and enhance oral bioavailability. This chapter will conclude with research objectives for expanding the understanding of cocrystal solution behavior and ultimately for streamlining their development.

Cocrystal Formation and Design

Multicomponent solid forms include both crystalline and amorphous systems. Figure 1.2 schematically demonstrates the differences in composition of cocrystals and other multicomponent solids.¹² While amorphous systems, polymorphs, solvates, and salts currently represent the most common solid forms in product development, cocrystals have been largely underutilized despite offering a unique set of advantages. Cocrystals differ from solvates in that both components are solids at room temperature. Crystallinity gives cocrystal stability advantage over amorphous materials, and lack of reliance on ionic interactions like salts allows nonionizable drugs and cofomers to be amenable to cocrystallization. Both cocrystals and salts can exhibit polymorphism and solvate formation, and their stoichiometric nature makes their solubilities uniquely tailorable with solution conditions.^{3, 13}

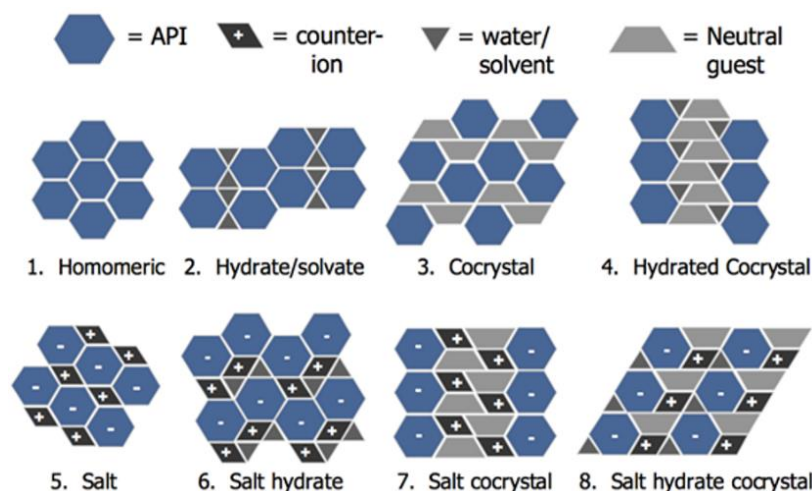


Figure 1.2. Multicomponent crystalline forms that can be used to alter the physicochemical properties of an active pharmaceutical ingredient (API) or drug without changing molecular structure.¹²

Cocrystal and salt formation have been described as a continuum, whereby complete proton transfer yields an ionic bond and salt formation, while incomplete transfer yields a noncovalent bond and cocrystal formation.¹³ ΔpK_a values (pK_a of base – pK_a of acid) serve as reliable parameters for predicting salt formation when greater than 2 or 3 and for predicting cocrystal formation when less than 0.^{14, 15} However, these predictions become more arbitrary when ΔpK_a is between 0 and 2.

By definition, cocrystals form in a stoichiometric ratio of drug and coformer.^{6, 11, 16} Instead of conducting cocrystal screens which can be costly in both material and time, rational coformer selection can be achieved by examining the functional groups capable of hydrogen bonding with the drug. Because of the directional interactions they impart on the respective components, hydrogen bonds are known to strongly influence molecular recognition.¹⁷ As a result, general guidelines have been established to predict which hydrogen bond interactions will result in crystal formation: (1) all acidic hydrogen atoms will participate in hydrogen bonding; (2) contingent on sufficient number of hydrogen bond donors, all good hydrogen bond acceptors

will be used; (3) hydrogen bonds will preferentially form between the best proton donor and acceptor; and (4) intramolecular hydrogen bonds in a six-membered ring will form preferentially over intermolecular hydrogen bonds.¹⁷⁻¹⁹

Common noncovalent intermolecular interactions of specified geometries and bonding motifs are referred to as synthons. By performing supramolecular retrosynthetic analysis for a target compound, the Cambridge Structural Database (CSD) can be used to identify both homosynthons, which are formed between identical functional moieties, and heterosynthons, which are formed between different functional moieties.²⁰⁻²² Some of the most common synthon pairs are shown in Figure 1.2.

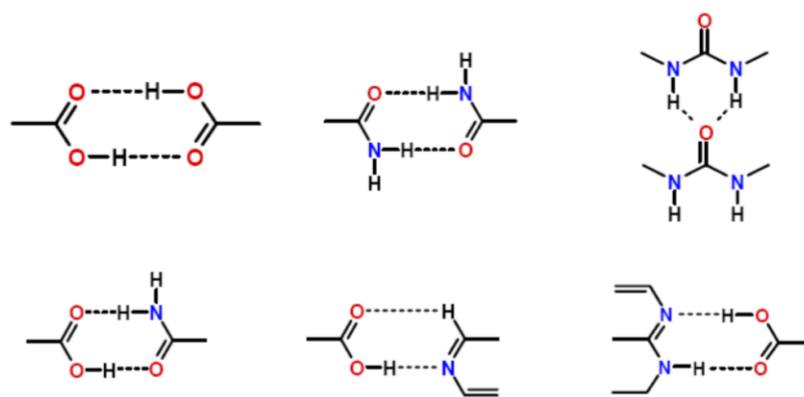


Figure 1.3. Common supramolecular synthons formed with hydrogen bonds between carboxylic acids, amides, pyridines, and other aromatic nitrogens.^{3, 18-20}

When designing cocrystals to be supersaturating drug delivery systems, it is also important to thoughtfully select a coformer for its solubility. As shown in Figure 1.3, a correlation has been observed between cocrystal SA and the ratio of coformer to drug solubilities.³ In general, cofomers 10 times more soluble than drug will yield cocrystals with SA = 1. Ionizable cofomers also have the ability to impart or alter the solubility – pH

dependence of the drug, so cognizant selection of highly soluble cofomers with complementary ionization to the drug has the greatest chance to yield cocrystals with solubility advantage.

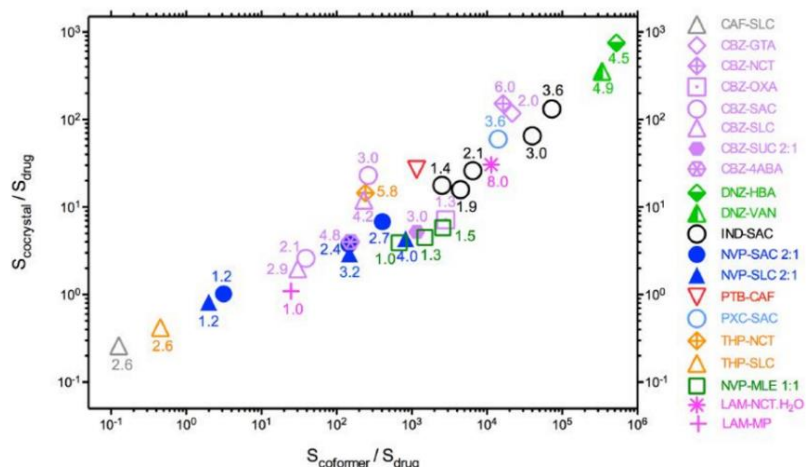


Figure 1.4. A correlation is observed between cocrystal solubility advantage ($S_{\text{cocrystal}} / S_{\text{drug}}$) and the ratio of cofomer to drug solubilities ($S_{\text{coformer}} / S_{\text{drug}}$). $S_{\text{coformer}} / S_{\text{drug}} > \sim 10$ relates to $S_{\text{cocrystal}} / S_{\text{drug}} = 1$. Final pH values from equilibrium solubility measurements at 25°C are shown as numbers by data points.³

Cocrystal Screening and Synthesis

While the CSD represents a useful basis for rationally identifying potential cocrystalline cofomers, it is not a definitive predictor of molecules that will cocrystallize. Nor can it predict cocrystal structure, conditions that promote cocrystallization, or physicochemical properties of formed cocrystals. Thus, cocrystal screening remains to be an important aspect of the synthesis process.³ A variety of cocrystal screening techniques can be found in the literature, including slow solvent evaporation,²³⁻²⁷ slurry conversion,²⁸ neat (dry) grinding,^{29, 30} solvent drop grinding,³¹⁻³³ and melt.^{34, 35} However, these techniques have limitations, as they often result in crystallization of individual components, cannot be readily upscaled, and are costly in both time and materials. By examining the basic equilibria and mathematical relationships that govern

crystallization, the nucleation and growth principles of cocrystals can be readily understood and controlled.

For the case of cocrystal A_yB_z , formation is characterized as the crystallization of a single phase with components A and B in an exact stoichiometric ratio according to



where A and B represent drug and coformer, and y and z represent their respective stoichiometric coefficients.³⁶ The forward reaction is dissociation and represents dissolution, while the reverse reaction is association and represents precipitation. The solubility product K_{sp} is the thermodynamic equilibrium constant for this reaction and is defined as the product of the molar activities or concentrations of cocrystal constituents. K_{sp} is given by

$$K_{\text{sp,a}} = \gamma_A[A]^y \gamma_B[B]^z \cong K_{\text{sp}} = [A]^y [B]^z \quad (1.2)$$

where γ represents the activity coefficients of components A and B. Under ideal conditions where activity is constant and $\gamma = 1$, the activity-based solubility product $K_{\text{sp,a}}$ can be replaced by the concentration product K_{sp} . It is important to note that K_{sp} is explicitly calculated as the product of the cocrystal components in the same molecular state as the cocrystal. While cocrystal K_{sp} considers [A] and [B], salt K_{sp} considers the ionized compounds as

$$K_{\text{sp}} = [AH^+]^y [B^-]^z \quad (1.3)$$

$K_{\text{sp}} \neq [A]_{\text{T}} [B]_{\text{T}}$ when there are molecular species in solution different from those in the corresponding solid phase. These K_{sp} values are not calculated from total analytical concentrations of salt or cocrystal components when there are molecular species in solution different from those in the salt or cocrystal solid phase.

Supersaturation (σ) is the driving force for cocrystal nucleation and growth and is represented as

$$\sigma = \left(\frac{a_A a_B}{K_{sp,a}} \right)^{1/2} \cong \left(\frac{[A][B]}{K_{sp}} \right)^{1/2} \quad (1.4)$$

This equation demonstrates that supersaturation with respect to cocrystal can be increased by increasing the product of the component concentrations in solution.³

The reaction crystallization method (RCM) utilizes this relationship between cocrystal supersaturation and solution component concentrations in order to avoid crystallization of pure components.³⁷ The phase solubility diagram of Figure 1.5 shows graphically how cocrystal supersaturation can be generated while component solution concentrations are only at or below saturation.^{11, 38}

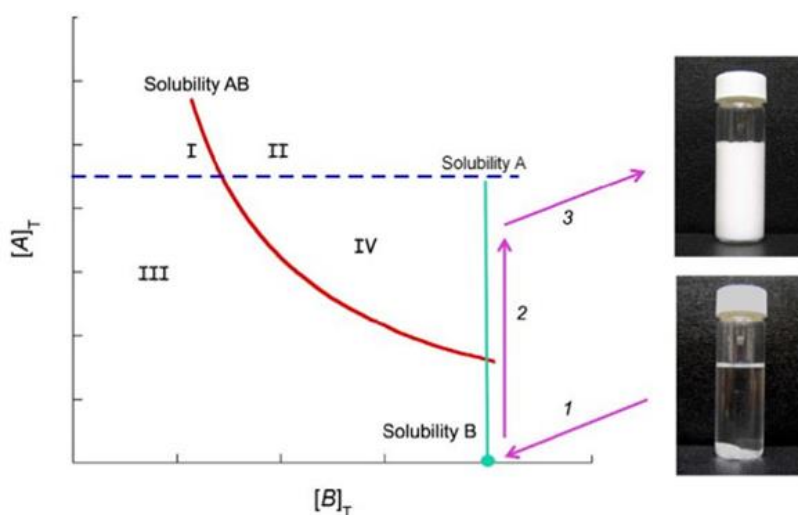


Figure 1.5. Phase solubility diagram defining regions where cocrystal can form or dissolve. Solubility of drug A is indicated with dashed blue line, solubility of coformer B is indicated with solid green line, and solubility of cocrystal AB is indicated with red curve. Nonstoichiometric cocrystal solubility decreases with increasing coformer concentration ($[B]_T$). Subscript T represents total analytical concentrations. Region I represents supersaturation with respect to drug, where the cocrystal can convert to drug. Region II represents supersaturation with respect to cocrystal and drug, where both forms can precipitate. Region III represents undersaturation, where cocrystal, drug, and coformer may dissolve. Region IV represents supersaturation with respect to cocrystal, but undersaturation with respect to drug. Pink arrows represent a possible cocrystal formation pathway, whereby drug in saturated coformer solution may dissolve above nonstoichiometric cocrystal solubility and convert to precipitate pure cocrystal. This method of cocrystal synthesis is known as reaction crystallization method (RCM).^{3, 37, 38}

In this case, cocrystal AB is more soluble than drug under stoichiometric conditions, and nonstoichiometric cocrystal solubility decreases with increasing coformer B concentration as governed by K_{sp} . In region III, the components and the cocrystal are all below saturation. In contrast, the solution is supersaturated with respect to drug in region I and with respect to both cocrystal and drug in region II, which charts the potential for undesired precipitation of the supersaturated component(s). However, region IV represents supersaturation with respect to only cocrystal. Assuming that coformer is more soluble than drug, cocrystal (the most thermodynamically stable phase) can be formed by saturating a solution with respect to coformer and then dissolving drug at or below its solubility.

Phase solubility diagrams are essential to guide cocrystal discovery and synthesis. Manipulating solution conditions to be within region IV of the diagram will maximize the likelihood of successful cocrystal synthesis by a controlled approach. Furthermore, RCM has the advantages of not being limited by differences in component solubilities, being amenable to a large range of solvents, and being adjustable for any reaction scale, including small scale *in situ* monitoring for cocrystal discovery and large scale cocrystal production.^{3, 37, 39-41}

Employment of supramolecular retrosynthetic analysis and proper selection of a cocrystal screening technique can effectively streamline the process of cocrystal formation. Both cocrystals and salts have been discovered by their tandem use.

Cocrystal Eutectic Point and K_{eu}

The cocrystal eutectic point has been well established as an important transition point that defines cocrystal thermodynamic stability relative to its components.^{11, 38, 39, 42} The phase solubility diagram denotes cocrystal eutectic points where the cocrystal solubility curve

intersects with the drug and coformer solubility lines (Figure 1.5). For cocrystals of highly soluble coformers and poorly soluble drugs, their resulting SA means that they are not the most thermodynamically stable phase and that stoichiometric cocrystal solubility is not experimentally measurable due to drug precipitation. However, the eutectic point, defined as drug or coformer and cocrystal solid phases in equilibrium with solution, represents experimentally measurable nonstoichiometric solubility that can be used to calculate stoichiometric cocrystal solubility according to

$$S_{CC} = \sqrt{\frac{y+z}{y^y z^z} [A]_T [B]_T} \quad (1.5)$$

where the total concentrations of components A and B represent the total analytical equilibrium concentrations of each component.

Pharmaceutically, the eutectic point between drug and cocrystal is most typically relevant since drug is typically the less soluble component.¹¹ Figure 1.6 shows the cocrystal and drug eutectic point for two different cocrystals in a particular solvent: a stable cocrystal 1 with low solubility and low K_{sp} , and metastable cocrystal 2 with high solubility and high K_{sp} . The dashed line indicates stoichiometric solution concentrations, which congruent cocrystal saturation would follow. Stoichiometric cocrystal solubilities are indicated with the blue and red dots, and nonstoichiometric cocrystal solubilities predictably decrease according to Equation 1.5. Intersection with the solid drug solubility line indicates the eutectic point. The metastable cocrystal 2 has stoichiometric solubility above drug solubility, meaning that it would incongruently saturate as generated supersaturation led to drug precipitation. As a result, stoichiometric solubility is not experimentally measurable, but can be estimated from eutectic point measurements. In contrast, stable cocrystal 1 congruently saturates and is less soluble than

parent drug, and therefore its solubility can be directly measured and need not be estimated from eutectic concentrations.

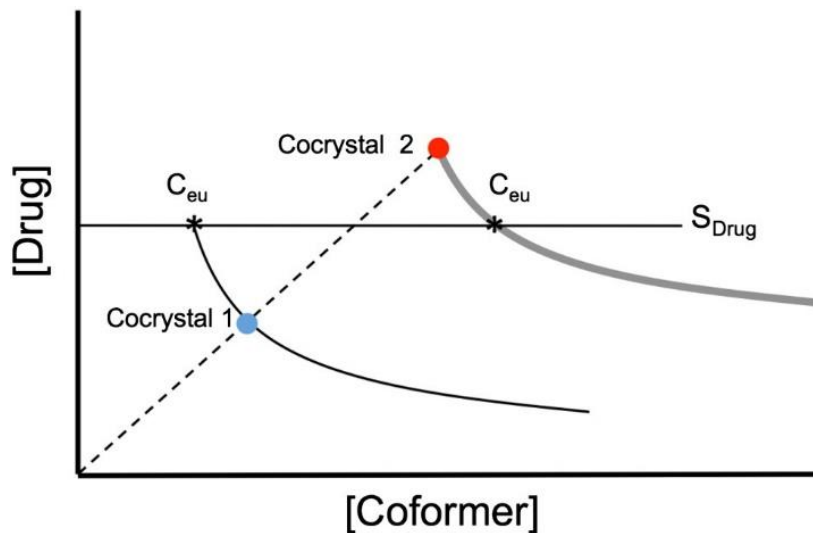


Figure 1.6. Schematic phase solubility diagram indicating the eutectic points (*) where cocrystal and drug solid phases are in equilibrium with solution.¹¹ C_{eu} represents the eutectic concentrations of drug and coformer. The circles represent stoichiometric cocrystal solubilities. Two different cocrystals are considered based on their stability with respect to drug under stoichiometric conditions: a stable cocrystal (cocystal 1), and a metastable cocrystal (cocystal 2) where the cocrystal generates supersaturation with respect to drug. Drug solubility (S_{drug}) is indicated and is much lower than the solubility of the coformer, which is not shown. The dashed line illustrates stoichiometric concentrations of cocrystal components, which congruent dissolution would follow.³

The eutectic constant K_{eu} also serves as an indicator of cocrystal stability and solubility.⁴²

K_{eu} is defined as

$$K_{eu} = \frac{[coformer]_{eu,T}}{[drug]_{eu,T}} \quad (1.6)$$

at the eutectic point where drug and cocrystal are in equilibrium with solution. Subscripts eu and T represent total analytical concentrations (ionized and nonionized) at the eutectic point.

K_{eu} represents a transition point when it is equal to the stoichiometric ratio of coformer to drug in a cocrystal. K_{eu} values greater than the stoichiometric ratio indicate that cocrystal is

more soluble than the drug ($SA > 1$), and vice versa for K_{eu} values less than the stoichiometric ratio ($SA < 1$). Mathematically, K_{eu} can also be used to calculate cocrystal SA according to

$$SA = \frac{y}{z} K_{eu}^{z/(y+z)} \quad (1.7)$$

Figure 1.7 shows excellent agreement between the experimental and predicted relationship between K_{eu} and SA for NVP cocrystals.⁴³ Because K_{eu} changes with pH, it can also serve as an indicator for a pH_{max} , the pH at which drug and cocrystal solubilities are equal. NVP-MLE is a 1:1 cocrystal, so the K_{eu} and SA values greater than 1 at all studied pH values indicate that cocrystal is more soluble than drug and there is no pH_{max} within this range. NVP-SAC and NVP-SLC are 2:1 cocrystals, so the transition point would occur at $K_{eu} = 0.5$. Figure 1.7 indicates that NVP-SAC exhibits a pH_{max} between 1.2 and 2.4, while NVP-SLC has a pH_{max} between 1.2 and 3.2.^{42, 43}

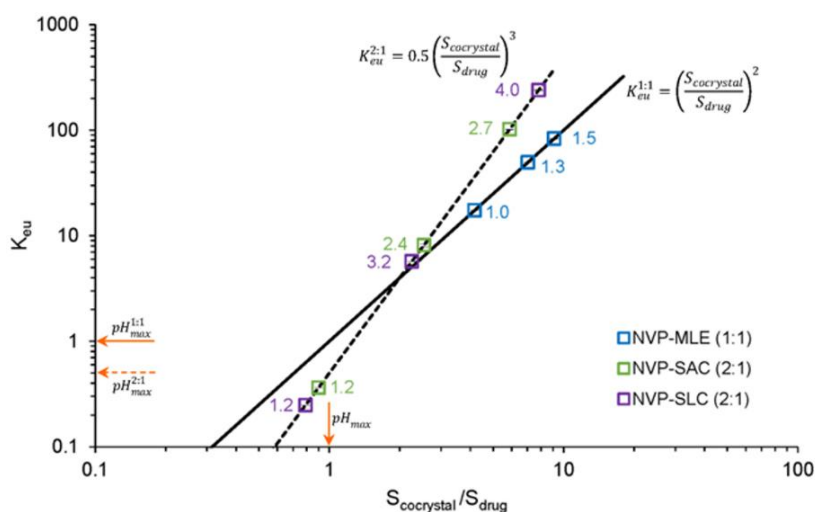


Figure 1.7. Predicted and experimental eutectic constant K_{eu} and solubility advantage ($SA = S_{cocrystal} / S_{drug}$) values for 1:1 NVP–MLE (solid line) and 2:1 NVP–SAC and NVP–SLC cocrystals (dashed line). K_{eu} is a key indicator of SA, and K_{eu} dependence on pH reveals the cocrystal pH_{max} . At pH_{max} , $K_{eu} = 1$ for 1:1 cocrystals and $K_{eu} = 0.5$ for 2:1 cocrystals. Symbols represent experimental values. The numbers next to data points indicate pH at eutectic point or equilibrium pH. Predicted lines were calculated according to Equation 1.7 (shown for 1:1 and 2:2 cocrystals on plot).⁴³

Figure 1.8 summarizes all the different cocrystal parameters, transition points, and diagrams that can be calculated and/or predicted from a single eutectic point measurement. Utilizing these relationships will not only provide a holistic characterization of cocrystal solubility and stability, but also can be time- and material-sparing during early cocrystal development.

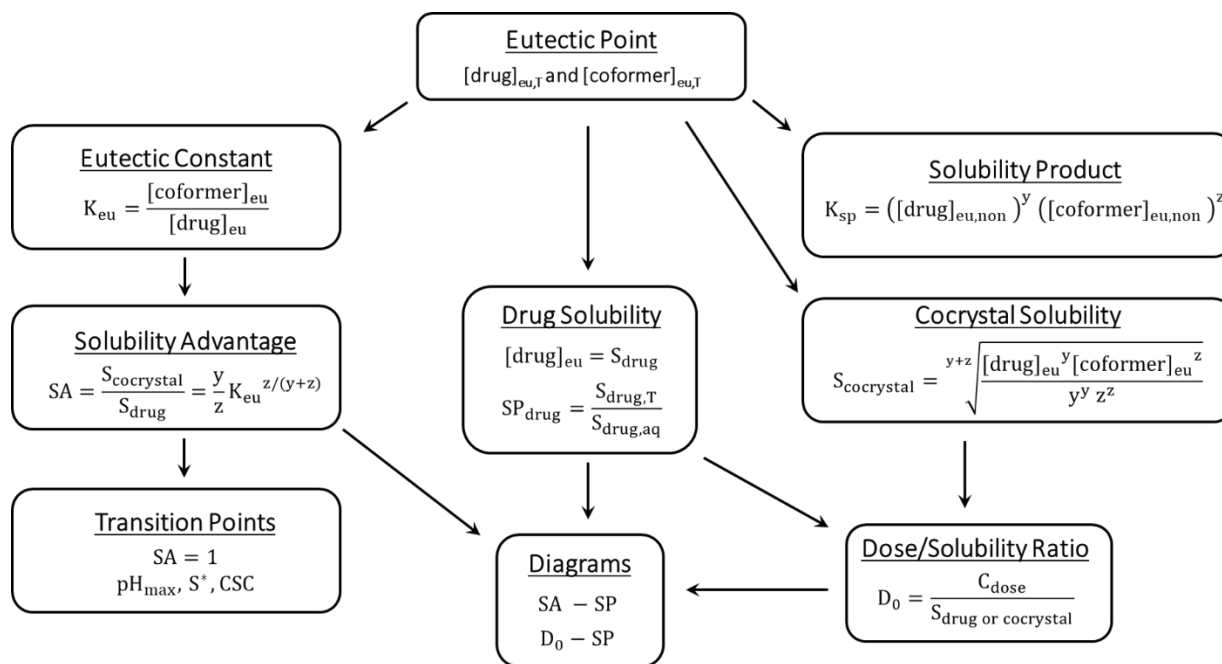


Figure 1.8. A single eutectic point measurement can be used to obtain important cocrystal parameters, transition points, and diagrams. General equations refer to a cocrystal of stoichiometry y:z.

Cocrystal Solubility and Transition Points

Mathematical Forms of Cocrystal Solubility and Stability

Although solubility is often reported as a single value, in reality it varies with changing solution conditions such as pH, presence of solubilizing agents, or excess coformer (Figure 1.1). Total solubility of a binary cocrystal A_yB_z may be expressed as a function of equilibrium constants and relevant concentrations as

$$S_{CC,T} = f(K_{sp}, K_a, K_s, K_c, [H^+], [M], y, z) \quad (1.8)$$

where K_{sp} , K_a , K_s , and K_c are the dissociation, ionization, solubilization by additives, and complexation equilibrium constants respectively; $[H^+]$ represents hydrogen ion concentration as determined by pH; $[M]$ represents total solubilizing agent concentration or micellar concentration; and y and z represent the stoichiometric coefficients of the drug and coformer respectively. For simplicity, complexation will not be considered here.

The total influence of both ionization and solubilization on cocrystal solubility may be summarized for both the drug and coformer using the representative terms $\delta_{D,T}$ and $\delta_{CF,T}$, where

$$\delta_{D,T} = \delta_{D,I} + \delta_{D,S} \quad (1.9)$$

and

$$\delta_{CF,T} = \delta_{CF,I} + \delta_{CF,S} \quad (1.10)$$

where subscripts I and S refer to ionization and solubilization. The ionization parameters $\delta_{D,I}$ and $\delta_{CF,I}$ are a function of K_a and $[H^+]$, and the solubilization parameters $\delta_{D,S}$ and $\delta_{CF,S}$ are a function of K_s and $[M]$. Thus, Equation 1.8 may be simplified as

$$S_{CC,T} = f(K_{sp}, \delta_{D,T}, \delta_{CF,T}, y, z) \quad (1.11)$$

Cocrystal solubility can be calculated from the general equation

$$S_{CC,T} = \sqrt{\frac{K_{sp}}{(y^y z^z)} \delta_{D,T}^y \delta_{CF,T}^z} \quad (1.12)$$

This equation can be used to calculate solubility for a cocrystal of given stoichiometry and under specific ionization and solubilization conditions by substituting δ_I and δ_S expressions in terms of the appropriate equilibrium constants (Table 1.1).⁴²

Table 1.1. Ionization (δ_I) and solubilization (δ_S) terms used to calculate cocrystal solubility according to Equations 1.9, 1.10, and 1.12. The expressions for cocrystal solubilities were previously derived and experimentally confirmed.^a

Ionization of Cocrystal Component	δ_I	δ_S
Nonionizable (R)	1	$K_S^R [M]$
Monoprotic Acidic (HA)	$1 + \frac{K_a^{HA}}{[H^+]}$	$K_S^{HA} [M]$
Diprotic Acidic (H ₂ A)	$1 + \frac{K_a^{H_2A}}{[H^+]} + \frac{K_a^{H_2A} K_a^{HA^-}}{[H^+]^2}$	$K_S^{H_2A} [M]$
Monoprotic Basic (BH ⁺)	$1 + \frac{[H^+]}{K_a^{BH^+}}$	$K_S^{BH^+} [M]$
Amphoteric (HAB)	$1 + \frac{K_a^{HAB}}{[H^+]} + \frac{[H^+]}{K_a^{H_2AB^+}}$	$K_S^{HAB} [M]$
Zwitterionic (⁻ ABH ⁺)	$1 + \frac{K_a^{-ABH^+}}{[H^+]} + \frac{[H^+]}{K_a^{HABH^+}}$	$K_S^{-ABH^+} [M]$

^aIt should be noted that these expressions for δ_S have excluded the K_S term(s) for all non-neutral species. In cases when $K_S^{\text{neutral}} \gg K_S^{\text{non-neutral}}$, the solubilization of non-neutral species will have a negligible effect on total cocrystal solubility.⁴⁴⁻⁴⁷

When cocrystal solubility is only influenced by dissociation ($\delta_{D,T} = 1$ and $\delta_{CF,T} = 1$),

Equation 1.12 becomes

$$S_{CC,T} = \frac{(y+z) \sqrt{K_{sp}}}{\sqrt{(y^y z^z)}} \quad (1.13)$$

For a 1:1 cocrystal, $y = z = 1$ and Equation 1.12 becomes

$$S_{CC,T} = \sqrt{K_{sp} \delta_{D,T} \delta_{CF,T}} \quad (1.14)$$

The equations associated with the expressions in Table 1.1 are mathematically derived from equilibrium and mass balance equations of a particular system. The equilibrium reactions corresponding to the δ terms in Table 1.1 are presented in Table 1.2.

Table 1.2. Equilibrium expressions and constants of drug or cofomer cocrystal components that are nonionizable, acidic, basic, amphoteric, or zwitterionic. Equilibrium constant equations can be used with knowledge of system mass balance to derive δ_1 and δ_5 equations. Subscripts m and aq refer to the micellar and aqueous pseudophases, respectively.

Ionization of Cocrystal Component	Equilibrium Expression	Equilibrium Constant
Nonionizable (R)	$R_{aq} \rightleftharpoons R_m$	$K_{S,R}$
Monoprotic Acidic (HA)	$HA_{aq} \rightleftharpoons H^+_{aq} + A^-_{aq}$	$K_{a,HA}$
	$HA_{aq} \rightleftharpoons HA_m$	$K_{S,HA}$
Diprotic Acidic (H ₂ A)	$H_2A_{aq} \rightleftharpoons H^+_{aq} + HA^-_{aq}$	K_{a,H_2A}
	$HA^-_{aq} \rightleftharpoons H^+_{aq} + A^{2-}_{aq}$	K_{a,HA^-}
	$H_2A_{aq} \rightleftharpoons H_2A_m$	K_{S,H_2A}
Monoprotic Basic (BH ⁺)	$BH^+_{aq} \rightleftharpoons H^+_{aq} + B_{aq}$	K_{a,BH^+}
	$BH^+_{aq} \rightleftharpoons BH^+_m$	K_{S,BH^+}
Amphoteric (HAB)	$HAB_{aq} \rightleftharpoons H^+_{aq} + AB^-_{aq}$	$K_{a,HAB}$
	$H_2AB^+_{aq} \rightleftharpoons HAB_{aq} + H^+_{aq}$	K_{a,H_2AB^+}
	$HAB_{aq} \rightleftharpoons HAB_m$	$K_{S,HAB}$
Zwitterionic (⁻ ABH ⁺)	$-ABH^+_{aq} \rightleftharpoons H^+_{aq} + AB^-_{aq}$	$K_{a,-ABH^+}$
	$HABH^+_{aq} \rightleftharpoons -ABH^+_{aq} + H^+_{aq}$	$K_{a,HABH^+}$
	$-ABH^+_{aq} \rightleftharpoons -ABH^+_m$	$K_{S,-ABH^+}$

The mass balance equation for the case of a 1:1 cocrystal RHA composed of nonionizable drug (R) and ionizable coformer (HA) is based upon the phase and chemical equilibria presented in Figure 1.9.³

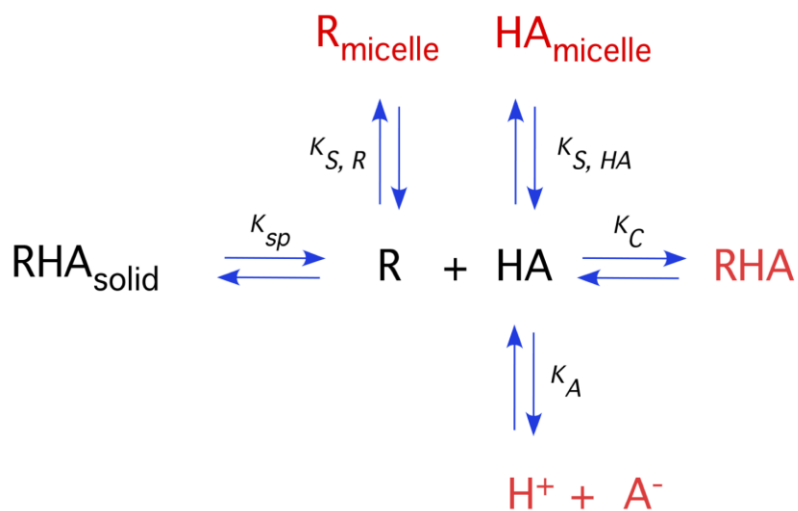


Figure 1.9. Cocrystal solubility is determined by the total analytical concentrations of its molecular constituents in solution. This diagram shows cocrystal-solution phase interactions for a cocrystal RHA composed of nonionizable drug (R) and acidic coformer (HA), as well as the associated equilibria common to pharmaceutical dosage forms, including dissociation, complexation, ionization, and solubilization. K_{sp} represents the cocrystal solubility product, K_a is the ionization constant, K_c is the complexation constant, and K_s^{HA} and K_s^R are the solubilization constants for HA and R, respectively.^{3, 48}

Mass balance on R and A gives the total solubility of cocrystal RHA under stoichiometric conditions as

$$S_{RHA,T} = [R]_T = [A]_T \quad (1.15)$$

where $[R]_T$ and $[A]_T$ represent the concentrations of all species in solution. The cocrystal solubility is

$$S_{RHA,T} = [R]_{aq} + [RHA]_{aq} + [R]_m = [HA]_{aq} + [A^-]_{aq} + [RHA]_{aq} + [HA]_m \quad (1.16)$$

where subscript aq represents the aqueous phase and subscript m represents the micellar phase.

The concentrations of all species in Equation 1.16 can be expressed in terms of the concentrations of cocystal components (free and nonionized) R and HA using the equilibrium constants. This analysis gives the cocystal solubility in terms of equilibrium constants (ionization and solubilization of cocystal components, K_a^{HA} , K_s^{HA} , and K_s^R) and micellar concentration of surfactant [M]:

$$S_{RHA,T} = \sqrt{K_{sp}(1 + K_S^R[M]) \left(1 + \frac{K_a^{HA}}{[H^+]} + K_s^{HA}[M]\right)} \quad (1.17)$$

where K_{sp} is the solubility product given by $[R][HA]$. The terms in parenthesis represent ionization and solubilization according to the equilibrium reactions in Figure 1.9.

The generalized form for a cocystal RHA under the solubility conditions in Figure 1.9 gives

$$S_{RHA,T} = \sqrt{K_{sp}\delta_{R,S}(\delta_{A,I} + \delta_{A,S})} \quad (1.18)$$

and shows how the expressions for the ionization and solubilization terms presented in Table 1.1 can be utilized to obtain the cocystal solubility equation. Note that solubilization of ionized species is not considered in the expressions in Table 1.1.

General Solubility Expressions

Ionization of cocystal components is defined as the sum of acidic and basic functional groups of cocystal components according to

$$\delta_{D,I} = 1 + \sum_{l=1}^m \left(\frac{\prod_{h=1}^l K_{a_h}^{acidic}}{[H^+]^l} \right) + \sum_{q=1}^r \left(\frac{[H^+]^q}{\prod_{t=1}^q K_{a_t}^{basic}} \right) \quad (1.19)$$

for drug, and

$$\delta_{CF,I} = 1 + \sum_{f=1}^g \left(\frac{\prod_{h=1}^f K_{a_h}^{acidic}}{[H^+]^f} \right) + \sum_{i=1}^j \left(\frac{[H^+]^i}{\prod_{k=1}^i K_{a_k}^{basic}} \right) \quad (1.20)$$

for coformer, where m and g are the total number of respective acidic groups, and r and j are the total number of respective basic groups.⁴² It should be noted from these equations that when ionization is not considered, both $\delta_{D,I}$ and $\delta_{CF,I}$ reduce to one (as predicted by Equation 1.13).

In solutions with additives that solubilize cocrystal components, the heterogeneous equilibria between cocrystal and its components are taken into consideration as illustrated in Figure 1.10.⁴⁸⁻⁵² This diagram only represents solubilization of the drug component of the cocrystal and assumes negligible solution complexation as well as non-ionizing solution conditions.^{44, 50}

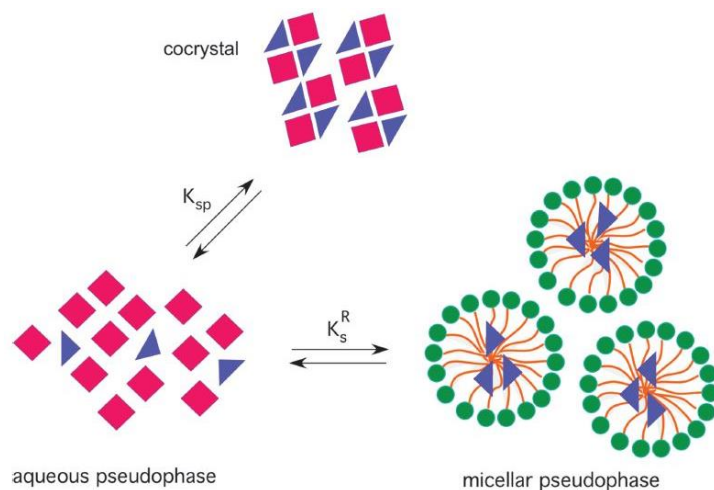


Figure 1.10. Schematic illustration of the equilibria between the cocrystal solid phase and its components in the aqueous and micellar solution pseudophases. This scheme represents preferential micellar solubilization of the drug component, which leads to excess coformer in the aqueous phase and stabilization of the cocrystal in the aqueous phase.^{44, 48}

Solubilization of cocrystal components is defined as the sum of all cocrystal dissolved species (ionized and nonionized) according to

$$\delta_{D,S} = \left[K_{s_1} [M] + \left(\sum_{l=1}^m \left(\frac{\prod_{n=1}^l K_{an}^{acidic}}{[H^+]^l} \right) K_{s_{l+1}} \right) + \sum_{q=1}^r \left(\left(\frac{[H^+]^q}{\prod_{t=1}^q K_{at}^{basic}} \right) K_{s_{q+1}} \right) \right] [M] \quad (1.21)$$

for drug, and

$$\delta_{CF,S} = \left[K_{S_1} [M] + \left(\sum_{f=1}^g \left(\left(\frac{\prod_{h=1}^f K_{a_h}^{\text{acidic}}}{[H^+]^f} \right) K_{S_{f+1}} \right) + \sum_{i=1}^j \left(\left(\frac{[H^+]^i}{\prod_{k=1}^i K_{a_k}^{\text{basic}}} \right) K_{S_{i+1}} \right) \right) [M] \right] \quad (1.22)$$

for coformer, where m and g are the total number of respective acidic groups, and r and j are the total number of respective basic groups. K_{S_1} represents the solubilization equilibrium constant for the nonionized species, while $K_{S_{l+1}}$, $K_{S_{q+1}}$, $K_{S_{f+1}}$, and $K_{S_{i+1}}$ represent the solubilization constants for the respective acidic and basic groups of the drug and coformer as ionization proceeds. It should be noted from these equations that when solubilization is not considered ($K_s = 0$), both $\delta_{D,S}$ and $\delta_{CF,S}$ reduce to zero.

Applications

Cocrystal solubility as a function of pH and solubilization can be predicted from knowledge of K_{sp} , K_a , and K_s values according to the equations presented above.

Solubility-pH profiles in Figure 1.11 generated from the appropriate equations, illustrate how cocrystal stoichiometry and ionization properties of drug and coformer can influence cocrystal and drug solubilities.³⁶ The predictive power of these equations has been confirmed for carbamazepine (CBZ),^{36, 39, 44} gabapentin (GBP),⁵³ indomethacin (IND),⁵⁴ ketoconazole (KTZ),¹⁰ NVP,⁴³ tadalafil (TDF),⁹ ibuprofen (IBU),⁵⁵ isoniazid (INH),⁵⁶ and meloxicam (MLX)⁵⁷ cocrystals.

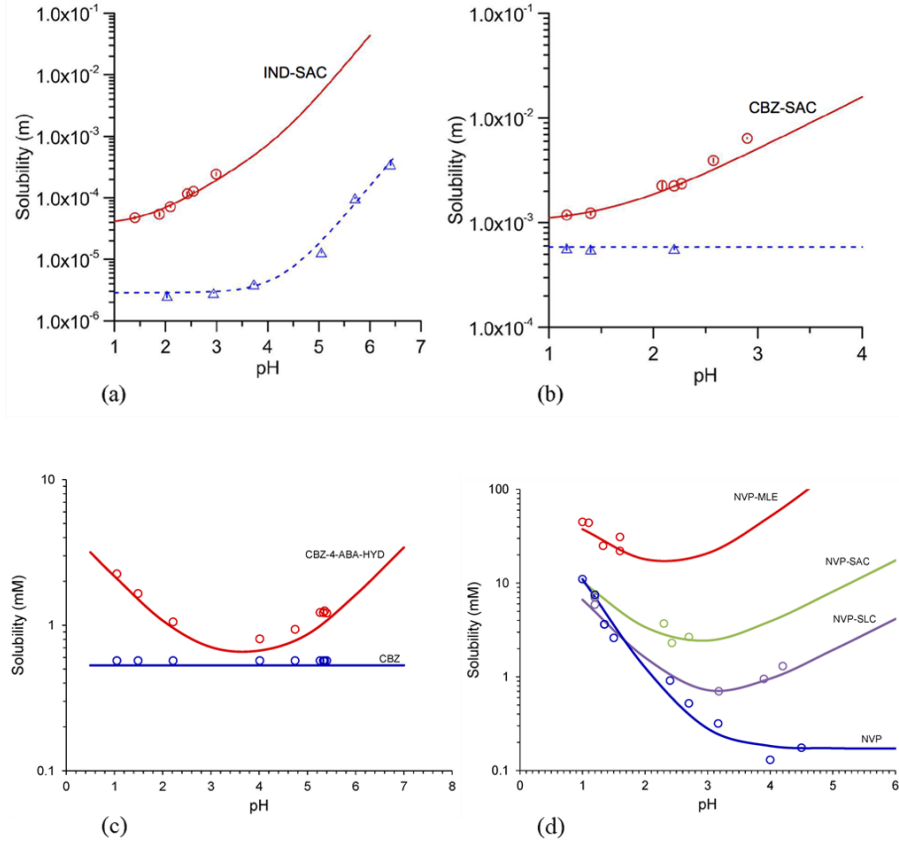


Figure 1.11. Solubility-pH profiles for (a) 1:1 HAHX cocrystal composed of two acidic components was calculated using $S_{\text{HAHX},T} = \sqrt{K_{\text{Sp}} \left(1 + \frac{K_{\text{a1}}^{\text{HA}}}{[\text{H}^+]}\right) \left(1 + \frac{K_{\text{a1}}^{\text{HX}}}{[\text{H}^+]}\right)}$, (b) 1:1 RHA cocrystal composed of nonionizable drug and acidic cofomer was calculated using Equation 1.17, (c) 2:1 R_2HAB cocrystal composed of nonionizable drug and amphoteric cofomer was calculated using $S_{\text{R}_2\text{HAB},T} = \sqrt[3]{\frac{K_{\text{Sp}}}{4} \left(1 + \frac{K_{\text{a1}}^{\text{HAB}}}{[\text{H}^+]} + \frac{[\text{H}^+]}{K_{\text{a2}}^{\text{H}_2\text{AB}^+}}\right)}$, and (d) 1:1 BH_2A and 2:1 B_2HA cocrystals composed of basic drug and diprotic and monoprotic acidic cofomers was calculated using $S_{\text{BH}_2\text{A},T} =$

$$\sqrt{K_{\text{Sp}} \left(1 + \frac{[\text{H}^+]}{K_{\text{a1}}^{\text{B}}}\right) \left(1 + \frac{K_{\text{a1}}^{\text{H}_2\text{A}}}{[\text{H}^+]} + \frac{K_{\text{a1}}^{\text{H}_2\text{A}} K_{\text{a2}}^{\text{H}_2\text{A}}}{[\text{H}^+]^2}\right)}$$

$$\text{and } S_{\text{B}_2\text{HA},T} = \sqrt[3]{\frac{K_{\text{Sp}}}{4} \left(1 + \frac{[\text{H}^+]}{K_{\text{a1}}^{\text{B}}}\right)^2 \left(1 + \frac{K_{\text{a1}}^{\text{HA}}}{[\text{H}^+]}\right)}$$

respectively. K_{Sp} values were either experimentally determined or estimated from published work for the selected cocrystal(s) in each graph (a) indomethacin-saccharin (IND-SAC),⁵⁴ (b) carbamazepine-saccharin (CBZ-SAC),⁵⁴ (c) carbamazepine-4-aminobenzoic acid hydrate (CBZ-4ABA) and (d) nevirapine-maleic acid (NVP-MLE), nevirapine-saccharin (NVP-SAC), and nevirapine-salicylic acid (NVP-SLC).³ Symbols represent experimentally measured data.

Cocrystals of nonionizable drugs can exhibit very different solubility-pH behavior depending on cofomer ionization properties (Figures 1.11a, b, and c). While an acidic cofomer results in increases in solubility with increasing pH (Figures 1.11a and b), an amphoteric cofomer leads to a U-shaped cocrystal solubility curve (Figure 1.11c). The solubility minimum of the curve will reside within the pH range between the drug and cofomer pK_a values. A basic drug and an acidic cofomer, as shown in Figure 1.11d, predict a similar U-shaped behavior where the ionizable groups reside in different molecules. The pH range of the minimum solubility for this type of cocrystal is dependent upon the difference between the drug and cofomer pK_a values.^{36, 58}

In regards to solubilization, Equation 1.17 predicts that cocrystal solubility $S_{RHA,T}$ will increase with corresponding increases in cocrystal K_{sp} , K_S^R , or $[M]$. Because $K_{sp} = (S_{RHA,aq})^2$, this equation can also be written in terms of $S_{RHA,aq}$ as

$$S_{RHA,T} = S_{RHA,aq} \sqrt{(1 + K_S^R[M])} \quad (1.23)$$

Likewise, the total solubility of the non-ionizable drug component R is given by

$$S_{R,T} = [R]_{aq} + [R]_m = S_{R,aq}(1 + K_S^R[M]) \quad (1.24)$$

where $S_{R,aq}$ represents the drug solubility in aqueous pseudophase.⁴⁸

While Equation 1.23 shows that cocrystal RHA solubility is a function of $\sqrt{[M]}$, Equation 1.24 demonstrates that drug R solubility is a function of $[M]$.⁴⁸ Therefore, by comparing these two equations, it becomes apparent that the solubilities of cocrystal RHA and drug R behave differently with changing surfactant concentration.^{44, 48-52, 59, 60}

It is also plausible to use Equation 1.12 with the appropriate δ expressions and K values as a guide for solubilizing agent selection that will yield a desired cocrystal solubility. When

values such as K_a and K_s are known, only cocrystal K_{sp} needs to be determined to obtain cocrystal solubility.⁴⁴

Behavior predicted by solubility equations of the form of Equation 1.12 is in excellent agreement with experimental values (Figure 1.12). Solubility curves of cocrystal and drug intersect at transition points defined by S^* and critical stabilization concentration (CSC). CSC is the solubilizing agent concentration at the transition point.

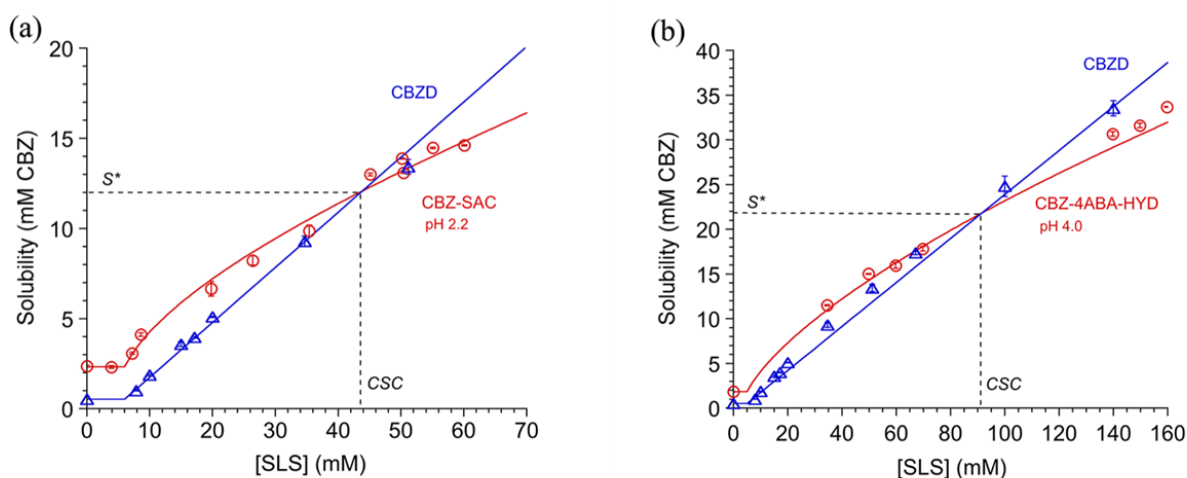


Figure 1.12. Solubilities and transition points of (a) 1:1 carbamazepine-saccharin (CBZ-SAC) and (b) 2:1 carbamazepine-4-aminobenzoic acid-hydrate (CBZ-4ABA-HYD) with carbamazepine dihydrate (CBZD) induced by sodium lauryl sulfate (SLS) preferential solubilization of CBZ.⁴⁴ Transition points are characterized by a solubility (S^*) and a solubilizing agent concentration (CSC) (dashed lines). S^* and CSC vary with cocrystal aqueous solubility and stoichiometry. Symbols represent experimentally measured cocrystal (\circ) and drug (Δ) solubility values. Predicted drug and cocrystal solubilities (solid lines) were calculated according to Equation 1.17 and $S_{R_2HAB,T} = \sqrt[3]{\frac{K_{sp}}{4} (1 + K_s^R[M])^2 \left(1 + \frac{[H^+]}{K_a^{H_2AB^+}} + \frac{K_a^{HAB}}{[H^+]} + K_s^{HAB}[M] \right)}$, with previously reported values.^{44, 60}

The transition point for a given cocrystal and its drug will vary with the extent of drug solubilization, as illustrated for different solubilizing agents in Figure 1.13.⁶⁰ A lower CSC is obtained with a stronger drug solubilizing agent ($K_s = 1.5 \text{ mM}^{-1}$) than with a weaker one ($K_s = 0.5 \text{ mM}^{-1}$). This means that a lower concentration of solubilizing agent is required to reach the

transition point when a stronger solubilizing agent is used. Despite a variable CSC, the transition points of a particular cocrystal and drug will exhibit a constant S^* . This property of S^* is found by examining the mathematical models that describe cocrystal and drug solubilization.⁶⁰

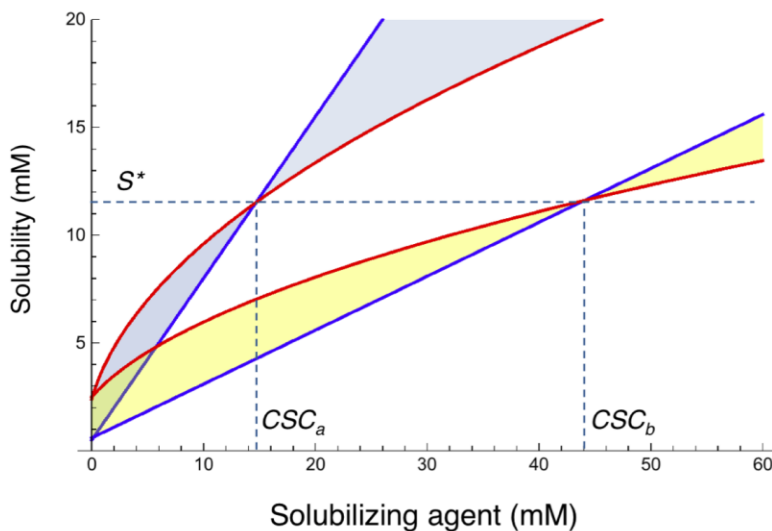


Figure 1.13. Transition points S^* and critical stabilization concentration (CSC) for a cocrystal (red line) and its constituent drug (blue line) in the presence of two different solubilizing agents, a and b. S^* is a constant for a given cocrystal, but CSC varies with the extent of drug solubilization by a particular solubilizing agent. For this case, drug is solubilized to a greater extent by a than by b, and thus $CSC_a < CSC_b$. The curves were generated from Equations 1.23 and 1.24 with parameter values $S_{D,aq} = 0.5$ mM, $S_{CC,aq} = 2.4$ mM ($K_{sp} = 5.76$ mM²), and $K_s^D = 1.5$ mM⁻¹ and 0.5 mM⁻¹ for solubilizing agents a and b, respectively.⁶⁰

Since the cocrystal and drug solubilities are equal at the transition point

$$S_{CC,T} = S_{D,T} = S^* \quad (1.25)$$

mathematical expressions that relate S^* to cocrystal and drug solubilities can be derived. For a

1:1 cocrystal

$$S^* = \frac{(S_{CC,aq})^2}{S_{D,aq}} \quad (1.26)$$

The general equation for a cocrystal A_yB_z is

$$S^* = \frac{(S_{CC,aq})^{y+z}}{(S_{D,aq})^y} \quad (1.27)$$

This equation shows that the solubility value at the transition point is governed by aqueous solubilities and not by solubilizing agents. S_{aq} refers to both the ionized and nonionized aqueous solubilities of cocrystal and drug, and therefore Equations 1.26 and 1.27 apply to a range of ionizing conditions.⁶⁰

From the equations presented in this section, it is possible to quantitatively predict the cocrystal and drug solubilization behaviors and the transition point as defined by S^* and CSC. Figure 1.12 shows how these theoretical relationships compare to the experimental data for two different CBZ cocrystals in the presence of surfactant.

Under some conditions the assumption that cofomer solubilization is negligible ($K_s^{CF} = 0$) is not justified, and an additional term must be included in the S^* equations to account for situations where $K_s^{CF} > 0$. The factor ϵ is used to quantitatively represent and correct for this deviation.⁶⁰ The solubility at the transition point is

$$S^* = \epsilon \frac{(S_{CC,aq})^2}{S_{D,aq}} \quad (1.28)$$

where

$$\epsilon = \frac{(1+10^{pH-pK_{a,CF}} + K_s^{CF}[M])}{(1+10^{pH-pK_{a,CF}})} \quad (1.29)$$

where $[M]$ represents the micellar concentration at the CSC. This equation shows the importance of both K_s and $[M]$ in determining the value of ϵ . Small K_s and large $[M]$ will have a significant influence on deviations of S^* . When $K_s^{CF} = 0$, then $\epsilon = 1$ and S^* values calculated from the simpler equation (Equation 1.26) will approach experimental values.⁶⁰

S^* and corresponding ϵ values for CBZ cocrystals in SLS are shown in Table 1.3.

Calculations with $\epsilon = 1$ provides a first good approximation of S^* as ϵ is less than 1.4.

Table 1.3. S* Deviations Due to Coformer Solubilization

Cocrystal	pH	K _s ^{coformer^a} (mM ⁻¹)	[SLS] at CSC (mM) ^a	ε ^b	S* pred ^c	S* pred with ε ^d	S* obs ^e
CBZ-SLC (1:1)	3.0	0.06	23	1.40	3.3	4.6	4.6
CBZ-SAC (1:1)	2.2	0.013	44	1.14	10.5	12.0	12.0

^aValues reported in reference.⁴⁴

^bCalculated from Equation 1.29.⁶⁰

^cCalculated from Equation 1.26.⁶⁰

^dCalculated from Equation 1.28.⁶⁰

^eDetermined from the intersection of S_{CC,T} and S_{D,T} curves in Figure 1.12.⁶⁰

Using Solubility Advantage Diagrams to Control Dissolution – Supersaturation –

Precipitation Behavior

While highly soluble cocrystals may be orders of magnitude more soluble than poorly soluble parent drug, highest SA does not always lead to the best dissolution performance. This is because as cocrystal systems undergo dissolution – supersaturation – precipitation (DSP) kinetics, their ability to generate supersaturation levels above critical supersaturation leaves them prone to spontaneous and rapid conversion. In the form of the Arrhenius rate equation, the steady-state rate of nucleation (J) is directly proportional to the free energy change (ΔG) as

$$J = A \exp\left(\frac{-\Delta G}{k_B T}\right) \quad (1.30)$$

where A is the pre-exponential factor, k_B is the Boltzmann constant, and T is temperature.⁶¹ For supersaturating drug delivery systems, SA is the driving force for conversions back to less soluble drug and is directly proportional to ΔG as

$$\Delta G_{CC \rightarrow D} = -RT \ln\left(\frac{S_{CC}}{S_D}\right) = -RT \ln(SA) \quad (1.31)$$

Highly soluble cocrystals with high SA are prone to rapid phase conversion during dissolution, often negating their SA and ability to generate enhanced drug exposure. However, while moderately soluble cocrystals may have lower SA, they also have lower driving force for conversion and are more likely to remain within the metastable zone, to sustain supersaturation, and to actually enhance drug exposure. This phenomenon is shown schematically in Figure 1.14, where the moderately soluble cocrystal achieves a higher area under the curve (AUC) and C_{\max} (kinetic parameters that represent the competing processes of dissolution and precipitation) despite lower $S_{\text{cocrystal}}$ and SA (thermodynamic parameters that represent the ability to generate supersaturation and the driving force for conversion).^{3, 48}

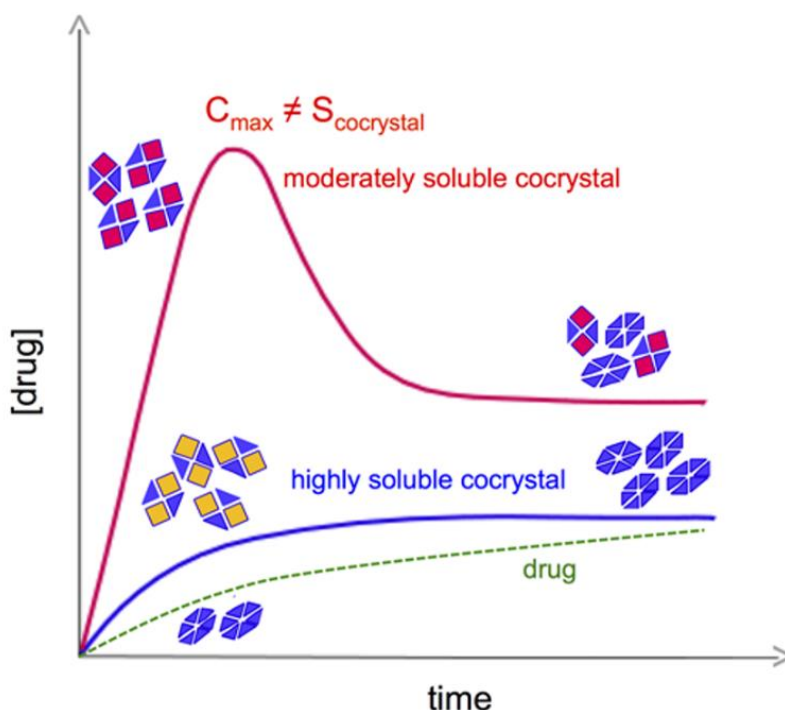


Figure 1.14. C_{\max} is a kinetic parameter determined by the rates of cocrystal dissolution and drug precipitation. C_{\max} is not proportional to cocrystal solubility advantage (SA), as the relation between dissolution and precipitation rates change with SA. For highly soluble cocrystals, C_{\max} will decrease and may elude detection as precipitation rates become much higher than dissolution.³

Despite the potential shortcomings of kinetic measurements, dissolution studies remain the most common approach to evaluating cocrystal solution behavior. However, knowledge of cocrystal thermodynamic parameters is essential to not only correctly interpret cocrystal concentration – time profiles, but also to effectively design cocrystals without unnecessarily high solubilities and conversion risk. The proposed use of solubilizing agents and cocrystal solubility advantage – drug solubilization power (SA – SP) diagrams represents a mechanistic approach to fine-tune SA and to design cocrystals with controlled DSP behavior.

Cocrystal Solubility Advantage – Drug Solubilization Power (SA – SP) Diagrams

Understanding the interplay between solubilizing agents and SA is of practical importance because of how commonly pharmaceutical entities encounter drug solubilizing agents in formulation and physiologically *in vivo*. As shown in Figure 1.12, cocrystal and drug solubilities increase to different extents with increasing solubilizing agent concentration. By combining Equations 1.23 and 1.24, the relationship between cocrystal and drug solubilization ratios can be related as

$$\left(\frac{S_T}{S_{aq}}\right)_{CC} = \sqrt{\left(\frac{S_T}{S_{aq}}\right)_D} \quad (1.32)$$

where S_T represents total cocrystal or drug solubility in the presence of a solubilizing agent ($S_T = S_{aq} + S_{solubilized}$), and S_{aq} represents the aqueous solubility in the absence of solubilizing agents.⁶⁰ Equation 1.32 applies to 1:1 cocrystals and their parent drug. The general form of Equation 1.32 for y:z cocrystal is

$$\left(\frac{S_T}{S_{aq}}\right)_{CC} = \left(\frac{S_T}{S_{aq}}\right)_D^{x/(x+y)} \quad (1.33)$$

Solubilization power (SP) of an additive for the drug or cocrystal is defined as

$$SP = \frac{S_T}{S_{aq}} \quad (1.34)$$

so that Equations 1.32 and 1.33 may be simplified as

$$SP_{CC} = \sqrt{SP_D} \quad (1.35)$$

and

$$SP_{CC} = SP_D^{x/(x+y)} \quad (1.36)$$

respectively. SP_{CC} is lower than SP_D due to preferential drug solubilization over the cofomer, and the lower the ratio of y/z the smaller the SP_{CC} .^{60, 62}

Because drug and cocrystal solubilities change in the presence of solubilizing agents (Figure 1.12), it follows that SA changes with solubilizing agent concentration.³ For a 1:1 cocrystal, SA can be related to SP_D as

$$\left(\frac{S_{CC}}{S_D}\right)_T = \frac{\left(\frac{S_{CC}}{S_D}\right)_{aq}}{\sqrt{\left(\frac{S_T}{S_{aq}}\right)_D}} \quad (1.37)$$

or

$$SA_T = \frac{SA_{aq}}{\sqrt{SP_D}} \quad (1.38)$$

SA_T represents the total cocrystal solubility advantage in the presence of solubilizing additives, whereas SA_{aq} represents the aqueous cocrystal solubility advantage in the absence of solubilizing additives. SP_D represents the ratio of total drug solubility (all dissolved species) in the presence of solubilizing agents ($S_{D,T} = S_{D,aq} + S_{D,solubilized}$) to aqueous drug solubility ($S_{D,aq} = S_{D,nonionized,aq} + S_{D,ionized,aq}$) at a given pH. Because solubilizing agents preferentially solubilize hydrophobic drugs over hydrophilic cofomers, cofomer solubilization is oftentimes negligible and not considered in Equations 1.37 and 1.38.

By considering the logarithmic form of Equation 1.38

$$\log SA_T = \log SA_{aq} - \frac{1}{2} \log SP_D \quad (1.39)$$

a linear relationship exists between $\log SA_T$ and $\log SP_D$ and is shown in Figure 1.15.³

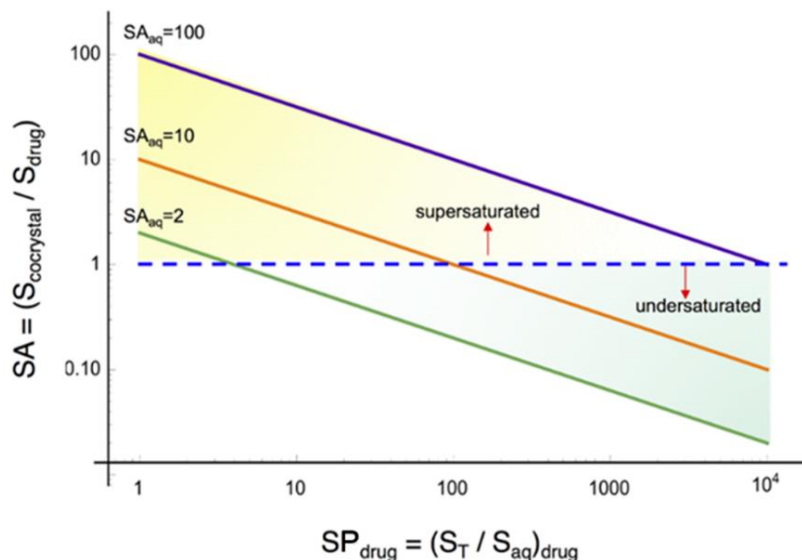


Figure 1.15. Cocystal solubility advantage over drug ($SA = S_{cocrystal} / S_{drug}$) predictably decreases with increasing drug solubilization power ($SP_{drug} = S_{drug,T} / S_{drug,aq}$). Solid lines represent 1:1 cocrystals with $SA_{aq} = 2, 10, \text{ and } 100$. The dashed line indicates transition point $SA = 1$, and its intersection with solid cocystal SA lines represents where $S_{cocrystal} = S_{drug}$ ($SP_{drug} = 4, 100, \text{ and } 10,000$ for the corresponding cocystals). Solubilizing additives and their concentrations can be rationally selected to promote sustained supersaturation by dialing SP_{drug} and corresponding SA to maximum theoretical supersaturations within the metastable zone width.³

Equation 1.39 and Figure 1.15 show that rationally selecting additives to dial to a particular SP_D value will allow for the predictable tailoring of SA_T . Cocystal supersaturation can therefore be controlled within the metastable zone so that the cocystal still has solubility advantage and can generate supersaturation, but the risk of conversion is mitigated with a modulated SA_T .

The linear plot of $\log SA$ versus $\log SP_D$ is characterized by a slope of $-1/2$ for 1:1 cocystals, and shows cocystal transition points as well as regions of supersaturation and undersaturation. SP_D^* represents the SP_D value at which $SA = 1$ for a given SA_{aq} . This transition

point represents drug saturation; drug can achieve supersaturation when $SA > 1$ but will remain undersaturated when $SA < 1$. $SA = 1$ also represents an inversion in solubility advantage, where cocrystal is more soluble than drug when $SA > 1$ but less soluble when $SA < 1$. Therefore, knowledge of SP_D^* allows supersaturation with respect to drug to be tailored to a desired level by adjusting SP_D to avoid conversion to less soluble forms or inversion in solubility advantage.

Figure 1.16 shows the $SA - SP$ diagram for 1:1 IND-SAC cocrystal at pH 2.1 and 5.0. The predicted dependence of SA_T on SP_D was calculated from $SA_{aq} = 25$ at pH 2.1 and $SA_{aq} = 220$ at pH 5.0 (Figure 1.11a) according to Equation 1.39.^{63, 64} Lines were experimentally validated with solubility measurements in the presence of Polyoxyethylene (20) oleyl ether (Brij99), sodium lauryl sulfate SLS), and polyoxyethylene (40) stearate (Myrj 52) at pH 2.1, and FeSSIF at pH 5.0. The results show that SA_T predictably decreased with increased surfactant concentration, and that the $SA-SP$ relationship is independent of surfactant type.

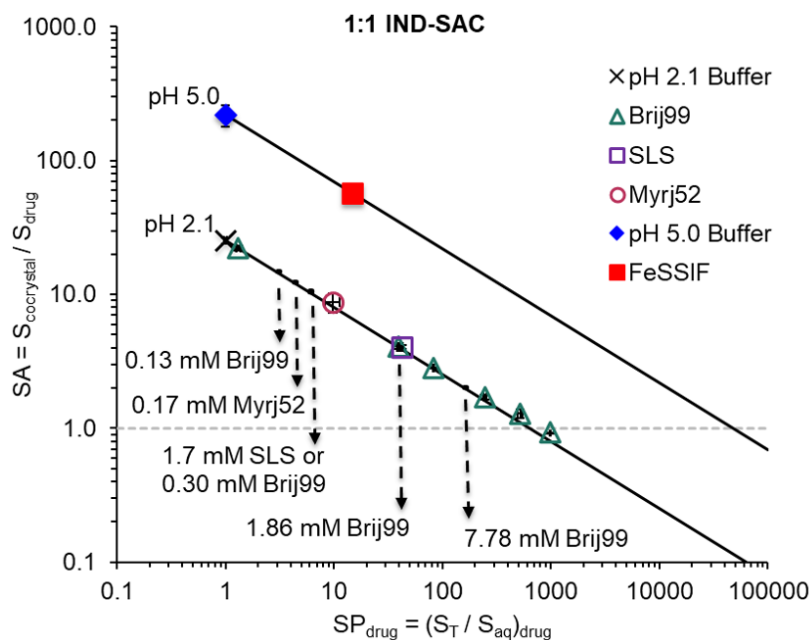


Figure 1.16. The log-linear dependence of cocystal solubility advantage (SA) on drug solubilization power (SP_D) for 1:1 IND-SAC cocystal at pH 2.1 and 5.0. Lines are predicted from Equation 1.39 $SA_{\text{aq}} = 25$ at pH 2.1 and $SA_{\text{aq}} = 220$ at pH 5.0. Symbols represent values calculated from experimental drug and cofomer eutectic concentrations in aqueous and surfactant media at 25°C. Dashed arrows represent media used to conduct dissolution studies at pH 2.1. Error bars (within the points) represent standard deviations.^{63, 64}

Both physiologically relevant surfactants such as bile salts encountered in the gastrointestinal tract and synthetic additives that may be used during formulation can solubilize drug and be used to modulate SA. The relationship between SA and DSP kinetics has been shown for IND-SAC cocystal for both classes of additives.

Physiologically Relevant Surfactants

Figure 1.17 shows the effect of modulating SA with FeSSIF on DSP kinetics. While IND-SAC cocystal generated high supersaturation within 10 minutes during powder dissolution in pH 5.0 buffer (blank FeSSIF), rapid precipitation followed and resulted in final IND concentration (0.034 mM) just above IND solubility (0.023 mM). The final solid phase of IND-SAC + IND confirmed cocystal conversion. However, when cocystal dissolution was

conducted in the presence of FeSSIF, supersaturation was sustained over the course of 4 hours and resulted in a final solid phase of IND-SAC, indicating no cocrystal conversion.⁶⁴

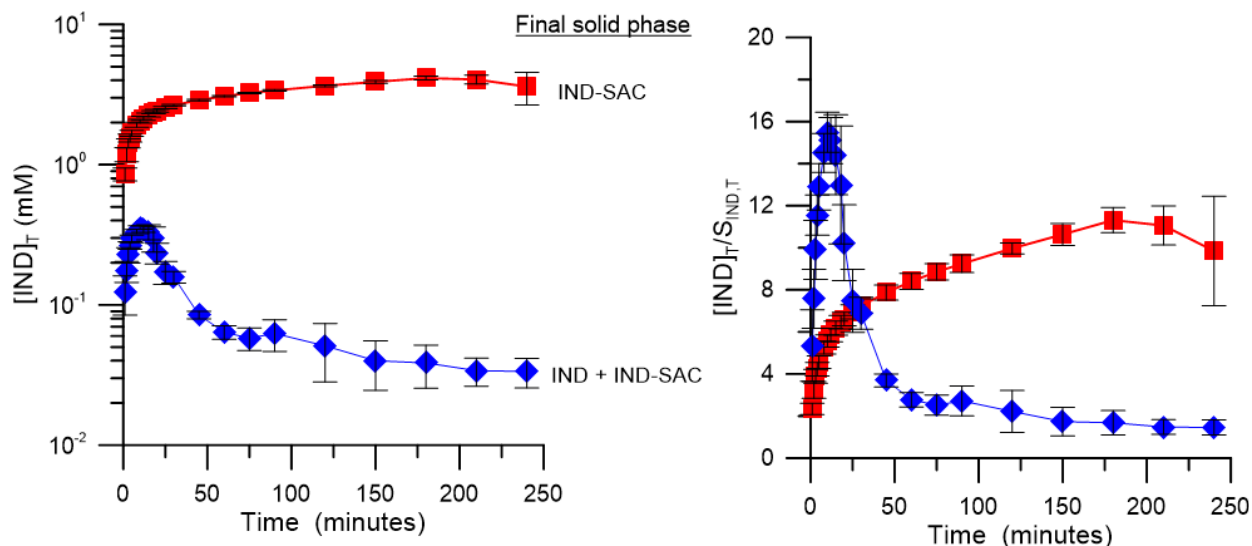


Figure 1.17. Influence of aqueous (blue diamond) and biorelevant medium FeSSIF (red square) on the (a) concentration – time and (b) supersaturation – time profiles of 1:1 indomethacin - saccharin (IND-SAC) cocrystal at 25°C. Cocrystal solubility advantage (SA) was modulated from 220 in blank buffer to approximately 57 in FeSSIF.^{3, 64}

The SA-SP diagram in Figure 1.16 showed that high $SA_{aq} = 220$ in pH 5.0 buffer (blank FeSSIF) was modulated to $SA_T = 57$ in FeSSIF. Because $SA_{aq} = 220$ represents a high driving force for conversion, drug precipitation began to outcompete cocrystal dissolution after only 10 minutes in blank FeSSIF and resulted in very little advantage to drug after about one hour. In contrast, the addition of FeSSIF modulated both SA_T and the driving force for conversion. Drug solubilization by FeSSIF not only increased cocrystal and drug solubilities, leading to a higher concentrations compared to blank FeSSIF, but also delayed drug precipitation, promoted sustained supersaturation over 4 hours, and led to higher AUC.⁶⁴ For some drugs and cocrystals, physiologically relevant surfactants may be sufficient to stabilize the cocrystal and achieve

desired drug exposure. For others, synthetic additives may be necessary to dial to the targeted SA_T .

Synthetic Additives

At pH 2.1, synthetic additives Brij 99, Myrj 52, and SLS were shown to modulate $SA_{aq} = 25$ to values less than 1 (Figure 1.16). Figure 1.18 shows the dissolution effect of modulating SA from 25 to 2 with increasing Brij99 concentrations. For all media conditions, the cocrystal induced faster and higher drug concentrations compared to the drug. Aqueous buffer conditions resulted in the lowest achieved concentrations (as a function of cocrystal and drug solubilities), and rapid conversion prevented the cocrystal from sustaining high supersaturation levels. With increasing Brij99 and decreasing SA, cocrystal solubility, drug solubility, and drug solubilization increased, resulting in higher achieved drug concentrations. However, modulating SA down to 2 resulted in the lowest achieved supersaturation levels, as drug supersaturation was limited by cocrystal solubility. Optimal sustainment of supersaturation was observed at $SA = 10$, which achieved and sustained the highest supersaturation levels over 3 hours.⁶³

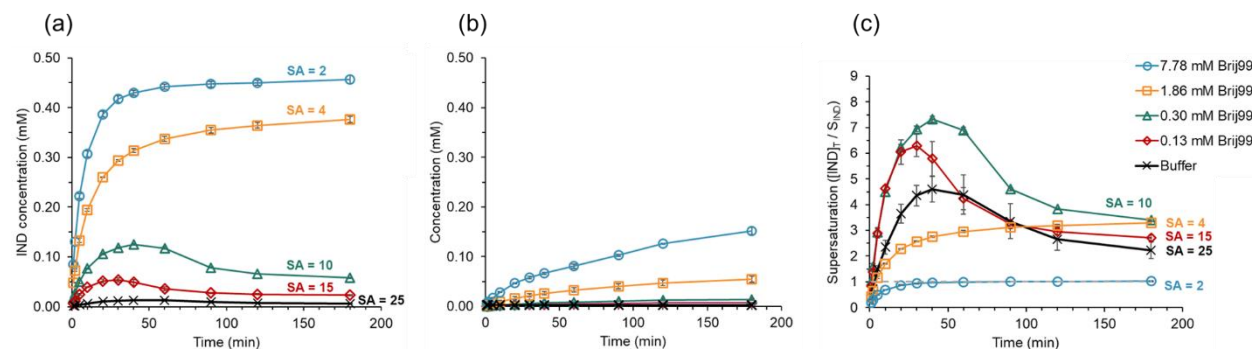


Figure 1.18. Influence of SA, $S_{cocrystal}$, and S_{drug} , on the concentration – time profiles of (a) 1:1 indomethacin – saccharin (IND-SAC) cocrystal and (b) indomethacin drug, and (c) the supersaturation – time profile of IND-SAC. SA was modulated from 25 to 2 by increasing surfactant concentration.⁶³

Figure 1.19 demonstrates the effect of targeting similar SA values in the range of 10 – 12 with three different surfactants. The optimized SA = 10 demonstrated by Brij99 resulted in similar DSP behavior when targeted by Myrj52 and SLS, even though different surfactant concentrations were required to dial to this value. This shows the critical importance of evaluating SA and utilizing the SA – SP diagram to control DSP behavior of cocrystal systems, rather than empirical selection of solubilizing additives and their concentrations.⁶³

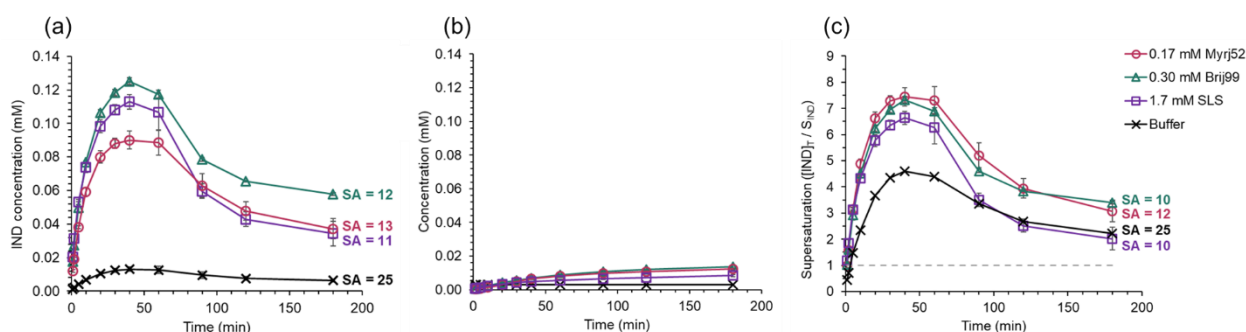


Figure 1.19. Influence of additive selection on the concentration – time profiles of (a) 1:1 indomethacin – saccharin (IND-SAC) cocrystal and (b) indomethacin drug, and (c) the supersaturation – time profile of IND-SAC. SA was tailored to 11 – 13 with three different surfactants.⁶³

Effect of pH on Cocrystal Dissolution

It is important to note that for cocrystals of ionizable components, SA_{aq} is a conditional constant and will change with pH. Figure 1.16 showed the resulting effect of changing pH on the SA – SP relationship for a cocrystal of two acidic components. However, because of their ability to impart or alter the solubility – pH dependence of parent drug, even in aqueous conditions cocrystals have the ability to mitigate the negative dissolution effects of low pH-dependent solubility regions for ionizable parent drugs.

Figure 1.20 shows the solubility - and SA – pH dependence of dibasic ketoconazole (KTZ) drug and 1:1 cocrystals. Coformers are diprotic acids and include adipic acid (ADP),

fumaric acid (FUM), and succinic acid (SUC). Cocrystal solubility – pH profiles were predicted according to

$$S_{CC,aq} = \sqrt{K_{sp} \left(1 + \frac{[H^+]}{K_a^{BH^+}} + \frac{[H^+]^2}{K_a^{BH^+} K_a^B} \right) \left(1 + \frac{K_a^{H_2A}}{[H^+]} + \frac{K_a^{H_2A} K_a^{HA^-}}{[H^+]^2} \right)} \quad (1.40)$$

and drug solubility – pH dependence was predicted according to

$$S_{D,aq} = S_0 \left(1 + \frac{[H^+]}{K_a^{BH^+}} + \frac{[H^+]^2}{K_a^{BH^+} K_a^B} \right) \quad (1.41)$$

and values in Table 1.4. SA was predicted as the ratio of Equations 1.40 and 1.41.

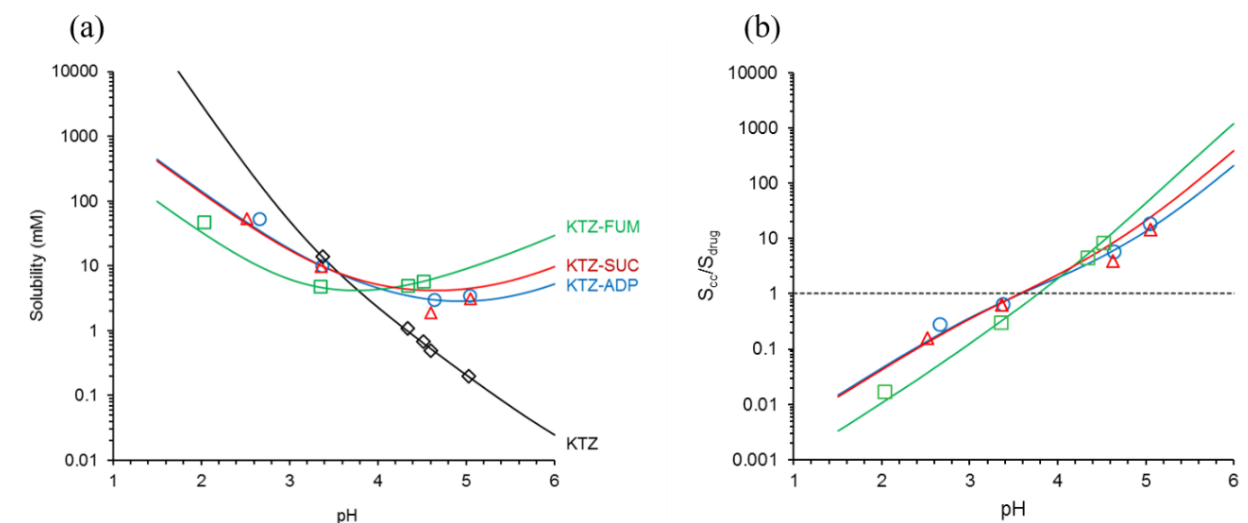


Figure 1.20. (a) Aqueous solubility and (b) aqueous solubility advantage (SA) of 1:1 ketoconazole cocrystals and drug. Solubility – pH curves for ketoconazole – fumaric acid (KTZ-FUM), ketoconazole – succinic acid (KTZ-SUC), and ketoconazole – adipic acid (KTZ-ADP) were predicted according to Equation 1.40 and values in Table 1.4. SA lines were predicted from the ratio of Equation 1.40 to Equation 1.41. Symbols represent experimental solubility values. pH values represent equilibrium pH. Standard errors are less than 7% and within points.¹⁰

Table 1.4. Values to Predict Cocrystal and Drug Solubility – pH Profiles.¹⁰

Solid Form	S ₀ (M)	K _{sp} (M ²)	KTZ pK _{a,1} , pK _{a,2}	CF pK _{a,1} , pK _{a,2}
KTZ	4.7 × 10 ⁻⁶	-	3.17, 6.63	-
KTZ-ADP	-	(3.4 ± 0.2) × 10 ⁻⁸	-	4.44, 5.44
KTZ-FUM	-	(2.7 ± 0.1) × 10 ⁻⁸	-	4.00, 5.24
KTZ-SUC	-	(1.5 ± 0.2) × 10 ⁻⁹	-	2.85, 4.10

Highly soluble acidic cofomers impart cocrystal SA above pH_{max} values of 3.6 – 3.8. Although the cocrystals are less soluble than KTZ in acidic conditions, the cocrystals have the advantage of softening the solubility – pH dependence across physiological pH, which reduces the risk of pH – dependent disproportionation in the gastrointestinal tract.¹⁰

Figure 1.21 shows the effect of SA – pH dependence on DSP parameters such as relative area under the curve (RAUC = AUC_{CC} / AUC_D) and σ_{max} for KTZ cocrystals. Lower SA was observed for all three cocrystals at initial pH 5.0, which led to modest increases in AUC and observed supersaturation levels. Much more variable behavior was observed with higher SA values of 440 – 3100 at initial pH 6.5. With the highest SA, KTZ-FUM cocrystal rapidly converted to parent drug and resulted in very low dissolution advantage compared to parent drug. At SA 440, KTZ-ADP cocrystal initially spiked in supersaturation, leading to a high σ_{max} value, before precipitation began to outcompete dissolution, resulting in a low RAUC value. KTZ-SUC was observed to reach and sustain the highest supersaturation levels of any studied condition, with the highest observed RAUC and σ_{max} values at SA 822.¹⁰ Besides SA, differences in KTZ cocrystal DSP kinetics may be the result of cofomer effect on precipitation or cocrystal influence on surface nucleation.

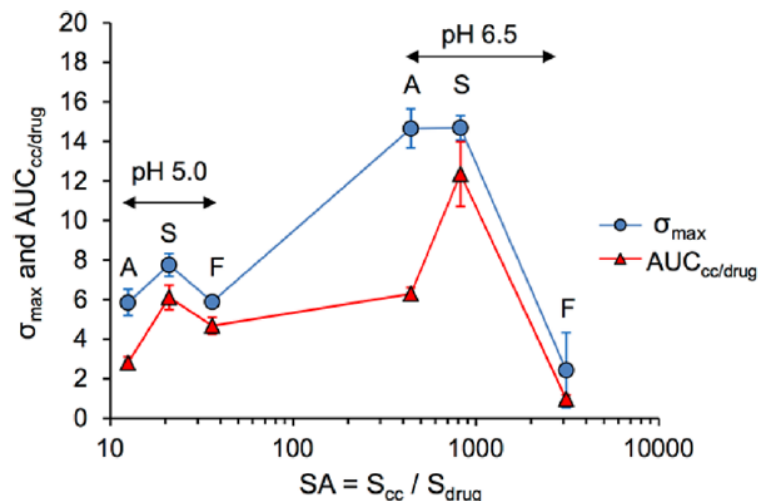


Figure 1.21. Cocystal σ_{max} and $AUC_{cocystal/drug}$ related to cocystal solubility advantage ($SA = S_{cocystal} / S_{drug}$). Letters A, S, and F represent ketoconazole – adipic acid cocystal, ketoconazole succinic acid cocystal, and ketoconazole – fumaric acid cocystal, respectively. pH 5.0 represents FeSSIF and blank FeSSIF media, and pH 6.5 represents FaSSIF and blank FaSSIF media. Error bars (some within points) represent standard error.¹⁰

In addition to the influence of bulk pH on cocystal solubility and dissolution, it has been shown that cocystals of ionizable components have the ability to modulate the microenvironment pH at the dissolving interface. Figure 1.22 shows the relationship between bulk and interfacial pH values for KTZ and cocystals. As bulk pH increases, cocystal interfacial pH plateaus due to the self-buffering effect of the cofomers, which are predominantly ionized in this region. This plateau pH occurs above pH_{max} for all three cocystals, meaning that the cocystals are thermodynamically unstable at the interface and may be prone to surface nucleation.⁶⁵

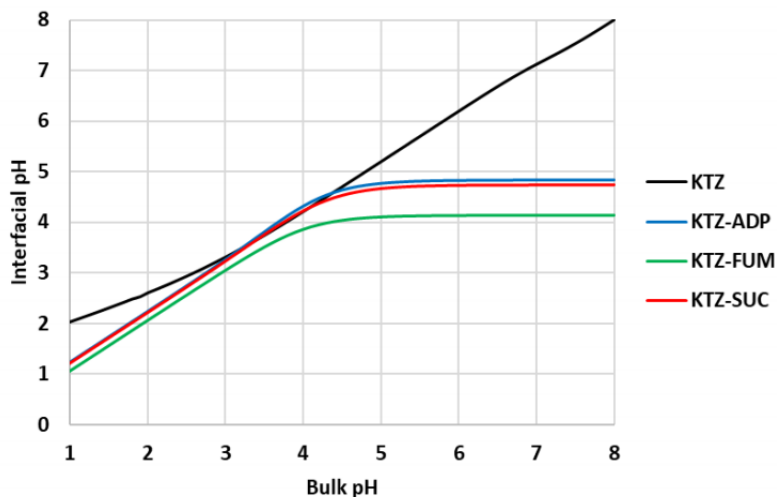


Figure 1.22. Interfacial pH of ketoconazole (KTZ), ketoconazole – adipic acid cocrystal (KTZ-ADP), ketoconazole – fumaric acid cocrystal (KTZ-FUM), and ketoconazole – succinic acid cocrystal (KTZ-SUC) as a function of bulk pH.⁶⁵

Statement of Dissertation Research

The purpose of this research is (1) to develop a quantitative, mechanistic-based approach through which known relationships between cocrystal SA and other key cocrystal solubility transition points can be used to fine-tune cocrystal inherent supersaturation, and (2) to assess and modulate the risk of conversion by rationally selecting additives that will exhibit thermodynamic and kinetic control over DSP behavior given the drug dose. Lack of critical understanding of cocrystal solution behavior and the underlying solution interactions that govern drug supersaturation and exposure as well as lack of streamlined development approaches have left cocrystals as appearing overly risky to develop. Dissolution remains the most common method for evaluating cocrystal solubility, despite the inability to correlate cocrystal conversion kinetics during dissolution to thermodynamic, equilibrium solubility values as well as to changing solution conditions. This makes dissolution time- and material-consuming as a primary cocrystal evaluation tool and controlling cocrystal DSP behavior with this strategy remains a largely

empirical process. The main objective of this work is to establish key thermodynamic parameters for evaluating cocrystal solubility and stability that can be used to rationally and mechanistically design cocrystal delivery systems that can generate both thermodynamically possible and kinetically sustainable supersaturation levels.

The findings of Chapter 2 have been published as “Understanding the Differences Between Cocrystal and Salt Aqueous Solubilities” in *Journal of Pharmaceutical Sciences* Volume 107, pages 113-120.⁷⁸ Chapter 2 describes the differences in cocrystal and salt aqueous solubilities and aims to address the commonly held notion that salts are inherently more soluble than cocrystals. Equations to predict the solubility – pH dependence of lamotrigine drug (LTG), lamotrigine – nicotinamide cocrystal (LTG-NCT),⁶⁶ lamotrigine – saccharin salt (LTG-SAC),⁶⁶ and lamotrigine – phenobarbital cocrystal (LTG-PB)⁶⁷ were derived and compared. The predicted equations were validated with experimental solubility measurements and showed that, depending on the interplay between the chemistry of the solid and solution phases, cocrystals can be more soluble than salts or vice-versa. The cocrystals, salt, and drug were also found to exhibit very different solubility – pH dependence, with one of the cocrystals and the salt exhibiting a pH_{max} , but the other cocrystal exhibiting $\text{SA} > 1$ across physiological pH range. SA and pH_{max} were found to be key cocrystal stability indicators. These findings were used to further interpret previously reported LTG, LTG-NCT, and LTG-SAC dissolution results at pH 1.0 and 5.1-5.5, where the cocrystal and salt relative dissolution performances were inverted in the different aqueous media.⁶⁶

The findings of Chapter 3 have been submitted for publication to *Molecular Pharmaceutics* as “Cocrystal Solubility Advantage and Dose/Solubility Ratio Diagrams: A Mechanistic Approach to Selecting Additives and Controlling Dissolution – Supersaturation –

Precipitation Behavior”. Chapter 3 presents a mechanistic approach to control DSP behavior of cocrystal systems through rational additive selection. 1:1 danazol – vanillin cocrystal (DNZ-VAN) has been previously shown to sustain supersaturation in the presence of additives, corresponding to a 10 times *in vivo* increase in AUC compared to the drug. In contrast, the cocrystal rapidly converted in the absence of additives and resulted in only a 1.7 times increase in AUC.⁶⁸ This important study demonstrated the essential role of formulation in developing cocrystals that can sustain supersaturation and improve oral bioavailability; however, additive selection to achieve this remains a largely empirical process. Chapter 3 describes a two-fold approach to predictably assess and modulate the risk of cocrystal conversion by optimizing thermodynamic (SA via solubilizing additives) and kinetic (precipitation and growth inhibitors) factors. The SA – SP diagram for DNZ-VAN was used to predictably modulate SA below critical supersaturation through rational additive selection, which resulted in sustained supersaturation and increased RAUC values during *in vitro* dissolution experiments. The addition of non-solubilizing precipitation and growth inhibitors was found to further promote sustained supersaturation despite not lowering SA. Furthermore, drug D_0 ($D_{0(D)} = C_{\text{dose}} / S_{D,T}$) is presented as an important parameter for assessing the potential for dose-limited supersaturation and how fast the cocrystal may (or may not) dissolve the drug dose. The SA – SP and $D_{0(D)} – SP$ relationships can be used in tandem to optimize maximum theoretical cocrystal supersaturation (thermodynamic limit) and to predictably modulate it below critical supersaturation (kinetic limit).

The findings of Chapter 4 are being prepared for publication. Chapter 4 reports the characterization of two novel posaconazole cocrystals: 2:3 posaconazole – 4-aminobenzoic acid (PSZ-4ABA)⁶⁹ and 2:3 posaconazole – 4-hydroxybenzoic acid (PSZ-4HBA). Posaconazole

(PSZ) is an antifungal agent and a third-generation azole drug, meaning that it has a broader spectrum of activity and is safer than earlier drugs of its class.⁷⁰ However, PSZ is a BCS Class II compound with extremely poor aqueous solubility (0.2 µg/mL at 25°C), high lipophilicity of Log P 4.6, and positive food-effect pharmacokinetics.⁷⁰⁻⁷² As a result, the marketed oral suspension and delayed-release tablets have highly variable bioavailability and require therapeutic monitoring.⁷³⁻⁷⁶ PSZ cocrystals were shown to increase solubility by orders of magnitude in aqueous media and biorelevant media. PSZ-4ABA cocrystal sustained supersaturation during *in vitro* dissolution studies in both FaSSIF (SA = 139) and FeSSIF (SA = 48) media, and increased AUC 4.1 – 13 times respectively compared to drug. SA was further decreased to 6 in the presence of excess 4ABA, and a quasi-equilibrium at supersaturation of 2 was achieved and sustained over 3 hours.

Chapter 5 presents the conclusions and proposed future research directions of this work. Several parts of this dissertation have been or will be submitted for publication. Portions of Chapter 1 have been published in a book chapter entitled “Measurement and Mathematical Relationships of Cocrystal Thermodynamic Properties” within *Pharmaceutical Crystals* edited by Tonglei Li and Alessandra Mattei.⁷⁷

References

1. Amidon, G. L.; Lennernas, H.; Shah, V. P.; Crison, J. R., A Theoretical Basis for a Biopharmaceutical Drug Classification - the Correlation of in-Vitro Drug Product Dissolution and in-Vivo Bioavailability. *Pharm Res* **1995**, *12* (3), 413-420.
2. Rinaki, E.; Valsami, G.; Macheras, P., Quantitative Biopharmaceutics Classification System: The Central Role of Dose/Solubility Ratio. *Pharm Res* **2003**, *20*, 1917-25.
3. Kuminek, G.; Cao, F.; Bahia de Oliveira da Rocha, A.; Goncalves Cardoso, S.; Rodríguez-Hornedo, N., Cocrystals to Facilitate Delivery of Poorly Soluble Compounds Beyond-Rule-of-5. *Adv Drug Deliv Rev* **2016**, *101*, 143-66.
4. Berry, D. J.; Steed, J. W., Pharmaceutical Cocrystals, Salts and Multicomponent Systems; Intermolecular Interactions and Property Based Design. *Adv Drug Deliv Rev* **2017**, *117*, 3-24.
5. Taylor, L. S.; Zhang, G. G. Z., Physical Chemistry of Supersaturated Solutions and Implications for Oral Absorption. *Adv Drug Deliv Rev* **2016**, *101*, 122-142.
6. Aitipamula, S.; Banerjee, R.; Bansal, A. K.; Biradha, K.; Cheney, M. L.; Choudhury, A. R.; Desiraju, G. R.; Dikundwar, A. G.; Dubey, R.; Duggirala, N.; Ghogale, P. P.; Ghosh, S.; Goswami, P. K.; Goud, N. R.; Jetti, R. K. R.; Karpinski, P.; Kaushik, P.; Kumar, D.; Kumar, V.; Moulton, B.; Mukherjee, A.; Mukherjee, G.; Myerson, A. S.; Puri, V.; Ramanan, A.; Rajamannar, T.; Reddy, C. M.; Rodríguez-Hornedo, N.; Rogers, R. D.; Row, T. N. G.; Sanphui, P.; Shan, N.; Shete, G.; Singh, A.; Sun, C. Q. C.; Swift, J. A.; Thaimattam, R.; Thakur, T. S.; Thaper, R. K.; Thomas, S. P.; Tothadi, S.; Vangala, V. R.; Vishweshwar, P.; Weyna, D. R.; Zaworotko, M. J., Polymorphs, Salts and Cocrystals: What's in a Name? (vol 12, pg 2147, 2012). *Cryst Growth Des* **2012**, *12* (8), 4290-4291.
7. Hancock, B. C.; Zografi, G., Characteristics and Significance of the Amorphous State in Pharmaceutical Systems. *J Pharm Sci* **1997**, *86* (1), 1-12.
8. Brouwers, J.; Brewster, M. E.; Augustijns, P., Supersaturating Drug Delivery Systems: The Answer to Solubility-Limited Oral Bioavailability? *J Pharm Sci* **2009**, *98* (8), 2549-2572.
9. Shimpi, M. R.; Alhayali, A.; Cavanagh, K. L.; Rodríguez-Hornedo, N.; Velaga, S. P., Tadalafil–Malonic Acid Cocrystal: Physicochemical Characterization, pH-Solubility, and Supersaturation Studies. *Cryst Growth Des* **2018**, *18* (8), 4378-4387.
10. Chen, Y. M.; Rodríguez-Hornedo, N., Cocrystals Mitigate Negative Effects of High pH on Solubility and Dissolution of a Basic Drug. *Cryst Growth Des* **2018**, *18* (3), 1358-1366.
11. Good, D. J.; Rodríguez-Hornedo, N., Solubility Advantage of Pharmaceutical Cocrystals. *Cryst Growth Des* **2009**, *9* (5), 2252-2264.
12. Schultheiss, N.; Newman, A., Pharmaceutical Cocrystals and Their Physicochemical Properties. *Cryst Growth Des* **2009**, *9* (6), 2950-2967.

13. Childs, S. L.; Stahly, G. P.; Park, A., The Salt-Cocrystal Continuum: The Influence of Crystal Structure on Ionization State. *Mol Pharm* **2007**, *4* (3), 323-338.
14. Bhogala, B. R.; Basavoju, S.; Nangia, A., Tape and Layer Structures in Cocrystals of Some Di- and Tricarboxylic Acids with 4,4'-Bipyridines and Isonicotinamide. From Binary to Ternary Cocrystals. *CrystEngComm* **2005**, *7*, 551-562.
15. Huang, K. S.; Britton, D.; Etter, M. C.; Byrn, S. R., A Novel Class of Phenol-Pyridine Co-crystals for Second Harmonic Generation. *J Mater Chem* **1997**, *7* (5), 713-720.
16. Jones, W.; Motherwell, S.; Trask, A. V., Pharmaceutical Cocrystals: An Emerging Approach to Physical Property Enhancement. *Mrs Bulletin* **2006**, *31* (11), 875-879.
17. Etter, M. C., Hydrogen-Bonds as Design Elements in Organic-Chemistry. *J Phys Chem* **1991**, *95* (12), 4601-4610.
18. Etter, M. C., Encoding and Decoding Hydrogen-Bond Patterns of Organic-Compounds. *Acc Chem Res* **1990**, *23* (4), 120-126.
19. Donohue, J., The Hydrogen Bond in Organic Crystals. *J Phys Chem* **1952**, *56* (4), 502-510.
20. Desiraju, G. R., Supramolecular Synthons in Crystal Engineering - a New Organic-Synthesis. *Angew Chem Int Edit* **1995**, *34* (21), 2311-2327.
21. Desiraju, G. R., Designer Crystals: Intermolecular Interactions, Network Structures and Supramolecular Synthons. *ChemComm* **1997**, (16), 1475-1482.
22. Almarsson, O.; Zaworotko, M. J., Crystal Engineering of the Composition of Pharmaceutical Phases. Do Pharmaceutical Co-crystals Represent a New Path to Improved Medicines? *ChemComm* **2004**, (17), 1889-1896.
23. Childs, S. L.; Chyall, L. J.; Dunlap, J. T.; Smolenskaya, V. N.; Stahly, B. C.; Stahly, G. P., Crystal Engineering Approach to Forming Cocrystals of Amine Hydrochlorides with Organic Acids. Molecular Complexes of Fluoxetine Hydrochloride with Benzoic, Succinic, and Fumaric Acids. *J Am Chem Soc* **2004**, *126* (41), 13335-13342.
24. Fleischman, S. G.; Kuduva, S. S.; McMahon, J. A.; Moulton, B.; Walsh, R. D. B.; Rodríguez-Hornedo, N.; Zaworotko, M. J., Crystal Engineering of the Composition of Pharmaceutical Phases: Multiple-Component Crystalline Solids involving Carbamazepine. *Cryst Growth Des* **2003**, *3* (6), 909-919.
25. Weyna, D. R.; Shattock, T.; Vishweshwar, P.; Zaworotko, M. J., Synthesis and Structural Characterization of Cocrystals and Pharmaceutical Cocrystals: Mechanochemistry vs Slow Evaporation from Solution. *Cryst Growth Des* **2009**, *9* (2), 1106-1123.
26. Kojima, T.; Tsutsumi, S.; Yamamoto, K.; Ikeda, Y.; Moriwaki, T., High-throughput Cocrystal Slurry Screening by Use of in situ Raman Microscopy and Multi-well Plate. *Int J Pharm* **2010**, *399* (1-2), 52-59.
27. Yu, Z. Q.; Chow, P. S.; Tan, R. B. H.; Ang, W. H., Supersaturation Control in Cooling Polymorphic Co-Crystallization of Caffeine and Glutaric Acid. *Cryst Growth Des* **2011**, *11* (10), 4525-4532.

28. Zhang, G. G. Z.; Henry, R. F.; Borchardt, T. B.; Lou, X. C., Efficient Co-crystal Screening Using Solution-mediated Phase Transformation. *J Pharm Sci* **2007**, *96* (5), 990-995.
29. Karki, S.; Friscic, T.; Jones, W., Control and Interconversion of Cocrystal Stoichiometry in Grinding: Stepwise Mechanism for the Formation of a Hydrogen-bonded Cocrystal. *CrystEngComm* **2009**, *11* (3), 470-481.
30. Friscic, T.; Jones, W., Recent Advances in Understanding the Mechanism of Cocrystal Formation via Grinding. *Cryst Growth Des* **2009**, *9* (3), 1621-1637.
31. Trask, A. V.; Jones, W., Crystal Engineering of Organic Cocrystals by the Solid-State Grinding Approach. In *Organic Solid State Reactions: Topics in Current Chemistry*, Toda, F., Ed. Springer Berlin Heidelberg: Berlin, Heidelberg, 2005; pp 41-70.
32. Trask, A. V.; Motherwell, W. D. S.; Jones, W., Solvent-drop Grinding: Green Polymorph Control of Cocrystallisation. *ChemComm* **2004**, (7), 890-891.
33. Shan, N.; Toda, F.; Jones, W., Mechanochemistry and Co-crystal Formation: Effect of Solvent on Reaction Kinetics. *ChemComm* **2002**, (20), 2372-2373.
34. McNamara, D. P.; Childs, S. L.; Giordano, J.; Iarriccio, A.; Cassidy, J.; Shet, M. S.; Mannion, R.; O'Donnell, E.; Park, A., Use of a Glutaric Acid Cocrystal to Improve Oral Bioavailability of a Low Solubility API. *Pharm Res* **2006**, *23* (8), 1888-1897.
35. Lu, E.; Rodríguez-Hornedo, N.; Suryanarayanan, R., A Rapid Thermal Method for Cocrystal Screening. *CrystEngComm* **2008**, *10* (6), 665-668.
36. Bethune, S. J.; Huang, N.; Jayasankar, A.; Rodríguez-Hornedo, N., Understanding and Predicting the Effect of Cocrystal Components and pH on Cocrystal Solubility. *Cryst Growth Des* **2009**, *9* (9), 3976-3988.
37. Rodríguez-Hornedo, N.; Nehm, S. J.; Seefeldt, K. F.; Pagán-Torres, Y.; Falkiewicz, C. J., Reaction Crystallization of Pharmaceutical Molecular Complexes. *Mol Pharm* **2006**, *3* (3), 362-367.
38. Nehm, S. J.; Rodríguez-Spong, B.; Rodríguez-Hornedo, N., Phase solubility diagrams of cocrystals are explained by solubility product and solution complexation. *Cryst Growth Des* **2006**, *6* (2), 592-600.
39. Childs, S. L.; Rodríguez-Hornedo, N.; Reddy, L. S.; Jayasankar, A.; Maheshwari, C.; McCausland, L.; Shipplett, R.; Stahly, B. C., Screening Strategies based on Solubility and Solution Composition Generate Pharmaceutically Acceptable Cocrystals of Carbamazepine. *CrystEngComm* **2008**, *10* (7), 856-864.
40. Gagniere, E.; Mangin, D.; Puel, F.; Bebon, C.; Klein, J.-P.; Monnier, O.; Garcia, E., Cocrystal Formation in Solution: In Situ Solute Concentration Monitoring of the Two Components and Kinetic Pathways. *Cryst Growth Des* **2009**, *9* (8), 3376-3383.
41. Gagnière, E.; Mangin, D.; Puel, F.; Rivoire, A.; Monnier, O.; Garcia, E.; Klein, J. P., Formation of Co-crystals: Kinetic and Thermodynamic Aspects. *J Cryst Growth* **2009**, *311* (9), 2689-2695.

42. Good, D. J.; Rodríguez-Hornedo, N., Cocrystal Eutectic Constants and Prediction of Solubility Behavior. *Cryst Growth Des* **2010**, *10* (3), 1028-1032.
43. Kuminek, G.; Rodríguez-Hornedo, N.; Siedler, S.; Rocha, H. V.; Cuffini, S. L.; Cardoso, S. G., How Cocrystals of Weakly Basic Drugs and Acidic Cofomers Might Modulate Solubility and Stability. *ChemComm* **2016**, *52* (34), 5832-5.
44. Huang, N.; Rodríguez-Hornedo, N., Engineering Cocrystal Solubility, Stability, and pH(max) by Micellar Solubilization. *J Pharm Sci* **2011**, *100* (12), 5219-34.
45. Jain, A.; Ran, Y. Q.; Yalkowsky, S. H., Effect of pH-Sodium Lauryl Sulfate Combination on Solubilization of PG-300995 (an Anti-HIV Agent): A Technical Note. *AAPS PharmSciTech* **2004**, *5* (3).
46. Li, P.; Tabibi, S. E.; Yalkowsky, S. H., Combined Effect of Complexation and pH on Solubilization. *J Pharm Sci* **1998**, *87* (12), 1535-1537.
47. Yan, H.; Yalkowsky, S. H., Solubilization of Monovalent Weak Electrolytes by Micellization or Complexation. *Int J Pharm* **2006**, *314* (1), 15-20.
48. Roy, L.; Lipert, M. P.; Rodríguez-Hornedo, N., Co-crystal Solubility and Thermodynamic Stability. *Rsc Drug Discov* **2011**, (16), 247-279.
49. Huang, N.; Rodríguez-Hornedo, N., Effect of Micellar Solubilization on Cocrystal Solubility and Stability. *Cryst Growth Des* **2010**, *10* (5), 2050-2053.
50. Huang, N.; Rodríguez-Hornedo, N., Engineering Cocrystal Thermodynamic Stability and Eutectic Points by Micellar Solubilization and Ionization. *CrystEngComm* **2011**, *13* (17), 5409-5422.
51. Roy, L.; Lipert, M. P.; Huang, N.; Rodríguez-Hornedo, N., Understanding and Predicting Cocrystal Solubility in Biorelevant Media. *Poster presentation at the 2010 AAPS Annual Meeting and Exposition 2010, New Orleans, LA* (November 14-18, 2010), Poster T3112.
52. Roy, L.; Rodríguez-Hornedo, N., A Rational Approach for Surfactant Selection to Modulate Cocrystal Solubility and Stability. *Poster presentation at the 2010 AAPS Annual Meeting and Exposition 2010, New Orleans, LA* (November 14-18, 2010), Poster R6072.
53. Reddy, L. S.; Bethune, S. J.; Kampf, J. W.; Rodríguez-Hornedo, N., Cocrystals and Salts of Gabapentin: pH Dependent Cocrystal Stability and Solubility. *Cryst Growth Des* **2009**, *9* (1), 378-385.
54. Alhalaweh, A.; Roy, L.; Rodríguez-Hornedo, N.; Velaga, S. P., pH-Dependent Solubility of Indomethacin-Saccharin and Carbamazepine-Saccharin Cocrystals in Aqueous Media. *Mol Pharm* **2012**, *9* (9), 2605-2612.
55. Wei, Y.; Zhang, L.; Wang, N.; Shen, P.; Dou, H.; Ma, K.; Gao, Y.; Zhang, J.; Qian, S., Mechanistic Study on Complexation-Induced Spring and Hover Dissolution Behavior of Ibuprofen-Nicotinamide Cocrystal. *Cryst Growth Des* **2018**, *18* (12), 7343-7355.

56. Rosa, J.; Machado, T. C.; da Silva, A. K.; Kuminek, G.; Bortolluzzi, A. J.; Caon, T.; Cardoso, S. G., Isoniazid-Resveratrol Cocrystal: A Novel Alternative for Topical Treatment of Cutaneous Tuberculosis. *Cryst Growth Des* **2019**, *19* (9), 5029-5036.
57. Machado, T. C.; Kuminek, G.; Cardoso, S. G.; Rodríguez-Hornedo, N., The Role of pH and Dose/solubility Ratio on Cocrystal Dissolution, Drug Supersaturation and Precipitation. *Eur J Pharm Sci* **2020**, 105422.
58. Yalkowsky, S. H., *Solubility and Solubilization in Aqueous Media*. American Chemical Society; Oxford University Press: Washington, D.C.; New York; Oxford, 1999; p xvi, 464.
59. Roy, L., Engineering Cocrystal and Cocrystalline Salt Solubility by Modulation of Solution Phase Chemistry. 2013. <http://hdl.handle.net/2027.42/98067>.
60. Lipert, M. P.; Rodríguez-Hornedo, N., Cocrystal Transition Points: Role of Cocrystal Solubility, Drug Solubility, and Solubilizing Agents. *Mol Pharm* **2015**, *12* (10), 3535-46.
61. Gong, J. a. T., W., Nucleation. In *Pharmaceutical Crystals*, pp 47-88.
62. Lipert, M. P.; Roy, L.; Childs, S. L.; Rodríguez-Hornedo, N., Cocrystal Solubilization in Biorelevant Media and its Prediction from Drug Solubilization. *J Pharm Sci* **2015**, *104* (12), 4153-4163.
63. Huang, Y.; Kuminek, G.; Roy, L.; Cavanagh, K. L.; Yin, Q.; Rodríguez-Hornedo, N., Cocrystal Solubility Advantage Diagrams as a Means to Control Dissolution, Supersaturation, and Precipitation. *Mol Pharm* **2019**, *16* (9), 3887-3895.
64. Lipert, M. P. Predicting the Influence of Drug Solubilizing Agents on Cocrystal Solubility, Stability, and Transition Points. Dissertations and Theses, University of Michigan, 2015.
65. Cao, F.; Amidon, G. L.; Rodríguez-Hornedo, N.; Amidon, G. E., Mechanistic Analysis of Cocrystal Dissolution as a Function of pH and Micellar Solubilization. *Mol Pharm* **2016**, *13* (3), 1030-1046.
66. Cheney, M. L.; Shan, N.; Healey, E. R.; Hanna, M.; Wojtas, L.; Zaworotko, M. J.; Sava, V.; Song, S. J.; Sanchez-Ramos, J. R., Effects of Crystal Form on Solubility and Pharmacokinetics: A Crystal Engineering Case Study of Lamotrigine. *Cryst Growth Des* **2010**, *10* (1), 394-405.
67. Kaur, R.; Cavanagh, K. L.; Rodríguez-Hornedo, N.; Matzger, A. J., Multidrug Cocrystal of Anticonvulsants: Influence of Strong Intermolecular Interactions on Physicochemical Properties. *Cryst Growth Des* **2017**.
68. Childs, S. L.; Kandi, P.; Lingireddy, S. R., Formulation of a Danazol Cocrystal with Controlled Supersaturation Plays an Essential Role in Improving Bioavailability. *Mol Pharm* **2013**, *10* (8), 3112-27.
69. Kuminek, G.; Cavanagh, K. L.; da Piedade, M. F. M.; Rodríguez-Hornedo, N., Posaconazole Cocrystal with Superior Solubility and Dissolution Behavior. *Cryst Growth Des* **2019**, *19* (11), 6592-6602.

70. Schiller, D. S.; Fung, H. B., Posaconazole: An Extended-Spectrum Triazole Antifungal Agent. *Clin Ther* **2007**, *29* (9), 1862-1886.
71. Diakidou, A.; Vertzoni, M.; Dressman, J.; Reppas, C., Estimation of Intra-gastric Drug Solubility in the Fed State: Comparison of Various Media with Data in Aspirates. *Biopharm Drug Dispos* **2009**, *30* (6), 318-325.
72. Cristofolletti, R.; Patel, N.; Dressman, J. B., Differences in Food Effects for 2 Weak Bases With Similar BCS Drug-Related Properties: What Is Happening in the Intestinal Lumen? *J Pharm Sci* **2016**, *105* (9), 2712-2722.
73. Dekkers, B. G. J.; Bakker, M.; van der Elst, K. C. M.; Sturkenboom, M. G. G.; Veringa, A.; Span, L. F. R.; Alffenaar, J.-W. C., Therapeutic Drug Monitoring of Posaconazole: an Update. *Curr Fungal Infect Rep* **2016**, *10* (2), 51-61.
74. Hens, B.; Bermejo, M.; Tsume, Y.; Gonzalez-Alvarez, I.; Ruan, H.; Matsui, K.; Amidon, G. E.; Cavanagh, K. L.; Kuminek, G.; Benninghoff, G.; Fan, J.; Rodríguez-Hornedo, N.; Amidon, G. L., Evaluation and Optimized Selection of Supersaturating Drug Delivery Systems of Posaconazole (BCS Class 2b) in the Gastrointestinal Simulator (GIS): An in vitro-in silico-in vivo Approach. *Eur J Pharm Sci* **2018**, *115*, 258-269.
75. Walravens, J.; Brouwers, J.; Spriet, I.; Tack, J.; Annaert, P.; Augustijns, P., Effect of pH and Comedication on Gastrointestinal Absorption of Posaconazole: Monitoring of Intraluminal and Plasma Drug Concentrations. *Clin Pharmacokinet* **2011**, *50* (11), 725-34.
76. Chen, Y. J.; Wang, S. J.; Wang, S.; Liu, C. Y.; Su, C.; Hageman, M.; Hussain, M.; Haskell, R.; Stefanski, K.; Qian, F., Sodium Lauryl Sulfate Competitively Interacts with HPMC-AS and Consequently Reduces Oral Bioavailability of Posaconazole/HPMC-AS Amorphous Solid Dispersion. *Mol Pharm* **2016**, *13* (8), 2787-2795.
77. Kuminek, G.; Cavanagh, K. L.; Rodríguez-Hornedo, N., Measurement and Mathematical Relationships of Cocrystal Thermodynamic Properties. In *Pharmaceutical Crystals*, Li, T.; Mattei, A., Eds. John Wiley & Sons, Inc.: 2019.
78. Cavanagh, K. L.; Maheshwari, C.; Rodríguez-Hornedo, N., Understanding the Differences Between Cocrystal and Salt Aqueous Solubilities. *J Pharm Sci* **2018**, *107* (1), 113-120.

CHAPTER 2

Understanding the Differences between Cocrystal and Salt Aqueous Solubilities

Introduction

Cocrystals constitute an important class of pharmaceutical materials that have the ability to enhance and fine-tune solubility. This property enables cocrystals to solve absorption and bioavailability problems of poorly water-soluble drugs. Cocrystals are thus receiving significant attention and numerous cocrystals have been reported.¹⁻⁸ In spite of their promise to solve solubility problems, there is a wide gap between the principles that explain cocrystal solution behavior and their application to cocrystal characterization and development.

Unlike other supersaturating delivery systems, cocrystal stoichiometric nature predisposes them to huge and predictable changes in solubility and thermodynamic stability as solution conditions change (pH, complexation, solubilization, among others). Cocrystals are therefore characterized not only by their solubility but also by the supersaturation that they generate. For cocrystals whose constituents may ionize in solution, understanding the influence of ionization (pH) on cocrystal solubility and supersaturation is essential to correctly evaluate their stability and potential for conversion to less soluble forms. The purpose of the work presented here is to develop mathematical relationships and determine thermodynamic parameters that explain the stability and solubility-pH dependence of cocrystals and salts of weakly basic drugs. *We also wish to address the commonly held notion that salts are more soluble than cocrystals.* To this end, we have studied the solubility behavior of salts and

cocrystals of lamotrigine (LTG), a weakly basic drug of equimolar composition. The cocrystals and salts studied, are summarized in Table 2.1.

Table 2.1. pK_a Values of Cocrystal and Salt Constituents.

Compound	Abbreviation	pK _a
Lamotrigine	LTG	5.7 ^a
Saccharin	SAC	1.6 ^b
Nicotinamide	NCT	3.4 ^c
Phenobarbital	PB	7.5 ^d , 11.8 ^e

^a O'Neil et al.⁹ and GlaxoSmithKline.¹⁰

^b Determined at 25°C in water¹¹

^c Determined at 20°C and 0.01 M ionic strength¹²

^d Determined at 25°C and 0.02 M ionic strength¹³

^e O'Neil et al.⁹

Materials and Methods

Materials

Cocrystal and Salt Constituents

LTG was purchased from Jai Radhe Sales, India with a purity of 99.6% w/w and was used as received. Nicotinamide (NCT) and saccharin (SAC) were purchased from Sigma-Aldrich and used as received. X-ray powder diffraction (XRPD) and differential scanning calorimetry (DSC) analyses were performed on all materials to confirm phase purity prior to use. Lamotrigine monohydrate (LTG·H₂O) was prepared by suspending anhydrous LTG for 72 hours in water at 25 ± 0.1°C. The slurry was vacuum filtered and the solid phase was confirmed by XRPD and DSC.

Solvents and Buffer Components

High performance liquid chromatography (HPLC) grade methanol was purchased from Fisher Scientific (Pittsburgh, PA). Trifluoroacetic acid spectrophometric grade 99% was purchased from Aldrich Company (Milwaukee, WI). All water used in this study was filtered through a double deionized purification system (Milli Q Plus Water System) from Millipore Company (Bedford, MA).

pH 2.0 phosphate buffer was prepared using sodium phosphate dibasic heptahydrate from Acros Organics, potassium dihydrogen phosphate from Sigma-Aldrich, and phosphoric acid from Acros Organics. pH 4.5 acetate buffer was prepared using acetic acid purchased from Sigma-Aldrich and sodium acetate purchased from Sigma Chemical Company. pH 6.8 phosphate buffer was prepared using monobasic potassium phosphate purchased from Sigma-Aldrich and sodium hydroxide pellets (NaOH) from J.T. Baker (Philipsburg, NJ).

Methods

Buffer Preparation

All buffers were prepared according to the pharmacopeial protocol.^{14, 15} pH 2.0 phosphate buffer was prepared by dissolving 1.41 g sodium phosphate dibasic heptahydrate and 0.85 g potassium dihydrogen phosphate in 250 mL of water. pH was adjusted to 2.0 using phosphoric acid (1.8 mL total). pH 4.5 acetate buffer was prepared by dissolving 147.5 mg sodium acetate and 3.5 mL of 2 M acetic acid in 246.5 mL of water. A quantity of 2 M acetic acid was prepared adding 28.8 mL of acetic acid to 250 mL of water. pH 6.8 phosphate buffer was prepared by adding 22.4 mL of 0.2 M NaOH solution to 50 mL of 0.2 M monobasic potassium phosphate solution. A quantity of 0.2 M NaOH solution was prepared by dissolving 0.8 g NaOH pellets in 100 mL of water. A quantity of 0.2 M monobasic potassium phosphate

solution was prepared by dissolving 2.7 g monobasic potassium phosphate in 100 mL of water. All buffers were prepared by stirring at room temperature.

Cocrystal and Salt Synthesis

LTG-NCT·H₂O was synthesized by reaction crystallization method.¹⁶ An aqueous solution of 2% w/w SLS and 3.5 M NCT was prepared, to which anhydrous LTG was added and stirred for 72 hours at ambient temperature. Cocrystalline solid phase was analyzed by XRPD, DSC, and HPLC to confirm crystalline form and phase purity. LTG-SAC salt was synthesized by adding stoichiometric weight fraction of anhydrous LTG to a SAC solution. The solid phase was filtered after approximately 24 hours and confirmed to be LTG-SAC salt by XRPD and DSC.

Drug Solubility Measurement

Intrinsic LTG·H₂O solubility ($S_{0,LTG\cdot H_2O}$) was measured in water by adding excess solid to solution. Solutions were magnetically stirred and maintained at $25.0 \pm 0.1^\circ\text{C}$ using a water bath for 72 hours. At 24 hour intervals, 0.50 mL aliquots were collected and filtered through a 0.45 μm pore membrane. After dilution with mobile phase, solution concentrations were analyzed by HPLC. LTG·H₂O was confirmed as the equilibrium solid phase by XRPD and DSC.

Cocrystal and Salt Solubility Measurements

Cocrystal equilibrium solubilities were measured in pH 2.0 phosphate buffer, pH 4.5 acetate buffer, pH 6.8 phosphate buffer, and water at the eutectic point, where LTG·H₂O and LTG-NCT·H₂O were in equilibrium with solution. The eutectic point between LTG-NCT·H₂O and LTG·H₂O was approached by equilibrating both solid phases in aqueous media. LTG-SAC solubilities were directly measured by suspending salt in aqueous media, and pH was adjusted by

adding pH 2 phosphate buffer or 0.1 M NaOH. Suspensions were stirred for 72 hours under constant temperature $25.0 \pm 0.1^\circ\text{C}$ using a water bath. At 24 hour intervals, 0.50 mL aliquots were collected and filtered through a 0.45 μm pore membrane. Solid phases were analyzed by XRPD and DSC to confirm solid phases at equilibrium. The equilibrium pH of the solution media was measured before dilution with mobile phase for concentration measurement of LTG cocrystal and salt constituents by HPLC. Solutions were considered to have reached equilibrium with solid phases when less than 5% change in concentration was detected in either component of the cocrystal or salt.

Stoichiometric solubility of the 1:1 cocrystal was calculated according to

$$S_{\text{LTG-NCT}\cdot\text{H}_2\text{O}} = \sqrt{[\text{LTG}]_{\text{T,eu}}[\text{NCT}]_{\text{T,eu}}} \quad (2.1)$$

from measured drug and coformer concentrations at the eutectic point ($[\text{LTG}]_{\text{T,eu}}$ and $[\text{NCT}]_{\text{T,eu}}$).¹⁷⁻¹⁹

Stoichiometric solubility of the 1:1 salt was calculated by a similar expression according to

$$S_{\text{LTG-SAC}} = \sqrt{[\text{LTG}]_{\text{T}}[\text{SAC}]_{\text{T}}} \quad (2.2)$$

K_{sp} for $\text{LTG-NCT}\cdot\text{H}_2\text{O}$ and LTG-SAC was calculated from solubility determinations from the above equations, as described in the results section.

X-ray Powder Diffraction (XRPD)

XRPD patterns of solid phases were recorded with a Rigaku MiniFlex X-ray diffractometer (Danvers, MA) using Cu K α radiation ($\lambda = 1.5418 \text{ \AA}$), a tube voltage of 30 kV, and a tube current of 15 mA. The intensities were measured at 2θ values from 2° to 35° with a continuous scan rate of $2.5^\circ/\text{min}$.

Thermal Analysis

Crystalline samples of 2-4 mg were analyzed by differential scanning calorimetry (DSC) using a TA instrument (Newark, DE) 2910 MDSC system equipped with a refrigerated cooling unit. DSC experiments were performed by heating the samples at a rate of 10°C/min under a dry nitrogen atmosphere. Temperature and enthalpy calibration of the instruments was achieved by using a high purity indium standard. Standard aluminum sample pans were used for all measurements.

High Performance Liquid Chromatography (HPLC)

Solution concentrations of drug and coformer were analyzed by Waters HPLC (Milford, MA) equipped with a UV/vis spectrometer detector. A reversed phase C18 Atlantis column (5 µm, 4.5 × 250 mm) at ambient temperature was used to separate the drug and the coformer or counterion. An isocratic method of 55% methanol, 45% water, and 0.1% trifluoroacetic acid mobile phase was used with a flow rate of 1 mL/min. Sample injection volume was 20 µL. Absorbance of the drug and coformer or counterion analytes was monitored between 210 and 300nm. The peak areas were integrated using Empower™ software.

Results and Discussion

Solubility-pH Dependence and Supersaturation Index

Figure 2.1 shows the solubility-pH dependence of the weakly basic drug LTG, a salt with a moderately strong acid, SAC, and two cocrystals, with a weakly basic coformer, NCT, or with a weakly acidic drug, phenobarbital (PB). We recently published the solubility-pH dependence of LTG-PB cocrystal and include it here for comparison.¹ These results demonstrate that pH has a huge influence on solubility and that both cocrystal and salt can exhibit pH_{max} where their

solubility curves intersect with the drug solubility curve. Furthermore, the cocrystal and salt solubility behaviors differ as a result of the ionization properties of their constituents.

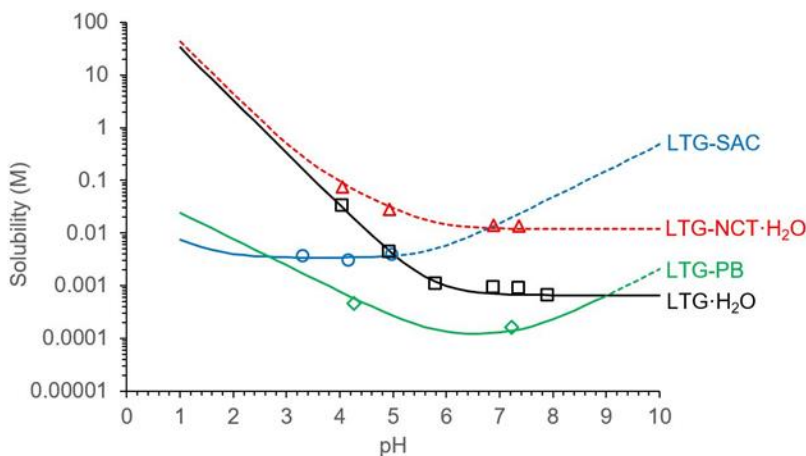


Figure 2.1. Solubility-pH dependence of drug, cocrystals, and salt of LTG. Solubility values for cocrystals and salt were determined under equilibrium conditions and calculated from Equations 2.1 and 2.2. Some of the solubility values are above LTG solubility and are useful as indicators of supersaturation. Solubility curves were generated using Equations 2.4-2.7, and previously published results for LTG-PB are included for comparison. Dashed lines represent supersaturated conditions with respect to LTG.¹ pH values represent equilibrium pH. Standard deviation of data points is less than 5%. Portions of data courtesy of Dr. Chinmay Maheshwari.

Solubility values for cocrystals and salt were determined under equilibrium conditions and calculated according to Equations 2.1 and 2.2. Some of the solubility values in Figure 2.1 represent supersaturated conditions with respect to the drug free base and are useful as a measure of the supersaturation index ($SA=S_{CC}/S_D$) that a cocrystal or a salt may generate, as presented in Figure 2.2.

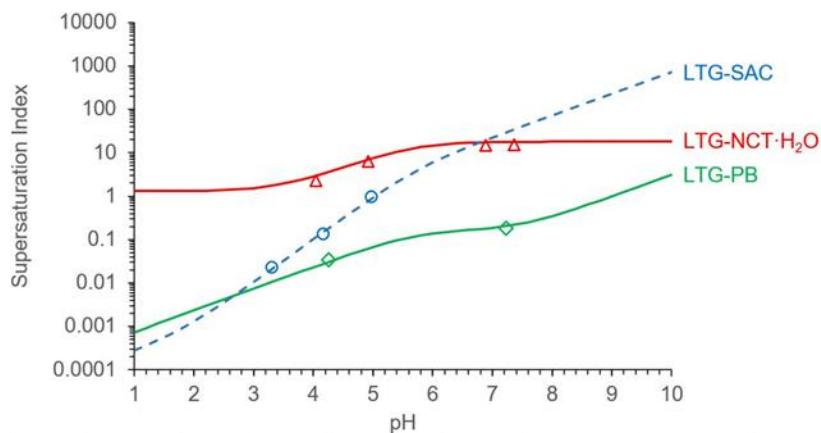


Figure 2.2. Supersaturation Index ($SA = S_{CC}/S_D$) is the ratio of salt or cocrystal solubility to parent drug. $SA = 1$ represents equal drug and salt or cocrystal solubility and corresponds to pH_{max} . $LTG-NCT \cdot H_2O$ is more soluble than drug ($SA = 1.2$ to 18). $LTG-SAC$ salt is less soluble than drug a $pH < pH_{max} = 5.0$, and $LTG-PB$ cocrystal is less soluble than LTG ($SA < 1$) below $pH_{max} 9.0$. Experimental measurements at $pH 4.0$ to 4.3 show that SA for NCT cocrystal is 2.8 , for SAC salt is 0.16 , and for PB cocrystal is 0.03 , demonstrating the range of behavior among these solid phase. Salt SA exhibits a fast increase with pH than cocrystal SA . Supersaturation index curves were generated by dividing Equations 2.5-2.7 by Equation 2.4.

SA is the driving force for conversions from cocrystal to the less soluble drug. The change in Gibbs-free energy for this conversion is

$$DG_{CC \rightarrow D} = -RT \ln \left(\frac{S_{CC}}{S_D} \right) = -RT \ln(SA) \quad (2.3)$$

where S is solubility and subscripts CC and D refer to cocrystal and drug phases. In this equation, S_{CC} is expressed in terms of moles of drug. A phase conversion from cocrystal to drug is favorable when $S_{CC} > S_D$, $SA > 1$. A similar analysis applies to salts and S_{CC} can be substituted for S_{salt} in Equation 2.3. When $S_{CC} = S_D$, $SA = 1$, and $\Delta G = 0$, the system is at equilibrium and the pH corresponding to these equilibria is pH_{max} .

Supersaturation can be sustained for some time until nucleation occurs, which is the reason for the importance of supersaturating drug delivery systems. The higher supersaturation is, the more negative is the free energy for conversion, the shorter is the time for nucleation to

occur, and the higher is the nucleation rate. This means that cocrystals with higher SA values may experience lower supersaturations and shorter induction times before conversion. In the context of the work presented here, SA is used to quantify the propensity of cocrystal conversions as their SA changes with pH.

The utility of SA versus pH plot (Figure 2.2) in assessing the risk of cocrystal and salt conversions to drug is shown by considering reported dissolution results for LTG-NCT·H₂O cocrystal and LTG-SAC salt.^{3,20} The cocrystal was reported to transform to the drug, whereas the salt did not transform during dissolution in aqueous unbuffered media at 25°C. Considering the SA values for cocrystal (18 at pH 6.6) and salt (1 at pH 5), one would expect the salt to be stable (as the dissolution pH is at pH_{max}) whereas the cocrystal will have a risk of conversion. In fact, the cocrystal was reported to transform to the less soluble drug as an SA of 18 was not sustainable and the salt did not transform was reported to be stable.

A common mistake in cocrystal solubility and stability studies is that solution conditions are not considered. Even when initial pH conditions are known, in aqueous or buffered solutions, the pH during cocrystal dissolution can change considerably, causing huge errors in data interpretation.

A word of caution about kinetically obtained C_{max} values during cocrystal/salt dissolution studies is in order. C_{max} is a result of two opposing kinetic processes, cocrystal/salt dissolution and drug precipitation, and is not proportional to solubility. C_{max} is a kinetic parameter and its values are variable due to its kinetic nature and to the differences in changing experimental conditions. Integrating dissolution and thermodynamic data provides a useful conceptual context to assess the risks associated with changing factors and conditions.

Relationships between Solubility, pK_a, and pH

LTG-NCT·H₂O is composed of two weakly basic components, which means the change in slope of the solubility-pH profile (Figure 2.1) is determined by the ionization behavior of both the drug (pK_a = 5.7) and the coformer (pK_a = 3.4). Cocrystal solubility remains constant above the drug pK_a as both components are predominantly nonionized. However, as the components become increasingly ionized, cocrystal solubility increases quite substantially as pH approaches the drug pK_a and even more so as pH approaches the coformer pK_a.

A multidrug cocrystal of basic LTG and acidic PB (pK_{a,1} = 7.5, pK_{a,2} = 11.8), exhibits a U-shaped solubility curve due the different ionization ranges of LTG and PB. Cocrystal solubility increases with LTG ionization and PB ionization. A pH of minimum solubility occurs between the pK_a of the basic and acidic constituents. The cocrystal and drug solubility curves intersect at a pH_{max}, which for this system is pH 9.

LTG-SAC salt with the acidic counterion SAC (pK_a = 1.6) also exhibits a U-shaped curve, including a plateau region between pH values of 2.5 and 5.0. Salt solubility increases below pH 2.5 and above pH 5.0 as ionization of the basic and acidic constituents change. A pH_{max} is observed at pH 5.

Solubilities of these four forms of LTG as a function of pH were predicted according to the following equations using pK_a values shown in Table 2.1. The drug solubility (S_{LTG·H₂O}) was predicted from

$$S_{\text{LTG}\cdot\text{H}_2\text{O}} = S_{0,\text{LTG}\cdot\text{H}_2\text{O}}(1 + 10^{\text{pK}_a,\text{LTG}-\text{pH}}) \quad (2.4)$$

where S_{0,LTG·H₂O} represents the solubility of LTG monohydrate under nonionizing conditions, also referred to as intrinsic drug solubility. S_{0,LTG·H₂O} was evaluated to be 6.6 × 10⁻⁴ M by fitting the above equation to the data.

For LTG-NCT·H₂O cocrystal, the solubility expression is given by

$$S_{\text{LTG-NCT}\cdot\text{H}_2\text{O}} = \sqrt{K_{\text{sp}}(1 + 10^{\text{pK}_a,\text{LTG}-\text{pH}})(1 + 10^{\text{pK}_a,\text{NCT}-\text{pH}})} \quad (2.5)$$

where K_{sp} is the cocrystal solubility product. This equation was derived by considering the mass balance of all cocrystal species in solution and expressing them in terms of the equilibrium constants that correspond to cocrystal dissociation (K_{sp}) and ionization (K_a)

Cocrystal K_{sp} was evaluated from Equation 2.5 and cocrystal solubility (S_{CC}) values obtained from Equation 2.1 by measurement of cocrystal component concentrations in equilibrium with cocrystal and drug phases at specific pH equilibrium values and pK_a values in Table 2.1.

The salt solubility-pH relationship is

$$S_{\text{LTG-SAC}} = \sqrt{K_{\text{sp}}(1 + 10^{\text{pH}-\text{pK}_a,\text{LTG}})(1 + 10^{\text{pK}_a,\text{SAC}-\text{pH}})} \quad (2.6)$$

This well recognized equation is analogous to that of the cocrystal (Equation 2.5) as it considers dissociation and ionization equilibrium reactions.²¹⁻²³ In this case, however, the salt K_{sp} is the product of activities of ionized constituents, whereas for a cocrystal, it is the non-ionized constituents. As a result of the different ionization states in the dissociation and ionization reactions, the ionization terms in the solubility equations for cocrystal and salt also have different signs.

Figure 2.1 shows excellent agreement between predicted and experimental solubility behavior. LTG-NCT cocrystal is more soluble than drug at $\text{pH} > 3$ and reaches solubilities 18 times the drug solubility at $\text{pH} \geq 6$. The cocrystal is also more soluble than the SAC salt at $\text{pH} < 7$ and is orders of magnitude more soluble than the salt at $\text{pH} < 3$. The SAC salt has a pH_{max} around pH 5, below which it is less soluble than the drug. Experimental measurement of salt

solubility above pH_{max} was not possible as the equilibrium pH decreased to pH 5 due to salt conversion to the less soluble drug at initial pH values of about 6.

The above results are compared with those recently reported for LTG-PB cocrystal.¹ The cocrystal solubility dependence on pH is given by

$$S_{\text{LTG-PB}} = \sqrt{K_{\text{sp}}(1 + 10^{\text{pK}_{\text{a,LTG}} - \text{pH}})(1 + 10^{\text{pH} - \text{pK}_{\text{a,PB1}}} + 10^{2\text{pH} - \text{pK}_{\text{a1,PB}} - \text{pK}_{\text{a2,PB}}})} \quad (2.7)$$

The cocrystal solubility curve generated by this equation²⁴ (Figure 2.1) predicts a pH_{max} of 9 and a solubility minimum between the pK_{a} of LTG and the first pK_{a} of PB.^{19, 24, 25} Another pH_{max} with PB occurs at pH 2.6 (not shown in this plot). The PB cocrystal is the least soluble of the four forms considered between pH 3 and 9. PB is also the least soluble constituent among the cocrystals. In fact, its intrinsic solubility is only about 10 times higher than the drug. The ratio of coformer to drug solubilities ($S_{\text{CF}}/S_{\text{D}} \leq 10$) has been generally observed to result in cocrystals that are less soluble than drug.^{17, 26} Solubility is however determined by pH, and these trends will change with the ionization of cocrystal and salt constituents as demonstrated in Figure 2.1.

Solubility Product, K_{sp}

Whereas solubility is a conditional constant and dependent on pH, the solubility product, K_{sp} , is not. K_{sp} is the constant associated with the equilibrium between cocrystal or salt and a solution phase. It involves dissociation of cocrystal and salt into its constituents according to



for a cocrystal, and



for a salt. A and B represent cocrystal constituents (or ionized constituents A^- and BH^+ for a salt), y and z are the stoichiometric coefficients. The forward reaction is dissociation and

represents dissolution, while the reverse reaction is association and represents precipitation. K_{sp} for a cocrystal is

$$K_{sp} = \frac{a_A^y a_B^z}{a_{A_y B_z}} \quad (2.10)$$

and for a salt

$$K_{sp} = \frac{a_A^y a_{BH^+}^z}{a_{A_y BH_z^+}} \quad (2.11)$$

where a represents activities, and subscripts represent cocrystal or salt constituents. Since the activity of the solid phase is assumed to be constant and equal to 1, K_{sp} is an activity product.

Activities are approximated by concentrations under the assumption of ideality, and K_{sp} becomes

$$K_{sp} = [A]^y [B]^z \quad (2.12)$$

for a cocrystal, and

$$K_{sp} = [A^-]^y [BH^+]^z \quad (2.13)$$

for a salt.

K_{sp} values for several salts and cocrystals of LTG are presented in Table 2.2. The K_{sp} expression for LTG-NCT cocrystal is

$$K_{sp} = [LTG][NCT] \quad (2.14)$$

For the saccharin salt, K_{sp} is

$$K_{sp} = [LTGH^+][SAC^-] \quad (2.15)$$

Similar equations with the corresponding cofomers or counterions were used to evaluate K_{sp} of other LTG forms as they were all of equimolar stoichiometry.

Table 2.2. Solubility Product K_{sp} , Intrinsic Solubility (S_0), and Solubility Advantage ($SA = \frac{S_{0,CC} \text{ or } S_{0,Salt}}{S_{0,LTG}}$) of LTG Cocrystals and Salts.

Solid Phase	K_{sp} (M^2)	$S_{0,CC}$ or $S_{0,Salt}$ (M)	$\frac{S_{0,CC} \text{ or } S_{0,Salt}}{S_{0,LTG}}$
LTG-NCT Cocrystal	$(1.4 \pm 0.4) \times 10^{-4}$	1.2×10^{-2}	18
LTG-HCl Salt	$(6.7 \pm 0.53) \times 10^{-5}$ ^a	8.2×10^{-3}	12
LTG-SAC Salt	$(1.1 \pm 0.2) \times 10^{-5}$	3.3×10^{-3}	5
LTG-MP Cocrystal	$(5.3 \pm 0.47) \times 10^{-7}$ ^b	7.3×10^{-4}	1.1
LTG-PB Cocrystal	$(1.2 \pm 0.5) \times 10^{-8}$	1.1×10^{-4}	0.18

^a K_{sp} of LTG-HCl was calculated from reported solubility of 0.46 mg/mL at 37°C (pH 1.2) from Floyd and Jain.²⁷ K_{sp} of the salt was estimated at 25°C from [LTGH⁺] and [Cl⁻] concentrations calculated from the dissolved salt and HCl concentrations, using a heat of solution value of 30 kJ/mol.

^b Steady state concentration from dissolution data in Cheney et al.³ was used to calculate the K_{sp} of lamotrigine-methylparaben (LTG-MP) cocrystal, where cocrystal was reported to be stable.

Results in Table 2.2 show that NCT cocrystal K_{sp} is higher than that of SAC and HCl salts. The PB cocrystal has the lowest K_{sp} among these forms. These findings challenge the popular notion that salts are more soluble than cocrystals. In fact, NCT cocrystal intrinsic solubility is 18 times higher than drug and even higher than the HCl and SAC salts.

It is important to note that K_{sp} is the *product of only the cocrystal or salt constituents in the non-ionized or ionized state, respectively*. $K_{sp} \neq [A]_T [B]_T$ when there are molecular species in solution different from those in the corresponding solid phase. The reader should be cautious of incorrect K_{sp} values calculated from total analytical concentrations of cocrystal or salt constituents that do not correspond to the K_{sp} definition according to the equilibrium in Equations 2.12 and 2.13.

K_{sp} values for cocrystals of several drugs in aqueous media are presented in Table 2.3 in terms of pK_{sp} . The low values of K_{sp} make use of $pK_{sp} = -\log K_{sp}$ more reasonable. Higher pK_{sp}

values refer to lower K_{sp} values. The range of values is similar to those reported for pharmaceutical salts.²⁸⁻³⁰ pK_{sp} values for CBZ cocrystals are in the range of 2 to 6, indicating increases in K_{sp} by orders of magnitude. When solubility is determined by solvation and not by solid-state lattice energy,^{17,31} cocrystal solubility is dependent on the solubility of its components. Nicotinamide and glutaric acid are among the most soluble cofomers and generally correspond to cocrystals with higher K_{sp} values for a given drug. The highest 1:1 cocrystal K_{sp} corresponds to theophylline-nicotinamide with a pK_{sp} of 0.7, among the most soluble combination of cocrystal constituents.

Comparing the pK_{sp} values of salts and cocrystals of the same drug (Table 2.3) shows that some cocrystals are more soluble than salts, or less soluble depending on the cofomers and counterions. Cocrystals with higher ratio of the less soluble drugs also have higher pK_{sp} values, as observed for 2:1 versus 1:1 cocrystals.

Table 2.3. Cocrystal and Salt pK_{sp}

Cocrystal (drug-coformer) or Salt (drug-counterion)	Solid Form	Stoichiometry (drug:coformer or drug:counterion)	pK_{sp}
Caffeine-Salicylic acid	Cocrystal	1:1	3.1 ¹⁷
Carbamazepine-Nicotinamide	Cocrystal	1:1	2.3 ¹⁷
Carbamazepine-Glutaric acid	Cocrystal	1:1	2.5 ¹⁷
Carbamazepine-Salicylic acid	Cocrystal	1:1	5.9 ²⁴
Carbamazepine-Saccharin	Cocrystal	1:1	6.0 ³²
Carbamazepine-Malonic acid ^a	Cocrystal	2:1 ^b	6.1 ¹⁷
Carbamazepine-Oxalic acid	Cocrystal	2:1 ^b	8.0 ¹⁷
Carbamazepine-Succinic acid	Cocrystal	2:1	8.2 ³³
Carbamazepine-4-aminobenzoic acid hydrate	Cocrystal	2:1	8.9 ²⁴
Danazol-Hydroxybenzoic acid	Cocrystal	1:1	8.0 ³⁴
Danazol-Vanillin	Cocrystal	1:1	8.5 ³⁴
Gabapentin Lactam-4-aminobenzoic acid	Cocrystal	1:1	3.1 ¹⁹
Gabapentin Lactam-Fumaric acid	Cocrystal	2:1	3.4 ¹⁹
Gabapentin Lactam-Benzoic acid	Cocrystal	1:1	3.5 ¹⁹
Gabapentin Lactam-4-hydroxybenzoic acid	Cocrystal	1:1	3.7 ¹⁹
Gabapentin Lactam-Gentisic acid	Cocrystal	1:1	3.9 ¹⁹
Indomethacin-Saccharin	Cocrystal	1:1	8.9 ³²
Ketoconazole-Oxalic acid	Salt	1:1	5.9 ^c
Ketoconazole-Adipic acid	Cocrystal	1:1	7.5 ³⁵

Ketoconazole-Succinic acid	Cocrystal	1:1	7.6 ³⁵
Ketoconazole-Fumaric acid	Cocrystal	1:1	8.8 ³⁵
Lamotrigine-Nicotinamide	Cocrystal	1:1	3.9
Lamotrigine-Hydrochloride	Salt	1:1	4.2 ^d
Lamotrigine-Saccharin	Salt	1:1	5.0
Lamotrigine-Methylparaben	Cocrystal	1:1	6.3 ^e
Lamotrigine-Phenobarbital	Cocrystal	1:1	7.9 ¹
Nevirapine-Maleic acid	Cocrystal	1:1	4.7 ²⁵
Nevirapine-Saccharin	Cocrystal	2:1	10.0 ²⁵
Nevirapine-Salicylic acid	Cocrystal	2:1	10.4 ²⁵
Pterostilbene-Caffeine	Cocrystal	1:1	5.3 ³⁶
Pterostilbene-Piperazine	Cocrystal	2:1	6.3 ³⁷
Piroxicam-Saccharin	Cocrystal	1:1	7.1 ³⁴
Theophylline-Nicotinamide	Cocrystal	1:1	0.7 ¹⁷
Theophylline-Salicylic acid	Cocrystal	1:1	3.8 ¹⁷

^a Form B (hydrated cocrystal).³⁸

^b Disordered crystal structure that does not provide definitive stoichiometry.²⁶

^c Calculated from reported solubility of 0.90 mg/mL at 25°C and pH 3.4.³⁹

^d Calculated described in Table 2.2 footnote a.

^e Calculated from steady state concentration during cocrystal dissolution as reported by Cheney et al.³

pH_{max} of Cocrystals and Salts

Knowledge of pH_{max} is important to determine phase stability regions. In this article, we are concerned with the LTG and cocrystal or salt pH_{max}, where LTG is the least soluble constituent under the conditions studied.

The pH_{max} of cocrystals is expected to vary over a wider pH range than that of salts due to the range of ionization properties of cocrystal constituents. Cocrystals can be composed of all possible combinations of acidic, basic, and nonionized constituents, unlike salts. For instance, binary cocrystals can be composed of two basic, two acidic, one basic and one acidic, or one or both nonionizable constituents.

We derived equations that predict cocrystal/salt pH_{max} values from K_a , K_{sp} , and $S_{0,D}$. Since at the pH_{max} the solution is doubly saturated with two solid phases, cocrystal or salt and drug, pH_{max} equations were derived by setting the cocrystal solubility equal to drug solubility and solving for pH_{max} . This approach is similar to that described for salts.⁴⁰⁻⁴²

pH_{max} values for cocrystals and salts with the ionization properties of the LTG solid forms studied here are shown in Table 2.4. These were calculated from the below relationships. Equations are presented in terms of $[\text{H}^+]_{\text{max}}$ and K as they are simpler than in terms of pH or pK.

For cocrystals with a basic drug and a basic coformer, such as LTG-NCT·H₂O, $[\text{H}^+]_{\text{max}}$ is

$$[\text{H}^+]_{\text{max}} = \frac{K_{a,\text{LTG}} K_{a,\text{NCT}}(S_{0,\text{LTG}\cdot\text{H}_2\text{O}}^2 - K_{\text{sp}})}{K_{a,\text{LTG}} K_{\text{sp}} - K_{a,\text{NCT}} S_{0,\text{LTG}\cdot\text{H}_2\text{O}}^2} \quad (2.16)$$

where $S_{0,D}$ is the drug intrinsic solubility and K_{sp} is the cocrystal or salt solubility product.

For cocrystals with a basic drug and a nonionic coformer, such as LTG-MP, $[\text{H}^+]_{\text{max}}$ is

$$[\text{H}^+]_{\text{max}} = -\frac{K_{a,\text{LTG}}(S_{0,\text{LTG}\cdot\text{H}_2\text{O}}^2 - K_{\text{sp}})}{S_{0,\text{LTG}\cdot\text{H}_2\text{O}}^2} \quad (2.17)$$

For cocrystals with a basic drug and an acidic coformer, such as LTG-PB $[\text{H}^+]_{\text{max}}$ is

$$[\text{H}^+]_{\text{max}} = \frac{K_{a,\text{LTG}} K_{\text{sp}} - K_{a,\text{LTG}} S_{0,\text{LTG}\cdot\text{H}_2\text{O}}^2 + \sqrt{4K_{a,\text{LTG}} K_{a1,\text{PB}} K_{\text{sp}} S_{0,\text{LTG}\cdot\text{H}_2\text{O}}^2 + (K_{a,\text{LTG}} K_{\text{sp}} - K_{a,\text{LTG}} S_{0,\text{LTG}\cdot\text{H}_2\text{O}}^2)^2}}{2S_{0,\text{LTG}\cdot\text{H}_2\text{O}}^2} \quad (2.18)$$

Equation 2.18 is for a monoprotic acid. While PB is a diprotic acid, the second $\text{p}K_a$ is 11.8 and the assumption of only using the lower $\text{p}K_a$ is justified at pH values below 10.

For salts with a basic drug and an acidic counterion, such as LTG-SAC, $[\text{H}^+]_{\text{max}}$ is

$$[\text{H}^+]_{\text{max}} = \frac{K_{\text{a,LTG}}^2 K_{\text{sp}} - K_{\text{a,LTG}} K_{\text{a,SAC}} S_{0,\text{LTG}\cdot\text{H}_2\text{O}}^2 + \sqrt{4K_{\text{a,LTG}}^2 K_{\text{a,SAC}}^2 K_{\text{sp}} S_{0,\text{LTG}\cdot\text{H}_2\text{O}}^2 + (K_{\text{a,LTG}}^2 K_{\text{sp}} - K_{\text{a,LTG}} K_{\text{a,SAC}} S_{0,\text{LTG}\cdot\text{H}_2\text{O}}^2)^2}}{2K_{\text{a,SAC}} S_{0,\text{LTG}\cdot\text{H}_2\text{O}}^2} \quad (2.19)$$

Results in Table 2.4 show the range in pH_{max} and solubility at pH_{max} , S_{pHmax} , for the cocrystals and salts studied. Of forms that exhibit a pH_{max} , the salt has the lowest pH_{max} and highest S_{pHmax} . This is consistent with SAC having the lowest pK_{a} and higher solubility than PB and MP. The NCT cocrystal approaches the drug solubility as pH approaches the NCT pK_{a} (3.4) at a solubility of about 0.6 M, although a pH_{max} is not achieved (Figure 2.1).

Table 2.4. pH_{max} ^a for LTG Cocrystals and Salts.

Solid Phase	pH_{max}	S_{pHmax} (M)
LTG-NCT·H ₂ O Cocrystal	None ^b	-
LTG-MP Cocrystal	6.4	8.0×10^{-4}
LTG-PB Cocrystal	9.0	6.5×10^{-4}
LTG-SAC Salt	5.0	3.7×10^{-3}

^a Calculated from Equations 2.16-2.19 with K_{a} and K_{sp} values in Tables 2.1 and 2.2.

^b Equation 2.16 gives an unreal solution for $[\text{H}^+]_{\text{max}}$, confirming that there is no pH_{max} .

How pH_{max} changes with pK_{sp} for basic drugs and acidic cofomers/counterions is shown in Figures 2.3 and 2.4 by using the above equations. The pK_{a} values for the simulations were selected for the purpose of understanding the influence of pK_{sp} and pK_{a} on cocrystal/salt pH_{max} and S_{pHmax} , even though it is generally accepted that salts may form when $\Delta\text{pK}_{\text{a}}$ ($\Delta\text{pK}_{\text{a}} = \text{pK}_{\text{a}}(\text{base}) - \text{pK}_{\text{a}}(\text{acid})$) is greater than 2 or 3.⁴³⁻⁴⁵

Figure 2.3 illustrates the influence of cofomer/counterion pK_{a} on cocrystal/salt pH_{max} - pK_{sp} dependence. Both cocrystal and salt pH_{max} values increase with pK_{sp} . Cocrystals have

lower pH_{max} values than salts. Cocrystal pH_{max} values also show higher sensitivity to changes in counterion pK_{a} values.

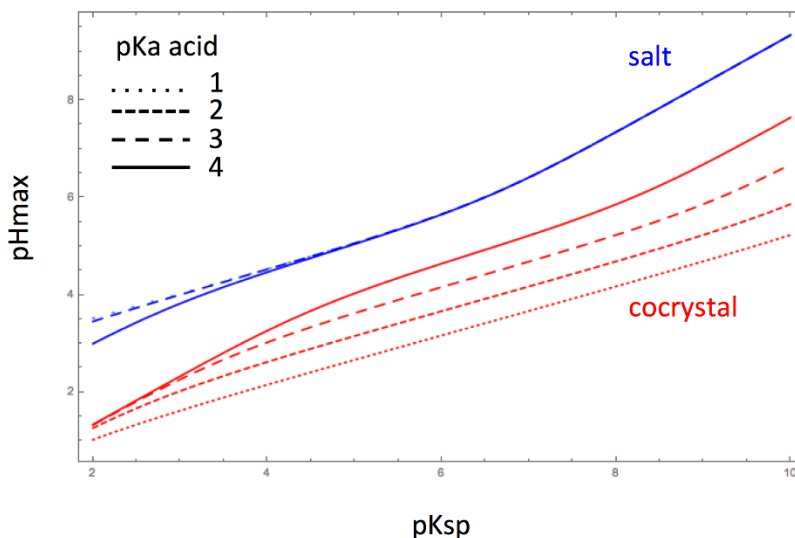


Figure 2.3. Cocrystal/salt pH_{max} dependence on pK_{sp} for basic drug with $\text{pK}_{\text{a}} = 5.71$ and acidic cofomer/counterion pK_{a} 1 to 4. Plots were generated using Equations 2.18 and 2.19 and $S_{0,D} = 6.6 \times 10^{-4}$ M. Cocrystals show lower pH_{max} values with higher sensitivity to cofomer pK_{a} than salts. For both cocrystals and salts, pH_{max} increases with pK_{sp} .

Figure 2.4 shows how the pH_{max} dependence on pK_{sp} varies with pK_{a} of a basic drug when the acidic cofomer/counterion $\text{pK}_{\text{a}} = 2.0$. At the same drug pK_{a} , salts have higher pH_{max} values. Salt pH_{max} changes by about one unit when drug pK_{a} is varied by one unit, and this trend appears to be almost constant throughout the studied pK_{sp} range. However, changes in cocrystal pH_{max} are smaller than those for salts, and they are not constant with changes in drug pK_{a} for all pK_{sp} values. While one unit change in drug pK_{a} results in about one unit change in pH_{max} at pK_{sp} 2, pH_{max} varies by 0.5 units at pK_{sp} 6 and by less than 0.2 units at pK_{sp} 10.

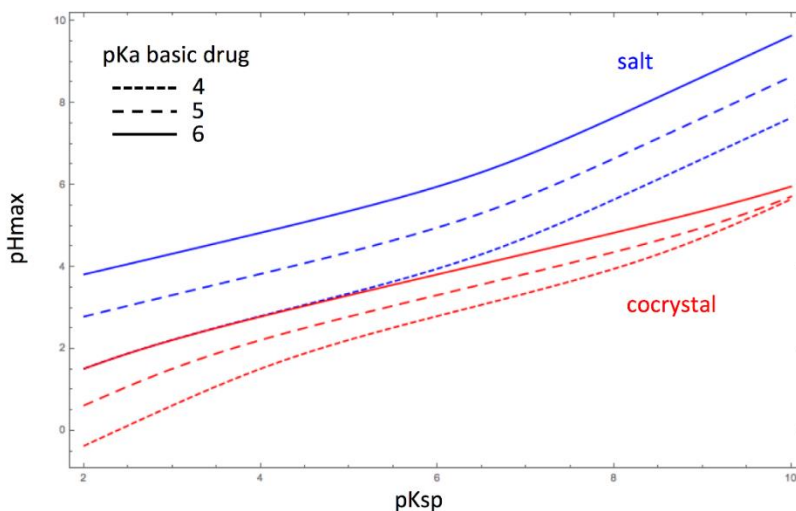


Figure 2.4. Cocrystal/salt pH_{max} dependence on pK_{sp} for basic drugs according to Equations 2.18 and 2.19 with pK_{a} 4 to 6, acidic cofomer/counterion $\text{pK}_{\text{a}} = 2.0$, and $S_{0,\text{D}} = 6.6 \times 10^{-4}$ M. Cocrystal pH_{max} values are lower than salt across the plotted pK_{sp} range. pH_{max} increases with pK_{sp} for both cocrystals and salts. Changes in salt pH_{max} with drug pK_{a} are larger than for cocrystals. Changes in cocrystal pH_{max} decrease with increasing K_{sp} .

These findings are consistent with the fact that salt pH_{max} values typically occur in the salt solubility plateau region where the counterion is almost completely ionized and solubility is independent of pH.^{21, 41, 46, 47} Changes in counterion pK_{a} (Figure 2.3) have minimal effect on pH_{max} dependence on pK_{sp} when $\Delta\text{pK}_{\text{a}}$ is large enough for the counterion to be fully ionized at pH_{max} . However, changes in drug pK_{a} will result in greater variability in pH_{max} versus pK_{sp} dependence as the solubility-pH dependencies of both the drug and salt shift. Unlike salts, the pH_{max} of cocrystals of basic drugs and acidic cofomers can occur on either side of the solubility minimum depending on pK_{sp} and $S_{0,\text{D}}$. pH_{max} occurs above minimum solubility for LTG-PB (Figure 2.1),¹ but has been shown to occur below minimum solubility for some ketoconazole nevirapine cocrystals.^{25, 35} For cocrystals with the same $S_{0,\text{D}}$, high pK_{sp} values show greater pH_{max} variability with changes in cofomer pK_{a} (Figure 2.3), but low pK_{sp} show greater pH_{max} variability with changes in drug pK_{a} (Figure 2.4).

The analysis presented shows that cocrystals and salts exhibit different dependencies of pH_{max} and K_{sp} . These cocrystal/salt properties are critical for cocrystal selection, stability, and solubility assessments.

Conclusions

This work shows that cocrystals can be more soluble than salts or vice-versa. The stoichiometric nature of cocrystals and salts predisposes them to huge, yet predictable changes in solubility, supersaturation index, and thermodynamic stability as solution pH changes. Supersaturation index is as important as solubility and pH_{max} in anticipating the potential for phase conversions. Cocrystal and salt solubility/supersaturation dependence on pH as well as pH_{max} can be predicted from knowledge of K_{sp} and pK_{a} .

Acknowledgements

We gratefully acknowledge the partial support from the National Institute of General Medical Sciences of the National Institutes of Health (NIH) under award number R01GM107146. The content is solely the responsibility of the authors and does not necessarily represent the official views of the NIH. We are grateful to Dr. Chinmay Maheshwari for his contributions in solubility data collection and equation derivations.

References

1. Kaur, R.; Cavanagh, K. L.; Rodríguez-Hornedo, N.; Matzger, A. J., Multidrug Cocrystal of Anticonvulsants: Influence of Strong Intermolecular Interactions on Physicochemical Properties. *Cryst Growth Des* **2017**.
2. Caira, M. R.; Bourne, S. A.; Samsodien, H.; Engel, E.; Liebenberg, W.; Stieger, N.; Aucamp, M., Co-crystals of the Antiretroviral Nevirapine: Crystal Structures, Thermal Analysis and Dissolution Behaviour. *CrystEngComm* **2012**, *14* (7), 2541-2551.
3. Cheney, M. L.; Shan, N.; Healey, E. R.; Hanna, M.; Wojtas, L.; Zaworotko, M. J.; Sava, V.; Song, S. J.; Sanchez-Ramos, J. R., Effects of Crystal Form on Solubility and Pharmacokinetics: A Crystal Engineering Case Study of Lamotrigine. *Cryst Growth Des* **2010**, *10* (1), 394-405.
4. Childs, S. L.; Hardcastle, K. I., Cocrystals of Piroxicam with Carboxylic Acids. *Cryst Growth Des* **2007**, *7* (7), 1291-1304.
5. Trask, A. V.; Motherwell, W. D. S.; Jones, W., Physical Stability Enhancement of Theophylline via Cocrystallization. *Int J Pharm* **2006**, *320* (1-2), 114-123.
6. McMahan, J. A.; Bis, J. A.; Vishweshwar, P.; Shattock, T. R.; McLaughlin, O. L.; Zaworotko, M. J., Crystal Engineering of the Composition of Pharmaceutical Phases. 3. Primary Amide Supramolecular Heterosynthons and their Role in the Design of Pharmaceutical Co-crystals. *Z Kristallogr* **2005**, *220* (4), 340-350.
7. Childs, S. L.; Chyall, L. J.; Dunlap, J. T.; Smolenskaya, V. N.; Stahly, B. C.; Stahly, G. P., Crystal Engineering Approach to Forming Cocrystals of Amine Hydrochlorides with Organic Acids. Molecular Complexes of Fluoxetine Hydrochloride with Benzoic, Succinic, and Fumaric Acids. *J Am Chem Soc* **2004**, *126* (41), 13335-13342.
8. Fleischman, S. G.; Kuduva, S. S.; McMahan, J. A.; Moulton, B.; Walsh, R. D. B.; Rodríguez-Hornedo, N.; Zaworotko, M. J., Crystal Engineering of the Composition of Pharmaceutical Phases: Multiple-Component Crystalline Solids involving Carbamazepine. *Cryst Growth Des* **2003**, *3* (6), 909-919.
9. M.J. O'Neil, A. S., and P.E. Heckelman, *The Merck Index: an Encyclopedia of Chemicals, Drugs, and Biologicals*. Whitehouse Station: NJ, 2001; Vol. 13th edn.
10. Lamotrigine [package insert]. In *GlaxoSmithKline*, Research Triangle Park, NC, 2009.
11. Bell, R. P.; Higginson, W. C. E., The Catalyzed Dehydration of Acetaldehyde Hydrate, and the Effect of Structure on the Velocity of Protolytic Reactions. *Proceedings of the Royal Society of London. Series A, Mathematical and Physical Sciences* **1949**, *197* (1049), 141-159.
12. Jellinek, H. H. G.; Wayne, M. G., Nicotinamide - Ultraviolet Absorption Spectra and Dissociation Constants. *J Phys Colloid Chem* **1951**, *55* (2), 173-180.
13. Geiser, L.; Henchoz, Y.; Galland, A.; Carrupt, P. A.; Veuthey, J. L., Determination of pK(a) Values by Capillary Zone Electrophoresis with a Dynamic Coating Procedure. *J Sep Sci* **2005**, *28* (17), 2374-2380.
14. *European Pharmacopoeia (EP)*. Council of Europe: Strasbourg, 2005.

15. *United States Pharmacopeia National Formulary (USP40-NF35)*. The United States Pharmacopeial Convention, Inc: Rockville, Maryland, 2017.
16. Rodríguez-Hornedo, N.; Nehm, S. J.; Seefeldt, K. F.; Pagán-Torres, Y.; Falkiewicz, C. J., Reaction Crystallization of Pharmaceutical Molecular Complexes. *Mol Pharm* **2006**, *3* (3), 362-367.
17. Good, D. J.; Rodríguez-Hornedo, N., Solubility Advantage of Pharmaceutical Cocrystals. *Cryst Growth Des* **2009**, *9* (5), 2252-2264.
18. Nehm, S. J.; Rodríguez-Spong, B.; Rodríguez-Hornedo, N., Phase Solubility Diagrams of Cocrystals are Explained by Solubility Product and Solution Complexation. *Cryst Growth Des* **2006**, *6* (2), 592-600.
19. Maheshwari, C.; Andre, V.; Reddy, S.; Roy, L.; Duarte, T.; Rodríguez-Hornedo, N., Tailoring Aqueous Solubility of a Highly Soluble Compound via Cocrystallization: Effect of Coformer Ionization, pH(max) and Solute-solvent Interactions. *CrystEngComm* **2012**, *14* (14), 4801-4811.
20. Chadha, R.; Saini, A.; Arora, P.; Jain, D. S.; Dasgupta, A.; Row, T. N. G., Multicomponent Solids of Lamotrigine with Some Selected Coformers and their Characterization by Thermoanalytical, Spectroscopic and X-ray Diffraction Methods. *CrystEngComm* **2011**, *13* (20), 6271-6284.
21. Stahl, P. H.; Wermuth, C. G., *Handbook of Pharmaceutical Salts : Properties, Selection, and Use*. 2nd, rev. ed.; VHCA ; Weinheim : Wiley-VCH: Zürich, 2011; p xvi, 446 p.
22. Serajuddin, A. T. M.; Rosoff, M., pH-Solubility Profile of Papaverine Hydrochloride and Its Relationship to the Dissolution Rate of Sustained-Release Pellets. *J Pharm Sci* **1984**, *73* (9), 1203-1208.
23. Yalkowsky, S. H., *Solubility and Solubilization in Aqueous Media*. American Chemical Society; Oxford University Press: Washington, D.C.; New York; Oxford, 1999; p xvi, 464.
24. Bethune, S. J.; Huang, N.; Jayasankar, A.; Rodríguez-Hornedo, N., Understanding and Predicting the Effect of Cocrystal Components and pH on Cocrystal Solubility. *Cryst Growth Des* **2009**, *9* (9), 3976-3988.
25. Kuminek, G.; Rodríguez-Hornedo, N.; Siedler, S.; Rocha, H. V.; Cuffini, S. L.; Cardoso, S. G., How Cocrystals of Weakly Basic Drugs and Acidic Coformers Might Modulate Solubility and Stability. *ChemComm* **2016**, *52* (34), 5832-5.
26. Childs, S. L.; Wood, P. A.; Rodríguez-Hornedo, N.; Reddy, L. S.; Hardcastle, K. I., Analysis of 50 Crystal Structures Containing Carbamazepine Using the Materials Module of Mercury CSD. *Cryst Growth Des* **2009**, *9* (4), 1869-1888.
27. Floyd, A. G.; Jain, S. Pharmaceutical composition containing lamotrigine. 1997.
28. Thakral, N. K.; Behme, R. J.; Aburub, A.; Peterson, J. A.; Woods, T. A.; Diserod, B. A.; Suryanarayanan, R.; Stephenson, G. A., Salt Disproportionation in the Solid State: Role of Solubility and Counterion Volatility. *Mol Pharm* **2016**, *13* (12), 4141-4151.

29. Guo, J.; Elzinga, P. A.; Hageman, M. J.; Herron, J. N., Rapid Throughput Screening of Apparent KSP values for Weakly Basic Drugs Using 96-Well Format. *J Pharm Sci* **2008**, *97* (6), 2080-2090.
30. Serajuddin, A. T. M.; Sheen, P.-C.; Augustine, M. A., Common Ion Effect on Solubility and Dissolution Rate of the Sodium Salt of an Organic Acid. *J Pharm Pharmacol* **1987**, *39* (8), 587-591.
31. Kuminek, G.; Cao, F.; Bahia de Oliveira da Rocha, A.; Goncalves Cardoso, S.; Rodríguez-Hornedo, N., Cocrystals to Facilitate Delivery of Poorly Soluble Compounds Beyond-Rule-of-5. *Adv Drug Deliv Rev* **2016**, *101*, 143-66.
32. Alhalaweh, A.; Roy, L.; Rodríguez-Hornedo, N.; Velaga, S. P., pH-Dependent Solubility of Indomethacin-Saccharin and Carbamazepine-Saccharin Cocrystals in Aqueous Media. *Mol Pharm* **2012**, *9* (9), 2605-2612.
33. Huang, N.; Rodríguez-Hornedo, N., Engineering Cocrystal Solubility, Stability, and pH(max) by Micellar Solubilization. *J Pharm Sci* **2011**, *100* (12), 5219-34.
34. Lipert, M. P.; University of Michigan. Library. Deep Blue., Predicting the Influence of Drug Solubilizing Agents on Cocrystal Solubility, Stability, and Transition Points. 2015. <http://hdl.handle.net/2027.42/111365>.
35. Chen, Y. M.; Rodríguez-Hornedo, N., Cocrystals Mitigate Negative Effects of High pH on Solubility and Dissolution of a Basic Drug. *Cryst Growth Des* **2018**, *18* (3), 1358-1366.
36. Schultheiss, N.; Bethune, S.; Henck, J. O., Nutraceutical Cocrystals: Utilizing Pterostilbene as a Cocrystal Former. *CrystEngComm* **2010**, *12* (8), 2436-2442.
37. Bethune, S. J.; Schultheiss, N.; Henck, J. O., Improving the Poor Aqueous Solubility of Nutraceutical Compound Pterostilbene through Cocrystal Formation. *Cryst Growth Des* **2011**, *11* (7), 2817-2823.
38. Childs, S. L.; Rodríguez-Hornedo, N.; Reddy, L. S.; Jayasankar, A.; Maheshwari, C.; McCausland, L.; Shipplett, R.; Stahly, B. C., Screening Strategies based on Solubility and Solution Composition Generate Pharmaceutically Acceptable Cocrystals of Carbamazepine. *CrystEngComm* **2008**, *10* (7), 856-864.
39. Martin, F. A.; Pop, M. M.; Borodi, G.; Filip, X.; Kacso, I., Ketoconazole Salt and Cocrystals with Enhanced Aqueous Solubility. *Cryst Growth Des* **2013**, *13* (10), 4295-4304.
40. Bogardus, J. B.; Blackwood, R. K., Solubility of Doxycycline in Aqueous-Solution. *J Pharm Sci* **1979**, *68* (2), 188-194.
41. Serajuddin, A. T. M., Salt Formation to Improve Drug Solubility. *Adv Drug Deliv Rev* **2007**, *59* (7), 603-616.
42. Avdeef, A., Solubility of Sparingly-soluble Ionizable Drugs. *Adv Drug Deliv Rev* **2007**, *59* (7), 568-90.
43. Huang, K. S.; Britton, D.; Etter, M. C.; Byrn, S. R., A Novel Class of Phenol-Pyridine Co-crystals for Second Harmonic Generation. *J Mater Chem* **1997**, *7* (5), 713-720.

44. Bhogala, B. R.; Basavoju, S.; Nangia, A., Tape and Layer Structures in Cocrystals of Some Di- and Tricarboxylic Acids with 4,4 '-Bipyridines and Isonicotinamide. From Binary to Ternary Cocrystals. *CrystEngComm* **2005**, *7*, 551-562.
45. Childs, S. L.; Stahly, G. P.; Park, A., The Salt-Cocrystal Continuum: The Influence of Crystal Structure on Ionization State. *Mol Pharm* **2007**, *4* (3), 323-338.
46. Bhattachar, S. N.; Deschenes, L. A.; Wesley, J. A., Solubility: It's Not Just for Physical Chemists. *Drug Discov Today* **2006**, *11* (21-22), 1012-1018.
47. Elder, D. P.; Holm, R.; de Diego, H. L., Use of Pharmaceutical Salts and Cocrystals to Address the Issue of Poor Solubility. *Int J Pharm* **2013**, *453* (1), 88-100.

CHAPTER 3

Cocrystal Solubility Advantage and Dose/Solubility Ratio Diagrams: A Mechanistic Approach to Selecting Additives and Controlling Dissolution – Supersaturation – Precipitation Behavior

Introduction

Dissolution- and solubility-limited absorption remain two of the major challenges in oral drug delivery. The Biopharmaceutics Classification System (BCS) defines solubility and permeability as the primary factors that influence oral drug absorption.¹ BCS Class II drugs are categorized as having low solubility and high permeability, where drug dissolution is the rate-limiting step to absorption. However, for BCS Class II drugs with very high dose/solubility ratios ($D_{0D} = \text{dose concentration} / S_D$), absorption has been shown to be only weakly dependent on dissolution rate and instead becomes solubility-limited.² In fact, the Quantitative Biopharmaceutics Classification System defines Category II drugs as having high permeability ($P_{app} > 10^{-5}$ cm/s) and D_{0D} values greater than 1.³ These drugs display dose/solubility-limited absorption, which becomes more and more pronounced with higher D_{0D} values. Depending on the required dose of a poorly-soluble drug, development efforts to improve both dissolution and solubility must be made for successful oral drug delivery.

Supersaturating drug delivery systems such as cocrystals, salts, and amorphous forms have been shown to enhance the solubility of crystalline drug, which can lead to increases in drug dissolution rate, exposure, and oral bioavailability.⁴⁻⁹ While salts and amorphous forms

have been routinely utilized in clinical development and have resulted in numerous marketed products, cocrystals remain largely underutilized despite continuing to gain interest for their ability to improve the biopharmaceutical properties of poorly-soluble drugs.¹⁰

Cocrystals are defined as multicomponent crystals composed of two or more neutral molecular components in a single homogeneous crystalline phase with well-defined stoichiometry. Cocrystals are characterized in that the components are solids at room temperature, which distinguishes them from solvates, and that they are formed through noncovalent interactions, which distinguishes them from salts.^{11, 12} When a poorly-soluble parent drug is cocrystallized with a highly soluble, generally regarded as safe (GRAS) cofomer, pharmaceutical cocrystals have been shown to impart solubility advantage orders of magnitude higher than parent drug.^{4, 13-15}

However, highly soluble, metastable cocrystals may appear to be risky to develop due to their vulnerability to convert to less soluble forms. Several studies have shown the ability of additives, both solubilizing and non-solubilizing, to improve the dissolution – supersaturation – precipitation (DSP) behavior of cocrystal systems.^{13, 16-23} One such study by Childs et al. demonstrated the ability of 1:1 danazol-vanillin cocrystal (DNZ-VAN) to sustain supersaturation and achieve 10 times higher area under the curve (AUC) *in vivo* than danazol drug (DNZ) in the presence of a solubilizing agent and a precipitation inhibitor, compared to only 1.7 times AUC increase and rapid conversion in the absence of additives.²⁴ While this study represents a landmark in demonstrating the “Essential Role” of cocrystal formulation, selecting additives in attempt to control DSP behavior of cocrystal systems remains a largely empirical and time-consuming process.

Without knowledge of thermodynamic solubility, interpreting cocrystal concentration – time profiles and their DSP behavior is difficult. Cocrystal solubility advantage over drug ($SA = S_{CC} / S_D$) is an important thermodynamic parameter that represents both the potential for drug supersaturation and the risk for drug precipitation. Likewise, D_{0D} and cocrystal dose/solubility ratio ($D_{0CC} = \text{dose concentration} / S_{CC}$) represent the extent of dose/solubility-limited absorption, but also whether drug supersaturation, or even saturation, may be dose-limited. Optimizing thermodynamic parameters SA , D_{0D} , and D_{0CC} is essential in order to achieve desired DSP behavior, and may be complemented through the kinetic role of precipitation and growth inhibitors. Previous studies from our laboratory have demonstrated the influence of solubilizing additives on thermodynamic cocrystal stability,²⁵⁻²⁷ and the log-log linear relationship between SA and the drug-solubilizing power of surfactants ($SP_D = S_{D,T} / S_{D,aq}$) has been shown.^{4, 17} This mathematical relationship suggests that SA can be fine-tuned as a function of SP_D through rational selection of solubilizing additives and their concentrations, and has thus far only been validated as a tool to optimize DSP behavior for one other cocrystal system.¹⁷ While D_{0D} has recently been shown to be a valuable parameter for interpreting cocrystal dissolution data,²⁸ the mathematical relationship of D_{0D} with SP_D has yet to be considered.

The purpose of the present study is to evaluate a mechanistic approach for rational additive selection by (1) fine-tuning SP_D , (2) predictably modulating SA and D_{0D} values to be near or below critical drug supersaturation, and ultimately (3) determining the interplay between thermodynamic and kinetic processes to optimize DSP behavior of cocrystal systems that sustain drug supersaturation and increase drug exposure. Drug solubilizers can have a two-fold effect: (a) to alter the thermodynamic driving force for precipitation (SA), and (b) to interfere with the kinetic processes of molecular self-association for drug nucleation and growth.

Based on the important results of Childs et al., DNZ-VAN was chosen as a model cocrystal.²⁴ DNZ is a nonionizable, BCS Class II drug with low oral bioavailability and positive food-effect pharmacokinetics, and it has been shown to be readily solubilized by a variety of additives.^{24, 29-33} Vanillin (VAN) is GRAS, nonionized across physiological pH, and over 100,000 times more soluble than DNZ in aqueous conditions at 37°C. In this work, DNZ-VAN is shown to have an aqueous SA of 183, leaving it prone to rapid phase conversion. Additives that have been shown to preferentially solubilize DNZ over VAN were selected at concentrations that lower SA. These included D- α Tocopherol polyethylene glycol 1000 succinate (TPGS) and Soluplus. Experimental results demonstrate how cocrystal SA and D_{0D} can be predictably modulated as a function of SP_D , and their relationships provide a mechanistic basis for rational additive selection and a framework for understanding and controlling thermodynamic and kinetic cocrystal behavior.

Theoretical

The goal of this section is to describe the theoretical basis for the mathematical relationships that define how cocrystal SA and drug D_{0D} can be predictably modulated as a function of SP_D and used to calculate the fraction of the cocrystal initial mass that can dissolve the drug dose (without drug precipitation). It is recognized that cocrystal dissolution may not achieve cocrystal SA for two main reasons: (1) the dose is not enough to reach cocrystal solubility, or (2) the threshold supersaturation for drug nucleation is below SA, which represents the maximum theoretical supersaturation. Throughout this text, the term supersaturation refers to the drug and the cocrystal relationships are based on a 1:1 cocrystal stoichiometry.

SA and D_{0D} can be used to assess and optimize relative cocrystal stability. Considering both parameters is important to provide a holistic framework for determining the risk of cocrystal conversion based on whether supersaturation is limited by S_{CC} (described by SA) or the dose concentration C_{dose} (described by D_{0D}). When $SA = D_{0D}$, $D_{0CC} = 1$ and there is a transition between supersaturation limited by S_{CC} and that limited by C_{dose} .

SA is calculated as the molar ratio of cocrystal to drug solubilities (S_{CC} and S_D , respectively) measured under the same conditions (solvent, temperature, pH, additive concentration, etc.) as

$$SA = \frac{S_{CC}}{S_D} \quad (3.1)$$

In the absence of drug solubilizers, SA becomes SA_{aq} and refers to the solubility advantage under aqueous conditions, as

$$SA_{aq} = \frac{S_{CC,aq}}{S_{D,aq}}$$

where $S_{CC,aq}$ and $S_{D,aq}$ represent aqueous cocrystal and drug solubilities, respectively. In the presence of drug solubilizers, the total SA (SA_T) is the sum of solubilized (micellar) and free (aqueous pseudophase) contributions, as

$$SA_T = \frac{S_{CC,T}}{S_{D,T}}$$

where $S_{CC,T}$ and $S_{D,T}$ represent total cocrystal and drug solubilities in the presence of drug solubilizers. SA is used when the reference could apply to both SA_{aq} and SA_T .

SP_D is the solubilization power of the additive for the drug and is obtained from

$$SP_D = \frac{S_{D,T}}{S_{D,aq}} \quad (3.2)$$

where $S_{D,T}$ represents drug solubility in the presence of an additive, and $S_{D,aq}$ represents aqueous drug solubility.

The influence of additives on SA_T can be calculated from knowledge of SA_{aq} and SP_D according to

$$SA_T = \frac{SA_{aq}}{\sqrt{SP_D}} \quad (3.3)$$

or, in logarithmic form,

$$\log SA_T = \log SA_{aq} - \frac{1}{2} \log SP_D \quad (3.4)$$

These equations have been previously described and applied to several different cocrystals and additives.^{4,17} Equations 3.3 and 3.4 assume negligible cofomer solubilization, and therefore generally apply to cocrystals of hydrophobic drugs and hydrophilic cofomers. Experimental measurements confirm the validity of this assumption with the present study. The impact of cofomer solubilization on SP_D has been previously presented,²⁵ which leads to nonlinear and positive deviations from the linear $\log SA_T - \log SP_D$ behavior of Equation 3.4.

Equation 3.4 clearly suggests that cocrystal SA_T can be fine-tuned by varying SP_D as a function of drug-solubilizing agents and their concentrations in order to control cocrystal inherent supersaturation. However, if the dissolved dose is below S_{CC} ($C_{dose} < S_{CC}$) then the theoretical maximum bulk supersaturation will be lower than SA_T . For this case, SA_T may still be representative of supersaturation at the solid-liquid interfaces (interfacial supersaturation),³⁴ but the well-recognized dimensionless parameter D_{0D} , referred to as both dose/solubility ratio and dose number,^{2,3} is representative of the maximum theoretical bulk supersaturation. D_{0D} has been defined as

$$D_{0(D)} = \frac{C_{dose}}{S_D} \quad (3.5)$$

where C_{dose} is the dose concentration, calculated as the dose per volume taken with dose or luminal volume (250 mL), and S_D is drug solubility. D_{0D} can be calculated under aqueous conditions ($D_{0D,aq}$) as a function of $S_{D,aq}$, or in the presence of an additive ($D_{0D,T}$) as a function of

$S_{D,T}$. D_{0D} is used when the reference could apply to both $D_{0D,aq}$ and $D_{0D,T}$. D_{0CC} can also be calculated as a function of S_{CC} as

$$D_{0(CC)} = \frac{C_{dose}}{S_{CC}} \quad (3.6)$$

where C_{dose} is the drug equivalent dose concentration, and S_{CC} is cocrystal solubility. D_{0CC} can be calculated under aqueous conditions ($D_{0CC,aq}$) as a function of $S_{CC,aq}$, or in the presence of an additive ($D_{0CC,T}$) as a function of $S_{CC,T}$. D_{0CC} is used when the reference could apply to both $D_{0CC,aq}$ and $D_{0CC,T}$.

According to Equations 3.2 and 3.5, $D_{0D,aq}$, $D_{0D,T}$, and SP_D can be mathematically related as

$$D_{0,T(D)} = \frac{D_{0,aq(D)}}{SP_D} \quad (3.7)$$

In logarithmic form, Equation 3.7 becomes a linear function:

$$\log D_{0,T(D)} = \log D_{0,aq(D)} - \log SP_D \quad (3.8)$$

Similar to Equation 3.4, Equation 3.8 suggests that $D_{0D,T}$ can be fine-tuned as a function of SP_D . Because $D_{0D,T}$, $D_{0D,aq}$, and SP_D are functions of drug solubility, Equations 3.7 and 3.8 are independent of cocrystal solubility and stoichiometry.

SA_T represents the theoretical maximum supersaturation as a function of S_{CC} , while $D_{0D,T}$ represents the theoretical maximum achievable supersaturation as a function of the drug dose. When $D_{0D} > SA$, cocrystal will not fully dissolve the drug dose even if it reaches cocrystal saturation at SA . Therefore, the maximum theoretical supersaturation is limited by S_{CC} and is quantified by SA . When $D_{0D} < SA$, cocrystal can fully dissolve the dose, since $C_{dose} < S_{CC}$ and the maximum theoretical supersaturation is limited by C_{dose} and is quantified by D_{0D} .

While SA and D_{0D} represent a theoretical, thermodynamic limit to supersaturation, critical supersaturation for drug precipitation or phase separation represents a practical, kinetic

limit to the concentrations that a supersaturating drug delivery system may achieve or sustain. Spontaneous and instantaneous nucleation will occur above critical supersaturation, which will ultimately lead to rapid precipitation and decreased drug exposure. Modulating SA_T and $D_{0D,T}$ as a function of SP_D to limit the maximum theoretical bulk supersaturation to be near or below critical supersaturation will reduce the driving force for rapid conversion and therefore promote sustained supersaturation. However, if SA_T and $D_{0D,T}$ are modulated to low values, then the ability to generate any meaningful supersaturation could be negated. This is especially relevant for systems with low C_{dose} values, where bulk supersaturation could inadvertently be dose-limited even when $SA > 1$. Furthermore, because cocrystals with $SA > D_0$ may still generate interfacial supersaturation as high as SA ,³⁴ it is important to be cognizant of the risk of rapid precipitation on the cocrystal surface that may hinder cocrystal dissolution and thereby limit bulk supersaturation.

Materials and Methods

Materials

Anhydrous DNZ was received as a gift from Renovo Research (Atlanta, GA). VAN was purchased from Fisher Chemical (Fair Lawn, NJ). D- α Tocopherol polyethylene glycol 1000 succinate (TPGS) was purchased from Sigma-Aldrich (St. Louis, MO). KlucelTM LF PHARM hydroxypropylcellulose (HPC) was received as a gift from Ashland (Wilmington, DE). Polyvinyl caprolactam – polyvinyl acetate – polyethylene glycol graft co-polymer (Soluplus[®]) was received as a gift from BASF (Florham Park, NJ).

Trifluoroacetic acid and sodium chloride were purchased from Sigma-Aldrich (St. Louis, MO). Sodium hydroxide and n-Heptane were purchased from J. T. Baker Chemical Company

(Philipsburg, NJ). Ethyl acetate was purchased from Acros Organics (Morris, NJ). High performance liquid chromatography (HPLC)-grade methanol and sodium phosphate monobasic monohydrate were purchased from Fisher Scientific (Fair Lawn, NJ). FaSSIF/FeSSIF/FaSSGF powder was purchased from Biorelevant.com Ltd (London, UK). All materials were used as received.

Cocrystal Synthesis

DNZ-VAN cocrystal²⁴ was prepared by reaction crystallization method³⁵ at room temperature. 450 mg DNZ and 60 mg VAN were added to 10 mL of saturated VAN solution in 1:2 ethyl acetate:heptane. The vial was then diluted with 4 mL of 1:2 ethyl acetate:heptane and allowed to stir for 24 hours. Suspensions were vacuum-filtered, and solids were analyzed by X-ray powder diffraction (XRPD) and differential scanning calorimetry (DSC). The effect of coformer impurity on cocrystal solubility and SA is shown in Appendix 3A.

Media Preparation

Phosphate buffer at pH 6.5 ± 0.1 (blank FaSSIF) was prepared at room temperature by dissolving 0.840 g of NaOH (pellets), 7.908 g of $\text{NaH}_2\text{PO}_4 \cdot \text{H}_2\text{O}$, and 12.372 g of NaCl in 2 L of purified deionized (DI) water. Acetate buffer at pH 5.0 ± 0.1 (blank FeSSIF) was prepared at room temperature by dissolving 4.040 g of NaOH (pellets), 8.650 g of acetic acid, and 11.87 g NaCl in 1 L of purified deionized (DI) water. The pH of the buffers was adjusted with 1 M NaOH or 1 M HCl solutions. FaSSIF and FeSSIF were prepared with the corresponding blank medium and FaSSIF/FeSSIF/FaSSGF powder according to manufacturer protocol. To prepare additive solutions, Soluplus, TPGS, and/or HPC were dissolved in pH 6.5 phosphate buffer at predetermined weight:volume (w/v) ratios. For media containing FaSSIF + Soluplus, TPGS, and/or HPC, twice concentrated FaSSIF and additive solutions were prepared and combined in

equal volumes (e.g., 15 mL 2× FaSSIF and 15 mL pH 6.5 phosphate buffer + 2% TPGS were combined to yield 30 mL FaSSIF + 1% TPGS). Molar concentrations of surfactant media are presented in Appendix 3B. Media were stored at room temperature, and all media containing FaSSIF or FeSSIF were used within 48 hours.

Eutectic Concentrations

Drug and coformer eutectic concentrations ($[\text{DNZ}]_{\text{eu}}$ and $[\text{VAN}]_{\text{eu}}$, respectively) were measured at the eutectic point, where the drug and cocrystal solid phases were in equilibrium with solution.^{4, 15, 27} Eutectic concentrations represent the total analytical concentrations of all species in solution. The eutectic point was approached by suspending excess cocrystal (150 mg) and drug (100 mg) in 3 mL of solution. The suspensions were kept in a 37.0 (\pm 1.0) °C water bath and magnetically stirred for up to 96 h. 0.5 mL aliquots of the suspensions were collected every 24 h and filtered through a 0.45 μm pore cellulose acetate membrane via centrifugation. pH of the filtered supernatant was measured. DNZ and VAN solution concentrations were analyzed by HPLC. Solid phases were analyzed by XRPD and DSC to verify the presence of both drug and cocrystal solid phases.

Eutectic Constant, Cocrystal Solubility, and Solubility Product

The eutectic constant K_{eu} , a key stability indicator defined as the ratio of coformer to drug eutectic concentrations,³⁶ was calculated according to

$$K_{\text{eu}} = \frac{[\text{VAN}]_{\text{eu}}}{[\text{DNZ}]_{\text{eu}}} \quad (3.9)$$

Cocrystal SA was calculated according to

$$SA = \sqrt{K_{\text{eu}}} \quad (3.10)$$

Cocrystal solubilities were calculated according to

$$S_{\text{CC}} = \sqrt{[\text{DNZ}]_{\text{eu}} [\text{VAN}]_{\text{eu}}} \quad (3.11)$$

The solubility product K_{sp} was calculated according to

$$K_{sp} = [\text{DNZ}]_{eu} [\text{VAN}]_{eu} \quad (3.12)$$

It should be noted that Equations 3.10, 3.11, and 3.12 only apply to 1:1 cocrystals. The reader is referred to the general $SA-K_{eu}$,³⁷ S_{CC} ,^{15, 38} and K_{sp} ^{15, 38} equations for cocrystals of other stoichiometries. Additionally, Equation 3.12 only applies when the component species are in the same molecular state as the cocrystal. For cocrystals or solution conditions where constituents are ionized at the eutectic point, nonionized eutectic species must be used to calculate K_{sp} .^{13, 14, 39}

Drug solubilities are reported as the eutectic drug concentrations and were used to calculate SP_D according to Equation 3.2. D_{0D} and D_{0CC} values were calculated according to Equations 3.5 and 3.6 from molar dose concentration and solubility values.

Cocrystal and Drug Powder Dissolution

Powder dissolution studies of drug or cocrystal were conducted in a water bath at 37.0 (\pm 1.0) °C using an overhead stirrer with a glass propeller at 100 rpm over two hours. The cocrystal and drug were sieved to a particle size range of 45 to 106 μm . Based on a 200 mg dose in 250 mL, 24 mg DNZ drug or 34.8 mg DNZ-VAN cocrystal (molar equivalent DNZ amount) were added to 30 mL of dissolution media. 0.5 mL aliquots were sampled with a syringe at time points up to two hours. The solution samples were filtered through syringe filter with PVDF membrane of a pore size of 0.45 μm . Initial solution pH was measured, as well as the pH of all aliquots. The solution concentrations of DNZ and VAN were analyzed by HPLC. Percentage cocrystal dissolved for 1:1 DNZ-VAN was calculated according to

$$\% \text{ cocrystal dissolved} = 100 \frac{\text{moles coformer dissolved}}{\text{initial moles cocrystal added}} \quad (3.13)$$

Percentage cocrystal dissolved represents the percentage of the initial cocrystal mass that has dissolved, and it does not represent drug concentrations in solution if the drug precipitates.

However, the cofomer solution concentrations are related to the mass of cocrystal dissolved as cofomer does not precipitate. Final solid phases were analyzed by DSC.

High Performance Liquid Chromatography (HPLC)

DNZ and VAN concentrations were analyzed by a Waters HPLC equipped with a UV spectrometer detector. A Waters Atlantis C18 column with 5 μm , 250 \times 4.6 mm dimensions was used for separation. The mobile phase composed of 80% methanol and 20% water + 0.1% trifluoroacetic acid. The flow was set at 1 mL/min, and the sample injection volume was 20 μL . Component absorbance was monitored at 285 nm for DNZ and 295 nm for VAN.

X-ray Powder Diffraction (XRPD)

X-ray powder diffractograms of solid phases were recorded on a benchtop Rigaku Miniflex X-ray diffractometer (Danvers, MA) using Cu-K α radiation ($\lambda = 1.54 \text{ \AA}$), a tube voltage of 30 kV, and a tube current of 15 mA. Data were collected between 5° and 40° in 2θ at a continuous scan rate of 2.5°/min.

Thermal Analysis

A TA Instruments DSC (Newark, DE) was used to analyze dried solid phases. Thermal measurements were performed by heating the samples at a rate of 10 °C/min under a dry nitrogen atmosphere (50 mL/min). Standard aluminum sample pans and lids were used for all measurements.

Inverted Light Microscopy

Cocrystal dissolution samples were visually inspected under bright field microscopy using a Leica DMI8 inverted optical microscope (Wetzlar, Germany). Upon sampling, 100 μL of dissolution aliquots were immediately transferred (before filtering) into a quartz 96-well plate to be observed under the microscope. Images were taken with a Leica DMC2900 camera

controlled with LAS v4.7 software (Leica Microsystems, Wetzlar, Germany). The 20x magnification lens was used for all observations.

Results and Discussion

Aqueous Cocrystal Solubility and Stability

Childs et. al. demonstrated the inability of DNZ-VAN cocrystal to sustain supersaturation during *in vitro* and *in vivo* studies in aqueous conditions. While the cocrystal showed enhanced dissolution behavior compared to drug, rapid conversion led to only a modest 1.7 times increase in AUC.²⁴

In this study, aqueous cocrystal solubility and stability were assessed by measuring constituent concentrations at the eutectic point, where cocrystal and drug solid phases are in equilibrium with solution.¹⁵ Cocrystal solubility represents the equilibrium solubility under stoichiometric conditions. Its value was calculated from the experimentally accessible thermodynamic condition at the eutectic point, as described in the methods section. The cocrystal solubility serves as a means to assess the potential to generate drug supersaturation and nucleation during cocrystal dissolution, even though it may not be experimentally achieved. Table 3.1 summarizes drug and coformer eutectic concentrations and the relevant solubility and stability parameters that can be calculated from them. $[\text{DNZ}]_{\text{eu}} = S_{\text{DNZ}}$ under the studied experimental conditions.

Table 3.1. Aqueous Cocrystal Solubility and Stability.

Parameter	Equation Number	Calculation	Value
$[\text{DNZ}]_{\text{eu}}$ ^{ab}	-	-	$(9.1 \pm 0.5) \times 10^{-4}$ mM
$[\text{VAN}]_{\text{eu}}$ ^a	-	-	30.3 ± 0.6 mM
$S_{\text{CC, aq}}$	3.11	$([\text{DNZ}]_{\text{eu}} [\text{VAN}]_{\text{eu}})^{1/2}$	$(1.7 \pm 0.1) \times 10^{-1}$ mM
K_{sp}	3.12	$[\text{DNZ}]_{\text{eu}} [\text{VAN}]_{\text{eu}}$ ^c	$(2.6 \pm 0.1) \times 10^{-8}$ M ² ^d
$\text{p}K_{\text{sp}}$	-	$-\log(K_{\text{sp}})$	7.6 ^d
K_{eu}	3.9	$[\text{VAN}]_{\text{eu}} / [\text{DNZ}]_{\text{eu}}$	33483 ± 2003
SA_{aq}	3.10	$S_{\text{CC, aq}} / S_{\text{D, aq}} = K_{\text{eu}}^{1/2}$	183 ± 12
$D_{0\text{D, aq}}$	3.5	$C_{\text{dose}} / S_{\text{D, aq}}$	2617 ± 148 ^e
$D_{0\text{CC, aq}}$	3.6	$C_{\text{dose}} / S_{\text{CC, aq}}$	14.3 ± 0.4 ^e

^a Eutectic concentrations were measured in pH 6.5 phosphate buffer at 37°C. Final pH was 6.28.

^b $[\text{DNZ}]_{\text{eu}} = S_{\text{D}}$ under the studied conditions.

^c K_{sp} is calculated as the product of the constituent concentrations in the same molecular state as the cocrystal (i.e. neutral). DNZ-VAN components are nonionized at pH 6.28. The reader is cautioned from using total analytical concentrations to calculate K_{sp} when cocrystal components are ionized at the eutectic point.^{38, 40}

^d Previously reported K_{sp} and $\text{p}K_{\text{sp}}$ values for DNZ-VAN were calculated from measurements at 25°C.^{40, 41}

^e Calculated based on a 200 mg DNZ dose in 250 mL luminal volume.

The results show that DNZ-VAN cocrystal is 183 times more soluble than DNZ drug under aqueous conditions, which is about an order of magnitude higher than critical supersaturation.^{24, 42-49} As a result, the ability of the cocrystal to initially generate high supersaturation during dissolution studies by Childs et. al. was quickly overcome by drug precipitation, essentially negating the cocrystal solubility advantage.²⁴

Cocrystal SA_{aq} was evaluated according to Equations 3.9 and 3.10 from eutectic concentration measurements and eutectic constant relationship (K_{eu}). K_{eu} is well recognized to be a key indicator of cocrystal stability/risk of conversion.³⁶ For a 1:1 cocrystal, a K_{eu} value of 1 indicates a transition point where drug and cocrystal solubilities are equal. When $K_{\text{eu}} > 1$, the

cocrystal has solubility advantage over drug ($SA > 1$); when $K_{eu} < 1$, the cocrystal is less soluble and more stable than drug ($SA < 1$). K_{eu} of 33483 is indicative of a highly soluble cocrystal.

Cocrystal SA can also be calculated as the ratio of cocrystal solubility (Equation 3.11) to drug solubility ($[DNZ]_{eu}$). SA values calculated from K_{eu} versus the ratio of cocrystal to drug solubilities may differ slightly due to experimental error propagation.

Solubility product K_{sp} was calculated according to Equation 3.12 as the product of the cocrystal components in the same molecular state as the cocrystal. DNZ-VAN constituents are nonionized at equilibrium pH 6.28, and therefore in this case the total analytical concentrations are the neutral species. K_{sp} values are proportional to cocrystal intrinsic solubility. Because the values are very small, it is common to express them as pK_{sp} values, where $pK_{sp} = -\log(K_{sp})$ and higher K_{sp} corresponds to lower pK_{sp} . 1:1 cocrystals of BCS Class II drugs have been reported to have pK_{sp} values in the range of 1 – 9.⁴⁰

Like many BCS Class II drugs, DNZ has a very high $D_{0D} = 2617$ under aqueous conditions, meaning that the C_{dose} of a 200 mg dose in 250 mL luminal volume is over 2000 times the drug solubility. Increased solubility of the cocrystal resulted in a much lower $D_{0CC} = 14.3$, meaning that the cocrystal will be able to dissolve a much greater fraction of the dose, and may even result in complete dose dissolution with the dynamic process of drug absorption.

While the parameters in Table 3.1 demonstrate the high aqueous solubility of DNZ-VAN and the potential of the cocrystal to overcome some of the challenges associated with the poorly water-soluble parent drug, an unnecessarily high SA_{aq} value allowed critical supersaturation to be more quickly reached, left the cocrystal at high risk for rapid phase conversion, and ultimately negated the cocrystal solubility advantage in studies by Childs et. al.²⁴ In order for cocrystals to be an effective development strategy to enhance drug exposure, cocrystal formulations should

consider both the thermodynamically possible and kinetically sustainable supersaturations that they generate.

Using Solubilizing Additives to Decrease Unnecessarily High Cocystal Solubility Advantage (SA)

DNZ and VAN eutectic concentrations were measured in blank and different additive media and are shown along with K_{eu} values in Figure 3.1. Results show that $K_{eu} > 1$ in all studied solution conditions, indicating that DNZ-VAN has solubility advantage over DNZ, or $SA > 1$. K_{eu} decreased with the increase of $[DNZ]_{eu}$ in biorelevant media, and K_{eu} further decreased in FaSSIF with solubilizing agents such as TPGS and Soluplus, which were selected based on their known ability to solubilize the drug and improve cocystal dissolution/supersaturation behavior.^{24, 33} This indicates that cocystal SA is reduced by the preferential solubilization of drug over coformer.

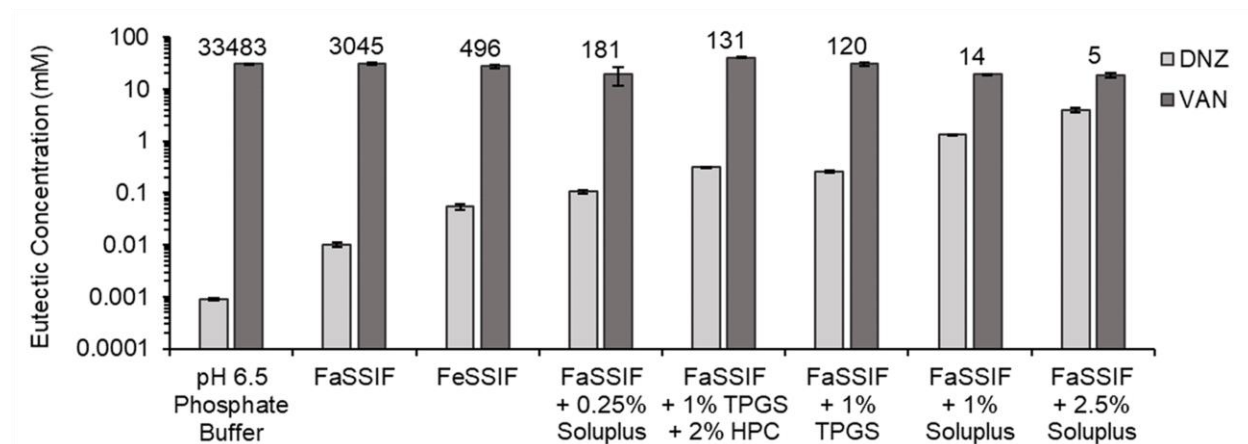


Figure 3.1. Danazol (DNZ) and vanillin (VAN) eutectic concentrations in both the presence and absence of different additives. $[DNZ]_{eu}$ is the drug solubility under the solution conditions studied. Numbers above bars represent K_{eu} values calculated from Equation 3.9. Initial pH was 6.5 and equilibrium pH values were 6.28 – 6.51 for all media except FeSSIF, which had an initial pH 5.0 and an equilibrium pH 4.95. pH values for each media are reported in Table 3.2. Error bars represent standard deviations.

Figure 3.2 shows the predicted and experimental SA- K_{eu} relationship according to the logarithmic form of Equation 3.10:

$$\log SA = \frac{1}{2} \log K_{eu} \quad (3.14)$$

The results indicate excellent agreement between the observed and predicted behavior of K_{eu} and SA. K_{eu} and SA are observed to decrease with increasing surfactant concentration, even though both drug solubility ($[DNZ]_{eu}$) and cocrystal solubility values increase (Figure 3.1 and Table 3.2). These trends are in agreement with previous findings from our laboratory on the behavior of cocrystals and drugs in the presence of surfactants.^{25, 26}

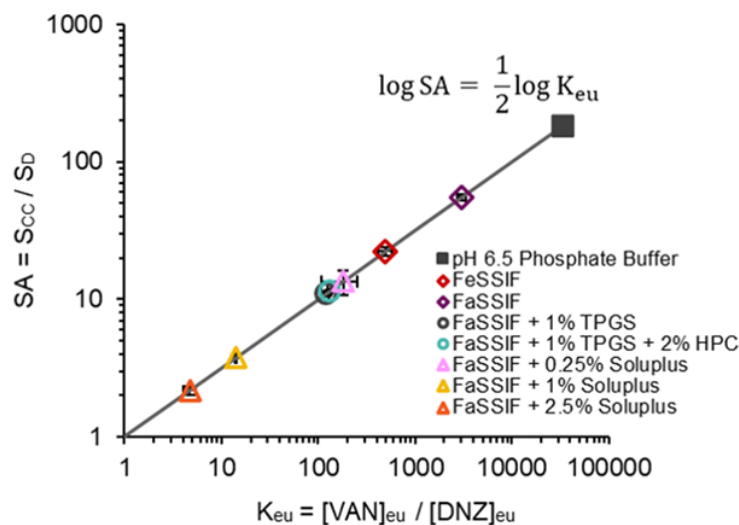


Figure 3.2. Predicted relationship between cocrystal solubility advantage (SA) and eutectic constant K_{eu} for 1:1 danazol – vanillin cocrystal (CC) and danazol drug (D). Symbols represent values calculated from experimental danazol (DNZ) and vanillin (VAN) eutectic concentrations (Figure 3.1 and Appendix 3B). Error bars (within the points) represent standard deviations.

Table 3.2. Cocrystal Solubility, Eutectic Constant K_{eu} , and Solubility Advantage (SA).

Additive(s)	$S_{DNZ-VAN}$ (mM) ^a	K_{eu} ^b	SA ^c	Final pH ^d
-	$(1.7 \pm 0.1) \times 10^{-1}$	33483 ± 2003	183 ± 5	6.28 ± 0.01
FaSSIF	$(5.6 \pm 0.3) \times 10^{-1}$	3045 ± 282	55 ± 3	6.33 ± 0.01
FeSSIF	1.2 ± 0.2	496 ± 77	22 ± 2	4.95 ± 0.01
FaSSIF + 0.25% Soluplus	1.4 ± 0.6	181 ± 72	13 ± 3	6.49 ± 0.05
FaSSIF + 1% TPGS + 2% HPC	3.6 ± 0.1	131 ± 6	11.5 ± 0.2	6.30 ± 0.01
1% TPGS + 2% HPC	3.4 ± 0.1	130 ± 4	11.4 ± 0.4	6.33 ± 0.01
FaSSIF + 1% TPGS	2.8 ± 0.1	120 ± 11	10.9 ± 0.5	6.37 ± 0.01
FaSSIF + 1% Soluplus	5.1 ± 0.1	14.0 ± 0.3	3.75 ± 0.04	6.51 ± 0.01
FaSSIF + 2.5% Soluplus	8.6 ± 1.2	4.7 ± 0.7	2.2 ± 0.2	6.50 ± 0.01

^a Calculated from $[DNZ]_{eu}$ and $[VAN]_{eu}$ in Appendix 3B according to Equation 3.11.

^b Calculated from $[DNZ]_{eu}$ and $[VAN]_{eu}$ in Appendix 3B according to Equation 3.9.

^c Calculated from K_{eu} values according to Equation 3.10.

^d Initial pH was 6.5 ± 0.1 for all studies except FeSSIF, which had an initial pH 5.0 ± 0.1 .

Importantly, these results also show that the addition of 2% HPC to 1% TPGS solutions did not affect K_{eu} nor SA. This finding is in agreement with that suggested by Childs et al., where HPC was classified as a precipitation inhibitor and not as a solubilizing agent.²⁴ Drug solubilization by 1% TPGS >>> drug solubilization by FaSSIF and its presence did not influence K_{eu} . Finally, because DNZ is a nonionizable drug and VAN is an acid with pK_a 7.4, DNZ-VAN cocrystal is expected to be predominantly nonionized at pH 5.0 – 6.5. Equilibrium pH values for solubility studies are reported in Table 3.2, although S_{CC} is not expected to change as a function of pH in the present study.

Modulation of Cocrystal Solubility Advantage (SA) and Critical Supersaturation

Figure 3.3 shows the SA – SP diagram for DNZ-VAN cocrystal. The SA – SP relationship is predicted according to $SA_{aq} = 183$ and Equation 3.4:

$$\log SA_T = \log SA_{aq} - \frac{1}{2} \log SP_D$$

Predicted line has a characteristic slope of -1/2 for 1:1 cocrystals. Points represent SP_D values calculated according to Equation 3.2 and values in Appendix 3B, and SA values in Table 3.2.

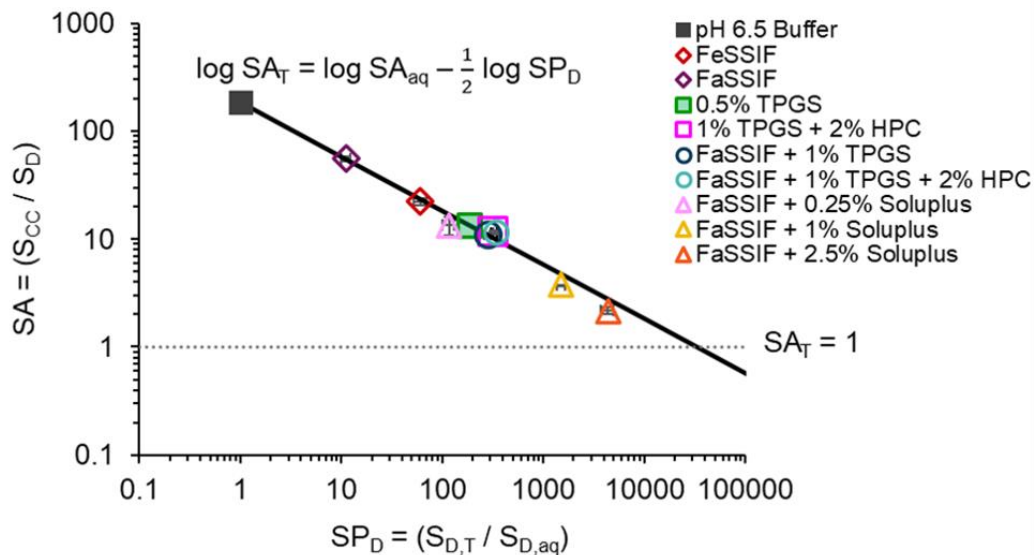


Figure 3.3. Cocrysal SA – SP diagram shows the linear dependence of log cocrysal solubility advantage (SA) on log drug solubilization power (SP_D) predicted from Equation 3.4. Symbols represent SA and SP_D values calculated from experimental measurements of drug (danazol) and cofomer (vanillin) eutectic concentrations (Appendix 3B). 0.5% TPGS SP_D and SA_T values were estimated from $S_{D,T} = 0.17$ mM reported by Childs et. al., $S_{D,aq}$ and SA_{aq} in Table 3.1, and Equation 3.3. Transition point $SA_T = 1$ shows where cocrysal and drug solubilities are equal and above which the cocrysal generates supersaturation with respect to the drug. Error bars (within the points) represent standard deviations of SA and SP_D .

The SA-SP diagram shows that cocrysal SA can be predictably modulated as a function of increasing SP_D , as $SA_{aq} = 183$ was modulated all the way to $SA_T = 2.2$ with FaSSIF + 2.5% Soluplus. Across the studied range, there is excellent agreement between the predicted and experimentally calculated SA and SP_D values, as has been shown for other cocrysal.^{4,17} The prediction is also independent of surfactant type, including both biorelevant and synthetic solubilizers. Formulations may require lower additive concentrations due to toxicity, such as for 1% TPGS.^{50,51} In this case, multiple solubilizing additives may be selected so that the targeted SP_D and SA values are reached at additive concentrations below GRAS values.

Literature examples have demonstrated various methods for generating DNZ supersaturation (i.e. cocrystals, amorphous solid dispersions, lipolysis-triggered, solvent-shift, etc.), with observed maximum supersaturation values (σ_{\max}) in the range of 2 – 10.^{24, 42-49} In this study, aqueous and biorelevant media corresponded to $SA \geq 22$, values that are likely much higher than DNZ critical supersaturation and leave the cocrystal at high risk to undergo rapid phase conversion during dissolution. The $SA - SP_D$ predicted relationship provides a means to tailor SA considering the critical supersaturation and the metastable zone for drug precipitation. The corresponding SP_D determines the selection of additional solubilizers and their concentrations. In our studies an $SA_T \leq 13$, which is near or below DNZ critical supersaturation, was achieved by the addition of $\geq 0.5\%$ TPGS or $\geq 0.25\%$ Soluplus to FaSSIF. $SA_T = 10.9 - 13$ corresponded to $SP_D = 117 - 343$. Lower SA_T values (2.2 – 3.75) were further obtained with higher SP_D values (1497 – 4364).

The basis of the SA - SP diagram is the different dependence of cocrystal and drug solubilities on additive solubilization and concentration, that changes SA_T in a predictable manner.^{4, 17, 26} Solubilizers in this work are micellar surfactants, and the relationship applies to other drug solubilizing approaches if the underlying mechanism is the differential selectivity of drug and coformer by an additive (where the coformer affinity is negligible compared to that of the drug).

Another important insight from the SA - SP diagram is that cocrystal SA_T is equal to the ratio of free or aqueous drug available for absorption in the aqueous pseudophase (SA_{aq}),

$$SA_T = SA_{aq} \quad (3.15)$$

where

$$SA_{aq} = \frac{S_{CC,aq}}{S_{D,aq}} \quad (3.16)$$

and will guide solubilizer selection that is not detrimental to drug absorption. The subscript T refers to the sum of free (aqueous) and bound (micellar) drug. Derivation is shown in SI. In the earlier section of this manuscript the term SA_{aq} referred to conditions without drug solubilizing agents, where SA_{aq} has its highest value.

Recent findings have shown that when micellar solubilization is used as a solubility enhancement technique for lipophilic drugs (single component phase), the surfactants can have a negative impact on intestinal drug permeation and absorption.^{52, 53} This is a result of the interplay between free drug, which is available for absorption, and bound drug solubilized by the micelle, which is not. With increasing surfactant concentration, the saturated concentration of free drug species in solution ($[D]_{aq}$) remains constant while the bound drug species ($[D]_{micellar}$) increases as shown in Fig. 4a. This trend is not the same for cocrystals where both free and bound drug concentrations change. The free drug concentration decreases with increasing drug solubilization as shown in Fig. 4b. The bound drug concentration increases but has a weaker dependence on drug solubilization than the single component drug phase. Thus, one has the option to select conditions that reduce the free drug concentration with cocrystals while maintaining a free drug concentration advantage over drug, $S_{CC,aq} > S_{D,aq}$ ($SA > 1$). While the predicted behavior has not yet been experimentally confirmed, micellar drug solubilization is likely to reduce the free drug from the cocrystal that is available for absorption, but the cocrystal will still maintain a free drug concentration higher than the drug as long as $SA > 1$.^{17, 26} This means that SA can be modulated using the SA - SP diagram to mitigate the risk for rapid conversion while also maintaining superior free drug concentration and promoting heightened drug absorption despite the presence of surfactants.

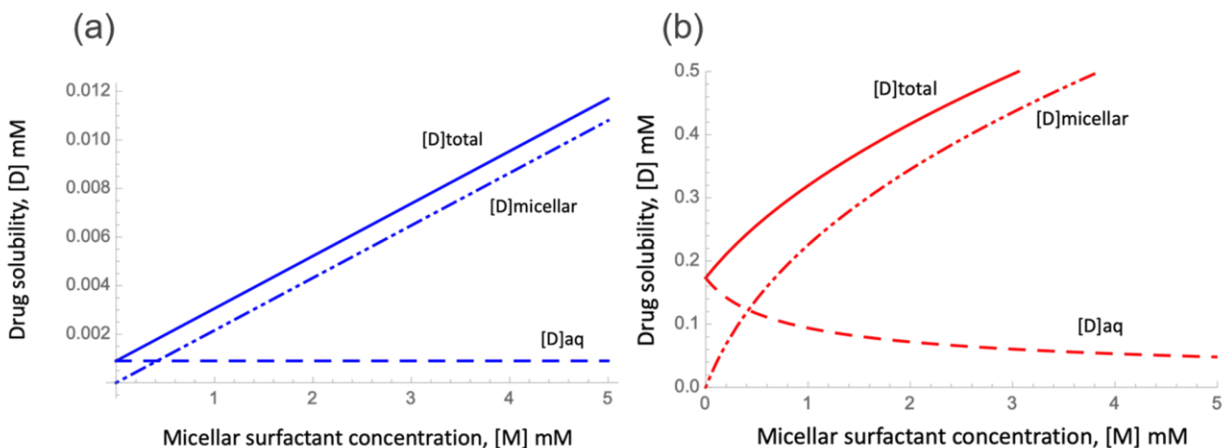


Figure 3.4. Predicted drug and cocrystal solubilities as a function of micellar surfactant concentrations showing total, micellar, and aqueous (free) drug contributions to solubility, represented by [D]. The following parameter values were used: $S_{D, \text{aq}} = 0.0009 \text{ mM}$, $K_{s(\text{DNZ,TPGS})} = 50 \text{ mM}^{-1}$, and $K_{\text{sp}} = 0.03 \text{ mM}^2$. (a) Drug solubility was calculated according to $S_{\text{drug}, T} = S_{\text{drug}, \text{aq}} (1 + K_s[M])$ and (b) cocrystal solubility was calculated according to $S_{\text{cocrystal}, T} = \sqrt{K_{\text{sp}} (1 + K_s[M])}$ and $[D]_{\text{aqueous}} = \frac{K_{\text{sp}}}{S_{\text{cocrystal}, T}}$. [D]_{micellar} was calculated from the difference of $[D]_{\text{total}} - [D]_{\text{aq}}$. K_s values for other surfactants are reported in Appendix 3B.

Figure 3.5 demonstrates how the aqueous contribution to the cocrystal solubility decreases with drug solubilization (micellar surfactant concentration). The cocrystal aqueous contribution curve intersects that of the drug at a given micellar concentration where $SA = 1$. This is a transition point where $S_{\text{CC}} = S_{\text{D}}$ in each pseudophase (aqueous and micellar) corresponding to equal thermodynamic drug activities in each as reported previously for three carbamazepine cocrystals (saccharin, 4-aminobenzoic acid, and succinic acid conformers) in sodium lauryl sulfate.²⁶

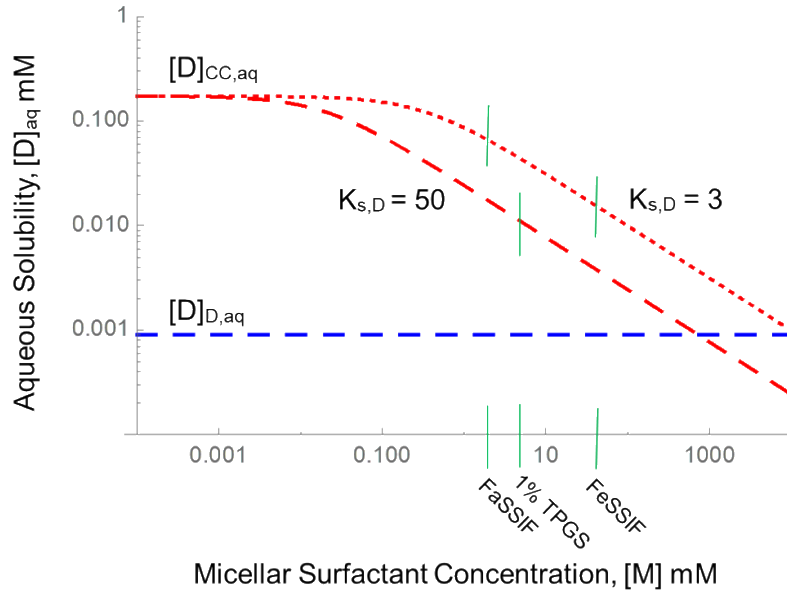


Figure 3.5. How free drug concentrations change with increasing surfactant micellar solubilization of drug. Green lines indicate surfactant concentrations of TPGS and biorelevant media used in this work. Aqueous cocrystal solubility was calculated from $[D]_{\text{aqueous}} = \frac{K_{\text{sp}}}{S_{\text{cocrystal,T}}}$. $[D]_{\text{micellar}}$ was calculated from the difference of $[D]_{\text{total}} - [D]_{\text{aq}}$. The following parameter values were used: $S_{\text{D, aq}} = 0.0009 \text{ mM}$, $K_{\text{s(DNZ,TPGS)}} = 50 \text{ mM}^{-1}$, $K_{\text{s(DNZ,FaSSiF/FeSSiF)}} = 3 \text{ mM}^{-1}$, and $K_{\text{sp}} = 0.03 \text{ mM}^2$.

Effect of Cocrystal Solubility Advantage (SA) and Additive Selection on Dissolution –

Supersaturation – Precipitation (DSP) Behavior

The cocrystal and drug dissolution profiles in Figure 3.6 show that cocrystal achieved higher drug concentrations in all studied media, demonstrating that the cocrystal has superior dissolution properties compared to drug. However, the supersaturation – precipitation behavior varied with the different additives and resulted in very different C_{max} , σ_{max} , and relative area under the curve ($\text{RAUC} = \text{AUC}_{\text{CC}} / \text{AUC}_{\text{D}}$) values (Table 3.3).

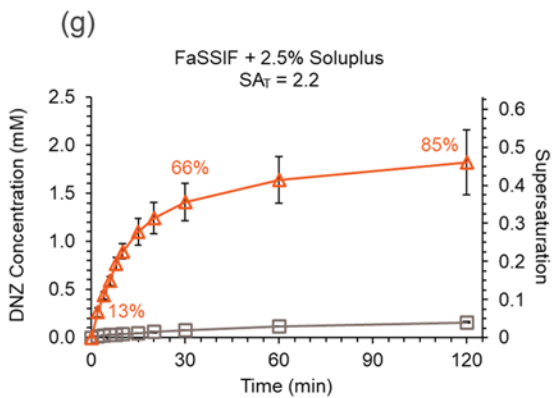
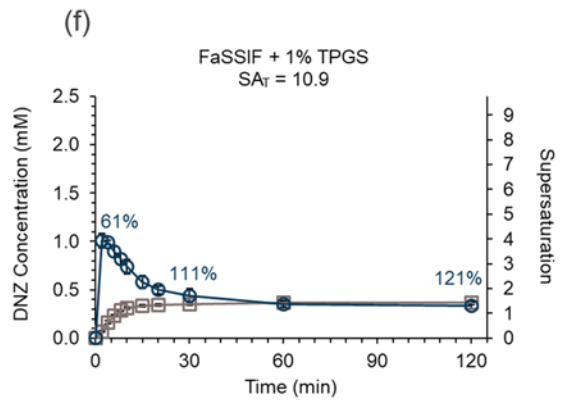
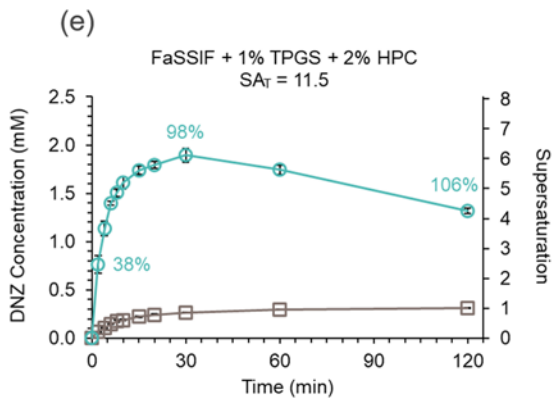
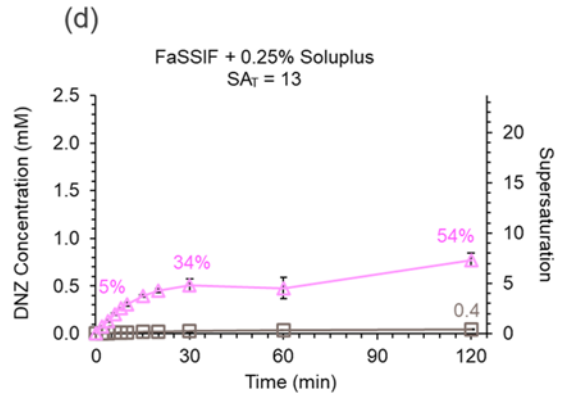
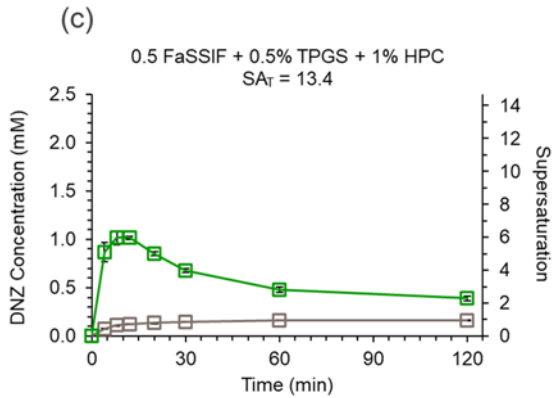
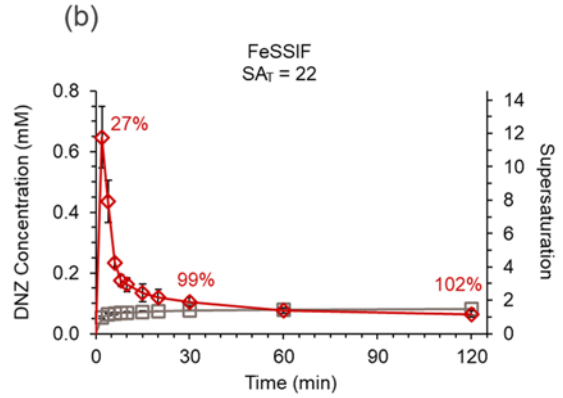
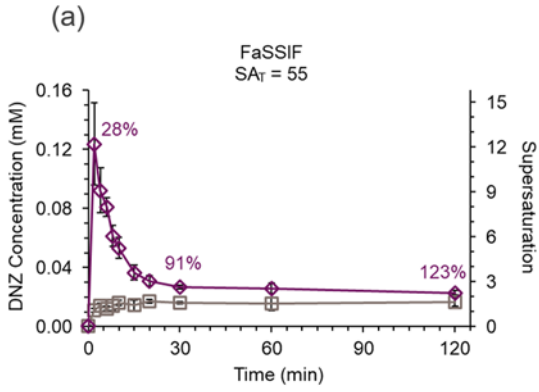


Figure 3.6. Concentration – time and supersaturation – time profiles of cocrystal DNZ-VAN (colored profiles) and drug DNZ (gray profiles) in surfactant media at 37°C with decreasing solubility advantage (SA_T): **(a)** FaSSIF, **(b)** FeSSIF, **(c)** 0.5 FaSSIF + 0.5% TPGS + 1% HPC, **(d)** FaSSIF + 0.25% Soluplus, **(e)** FaSSIF + 1% TPGS + 2% HPC, **(f)** FaSSIF + 1% TPGS, and **(g)** FaSSIF + 2.5% Soluplus. Different additives and concentrations corresponding to different cocrystal SA_T were selected to study their influence on dissolution – supersaturation – precipitation behavior. Dissolution in Figure **(c)** was conducted by Childs et. al, labeled as 1% TPGS + 2% HPC but described in their Methods and Results sections as the final solution being half concentrated.²⁴ $SA_T = 13.4$ for 0.5% TPGS was used to analyze this dissolution since HPC does not solubilize the drug and drug solubilization by FaSSIF $\ll\ll$ drug solubilization by TPGS. Supersaturation values are calculated as $\sigma = ([DNZ] / S_{DNZ})$, according to solubility values in Appendix 3B. Percentages represent cumulative percent cocrystal dissolved at 2, 30, and 120 minutes relative to the initial cocrystal mass added and calculated according to Equation 13. Percentages increase even as [DNZ] decreases when drug precipitation begins to outcompete cocrystal dissolution. Values above 100% are due to experimental error. Percentage component dissolved plots are shown in Figure S1 and selected values in Table S5. Error bars represent standard deviations.

Table 3.3. Cocrystal Dissolution Parameters in Different Media.^a

Media	C _{max} (mM)	σ _{max} ^b	AUC (mM × min)	RAUC ^c	Final pH
FaSSIF	$(1.2 \pm 0.2) \times 10^{-1}$	12 ± 3	3.7 ± 0.2	2.0 ± 0.2	6.48 ± 0.01
FeSSIF	$(6.5 \pm 1.0) \times 10^{-1}$	12 ± 2	13.3 ± 0.4	1.45 ± 0.05	4.86 ± 0.01
0.5 FaSSIF + 0.5% TPGS + 1% HPC ^d	1.0	6.0	68	3.8	-
FaSSIF + 0.25% Soluplus ^e	$(7.7 \pm 0.7) \times 10^{-1}$	7.3 ± 0.7	63 ± 5	16 ± 1	6.46 ± 0.01
FaSSIF + 1% TPGS	1.0 ± 0.1	3.9 ± 0.3	52 ± 2	1.3 ± 0.1	6.48 ± 0.01
FaSSIF + 1% TPGS + 2% HPC	1.9 ± 0.1	6.1 ± 0.2	193 ± 2	5.9 ± 0.1	6.46 ± 0.01
FaSSIF + 2.5% Soluplus ^e	1.8 ± 0.3	0.5 ± 0.1	178 ± 15	14 ± 1	6.41 ± 0.01

^a Drug dissolution parameters are reported in Appendix 3C.

^b $\sigma_{\max} = [\text{DNZ}]_{\max} / S_{\text{DNZ}}$.

^c $\text{RAUC} = \text{AUC}_{\text{DNZ-VAN}} / \text{AUC}_{\text{DNZ}}$. RAUC values are presented with standard error. All other table values are shown with standard deviations.

^d Dissolution performed by Childs et. al *in vitro*. Cocrystal achieved RAUC = 10 *in vivo* under these conditions. This dissolution was reported with a label as 1% TPGS + 2% HPC, but the final solution was described in their Methods and Results as being half concentrated with respect to each surfactant.

^e DNZ-VAN C_{max} and σ_{max} in FaSSIF + 0.25% Soluplus and FaSSIF + 2.5% Soluplus media refer to the final time point of 120 minutes.

Some of these trends are best appreciated in conjunction with Figure 3.7, which compares cocrystal dissolution in different media for the effect of changing SA_T with the same classes of additives (Figure 3.7a, 3.7c, and 3.7e) and the effect of different additives at similar SA_T values (Figure 3.7b, 3.7d, and 3.7f).

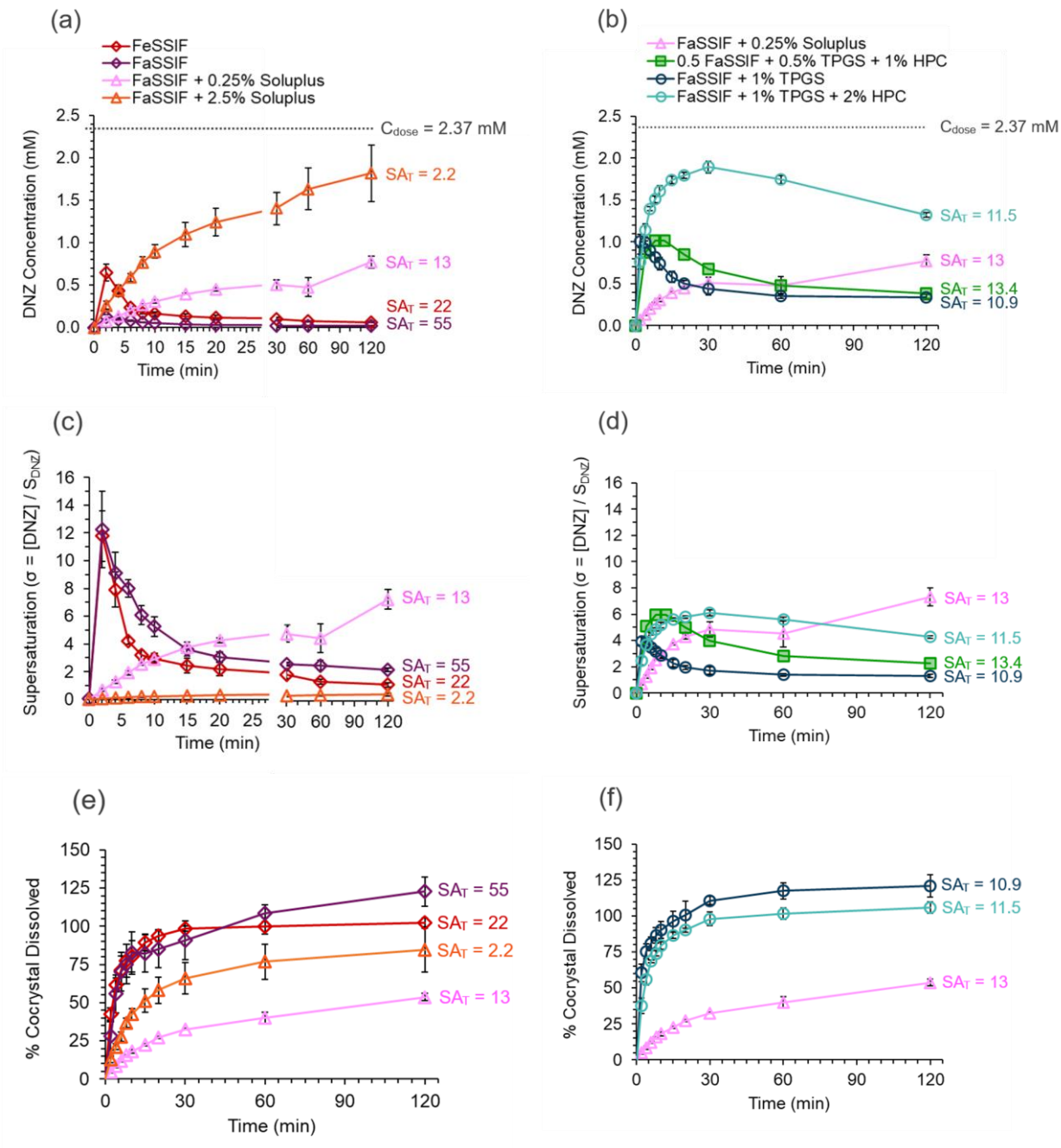


Figure 3.7. Cocryystal dissolution in surfactant media shows the effect of modulating cocryystal solubility advantage (SA_T) with the same additives of FaSSIF, FeSSIF, and Soluplus in (a), (c), and (e), and the effect of targeting similar SA_T 10.9 – 13.4 with different surfactants and precipitation and growth inhibitors in (b), (d), and (f). Concentration – time profiles are shown in (a) and (b) compared to dose concentration (C_{dose}) of 2.37 mM. Dissolution in 0.5 FaSSIF + 0.5% TPGS + 1% HPC was performed by Childs et. al. (reported with a label of 1% TPGS + 2% HPC, but described in the Methods and Results with final surfactant concentrations as presented here) with a C_{dose} of 2.0 mM. Supersaturation – time profiles are shown in (c) and (d). Percentage cocryystal dissolved values shown in (e) and (f) were calculated from Equation 13 as

previously described. Values over 100 are due to experimental error. Percentage component dissolved plots are shown in Figure S1 and selected values in Table S5. Percentage cocrystal dissolved was not reported by Childs et. al.²⁴ $SA_T = 13.4$ for 0.5% TPGS was used to analyze this dissolution since HPC does not solubilize the drug and drug solubilization by FaSSIF <<< drug solubilization by TPGS. Percentage component dissolved plots and selected values in Appendix 3C. Error bars represent standard deviations.

In general, Figure 3.7a shows that C_{max} increased with decreasing SA_T . This is a result of increasing S_{CC} and S_D as a function of increasing additive concentration and drug solubilization (Figure 3.4). In contrast, Figure 3.7c shows that the highest $\sigma_{max} = 12$ was observed in both FaSSIF and FeSSIF, which corresponded to the highest SA_T values and therefore the supersaturation threshold for nucleation under these conditions. A steady undersaturated state ($\sigma_{max} = 0.5$) was observed in FaSSIF + 2.5% Soluplus corresponding to the lowest $SA_T = 2.2$.

AUC is indicative of drug exposure and, for cocrystals, is directly proportional to dissolution rate and inversely proportional to precipitation rate. C_{max} represents the point at which drug precipitation begins to outcompete cocrystal dissolution and occurred at a t_{max} of 2 minutes with higher SA values (≥ 22) in biorelevant media. The cocrystal appears to have converted back to drug by 30 minutes in FaSSIF and FeSSIF. Figure 3.7e shows that the cocrystal had nearly completely dissolved in both of these conditions by this time point. This behavior resulted in $RAUC \leq 2.0$ in these media (Figures 3.6a and 3.6b).

Soluplus, which forms polymeric micelles, appears to have slowed the dissolution rates of both cocrystal and drug, and its polymeric nature may have also played a role in inhibiting nucleation. After 120 minutes, cocrystal was still not completely dissolved in both 0.25% and 2.5% Soluplus media (Figure 3.7e). Slower dissolution rates led to slower supersaturation (interfacial for 2.5% Soluplus)³⁴, which reduced the driving force for conversion. This behavior, combined with solutions remaining undersaturated during drug dissolution (Figures 3.6d and 3.6g), resulted in the highest observed $RAUC = 14 - 16$.

Supersaturation was sustained over 120 minutes for SA values modulated to 10.9 – 13.4 that included HPC or Soluplus (Figure 3.7d). Unlike in FaSSIF + 0.25% Soluplus, the cocrystal still completely dissolved by 30 minutes in the 2% HPC medium (Figure 3.7f), but slower precipitation and growth mediated by HPC resulted in sustained supersaturation and the highest observed cocrystal AUC of any studied media. In fact, this AUC was observed to be almost four times higher than the cocrystal AUC in FaSSIF + 1% TPGS without HPC (Table 3.3), which rapidly converted back to drug after $t_{\max} = 2$ minutes and resulted in the lowest observed RAUC = 1.3 (Figure 3.6f). Despite having lower TPGS concentration and cocrystal solubility, dissolution in 0.5 FaSSIF + 0.5% TPGS + 1% HPC reported by Childs et. al. also achieved higher AUC than FaSSIF + 1% TPGS. These results reiterate the conclusions of Childs et. al. of the importance of considering both solubilizing agents and precipitation/growth inhibitors to achieve sustained supersaturation,²⁴ and they also demonstrate that drug exposure generated by cocrystals can be tailored with simple formulation optimization.

Influence of Additive on Drug Nucleation

Visually examining the cocrystal dissolution aliquots can provide insights to possible differences in the nucleation mechanisms in different media, leading to differences in DSP behavior even at similar SA_T values 10.9 – 13. Figure 3.8 shows photomicrographs of cocrystal dissolution samples withdrawn from the reaction media at 120 minutes (other time points and media shown in Appendix 3C), and Table 3.4 shows the observed time to nucleation.

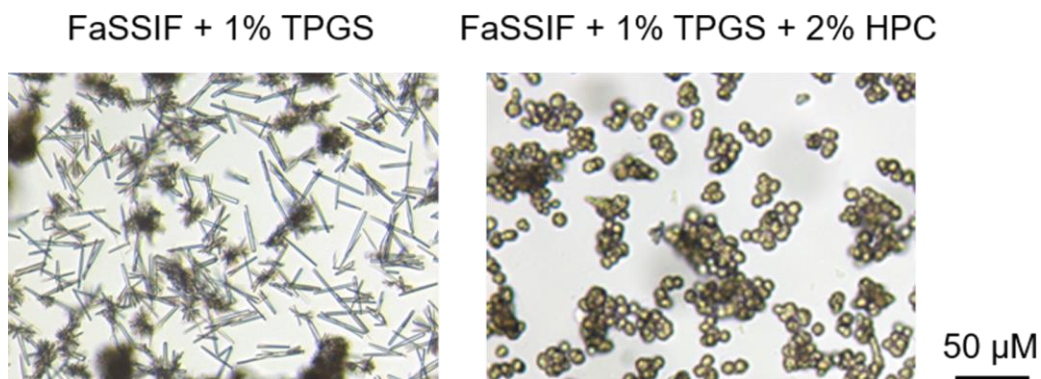


Figure 3.8. Photomicrographs of danazol – vanillin cocrystal (DNZ-VAN) dissolution aliquots at 120 minutes showing the cocrystal induced drug crystallization in the presence of drug solubilizer (1% TPGS) with and without growth inhibitor (2% HPC). DNZ crystals grow as elongated or isomorphous shapes depending on the additive. The addition of HPC sustains supersaturation and slows DNZ crystal growth rate along the elongated crystal axis (fastest growth axis). Nucleation is observed to occur on the surface of the dissolving cocrystal and in the bulk solution. Darker regions represent original sites of surface nucleation before cocrystal completely dissolved. Photomicrographs in other dissolution media and time points are presented in Appendix 3C.

Table 3.4. Time to Nucleation during Dissolution Varies with Different Additives.

Media: FaSSIF +	SA_T	2 Minute Aliquot	30 Minute Aliquot	120 Minute Aliquot	Final Solid Phase ^a
0.25% Soluplus	13 ± 3	-	-	-	DNZ-VAN
1% TPGS	10.9 ± 0.5	Surface	Surface + Bulk	Surface + Bulk	DNZ
1% TPGS + 2% HPC	11.5 ± 0.2	-	Surface + Bulk	Surface + Bulk	DNZ

^a Final solid phases confirmed by DSC.

DNZ-VAN was the final solid phase for cocrystal dissolution in FaSSIF + 0.25% Soluplus, and no drug precipitation was observed. This led to sustained supersaturation over 120 minutes. Conversely, DNZ was the final solid phase in both TPGS media, with complete cocrystal dissolution achieved at 120 minutes. However, while DNZ-VAN rapidly converted to drug in FaSSIF + 1% TPGS and surface nucleation was observed as early as 2 minutes, precipitation was delayed with the addition of 2% HPC until around 30 minutes. Furthermore,

the morphology of the precipitated drug was altered from needle-like rods in FaSSIF + 1% TPGS to spherical particles in FaSSIF + 1% TPGS + 2% HPC.

The sustainment of supersaturation and the lack of precipitation observed during cocrystal dissolution in FaSSIF + 0.25% Soluplus suggests that not only did the additives solubilize the drug, but the polymeric nature of Soluplus may have also served as a precipitation inhibitor. In contrast, addition of the polymer HPC to FaSSIF + 1% TPGS still led to conversion, but precipitation was delayed, and the precipitant morphology was altered. This finding suggests that HPC may be better classified as a growth inhibitor, rather than as a precipitation inhibitor as first suggested by Childs et al.²⁴

Drug Dose/Solubility – Limited Supersaturation

Using SA as a parameter to assess the risk of cocrystal conversion as well as the potential for drug supersaturation lies with the knowledge that a cocrystal cannot generate concentrations higher than its solubility, and therefore cannot generate supersaturation levels higher than SA_T (or critical supersaturation). Tailoring SA_T to be near or within the metastable zone therefore reduces the risk of quickly reaching critical supersaturation and thereby promotes sustained supersaturation.

However, if $C_{dose} < S_{CC}$, then C_{dose} represents the maximum concentration that a cocrystal may generate, and D_{0D} (Equation 3.5) represents the maximum bulk supersaturation level. In this case, considering only SA misses important information of cocrystal conversion risk versus supersaturation potential, and may even lead to inadvertently dosing cocrystals with dose-limited supersaturation.

As shown in Table 3.1, under aqueous conditions DNZ-VAN has $SA_{aq} = 183$ and $D_{0D,aq} = 2617$. When $SA < D_{0D}$, then $S_{CC} < C_{dose}$ and supersaturation is not dose-limited. This behavior

is likely true for many poorly-soluble drugs and their cocrystals, as BCS Class II drugs characteristically have high D_{0D} . However, as S_D and S_{CC} increase with increasing surfactant concentration and drug solubilization, there is the possibility that the relative concentrations of S_{CC} , S_D , and C_{dose} will invert, and bulk supersaturation (or even saturation) will become dose-limited. $D_{0D} > 1$ but $D_{0CC} < 1$ (Equation 3.6) represents C_{dose} values where the cocrystal can generate supersaturation, but not at levels as high as SA (i.e., $S_D < C_{dose} < S_{CC}$). $D_{0D} < 1$ represents C_{dose} values where the cocrystal cannot achieve drug saturation (i.e., $C_{dose} < S_D < S_{CC}$). The theoretical influence of SP_D , SA, D_{0D} , and D_{0CC} on cocrystal solubility, dissolution, supersaturation, and absorption are summarized in Table 3.5.

Table 3.5. How drug solubilization power (SP_D), cocrystal solubility advantage (SA), drug dose/solubility ratio (D_{0D}), and cocrystal dose/solubility ratio (D_{0CC}) influence solubility, dissolution, supersaturation, and absorption.

Ratio Value	$SP_D = S_{D,T} / S_{D,aq}$ ^a	$SA = S_{CC} / S_D$	$D_{0D} = C_{dose} / S_D$ ^b	$D_{0CC} = C_{dose} / S_{CC}$ ^{bc}
> 1	Additive increases drug solubility ²⁵	<p>$S_{CC} > S_D$</p> <p>Cocrystal has solubility advantage and generates supersaturation ¹⁵</p> <p>Driving force for cocrystal conversion ^{4, 14, 17}</p>	<p>$C_{dose} > S_D$</p> <p>Drug dose cannot completely dissolve (sans absorption) ^{1-3, 39}</p> <p>Fraction dose dissolved limited by S_D</p> <p>Supersaturating drug delivery systems may be required to dissolve the full dose</p> <p>Drug has dose/solubility-limited absorption ¹⁻³</p>	<p>$C_{dose} > S_{CC}$</p> <p>Cocrystal dose cannot completely dissolve (sans precipitation or absorption)</p> <p>Supersaturation is limited by S_{CC} (not dose-limited)</p> <p>Maximum theoretical supersaturation represented by SA</p> <p>Cocrystal has dose/solubility-limited absorption</p>
= 1	No additive, or additive does not increase drug solubility	<p>$S_{CC} = S_D$</p> <p>CSC ^{d 26, 54}</p> <p>S^* ^{e 25}</p> <p>$D_{0D} = D_{0CC}$</p>	$C_{dose} = S_D$	<p>$C_{dose} = S_{CC}$</p> <p>$SA = D_{0D}$</p>
< 1	-	<p>$S_{CC} < S_D$</p> <p>Cocrystal does not have solubility advantage and does not generate supersaturation</p>	<p>$C_{dose} < S_D$</p> <p>Drug dose can completely dissolve</p> <p>Bulk supersaturation cannot be generated</p> <p>Drug does not have dose/solubility-limited absorption</p>	<p>$C_{dose} < S_{CC}$</p> <p>Cocrystal dose can completely dissolve</p> <p>Supersaturation is dose-limited</p> <p>Maximum theoretical supersaturation represented by D_{0D}</p> <p>Cocrystal does not have dose/solubility-limited absorption</p>

^a Subscript T refers to total solubility in the presence of a solubilizing additive. Subscript aq refers to aqueous solubility.

^b C_{dose} calculated as molar equivalent of dose mass per 250 mL luminal volume.

^c $D_{\text{OCC}} = C_{\text{dose}} / S_{\text{CC}} = D_{\text{OD}} / SA$.

^d Critical stabilization concentration.

^e $S^* = S_{\text{CC,T}} = S_{\text{D,T}}$. For 1:1 cocrystals, $S^* = (S_{\text{CC,aq}})^2 / S_{\text{D,aq}}$.

Table 3.6 shows the calculated SP_{D} , SA , D_{OD} , and D_{OCC} values for DNZ-VAN in different media. As surfactant concentration and SP_{D} increase, SA , D_{OD} , and D_{OCC} decrease. Even though all studied media yielded $SA > 1$, the selected cocrystal dose is able to fully dissolve in some media, but not in others (sans precipitation).

Table 3.6. Calculated drug solubilization power (SP_D), cocrystal solubility advantage (SA), drug dose/solubility ratio (D_{0D}), and cocrystal dose/solubility ratio (D_{0CC}) in different media.

Additive	$SP_D = S_{D,T} / S_{D,aq}$ ^a	$SA = S_{CC} / S_D$ ^b	$D_{0D} = C_{dose} / S_D$ ^c	$D_{0CC} = C_{dose} / S_{CC}$ ^d
-	1	183 ± 5	2617 ± 148	14.3 ± 0.4
FaSSIF	11 ± 1	55 ± 3	234 ± 20	4.2 ± 0.2
FeSSIF	61 ± 8	22 ± 2	43 ± 5	1.9 ± 0.3
0.5% TPGS ^e	187	13.4	11.7	0.9
FaSSIF + 0.25% Soluplus	117 ± 15	13 ± 3	22 ± 2	1.7 ± 0.7
FaSSIF + 1% TPGS + 2% HPC	342 ± 24	11.5 ± 0.2	8.0 ± 0.3	0.67 ± 0.01
FaSSIF + 1% TPGS	283 ± 20	10.9 ± 0.5	9.2 ± 0.4	0.8 ± 0.1
FaSSIF + 1% Soluplus	1497 ± 138	3.75 ± 0.04	1.75 ± 0.02	0.47 ± 0.01
FaSSIF + 2.5% Soluplus	4364 ± 612	2.2 ± 0.2	0.6 ± 0.1	0.28 ± 0.04

^a Calculated from values in Appendix 3B according to Equation 3.2.

^b Calculated from values in Appendix 3B according to Equation 3.1.

^c Calculated from values in Appendix 3B and $C_{dose} = 2.37$ mM (molar equivalent of 200 mg DNZ dose in 250 mL luminal volume) according to Equation 3.5.

^d $D_{0CC} = C_{dose} / S_{CC} = D_{0D} / SA$. Calculated from values in Table 3.2 and $C_{dose} = 2.37$ mM (molar equivalent of 200 mg DNZ dose in 250 mL luminal volume) according to Equation 3.6.

^e SP_D was estimated from $S_{D,T} = 0.17$ mM reported by Childs et. al. and $S_{D,aq}$ in Table 3.1. SA_T was estimated from calculated SP_D , SA_{aq} in Table 3.1, and Equation 3.3. D_{0D} was estimated from $C_{dose} = 2.0$ mM used in dissolution experiments by Childs et. al. and $S_{D,T} = 0.17$ mM. D_{0CC} was estimated from $C_{dose} = 2.0$ mM and S_{CC} estimated from calculated SA_T and $S_{D,T} = 0.17$ mM.²⁴

When $D_{0CC,T} < 1$, solubilizing additives have increased S_{CC} above C_{dose} , meaning that the dose can fully dissolve and cocrystal supersaturation is limited by C_{dose} . This is the case for $\geq 0.5\%$ TPGS and $\geq 1\%$ Soluplus media, for which maximum theoretical supersaturation is quantified by $D_{0D,T}$ instead of SA_T . While cocrystal quickly converted in FaSSIF + 1% TPGS, supersaturation was sustained with the addition of 2% HPC and reached a maximum of 6.1

(Table 3.3). This observed σ_{\max} value is much closer to its theoretical maximum supersaturation of $D_{0D} = 8.0$ rather than $SA_T = 11.5$. This shows that when these values are dialed within the metastable zone and precipitation/growth inhibitors are utilized, cocrystals can generate and sustain supersaturation levels very close to their theoretical maxima.

One studied condition, FaSSIF + 2.5% Soluplus, resulted in $D_{0D} < 1$. This indicates insufficient dose to reach S_D in the bulk ($C_{\text{dose}} < S_D$) and to generate bulk supersaturation. In fact, $D_{0D,T} = 0.6$ in this condition is within error of $\sigma_{\max} = 0.5$ that the cocrystal achieved during dissolution (Figure 3.6g). This study highlights the danger of not considering D_{0D} when tailoring SA, as bulk supersaturation was unable to be generated despite $SA_T = 2.2$. However, because $SA > 1$ for this condition, interfacial supersaturation may be achieved as high as SA even when $D_{0D} < 1$ and bulk supersaturation is dose-limited.³⁴

For some drugs and cocrystals, D_{0D} may be greater than SA in all solution conditions and doses (i.e., $C_{\text{dose}} \gg S_{CC}$) and supersaturation will never be dose-limited. The opposite may be true for other cases. However, because solubility is not just one value, and because many drugs such as DNZ are prescribed at multiple doses, considering both SA and D_{0D} values in tandem is essential for many drugs in designing effective cocrystal formulations for reaching targeted bulk supersaturation and drug exposure.

Figure 3.9 shows a theoretical plot of the SA – SP and D_{0D} – SP diagram. In addition to the SA – SP relationship predicted by Equation 3.4, the D_{0D} – SP line is predicted according to Equation 3.8:

$$\log D_{0,T(D)} = \log D_{0,aq(D)} - \log SP_D$$

While the SA – SP_D predicted line has a theoretical slope of -1/2 for 1:1 cocrystals, the D_{0D} – SP_D line has a theoretical slope of -1. Unlike the SA- SP_D plot, it is independent of cocrystal

stoichiometry and solubility. The intersection of these lines marks the point where $SA_T = D_{0D,T}$, or where $D_{0CC,T} = 1$, and the transition between cocrystal solubility-limited supersaturation and dose-limited bulk supersaturation.

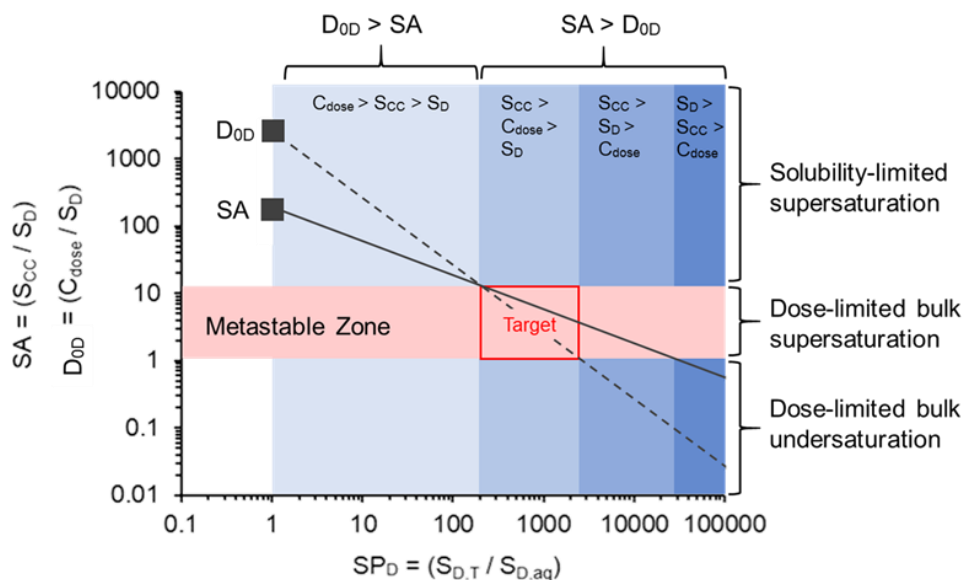


Figure 3.9. Schematic cocrystal solubility advantage (SA) and drug dose/solubility ratio (D_{0D}) diagram shows how the parameters predictably decrease with log-log linear dependence on drug solubilization power (SP_D) according to Equations 3.4 and 3.8. In tandem, SA and D_{0D} represent maximum theoretical supersaturation that a cocrystal can generate as a function of cocrystal solubility (S_{CC}) or the dose concentration (C_{dose}). $SA < D_{0D}$ represents solubility-limited supersaturation, while $SA > D_{0D}$ represents dose-limited saturation or supersaturation. SA and/or D_{0D} can be predictably decreased within the metastable zone by rational additive selection in order to promote sustained supersaturation.

When dialing SP_D , the target SA_T is near or within the metastable zone. Figure 3.9 is drawn based on DNZ-VAN cocrystal $SA_{aq} = 183$, $D_{0D,aq} = 2617$, and critical supersaturation 12 (σ_{max} in FaSSIF and FeSSIF). For this cocrystal, $SA_T = D_{0D,T} = 12.8$, which happens to be slightly above estimated critical supersaturation. This means that targeting SA_T values within the metastable zone will result in dose-limited bulk supersaturation. Inadvertently modulating maximum theoretical supersaturation too low can be avoided by also considering $D_{0D,T}$.

Figure 3.10 shows SP_D , SA , and D_{0D} values of Table 3.6 plotted on the $SA - SP$ and $D_{0D} - SP$ diagram. The log-log linear relationship between D_{0D} and SP_D facilitates determination of conditions with dose-limited supersaturation ($D_{0CC,T} < 1$) and with dose-limited drug undersaturation ($D_{0D,T} < 1$) as shown.

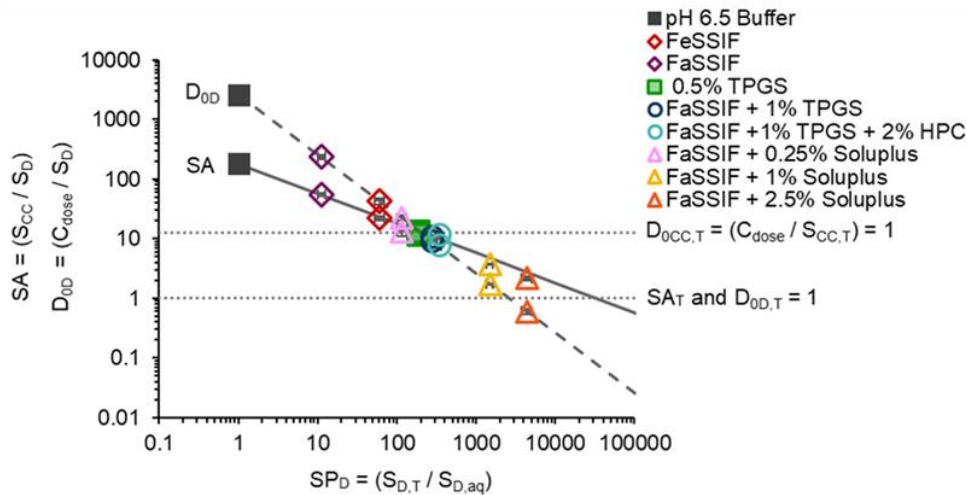


Figure 3.10. Cocrystal $SA - SP$ and drug $D_{0D} - SP$ diagram shows the log-log linear dependence of cocrystal solubility advantage (SA) and drug dose/solubility ratio (D_{0D}) on drug solubilization power (SP_D), predicted from Equations 3.4 and 3.8, respectively. SA_T should be modulated with cognizance of D_{0D} to avoid inadvertently dose-limiting supersaturation. Symbols represent SA , D_{0D} , and SP_D values calculated from experimental measurements of drug (danazol) and coformer (vanillin) eutectic concentrations (Appendix 3B), and $C_{dose} = 2.37$ mM (molar equivalent of 200 mg dose in 250 mL luminal volume). 0.5% TPGS D_{0D} was calculated from $C_{dose} = 2.0$ mM. Transition point $SA_T = 1$ shows where cocrystal and drug solubilities are equal and above which the cocrystal generates supersaturation with respect to the drug. Below $D_{0D,T} = 1$, supersaturating drug delivery systems such as cocrystals are unable to generate bulk supersaturation at the given dose. $D_{0CC,T} = 1$ shows where $SA_T = D_{0D,T}$ and below which bulk supersaturation is generated but is dose-limited. Error bars (within the points) represent standard deviations of SA , D_{0D} , and SP_D .

It is important to note that different doses will yield different C_{dose} values, D_{0D} values, and intersections with the $SA - SP$ line. Depending on indication and severity of disease, DNZ may be dosed at 100 – 800 mg daily. This would correspond to C_{dose} 1.18 – 9.48 mM in 250 mL luminal volume and $D_{0D,aq} = 1309 - 10469$. Our dissolution studies were conducted at the

equivalent of a 200 mg dose in 250 mL, or $C_{\text{dose}} = 2.37$ mM, but dissolution studies conducted by Childs et. al. were conducted at $C_{\text{dose}} = 2.00$ mM.²⁴ There is not a drastic difference between these values, and $D_{0D,T}$ calculated from $C_{\text{dose}} = 2.00$ mM for 0.5% TPGS from Childs et. al. still appears to follow the $D_{0D} - SP$ line predicted from $C_{\text{dose}} = 2.37$ mM for our studies (Figure 3.10). However, Table 3.6 shows that different C_{dose} values did cause $D_{0D,T}$ and $D_{0CC,T}$ values for 0.5% TPGS to slightly deviate from the linear decrease with increasing SP_D .

Cocrystal dissolution studies without considering dose-limited supersaturation are abundant in the literature. When comparing cocrystal dissolution in different solution conditions where S_{CC} and S_D change (with surfactant concentration, pH, temperature, etc.), one medium may have dose-limited supersaturation while the other may not. The same may also be true for two cocrystals in the same medium. Lack of consideration of this effect can lead to incorrect analyses regarding the ability of cocrystals to generate and sustain supersaturation. Small differences between our chosen C_{dose} and that of Childs et. al. does not appear to be a primary factor in differences between our cocrystal dissolution studies, but this could have been much more pronounced if the C_{dose} values were very different.³⁹

A Simple, Rational Approach to Control Dissolution – Supersaturation – Precipitation Behavior

Figure 3.11 summarizes the influence of modulating thermodynamic parameters SA, D_{0D} , and D_{0CC} on optimizing kinetic DSP parameters such as σ_{max} and RAUC. σ_{max} was highest when SA_T , $D_{0D,T}$, and $D_{0CC,T}$ were highest (12 in both FaSSIF and FeSSIF), ranking among the highest of literature reported DNZ supersaturation levels, but among the lowest observed RAUC values (2.0 in FaSSIF and 1.45 in FeSSIF) in this study due to rapid conversion. When SA and D_{0D} were modulated with the addition of solubilizers TPGS and Soluplus, σ_{max} was observed to decrease with the decrease in maximum theoretical supersaturation. However, RAUC values

increased in Soluplus (RAUC = 14 – 16) and HPC (RAUC = 3.8 – 5.9) media. While modulating SA and D_{0D} below critical supersaturation certainly promoted sustained supersaturation in these media, the polymeric nature of Soluplus and HPC likely also had a kinetic effect in inhibiting precipitation and growth.

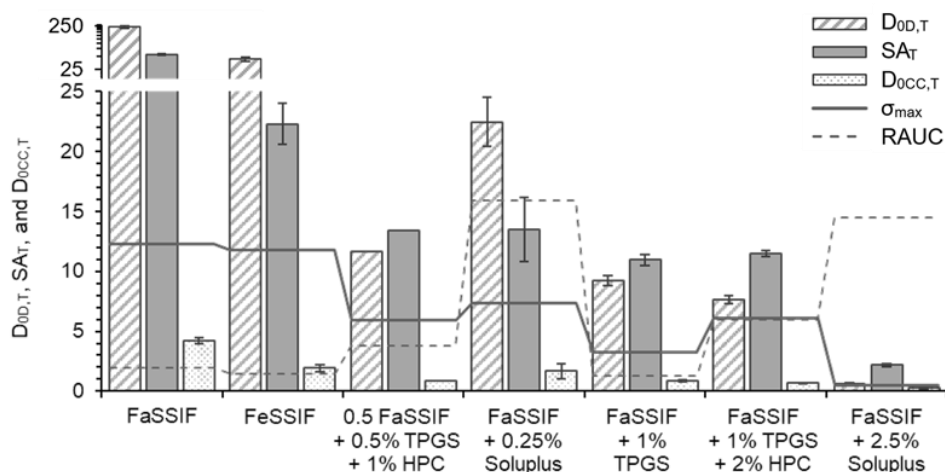


Figure 3.11. Comparison of drug dose/solubility ratio ($D_{0D,T} = C_{dose} / S_{drug}$), cocrystal solubility advantage ($SA_T = S_{cocrystal} / S_{drug}$), cocrystal dose/solubility ratio ($D_{0CC,T} = C_{dose} / S_{cocrystal}$), maximum supersaturation ($\sigma_{max} = [drug] / S_{drug}$), and relative area under the curve ($RAUC = AUC_{cocrystal} / AUC_{drug}$) during *in vitro* dissolution experiments. Dissolution in 0.5 FaSSIF + 0.5% TPGS + 1% HPC was performed by Childs et. al.²⁴ SA_T , $D_{0D,T}$, and $D_{0CC,T}$ are important thermodynamic parameters to assess the maximum theoretical supersaturation that a cocrystal may generate, and can be predictably modulated below critical supersaturation. Precipitation and growth inhibitors play an important role in sustaining supersaturation and increasing RAUC. Error bars represent standard deviations of SA_T and $D_{0D,T}$. σ_{max} and RAUC error are shown in Table 3.3.

These results demonstrate that optimizing DSP behavior of cocrystal systems may be achieved by both thermodynamic and kinetic approaches to mitigate nucleation and promote sustained supersaturation. Modulating SA and D_{0D} near critical supersaturation will maximize theoretical supersaturation, resulting in the highest σ_{max} values, while also minimizing the risk for conversion, resulting in the highest RAUC values. As observed in other cocrystal systems, this suggests optimal SA and $D_{0(D)}$ values exist for sustaining supersaturation and maximizing

drug exposure,^{14, 17, 39} which may be further aided through the use of precipitation and growth inhibitors.

This mechanistic approach of modulating SA and D_{0D} is not only effective in controlling DSP behavior of cocrystal systems, but can also be time, material, and cost sparing. Figure 12 shows how key cocrystal thermodynamic parameters, equilibrium constants, solubility transition points, and SA – SP and D_{0D} – SP diagrams can all be evaluated or predicted from a single eutectic point measurement. These values and relationships provide a framework to assess the cocrystal conversion risk from one simple experiment. Additives can then be readily screened and ranked for their ability to solubilize the drug and modulate SA and D_{0D} at GRAS concentrations. Depending on the dose, required drug exposure, and critical supersaturation, further formulation optimization and selection of precipitation and growth inhibitors may be necessary. However, much of the empiricism currently associated with cocrystal development can be eliminated by utilizing this simple yet science-based approach.

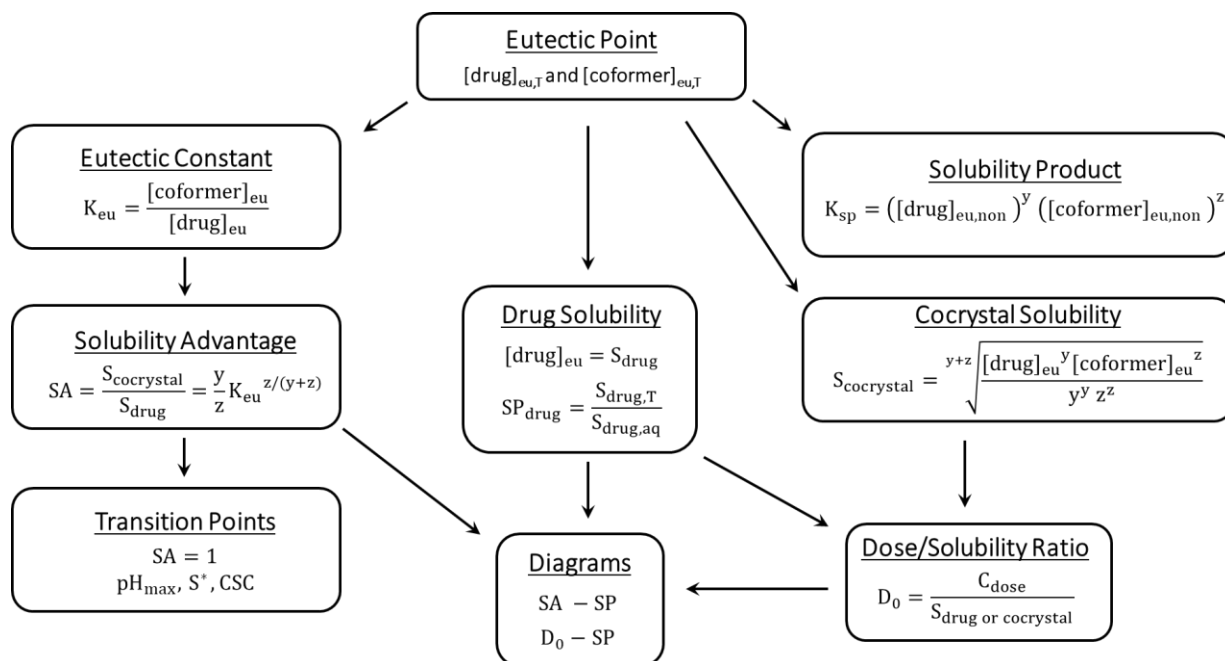


Figure 3.12. Summary of properties and relationships to characterize and formulate pharmaceutical cocrystals. Cocrystal solubility, thermodynamic parameters, transition points, equilibrium constants, and SA – SP and D_{0D} – SP diagrams can be determined or predicted from a single eutectic point measurement. The eutectic point is measured at saturation with both cocrystal and drug solid phases. The cocrystal conversion risk is assessed and modulated by additive selection at SA and D_{0D} below critical supersaturation, to control cocrystal dissolution – supersaturation – precipitation behavior. Drug and coformer stoichiometric coefficients are represented by y and z, respectively.

Conclusions

SA and D_{0D} are meaningful parameters to assess the risk of cocrystal conversion against the ability to generate and sustain supersaturation. This work proposes a mechanistic approach to modulate SA and D_{0D} as a function of additive SP_D in order to control DSP behavior of cocrystal systems, where SA – SP and D_{0D} – SP diagrams provide a framework for critically evaluating cocrystal concentration – time profiles. Mechanistically designing effective cocrystal formulations with the use of both solubilizing agents and precipitation and/or growth inhibitors allows for the increase of drug exposure and demonstrates cocrystals as a valuable tool for overcoming some of the challenges of solubility-limited oral drug absorption.

Acknowledgements

Research reported in this publication received financial support from the Upjohn Award from the College of Pharmacy, University of Michigan, and the National Institute of General Medical Sciences of the National Institutes of Health under Award Numbers R01GM107146. The content is solely the responsibility of the authors and does not necessarily represent the official views of the National Institutes of Health and other funding sources. We also gratefully acknowledge Dr. Gislaine Kuminek for helpful discussions.

References

1. Amidon, G. L.; Lennernas, H.; Shah, V. P.; Crison, J. R., A Theoretical Basis for a Biopharmaceutical Drug Classification - the Correlation of in-Vitro Drug Product Dissolution and in-Vivo Bioavailability. *Pharm Res* **1995**, *12* (3), 413-420.
2. Oh, D.-M.; Curl, R. L.; Amidon, G. L., Estimating the Fraction Dose Absorbed from Suspensions of Poorly Soluble Compounds in Humans: A Mathematical Model. *Pharm Res* **1993**, *10* (2), 264-270.
3. Rinaki, E.; Valsami, G.; Macheras, P., Quantitative Biopharmaceutics Classification System: The Central Role of Dose/Solubility Ratio. *Pharm Res* **2003**, *20*, 1917-25.
4. Kuminek, G.; Cao, F.; Bahia de Oliveira da Rocha, A.; Goncalves Cardoso, S.; Rodríguez-Hornedo, N., Cocrystals to Facilitate Delivery of Poorly Soluble Compounds Beyond-Rule-of-5. *Adv Drug Deliv Rev* **2016**, *101*, 143-66.
5. Berry, D. J.; Steed, J. W., Pharmaceutical Cocrystals, Salts and Multicomponent Systems; Intermolecular Interactions and Property Based Design. *Adv Drug Deliv Rev* **2017**, *117*, 3-24.
6. Taylor, L. S.; Zhang, G. G. Z., Physical Chemistry of Supersaturated Solutions and Implications for Oral Absorption. *Adv Drug Deliv Rev* **2016**, *101*, 122-142.
7. Aitipamula, S.; Banerjee, R.; Bansal, A. K.; Biradha, K.; Cheney, M. L.; Choudhury, A. R.; Desiraju, G. R.; Dikundwar, A. G.; Dubey, R.; Duggirala, N.; Ghogale, P. P.; Ghosh, S.; Goswami, P. K.; Goud, N. R.; Jetty, R. K. R.; Karpinski, P.; Kaushik, P.; Kumar, D.; Kumar, V.; Moulton, B.; Mukherjee, A.; Mukherjee, G.; Myerson, A. S.; Puri, V.; Ramanan, A.; Rajamannar, T.; Reddy, C. M.; Rodríguez-Hornedo, N.; Rogers, R. D.; Row, T. N. G.; Sanphui, P.; Shan, N.; Shete, G.; Singh, A.; Sun, C. Q. C.; Swift, J. A.; Thaimattam, R.; Thakur, T. S.; Thaper, R. K.; Thomas, S. P.; Tothadi, S.; Vangala, V. R.; Vishweshwar, P.; Weyna, D. R.; Zaworotko, M. J., Polymorphs, Salts and Cocrystals: What's in a Name? (vol 12, pg 2147, 2012). *Cryst Growth Des* **2012**, *12* (8), 4290-4291.
8. Hancock, B. C.; Zografi, G., Characteristics and Significance of the Amorphous State in Pharmaceutical Systems. *J Pharm Sci* **1997**, *86* (1), 1-12.
9. Brouwers, J.; Brewster, M. E.; Augustijns, P., Supersaturating Drug Delivery Systems: The Answer to Solubility-Limited Oral Bioavailability? *J Pharm Sci* **2009**, *98* (8), 2549-2572.
10. Kavanagh, O. N.; Croker, D. M.; Walker, G. M.; Zaworotko, M. J., Pharmaceutical Cocrystals: from Serendipity to Design to Application. *Drug Discov Today* **2019**, *24* (3), 796-804.
11. Almarsson, O.; Zaworotko, M. J., Crystal Engineering of the Composition of Pharmaceutical Phases. Do Pharmaceutical Co-crystals Represent a New Path to Improved Medicines? *ChemComm* **2004**, (17), 1889-1896.
12. Schultheiss, N.; Newman, A., Pharmaceutical Cocrystals and Their Physicochemical Properties. *Cryst Growth Des* **2009**, *9* (6), 2950-2967.
13. Shimpi, M. R.; Alhayali, A.; Cavanagh, K. L.; Rodríguez-Hornedo, N.; Velaga, S. P., Tadalafil–Malonic Acid Cocrystal: Physicochemical Characterization, pH-Solubility, and Supersaturation Studies. *Cryst Growth Des* **2018**, *18* (8), 4378-4387.

14. Chen, Y. M.; Rodríguez-Hornedo, N., Cocrystals Mitigate Negative Effects of High pH on Solubility and Dissolution of a Basic Drug. *Cryst Growth Des* **2018**, *18* (3), 1358-1366.
15. Good, D. J.; Rodríguez-Hornedo, N., Solubility Advantage of Pharmaceutical Cocrystals. *Cryst Growth Des* **2009**, *9* (5), 2252-2264.
16. Ullah, M.; Shah, M. R.; Asad, M. H. H. B.; Hasan, S. M. F.; Hussain, I., Improved in vitro and in vivo Performance of Carbamazepine Enabled by using a Succinic Acid Cocrystal in a Stable Suspension Formulation. *Pak J Pharm Sci* **2017**, *30*, 2139+.
17. Huang, Y.; Kuminek, G.; Roy, L.; Cavanagh, K. L.; Yin, Q.; Rodríguez-Hornedo, N., Cocrystal Solubility Advantage Diagrams as a Means to Control Dissolution, Supersaturation, and Precipitation. *Mol Pharm* **2019**, *16* (9), 3887-3895.
18. Remenar, J. F.; Peterson, M. L.; Stephens, P. W.; Zhang, Z.; Zimenkov, Y.; Hickey, M. B., Celecoxib:Nicotinamide Dissociation: Using Excipients To Capture the Cocrystal's Potential. *Mol Pharm* **2007**, *4* (3), 386-400.
19. Aitipamula, S.; Wong, A. B. H.; Kanaujia, P., Evaluating Suspension Formulations of Theophylline Cocrystals With Artificial Sweeteners. *J Pharm Sci* **2018**, *107* (2), 604-611.
20. Venczel, M.; Szvoboda, I.; Podányi, B.; Valente, D.; Menegotto, J.; Pintye-Hódi, K.; Ujhelyi, G., Formulation Possibilities of a Weak Base with a Narrow Solubility Range. *Cryst Growth Des* **2012**, *12* (3), 1101-1110.
21. Wang, C.; Tong, Q.; Hou, X.; Hu, S.; Fang, J.; Sun, C. C., Enhancing Bioavailability of Dihydromyricetin through Inhibiting Precipitation of Soluble Cocrystals by a Crystallization Inhibitor. *Cryst Growth Des* **2016**, *16* (9), 5030-5039.
22. Salas-Zúñiga, R.; Rodríguez-Ruiz, C.; Höpfl, H.; Morales-Rojas, H.; Sánchez-Guadarrama, O.; Rodríguez-Cuamatzi, P.; Herrera-Ruiz, D., Dissolution Advantage of Nitazoxanide Cocrystals in the Presence of Cellulosic Polymers. *Pharmaceutics* **2019**, *12* (1), 23.
23. Jasani, M. S.; Kale, D. P.; Singh, I. P.; Bansal, A. K., Influence of Drug–Polymer Interactions on Dissolution of Thermodynamically Highly Unstable Cocrystal. *Mol Pharm* **2019**, *16* (1), 151-164.
24. Childs, S. L.; Kandi, P.; Lingireddy, S. R., Formulation of a Danazol Cocrystal with Controlled Supersaturation Plays an Essential Role in Improving Bioavailability. *Mol Pharm* **2013**, *10* (8), 3112-27.
25. Lipert, M. P.; Rodríguez-Hornedo, N., Cocrystal Transition Points: Role of Cocrystal Solubility, Drug Solubility, and Solubilizing Agents. *Mol Pharm* **2015**, *12* (10), 3535-46.
26. Huang, N.; Rodríguez-Hornedo, N., Engineering Cocrystal Solubility, Stability, and pH(max) by Micellar Solubilization. *J Pharm Sci* **2011**, *100* (12), 5219-34.
27. Huang, N.; Rodríguez-Hornedo, N., Engineering Cocrystal Thermodynamic Stability and Eutectic Points by Micellar Solubilization and Ionization. *CrystEngComm* **2011**, *13* (17), 5409-5422.
28. Rosa, J.; Machado, T. C.; da Silva, A. K.; Kuminek, G.; Bortolluzzi, A. J.; Caon, T.; Cardoso, S. G., Isoniazid-Resveratrol Cocrystal: A Novel Alternative for Topical Treatment of Cutaneous Tuberculosis. *Cryst Growth Des* **2019**, *19* (9), 5029-5036.
29. Sunesen, V. H.; Vedelsdal, R.; Kristensen, H. G.; Christrup, L.; Müllertz, A., Effect of Liquid Volume and Food Intake on the Absolute Bioavailability of Danazol, a Poorly Soluble Drug. *Eur J Pharm Sci* **2005**, *24* (4), 297-303.

30. Vinarov, Z.; Katev, V.; Radeva, D.; Tcholakova, S.; Denkov, N. D., Micellar Solubilization of Poorly Water-Soluble Drugs: Effect of Surfactant and Solubilizate Molecular Structure. *Drug Dev Ind Pharm* **2018**, *44* (4), 677-686.
31. Lehto, P.; Kortejärvi, H.; Liimatainen, A.; Ojala, K.; Kangas, H.; Hirvonen, J.; Tanninen, V. P.; Peltonen, L., Use of Conventional Surfactant Media as Surrogates for FaSSIF in Simulating in vivo Dissolution of BCS Class II Drugs. *Eur J Pharm Biopharm* **2011**, *78* (3), 531-538.
32. Bakatselou, V.; Oppenheim, R. C.; Dressman, J. B., Solubilization and Wetting Effects of Bile Salts on the Dissolution of Steroids. *Pharm Res* **1991**, *8* (12), 1461-1469.
33. Linn, M.; Collnot, E.-M.; Djuric, D.; Hempel, K.; Fabian, E.; Kolter, K.; Lehr, C.-M., Soluplus® as an effective absorption enhancer of poorly soluble drugs in vitro and in vivo. *Eur J Pharm Sci* **2012**, *45* (3), 336-343.
34. Cao, F.; Amidon, G. L.; Rodríguez-Hornedo, N.; Amidon, G. E., Mechanistic Analysis of Cocrystal Dissolution as a Function of pH and Micellar Solubilization. *Mol Pharm* **2016**, *13* (3), 1030-1046.
35. Rodríguez-Hornedo, N.; Nehm, S. J.; Seefeldt, K. F.; Pagán-Torres, Y.; Falkiewicz, C. J., Reaction Crystallization of Pharmaceutical Molecular Complexes. *Mol Pharm* **2006**, *3* (3), 362-367.
36. Good, D. J.; Rodríguez-Hornedo, N., Cocrystal Eutectic Constants and Prediction of Solubility Behavior. *Cryst Growth Des* **2010**, *10* (3), 1028-1032.
37. Kuminek, G.; Cavanagh, K. L.; da Piedade, M. F. M.; Rodríguez-Hornedo, N., Posaconazole Cocrystal with Superior Solubility and Dissolution Behavior. *Cryst Growth Des* **2019**, *19* (11), 6592-6602.
38. Kuminek, G.; Cavanagh, K. L.; Rodríguez-Hornedo, N., Measurement and Mathematical Relationships of Cocrystal Thermodynamic Properties. In *Pharmaceutical Crystals*, Li, T.; Mattei, A., Eds. John Wiley & Sons, Inc.: 2019.
39. Machado, T. C.; Kuminek, G.; Cardoso, S. G.; Rodríguez-Hornedo, N., The Role of pH and Dose/solubility Ratio on Cocrystal Dissolution, Drug Supersaturation and Precipitation. *Eur J Pharm Sci* **2020**, 105422.
40. Cavanagh, K. L.; Maheshwari, C.; Rodríguez-Hornedo, N., Understanding the Differences Between Cocrystal and Salt Aqueous Solubilities. *J Pharm Sci* **2018**, *107* (1), 113-120.
41. Lipert, M. P.; University of Michigan. Library. Deep Blue., Predicting the Influence of Drug Solubilizing Agents on Cocrystal Solubility, Stability, and Transition Points. 2015. <http://hdl.handle.net/2027.42/111365>.
42. Alskar, L. C.; Keemink, J.; Johannesson, J.; Porter, C. J. H.; Bergstrom, C. A. S., Impact of Drug Physicochemical Properties on Lipolysis-Triggered Drug Supersaturation and Precipitation from Lipid-Based Formulations. *Mol Pharm* **2018**, *15* (10), 4733-4744.
43. Bevernage, J.; Forier, T.; Brouwers, J.; Tack, J.; Annaert, P.; Augustijns, P., Excipient-Mediated Supersaturation Stabilization in Human Intestinal Fluids. *Mol Pharm* **2011**, *8* (2), 564-70.
44. Palmelund, H.; Madsen, C. M.; Plum, J.; Mullertz, A.; Rades, T., Studying the Propensity of Compounds to Supersaturate: A Practical and Broadly Applicable Approach. *J Pharm Sci* **2016**, *105* (10), 3021-3029.

45. Jackson, M. J.; Kestur, U. S.; Hussain, M. A.; Taylor, L. S., Dissolution of Danazol Amorphous Solid Dispersions: Supersaturation and Phase Behavior as a Function of Drug Loading and Polymer Type. *Mol Pharm* **2016**, *13* (1), 223-31.
46. Ozaki, S.; Kushida, I.; Yamashita, T.; Hasebe, T.; Shirai, O.; Kano, K., Evaluation of Drug Supersaturation by Thermodynamic and Kinetic Approaches for the Prediction of Oral Absorbability in Amorphous Pharmaceuticals. *J Pharm Sci* **2012**, *101* (11), 4220-4230.
47. Murdande, S. B.; Pikal, M. J.; Shanker, R. M.; Bogner, R. H., Solubility Advantage of Amorphous Pharmaceuticals: II. Application of Quantitative Thermodynamic Relationships for Prediction of Solubility Enhancement in Structurally Diverse Insoluble Pharmaceuticals. *Pharm Res* **2010**, *27* (12), 2704-2714.
48. Vaughn, J. M.; McConville, J. T.; Crisp, M. T.; Johnston, K. P.; Williams, R. O., Supersaturation Produces High Bioavailability of Amorphous Danazol Particles Formed by Evaporative Precipitation into Aqueous Solution and Spray Freezing into Liquid Technologies. *Drug Dev Ind Pharm* **2006**, *32* (5), 559-567.
49. Kataoka, M.; Sugano, K.; da Costa Mathews, C.; Wong, J. W.; Jones, K. L.; Masaoka, Y.; Sakuma, S.; Yamashita, S., Application of Dissolution/Permeation System for Evaluation of Formulation Effect on Oral Absorption of Poorly Water-Soluble Drugs in Drug Development. *Pharm Res* **2012**, *29* (6), 1485-94.
50. Maras, J. E.; Bermudez, O. I.; Qiao, N.; Bakun, P. J.; Boody-Alter, E. L.; Tucker, K. L., Intake of α -tocopherol is Limited among US Adults. *J Am Diet Assoc* **2004**, *104* (4), 567-575.
51. Jae-Young, L.; Wie-Soo, K.; Piao, J.; Yoon, I.-S.; Kim, D.-D.; Cho, H.-J., Soluplus®/TPGS-based Solid Dispersions Prepared by Hot-melt Extrusion Equipped with Twin-screw Systems for Enhancing Oral Bioavailability of Valsartan. *Drug Des. Devel. Ther.* **2015**, *9*, 2745-2756.
52. Miller, J. M.; Beig, A.; Krieg, B. J.; Carr, R. A.; Borchardt, T. B.; Amidon, G. E.; Amidon, G. L.; Dahan, A., The Solubility–Permeability Interplay: Mechanistic Modeling and Predictive Application of the Impact of Micellar Solubilization on Intestinal Permeation. *Mol Pharm* **2011**, *8* (5), 1848-1856.
53. Beig, A.; Miller, J. M.; Lindley, D.; Dahan, A., Striking the Optimal Solubility–Permeability Balance in Oral Formulation Development for Lipophilic Drugs: Maximizing Carbamazepine Blood Levels. *Mol Pharm* **2017**, *14* (1), 319-327.
54. Huang, N.; Rodríguez-Hornedo, N., Effect of Micellar Solubilization on Cocrystal Solubility and Stability. *Cryst Growth Des* **2010**, *10* (5), 2050-2053.

Appendix 3A

Effect of Coformer Impurity on Cocrystal Solubility and SA

The effect of increasing coformer impurity on aqueous cocrystal solubility and SA is shown in Figure 3A.1 and Table 3A.1. Nonstoichiometric cocrystal solubility and SA predictably decrease with excess coformer concentration according to the K_{sp} , with greater coformer impurity corresponding to greater decreases. The coformer impurity effect in terms of percentage yields a greater effect with higher doses, as they have greater coformer (and drug) composition and the same percentage impurity therefore corresponds to higher impurity mass. Stoichiometric cocrystal solubility and SA are independent of the dose, as well as nonstoichiometric values calculated in terms of impurity mass. This finding shows that small coformer impurities generated during cocrystal synthesis can have a meaningful impact on purposefully or inadvertently modulating cocrystal solubility and SA.

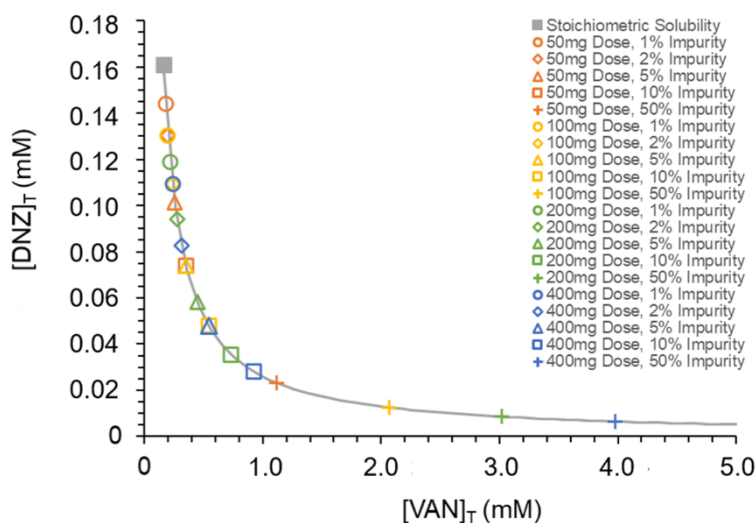


Figure 3A.1. Increasing coformer impurity decreases nonstoichiometric cocrystal solubility and SA. Line was calculated according to $K_{sp} = (2.6 \pm 0.1) \times 10^{-8} \text{ M}^2$.

Table 3A.1. Effect of Coformer Impurity on Cocrystal Solubility and SA for Different Doses.

Dose	% VAN Impurity	S _{CC} (mM)	SA ^a
-	0	0.17 ^b	183 ^b
50 mg	1	0.14	158
	2	0.13	143
	5	0.10	111
	10	0.07	81
	50	0.02	26
100 mg	1	0.13	143
	2	0.11	120
	5	0.07	81
	10	0.05	53
	50	0.01	14
200 mg	1	0.12	131
	2	0.09	104
	5	0.06	64
	10	0.04	39
	50	0.01	9
400 mg	1	0.11	120
	2	0.08	91
	5	0.05	53
	10	0.03	31
	50	0.01	7

^a SA calculated from $S_D = (9.1 \pm 0.5) \times 10^{-4}$ mM (Table 3.1).

^b Values in Table 3.1.

Appendix 3B

Eutectic Concentration Measurements in the Presence of Additives

Table 3B.1 shows the molar concentrations of surfactant media used within Chapter 3.

Table 3B.1. Selected Solubilizing Additives and their Concentrations.

Solubilizing Additive	Concentration (mM)
0.25% Soluplus	0.02
1% Soluplus	0.09
2.5% Soluplus	0.2
FaSSIF	3
0.5% TPGS	3.3
1% TPGS	6.6
FeSSIF	15

Table 3B.2 shows the measured drug and cofomer eutectic concentrations in various surfactant media. Eutectic concentrations were used to calculate cocrystal solubility and K_{eu} values reported in Table 3.2 according to Equations 3.9 and 3.11. Equilibrium pH values for the measurements are reported.

Table 3B.2. Drug and Coformer Eutectic Concentrations to Calculate Cocystal Solubility and Eutectic Constant K_{eu} .

Additive(s)	[DNZ] _{eu} (mM) ^a	[VAN] _{eu} (mM)	Final pH ^b
-	$(9.1 \pm 0.5) \times 10^{-4}$	30.3 ± 0.6	6.28 ± 0.01
FaSSIF	$(1.0 \pm 0.1) \times 10^{-2}$	30.8 ± 0.9	6.33 ± 0.01
FeSSIF	$(5.5 \pm 0.7) \times 10^{-2}$	27.3 ± 2.5	4.95 ± 0.01
FaSSIF + 0.25% Soluplus	$(1.1 \pm 0.1) \times 10^{-1}$	19.1 ± 7.4	6.49 ± 0.05
FaSSIF + 1% TPGS + 2% HPC	$(3.1 \pm 0.1) \times 10^{-1}$	40.7 ± 0.9	6.30 ± 0.01
FaSSIF + 1% TPGS	$(2.6 \pm 0.1) \times 10^{-1}$	30.7 ± 2.4	6.37 ± 0.01
FaSSIF + 1% Soluplus	1.36 ± 0.02	19.0 ± 0.3	6.51 ± 0.01
FaSSIF + 2.5% Soluplus	4.0 ± 0.4	18.5 ± 1.8	6.50 ± 0.01

^a [DNZ]_{eu} = S_D under the studied conditions.

^b Initial pH was 6.5 ± 0.1 for all studies except FeSSIF, which had an initial pH 5.0 ± 0.1 .

Speciation and SA in Micellar Solutions Derivation

The chemical and phase equilibria for cocystal solubilization when only drug is solubilized by micelle are



The expression for cocystal solubility has been previously derived^{1,2} by considering the above equilibrium constants, solubility product (K_{sp}), and drug solubilization (K_s), where

$$K_{sp} = [D]_{\text{aqueous}} [CF]_{\text{aqueous}} \quad (3B.3)$$

and

$$K_s = \frac{[D]_{\text{micellar}}}{[D]_{\text{aqueous}} [M]} \quad (3B.4)$$

Considering the mass balance of cocrystal components dissolved at equilibrium

$$S_{\text{cocrystal},T} = [D]_T = [CF]_T \quad (3B.5)$$

where the subscript T represents the sum of aqueous (free) and solubilized (micellar) cocrystal components. The total drug in equilibrium with cocrystal in micellar solutions is then

$$[D]_T = [D]_{\text{aqueous}} + [D]_{\text{micellar}} \quad (3B.6)$$

When the cofomer is not solubilized by the micelle as it is with the systems studied here, it remains in the aqueous pseudophase such that

$$[CF]_T = [CF]_{\text{aqueous}} = S_{\text{cocrystal},T} \quad (3B.7)$$

while the drug concentration in the aqueous pseudophase decreases according to the solubility product behavior given by

$$[D]_{\text{aqueous}} = \frac{K_{sp}}{[CF]_{\text{aqueous}}} = \frac{K_{sp}}{S_{\text{cocrystal},T}} \quad (3B.8)$$

Cocrystal and drug solubilities are expressed in terms of equilibrium constants and micelle concentration, based on the phase and chemical equilibria (Equations 3B.1-4), as

$$[CF]_T = S_{\text{cocrystal},T} = \sqrt{K_{sp} (1 + K_s[M])} \quad (3B.9)$$

and

$$S_{\text{drug},T} = S_{\text{drug,aq}} (1 + K_s[M]) \quad (3B.10)$$

Expressing $[D]_{\text{aqueous}}$ (Equation 3B.8) in terms of $S_{\text{cocrystal},T}$, $S_{\text{drug,aq}}$, and $S_{\text{drug},T}$ (Equations 3B.9-10) gives

$$[D]_{\text{aqueous}} = \frac{S_{\text{cocrystal},T} S_{\text{drug,aq}}}{S_{\text{drug},T}} \quad (3B.11)$$

$$\text{Substituting } [D]_{\text{aqueous}} = S_{\text{cocrystal,aq}} \quad (3B.12)$$

into Equation 3B.11 gives

$$\frac{S_{\text{cocrystal, aq}}}{S_{\text{drug, aq}}} = \frac{S_{\text{cocrystal, T}}}{S_{\text{drug, T}}} \quad (3B.13)$$

Demonstrating that the aqueous (free) solubility advantage (SA) is equal to the total SA

$$SA_{\text{aqueous}} = SA_{\text{T}} \quad (3B.14)$$

Table 3B.3 shows K_s values for FaSSiF/FeSSiF, TPGS, and Soluplus calculated according to Equation 3B.4, as well as the corresponding critical micellar concentration (CMC), critical stabilization concentration (CSC), and S^* values.

Table 3B.3. Drug Solubilization Constants and Associated Solubility and Stability Parameters.

Solubilizing Additive	K_s (mM ⁻¹) ^a	CMC (mM) ^b	CSC (mM) ^c	S^* (mM) ^d
FaSSiF/FeSSiF	2.4	0.025	-	-
TPGS	51	0.13	662	30.4
Soluplus	20162	0.02	1.7	32

^a Drug solubilization constant calculated according to Equation 3B.10 and values in Tables 3B.1 and 3B.2.^{2,3}

^b Critical micellar concentration.

^c Critical stabilization concentration where $S_{D,T} = S_{CC,T}$, predicted according to Equations 3B.9 and 3B.10.^{2,3}

^d $S^* = S_{CC,T} = S_{D,T}$. For 1:1 cocrystals, $S^* = (S_{CC, aq})^2 / S_{D, aq}$.⁴

References

1. Good, D. J.; Rodríguez-Hornedo, N., Solubility Advantage of Pharmaceutical Cocrystals. *Cryst Growth Des* **2009**, *9* (5), 2252-2264.
2. Huang, N.; Rodríguez-Hornedo, N., Engineering Cocrystal Solubility, Stability, and pH(max) by Micellar Solubilization. *J Pharm Sci* **2011**, *100* (12), 5219-34.
3. Huang, N.; Rodríguez-Hornedo, N., Effect of Micellar Solubilization on Cocrystal Solubility and Stability. *Cryst Growth Des* **2010**, *10* (5), 2050-2053.
4. Lipert, M. P.; Rodríguez-Hornedo, N., Cocrystal Transition Points: Role of Cocrystal Solubility, Drug Solubility, and Solubilizing Agents. *Mol Pharm* **2015**, *12* (10), 3535-46.

Appendix 3C

Table 3C.1 reports additional cocrystal and drug dissolution parameters to Table 3.3.

Table 3C.1. Dissolution Parameters for DNZ-VAN and DNZ in Different Media.

Media	Solid Form	t _{max} (min)	C _{max} (mM)	σ _{max} ^a	AUC (mM × min)	RAUC ^b	Final pH
FaSSIF	DNZ-VAN	2	(1.2 ± 0.2) × 10 ⁻¹	12 ± 3	3.7 ± 0.2	2.0 ± 0.2	6.48 ± 0.01
	DNZ	20	(1.7 ± 0.1) × 10 ⁻²	1.7 ± 0.1	1.9 ± 0.2	-	6.48 ± 0.01
FeSSIF	DNZ-VAN	2	(6.5 ± 1.0) × 10 ⁻¹	12 ± 2	13.3 ± 0.4	1.45 ± 0.05	4.86 ± 0.01
	DNZ	120	(8.1 ± 0.2) × 10 ⁻²	1.47 ± 0.04	9.15 ± 0.05	-	4.93 ± 0.01
FaSSIF + 0.25% Soluplus	DNZ-VAN ^c	120	(7.7 ± 0.7) × 10 ⁻¹	7.3 ± 0.7	63 ± 5	16 ± 1	6.46 ± 0.01
	DNZ	120	(4.6 ± 0.3) × 10 ⁻²	0.44 ± 0.03	4.0 ± 0.1	-	6.47 ± 0.01
FaSSIF + 1% TPGS	DNZ-VAN	2	1.0 ± 0.1	3.9 ± 0.3	52 ± 2	1.3 ± 0.1	6.48 ± 0.01
	DNZ	60	(3.6 ± 0.2) × 10 ⁻¹	1.4 ± 0.1	41 ± 1	-	6.498 ± 0.003
FaSSIF + 1% TPGS + 2% HPC	DNZ-VAN	30	1.9 ± 0.1	6.1 ± 0.2	193 ± 2	5.9 ± 0.1	6.46 ± 0.01
	DNZ	120	(3.15 ± 0.04) × 10 ⁻¹	1.01 ± 0.01	32.5 ± 0.3	-	6.49 ± 0.02
FaSSIF + 2.5% Soluplus	DNZ-VAN ^c	120	1.8 ± 0.3	0.5 ± 0.1	178 ± 15	14 ± 1	6.41 ± 0.01
	DNZ	120	(1.6 ± 0.1) × 10 ⁻¹	0.040 ± 0.002	12.4 ± 0.4	-	6.42 ± 0.02

^a σ_{max} = [DNZ]_{max} / S_{DNZ}. DNZ supersaturation values greater than 1 are likely the result of error in solubility measurements.

^b RAUC = AUC_{DNZ-VAN} / AUC_{DNZ}. RAUC values are presented with standard error. All other table values are shown with standard deviations.

^c DNZ-VAN t_{max}, C_{max}, and σ_{max} in FaSSIF + 0.25% Soluplus and FaSSIF + 2.5% Soluplus media refer to the final time point of 120 minutes.

Percentage component dissolved plots are shown in Figure 3C.1 and selected values in Table 3C.2.

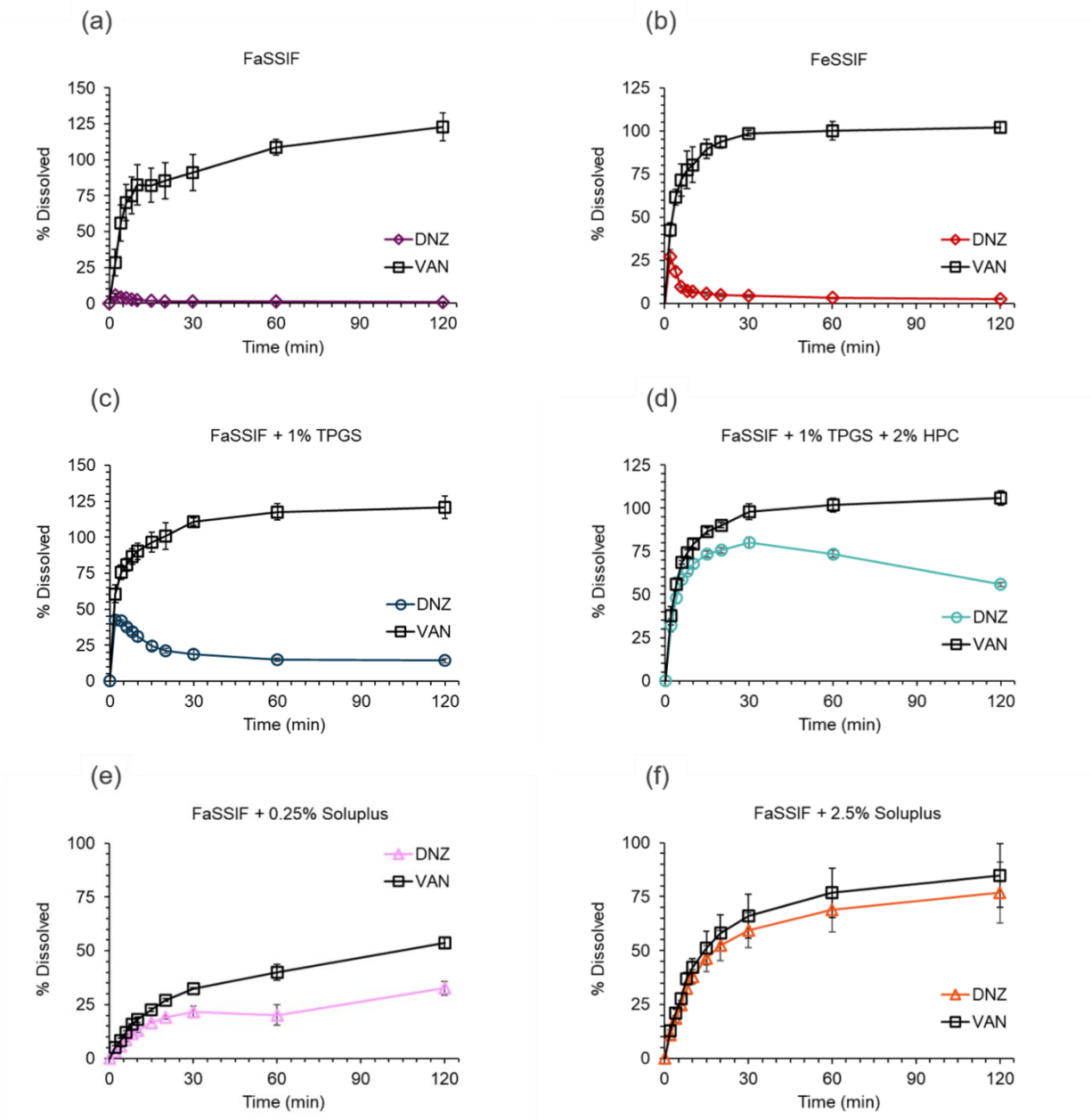


Figure 3C.1. Percentage DNZ and VAN dissolved during DNZ-VAN cocrystal dissolution in (a) FaSSIF, (b) FeSSIF, (c) FaSSIF + 1% TPGS, (d) FaSSIF + 1% TPGS + 2% HPC, (e) FaSSIF + 0.25% Soluplus, and (f) FaSSIF + 2.5% Soluplus at 37°C. Percent dissolved was calculated from the ratio of measured DNZ or VAN in solution to the theoretical concentration from the initial mass added ($100 \times [\text{DNZ or VAN}] \text{ dissolved} / [\text{DNZ or VAN}] \text{ total added}$ from the cocrystal). Error bars represent standard deviations.

Table 3C.2. Percent Cocystal Dissolved during Dissolution Studies.^a

	2 Minutes	30 Minutes	120 Minutes
FaSSIF	28 ± 9 ^b	91 ± 13	123 ± 10
FeSSIF	27 ± 4 ^b	99 ± 2	102 ± 3
FaSSIF + 0.25% Soluplus	5 ± 1	33.6 ± 0.4	54 ± 2 ^b
FaSSIF + 1% TPGS	61 ± 6 ^b	111 ± 3	121 ± 8
FaSSIF + 1% TPGS + 2% HPC	38 ± 5	98 ± 5 ^b	106 ± 4
FaSSIF + 2.5% Soluplus	13 ± 2	66 ± 10	85 ± 15 ^b

^a Calculated according to Equation 13. Percent component dissolved versus time plots are shown in Figure 3C.1.

^b Percent cocystal dissolved at t_{\max} (or up to 120 minutes).

Figure 3C.2 shows photomicrographs of cocystal dissolution aliquots in various surfactant media 2, 30, and 120 minutes. Percentage cocystal dissolved was observed to change with S_{CC} and SA, and precipitant morphology was observed to change with additives (Figure 3.8).

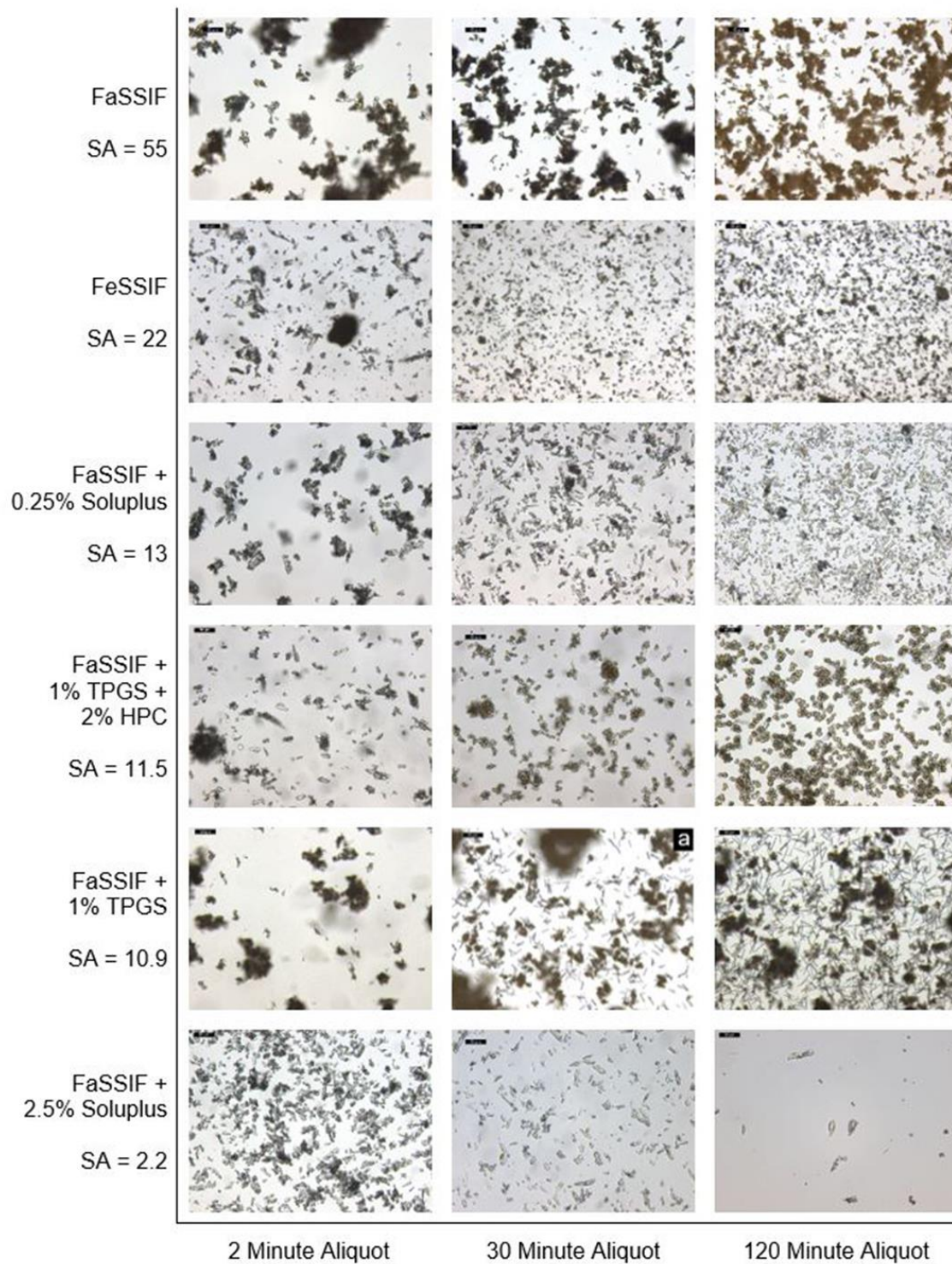


Figure 3C.2. Photomicrographs of DNZ-VAN dissolution aliquots at different time points (x-axis) show dissolution – supersaturation – precipitation (DSP) behavior in the presence of different additives (y-axis). Scale bar represents 50 μm . ^a Photo of 20 minute aliquot.

CHAPTER 4

Novel Posaconazole Cocrystals with Potential to Overcome Clinical Challenges

Introduction

Posaconazole (PSZ) is a third-generation azole drug indicated as an antifungal agent for the treatment of invasive yeast and mold.¹ While safer and with a broader spectrum of activity than many earlier generation azole drugs, PSZ remains challenging to administer orally. The marketed suspension formulation of PSZ has been shown to have both low and highly variable oral bioavailability as a result of positive food-effect pharmacokinetics, abnormal gastric pH levels common in patients due to disease state, and high solubility – pH dependence leading to precipitation when transferred from the stomach to the intestines.²⁻⁴ An amorphous delayed-release tablet was later developed to mitigate some of these problems, but therapeutic drug monitoring is still required and treatment is commonly inadequate compared to intravenous administration.^{3, 5}

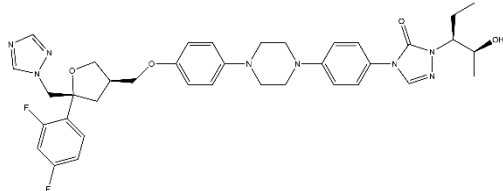
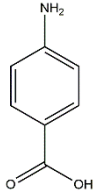
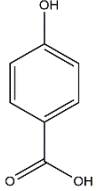
We have previously reported the discovery a 2:3 PSZ cocrystal with 4-aminobenzoic acid (4ABA) and its superior pharmaceutical properties compared to crystalline PSZ.⁶ PSZ is a Biopharmaceutics Classification System (BCS) Class II drug, characterized by its high lipophilicity (Log P 4.6) and low aqueous solubility (< 1 µg/mL).^{1, 7, 8} Like many cocrystals of BCS Class II drugs with highly soluble cofomers, PSZ-4ABA was found to have high solubility advantage ($SA = S_{\text{cocrystal}} / S_{\text{drug}}$) over the drug in biorelevant media ($SA = 139$ in FaSSIF and $SA = 48$ in FeSSIF).^{6, 9} PSZ-4ABA also had superior dissolution performance in FaSSIF and

FeSSIF, sustaining supersaturation > 3 for the course of both experiments (up to 180 minutes) and increasing area under the curve (AUC) 4.1 and 13 times, respectively.⁶

Cocrystals such as PSZ-4ABA continue to gain interest for their unique properties compared to other supersaturating drug delivery systems, such as amorphous forms, polymorphs, and salts.^{10, 11} Cocrystals are distinguished in that they form via noncovalent interactions (unlike salts) and can be composed of both ionizable and nonionizable components, have crystalline stability advantage compared amorphous solids, have the ability to impart or alter the solubility – pH dependence of parent drug, and mitigate the negative effects of pH – dependent dissolution.^{9, 12-16} Because cocrystals are formed in a crystal lattice with well-defined stoichiometry, their SA has been shown to be fine-tunable as a function of solution conditions, a unique property that does not apply to nonstoichiometric solids.^{9, 12, 17}

Given the unique advantages that cocrystals provide, PSZ cocrystals have the potential to overcome some of the clinical challenges with oral PSZ administration. In this work, we report the discovery of a second PSZ cocrystal with 4-hydroxybenzoic acid and its characterization. Component structures and pK_a values for both PSZ cocrystals are shown in Table 4.1. Solubility of PSZ-4ABA, PSZ-4HBA, and crystalline PSZ are compared in both aqueous and biorelevant media, and mathematical models to predict cocrystal solubility – pH dependence are derived and validated with experimental measurements. Finally, excess coformer concentration is evaluated as a tool to enhance cocrystal dissolution behavior by predictably fine-tuning cocrystal solubility and SA as a function of cocrystal solubility product K_{sp} .

Table 4.1. Chemical Structures and pK_a Values of Drug and Coformers.

Cocrystal Component	Structure	pK _{a,1} , pK _{a,2}
PSZ		3.6, 4.6 (basic) ¹⁸
4ABA		2.6 (basic), 4.6 (acidic) ¹⁹
4HBA		4.6 (acidic) ²⁰

Materials and Methods

Materials

Posaconazole was purchased from BOC Sciences (Shirley, NY) and used as received. 4-aminobenzoic acid, acetic acid, sodium acetate anhydrous, dipotassium hydrogen phosphate, trifluoroacetic acid, and sodium chloride were purchased from Sigma-Aldrich (St. Louis, MO) and used as received. 4-hydroxybenzoic acid was purchased from Acros Organics (Fair Lawn, NJ) and used as received. Sodium hydroxide was purchased from J. T. Baker Chemical Company (Phillipsburg, NJ) and used as received. High performance liquid chromatography (HPLC)-grade methanol, HPLC-grade acetonitrile, sodium phosphate monobasic, and hydrochloric acid were purchased from Fisher Scientific (Fair Lawn, NJ). FaSSIF/FeSSIF/FaSSGF powder was purchased from Biorelevant.com Ltd (London, UK).

Cocrystal Synthesis

PSZ-4ABA⁶ and PSZ-4HBA cocrystals for solubility and dissolution studies were prepared by reaction crystallization method²¹ (RCM) in acetonitrile at room temperature (22 to 25 °C). Acetonitrile was chosen to maximize drug solubility (18 mM) relative to coformer solubility (345 mM for 4ABA and 270 mM for 4HBA) and to avoid the formation of solvates.²² Half saturated 4ABA solution was prepared by adding 1.7 g 4ABA to 25 mL of acetonitrile, allowing to stir for 2 hours, filtering the suspension through a 0.45 μM pore membrane, and diluting 1:1 with pure acetonitrile. PSZ-4ABA was prepared by adding 350 mg PSZ to 10 mL of a half saturated 4ABA solution in acetonitrile and allowing to stir for 2 hours. For PSZ-4HBA, saturated solutions of PSZ in acetonitrile were prepared by adding 130 mg of PSZ to 10 mL of acetonitrile. Saturated solutions of 4HBA in acetonitrile were prepared by adding 800 mg of 4HBA to 22 mL of acetonitrile. Respective PSZ and 4HBA solutions were filtered through 0.45

μM pore membranes, and 10 mL filtered 4HBA solution was added to 10 mL filtered PSZ solution and allowed to stir for two hours. Suspensions were vacuum-filtered and washed with 10 mL acetonitrile. Dried solids were analyzed by powder X-ray diffraction (PXRD) and differential scanning calorimetry (DSC).

Single crystals of PSZ-4HBA were obtained by slow evaporation in acetonitrile at room temperature. Saturated component solutions were prepared by suspending PSZ and 4HBA respectively in acetonitrile, allowing to stir at room temperature, and filtering after one hour. Filtered saturated 4HBA solution was diluted in a 1:1 ratio with pure acetonitrile. 0.8 mL of the saturated PSZ solution in acetonitrile was combined with 0.8 mL of the half saturated 4HBA solution in acetonitrile in a glass HPLC vial with a hole poked through the lid. Colorless, needle-like crystals were obtained and isolated from the solution by 48 h.

Phase Purity and Cocrystal Stoichiometry

To improve cocrystal phase purity during PSZ-4HBA synthesis, RCM was performed in conditions that were undersaturated with respect to both components. Synthesized solid was thoroughly washed with pure acetonitrile to prevent precipitation of components during vacuum filtration and drying.

Cocrystal stoichiometry was determined by analytical measurement of drug and coformer concentrations of the completely dissolved cocrystal by HPLC. 15 mg of cocrystal were fully dissolved in 10 mL of high-performance liquid chromatography (HPLC) mobile phase (50:50 methanol:water with 0.1% trifluoroacetic acid) in triplicate for each prepared cocrystal batch. Solutions were analyzed by HPLC to determine the drug and coformer molar concentrations and from these their stoichiometric ratio in the cocrystal.

Synchrotron X-ray Diffraction (SXR)

PSZ-4HBA crystal structure was determined from synchrotron X-ray diffraction at Argonne National Laboratory in Lemont, IL, USA. Data collection was temperature controlled at 300 K.

Powder X-ray Diffraction (PXRD)

Powder X-ray diffractograms of solid phases were obtained on a benchtop Rigaku Miniflex X-ray diffractometer (Danvers, MA) using Cu-K α radiation ($\lambda = 1.54 \text{ \AA}$), a tube voltage of 30 kV, and a tube current of 15 mA. Data were collected at room temperature between 5° and 40° in 2θ at a continuous scan rate of 2.5°/min.

Differential Scanning Calorimetry (DSC)

A TA Instruments DSC (Newark, DE) was used to analyze solid phases. Thermal measurements were performed by heating the samples at a rate of 10 °C/min under a dry nitrogen atmosphere (50 mL/min). Standard aluminum sample pans and lids were used for all measurements.

Raman Spectroscopy

Raman analysis was conducted using a WiTec alpha300R confocal Raman microscope (Ulm, Germany) equipped with a 532 nm solid-state excitation laser, and a Zeiss EC EPIPLAN 50X objective (N.A. = 0.75). Single point spectra of PSZ, 4HBA, 1:2 PSZ-4HBA, and 2:3 PSZ-4HBA were obtained by focusing the laser on the samples with an integration time of 500 ms. Large area scans were done across 25 μm by 25 μm areas throughout 1:2 PSZ-4HBA single crystals and across 100 μm by 100 μm areas throughout 2:3 PSZ-4HBA, PSZ, and 4HBA with an integration time of 500 ms per pixel. A MATLAB[®] processing algorithm developed in-house²³ was used to obtain averages and standard deviations of the spectra. Spectra were also

normalized, baseline-subtracted, and overlaid using the MATLAB[®] processing algorithm. Cosmic ray removal was done on all spectra using the WiTec Project FOUR software.

High-Performance Liquid Chromatography (HPLC)

PSZ, 4ABA, and 4HBA concentrations were analyzed by a Waters HPLC equipped with a UV spectrometer detector. A Waters Atlantis C18 column with 5 μm , 250 \times 4.6 mm dimensions was used for separation. A gradient method using methanol and water with 0.1% trifluoroacetic acid was used with a flow rate of 1 mL/min. The gradient consisted of 50:50 methanol : water with 0.1% trifluoroacetic acid at 0 min, 90:10 methanol : water with 0.1% trifluoroacetic acid at 4.2 min, and 50:50 methanol : water with 0.1% trifluoroacetic acid at 8.2 min. Total run time was 11 min. Samples were diluted with mobile phase composed of 50% methanol and 50% water + 0.1% trifluoroacetic acid. For PSZ, injection volume was 20 μL for studies in FaSSIF and FeSSIF biorelevant media and 60 μL for studies in blank, aqueous media. Coformers were analyzed at injection volume of 20 μL for all studies. Analytes were monitored at wavelengths of 259 nm for PSZ, 287 nm for 4ABA, and 255 nm for 4HBA.

Dissolution and Solubility Media Preparation

pH 6.5 ± 0.1 phosphate buffer (blank FaSSIF) was prepared at room temperature by dissolving 0.840 g of NaOH (pellets), 7.908 g of $\text{NaH}_2\text{PO}_4 \cdot \text{H}_2\text{O}$, and 12.372 g NaCl in 2 L of purified deionized (DI) water. Acetate buffer at pH 5.0 ± 0.1 (blank FeSSIF) was prepared at room temperature by dissolving 4.040 g of NaOH (pellets), 8.650 g of acetic acid, and 11.87 g NaCl in 1 L of DI water. 1 M NaOH or 1 M HCl solutions were used to adjust the pH of the buffers. FaSSIF and FeSSIF were prepared with the corresponding blank medium and FaSSIF/FeSSIF/FaSSGF powder according to manufacturer protocol. 4ABA was pre-dissolved in FeSSIF for use in excess coformer dissolution studies.

Eutectic Concentrations

Drug and coformer concentrations were measured at the eutectic point, where drug and cocrystal solid phases were in equilibrium with solution. Excess cocrystal (150 mg) and drug (75 mg) were suspended in 3 mL of solution. The suspensions were magnetically stirred for 96 h in a 25.0 (\pm 0.5) °C water bath. Every 24 h, 0.5 mL aliquots were collected, filtered through a 0.45 μ m pore cellulose acetate membrane via centrifuge, and analyzed by HPLC. pH was measured and collected solid phases were characterized by DSC and PXRD.

Cocrystal and Drug Powder Dissolution

PSZ-4ABA cocrystal and drug powder dissolution studies were conducted in a water bath at 25.0 (\pm 0.5) °C over three hours using an overhead stirrer with a glass propeller at 150 rpm. Both cocrystal and drug were sieved to a particle size range of 106 to 125 μ m. 36 mg PSZ drug or 46.6 mg PSZ-4ABA cocrystal (molar equivalent PSZ amount) were added to 30 mL of dissolution media based on a 300 mg dose in 250 mL. 0.5 mL aliquots were sampled with a syringe at time points up to three hours. The solution samples were filtered through syringe filter with PVDF membrane of a pore size of 0.45 μ m. Initial solution pH was measured, as well as the pH of all aliquots. The solution concentrations of PSZ and 4ABA were analyzed by HPLC. Final solid phases were analyzed by DSC.

Dissolution and Precipitation Pathways

Samples from cocrystal dissolution were visually inspected under bright field microscopy using a Leica DMI8 inverted optical microscope (Wetzlar, Germany). For each aliquot, 100 μ L were immediately transferred (before filtering) into a quartz 96-well plate to be observed under the microscope. Images were taken with a Leica DMC2900 camera controlled with LAS v4.7

software (Leica Microsystems, Wetzlar, Germany). The 20x magnification lens was used for all reported observations.

Results and Discussion

Characterization of PSZ-4HBA Cocrystal

Single crystal growth of PSZ-4HBA was attempted by slow evaporation methods but was largely unsuccessful due to the rapid crystallization of large spherical particles at higher component concentrations. Longer times for crystallization (over one week) led to chemical degradation. Very thin needle-like single crystals were isolated by slow evaporation at about 48 hours in acetonitrile at room temperature. Crystal analysis by synchrotron revealed a 1:2 stoichiometry (PSZ:4HBA) and an orthorhombic unit cell. Crystal structure analysis results are presented in Appendix 4A. This stoichiometry is different from that of the cocrystal prepared by RCM (2:3), determined by dissolving the cocrystal and measuring the component concentrations by HPLC analysis as described in the methods section. Stoichiometric analysis results are presented in Appendix 4A. It appears that this cocrystal can exist in two different stoichiometries, and this section presents the similarities and differences in the solid-state characterization of the RCM cocrystal (2:3) and the single crystal prepared by slow evaporation (1:2). Subsequent solution phase analyses were conducted with cocrystal obtained by RCM and solubility assessment is based on the 2:3 cocrystal stoichiometry determined by HPLC. Solubility values calculated according to a 1:2 stoichiometry show higher cocrystal solubility and SA. These values are presented and compared to 2:3 solubility values in Appendix 4B.

Figure 4.1 shows the PXRD pattern of PSZ-4HBA, PSZ, and 4HBA. The PXRD pattern of 2:3 PSZ-4HBA obtained by RCM and the 1:2 single crystal have unique patterns compared to

PSZ and 4HBA. Differences in the cocrystal and component patterns demonstrate the formation of a new solid phase. However, the RCM cocrystal pattern does not match the calculated cocrystal pattern simulated by Mercury for SXRD data as these are two different stoichiometries, with a 1:2 cocrystal forming during single crystal growth and a 2:3 cocrystal forming during RCM.

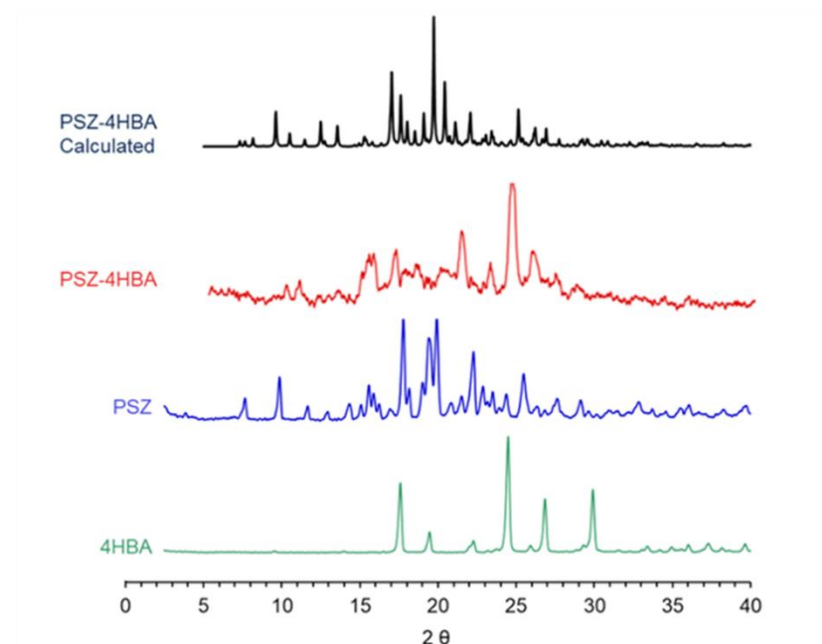


Figure 4.1. Powder X-ray diffraction (PXRD) patterns of cocrystal (PSZ-4HBA), drug (PSZ), and coformer (4HBA). PXRD pattern of 2:3 PSZ-4HBA obtained from reaction crystallization method (RCM) does not match the calculated pattern simulated by Mercury for the synchrotron X-ray diffraction (SXRD) data. Cocrystal PXRD courtesy of Prof. Adam Matzger. SXRD was calculated from single crystal analysis courtesy of Dr. Dongzhou Zhang and Prof. M. Fátima M. da Piedade.

Results of the Raman analysis in Figure 4.2 display a distinct chemical fingerprint for 2:3 PSZ-4HBA obtained by RCM and 1:2 PSZ-4HBA compared with its components, PSZ and 4HBA. A comparison between the spectra of PSZ and the cocrystals showed a blue shift of shared peaks within the spectral region of $700\text{--}850\text{ cm}^{-1}$. Raman spectra of the cocrystals also display new peaks at 1685 cm^{-1} , 2834 cm^{-1} , and 3134 cm^{-1} that are not present in its components.

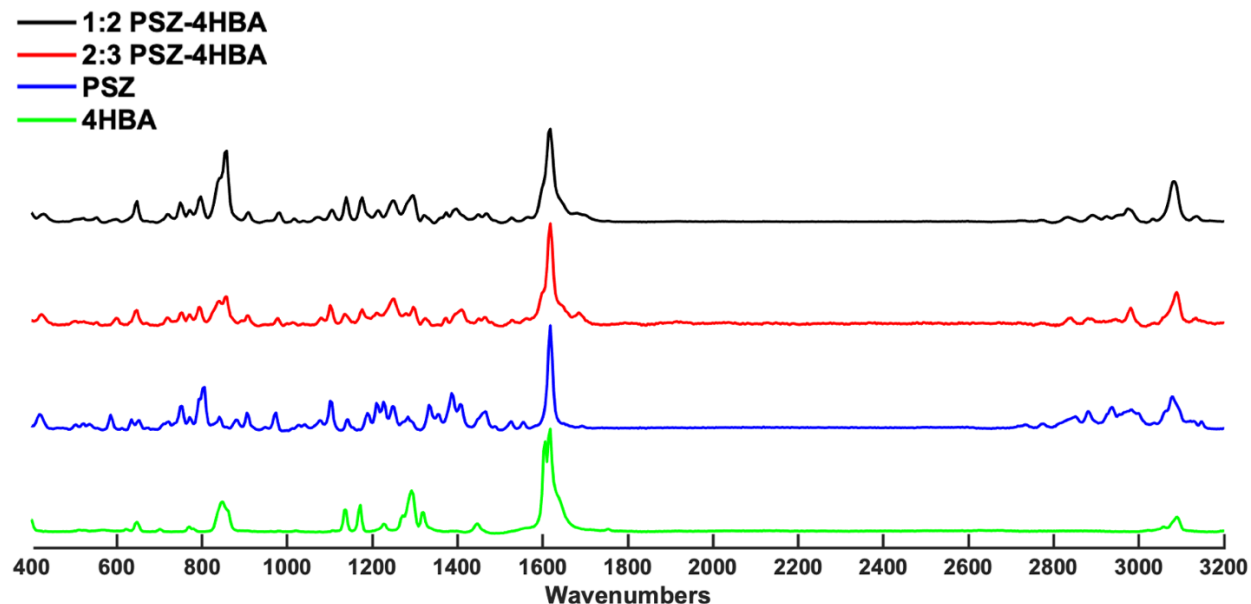


Figure 4.2. Raman spectra of cocrystals (PSZ-4HBA), drug (PSZ), and coformer (4HBA) show unique chemical fingerprints. The spectra displayed are the averages of large area scans. Courtesy of Jennifer Diaz-Espinosa.

Even though 1:2 PSZ-4HBA and 2:3 PSZ-4HBA share peaks and shifts that distinguish them from their components, the cocrystals also contain spectral differences between them. One difference in the spectra of the cocrystals is the morphology of the shared peaks located at 909 cm^{-1} and 1296 cm^{-1} . 1:2 PSZ-4HBA has a single peak at both 909 cm^{-1} and 1296 cm^{-1} ; however, these peaks split in the 2:3 PSZ-4HBA spectra. The peak morphology found at 1296 cm^{-1} in 2:3 PSZ-4HBA matches the morphology and the location of a peak in 4HBA. Also, there is a peak height difference located at 858 cm^{-1} in the cocrystals' spectra. In Figure 4.3, the averaged spectra obtained by using the single point Raman method shows that the peak located at 858 cm^{-1} is taller in 1:2 PSZ-4HBA than it is in 2:3 PSZ-4HBA. The standard deviation that is also shown in Figure 4.3 displays instances where the peak located at 858 cm^{-1} in the 1:2 PSZ-4HBA spectra is as tall as the peak located at 1618 cm^{-1} ; for reference, this peak located at 1618 cm^{-1} is the tallest peak in all the 2:3 PSZ-4HBA spectra. The peak at 858 cm^{-1} displayed in the

cocrystals' spectra originates from PSZ and can be found at 806 cm^{-1} in the PSZ spectra. Also, the 1:2 PSZ-4HBA morphology of the 858 cm^{-1} peak matches the morphology of the 806 cm^{-1} drug peak. The peak differences found between the cocrystals reveals that the spectra of 1:2 PSZ-4HBA that contains less 4HBA than 2:3 PSZ-4HBA, resembles the drug spectra more closely than 2:3 PSZ-4HBA; whereas, the spectra of 2:3 PSZ-4HBA that contains more 4HBA than 1:2 PSZ-4HBA, resembles the 4HBA spectra more closely than 1:2 PSZ-4HBA.

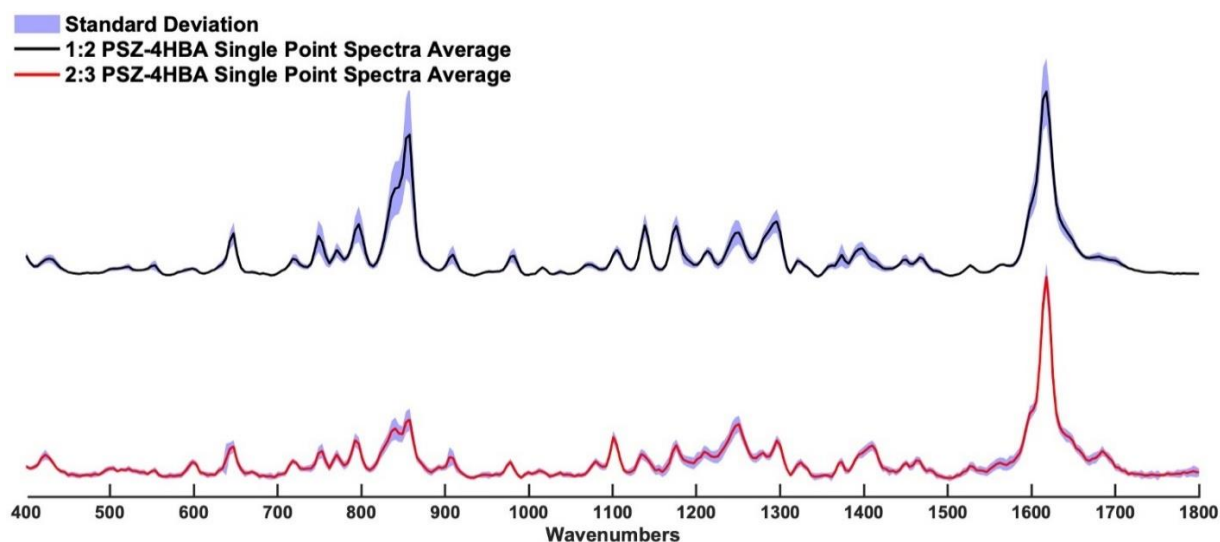


Figure 4.3. Raman spectra of 1:2 PSZ-4HBA single crystal and 2:3 PSZ-4HBA powder from reaction crystallization method (RCM). The spectra are shown as average and standard deviation obtained from single point scans. Courtesy of Jennifer Diaz-Espinosa.

Figure 4.4 shows the thermal behavior of 2:3 PSZ-4HBA cocrystal prepared by RCM and its components. A single endothermic event at $166.9 \pm 1.0\text{ }^{\circ}\text{C}$ is the melting point of 2:3 PSZ-4HBA and was consistently $1 - 2\text{ }^{\circ}\text{C}$ lower than the melting point of PSZ ($168.2 \pm 1.0\text{ }^{\circ}\text{C}$) and much lower than the melting point of 4HBA ($215.5 \pm 1.0\text{ }^{\circ}\text{C}$). PSZ-4ABA was previously characterized as having a melting point of $154.1 \pm 0.6\text{ }^{\circ}\text{C}$, which was also lower than both components.⁶ PSZ is observed to have two endothermic events, the first of which occurs at $134.0 \pm 1.0\text{ }^{\circ}\text{C}$ and corresponds to an impurity.²⁴

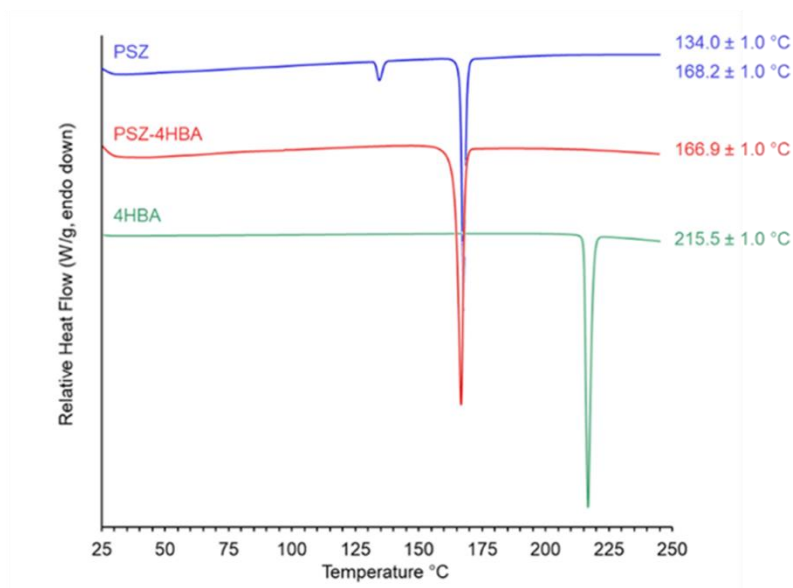


Figure 4.4. Differential scanning calorimetry (DSC) thermograms of cocrystal (PSZ-4HBA), drug (PSZ), and coformer (4HBA).

Cocrystal Eutectic Constant K_{eu} , Solubility, and Solubility Advantage (SA)

Cocrystal solubility was calculated as a function of relevant solution equilibria, solution conditions, and cocrystal stoichiometry. The analyses in this section are conducted for the case of a 2:3 PSZ-4HBA cocrystal, which was the solid phase used in these studies. Solubility values for the 2:3 PSZ-4HBA are compared with those of a 1:2 PSZ-4HBA cocrystal in Appendix 4B.

The eutectic constant K_{eu} has been well-recognized to be a key indicator of cocrystal stability and can be usefully applied to calculate cocrystal SA. K_{eu} is defined as the ratio of coformer to drug concentrations at the eutectic point, where drug and cocrystal solid phases are in equilibrium with solution, according to

$$K_{eu} = \frac{[\text{coformer}]_{eu}}{[\text{drug}]_{eu}} \quad (4.1)$$

Figure 4.5 shows K_{eu} values calculated from drug and coformer eutectic concentrations in blank and biorelevant media for both 2:3 PSZ-4ABA and 2:3 PSZ-4HBA cocrystals. PSZ-

4ABA eutectic concentrations in biorelevant media have been previously reported but are repeated here for comparison.⁶

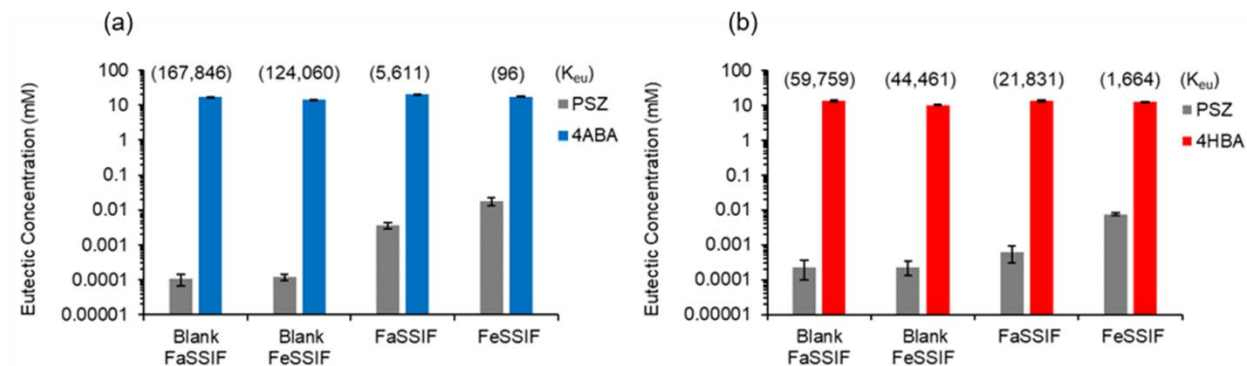


Figure 4.5. Drug and coformer eutectic concentrations in blank and biorelevant media. Figure (a) shows posaconazole – 4-aminobenzoic acid (PSZ-4ABA) cocrystal and (b) shows posaconazole – 4-hydroxybenzoic acid (PSZ-4HBA) cocrystal. Eutectic constant K_{eu} values are above bars and were calculated according to Equation 4.1. PSZ and 4ABA eutectic concentrations in FaSSIF and FeSSIF has been previously reported and are included here for comparison.⁶ Error bars represent standard deviations. PSZ-4ABA data courtesy of Dr. Gislaine Kuminek.

Equation 4.1 is independent of cocrystal stoichiometry, however interpretations of cocrystal stability are dependent on stoichiometry. The transition point where both cocrystal and drug are thermodynamically stable is indicated by the value of K_{eu} relative to the cocrystal stoichiometric ratio z/y , where y and z represent the drug and coformer stoichiometric coefficients, respectively. For 2:3 cocrystals, the transition point corresponds to $K_{eu} = 1.5$. $K_{eu} >$, $=$, or < 1.5 corresponds to higher, equal, or lower cocrystal solubility over drug, respectively. The results in Figure 4.5 and Table 4.2 indicate that $K_{eu} \gg 1.5$ in all studied media, meaning that the cocrystals have high solubility advantage compared to drug under these conditions. Initial pH 6.5 in FaSSIF conditions equilibrated to pH 5.0 – 5.1 for both cocrystals due to self-buffering by cocrystal components. Equilibrium pH values are the relevant values to solubility measurements and are used in this analysis.

Table 4.2. Component Eutectic Concentrations and Calculated Cocystal Solubility Values in Blank and Biorelevant Media.

Cocystal	Media	Final pH ^a	[PSZ] _T (mM)	[CF] _T (mM)	K _{eu} ^b
2:3 PSZ-4ABA	Blank FaSSIF	5.1 ± 0.1	(1.0 ± 0.4) × 10 ⁻⁴	17.4 ± 0.1	(1.7 ± 0.6) × 10 ⁵
	Blank FeSSIF	5.1 ± 0.1	(1.2 ± 0.3) × 10 ⁻⁴	14.5 ± 0.3	(1.2 ± 0.3) × 10 ⁵
	FaSSIF	5.1 ± 0.1	(3.6 ± 0.8) × 10 ⁻³	20.2 ± 0.4	(5.6 ± 1.3) × 10 ³
	FeSSIF	5.0 ± 0.1	(1.8 ± 0.5) × 10 ⁻²	17.3 ± 0.5	(9.6 ± 2.7) × 10 ²
2:3 PSZ-4HBA	Blank FaSSIF	5.1 ± 0.1	(2.2 ± 1.3) × 10 ⁻⁴	13.3 ± 0.6	(6.0 ± 3.4) × 10 ⁴
	Blank FeSSIF	4.8 ± 0.1	(2.3 ± 1.0) × 10 ⁻⁴	10.2 ± 0.4	(4.5 ± 1.9) × 10 ⁴
	FaSSIF	5.0 ± 0.1	(6.1 ± 3.0) × 10 ⁻⁴	13.3 ± 0.5	(2.2 ± 1.1) × 10 ⁴
	FeSSIF	4.8 ± 0.1	(7.5 ± 0.7) × 10 ⁻³	12.5 ± 0.1	(1.7 ± 0.2) × 10 ³

^a Initial pH was 6.5 ± 0.1 for Blank FaSSIF and FaSSIF media, and 5.0 ± 0.1 for Blank FeSSIF and FeSSIF media.

^b Calculated according to Equation 4.1.

Under the studied conditions, [PSZ]_{eu} = S_{drug}. However, a two-way ANOVA test showed significant difference between the [PSZ]_{eu} measurements between the two cocystals (p value < 0.0001) in Table 4.2. While it is possible that this difference is due to solution interactions between the drug and respective cofomers, it should be noted that these concentrations are at the limit of quantification due to the low solubility of PSZ. Solubility of crystalline PSZ has been previously reported as 2.4 × 10⁻³ mM in pH 6.5 FaSSIF at 37°C, which is lower than [PSZ]_{eu} measured from PSZ-4ABA and higher than [PSZ]_{eu} from PSZ-4HBA in FaSSIF at 25°C.²⁵ Given the scale of these solubility values, functionally small yet statistically significant variation between the [PSZ]_{eu} measurements for the two cocystals are compounded into larger differences in calculations that rely on the eutectic measurements. High standard deviation (9 - 59%) is also

observed within the triplicated measurements. For these and subsequent calculations, the high propagated variance between the cocrystals and deviation within triplicate measurements should be noted, but the level of uncertainty associated with the $[\text{PSZ}]_{\text{eu}}$ data does not preclude the observation that PSZ is a very poorly soluble drug and that the PSZ-4ABA and PSZ-4HBA cocrystals have high solubility advantage in the studied media.

K_{eu} has been shown to be directly proportional to cocrystal SA according to

$$SA = \left(\frac{y}{z} K_{\text{eu}}^{y:z} \right)^{z/(y+z)} \quad (4.2)$$

which for a 2:3 cocrystal simplifies to

$$SA = \left(\frac{2}{3} K_{\text{eu}}^{2:3} \right)^{3/5} \quad (4.3)$$

The predicted and experimental SA – K_{eu} relationship is shown for both PSZ cocrystals in Figure 4.6. Because the values are very large, the log – log relationship is presented according to

$$\log SA = \frac{3}{5} \log \left(\frac{2}{3} K_{\text{eu}}^{2:3} \right) \quad (4.4)$$

The results indicate excellent agreement between predicted and experimental values. In aqueous conditions, PSZ cocrystals are shown to have solubility advantage orders of magnitude higher than parent drug. This also means that equilibrium pH 4.8 – 5.1 for these measurements are above pH_{max} , the transition pH at which cocrystal and drug solubilities are equal ($K_{\text{eu}} = 1.5$ and $SA = 1$). K_{eu} and SA both decrease in biorelevant media compared to aqueous media, a trend that is supported by previous findings from our laboratory that show these parameters can be modulated in the presence of drug solubilizing agents such as those present in FaSSIF and FeSSIF.^{17, 26, 27}

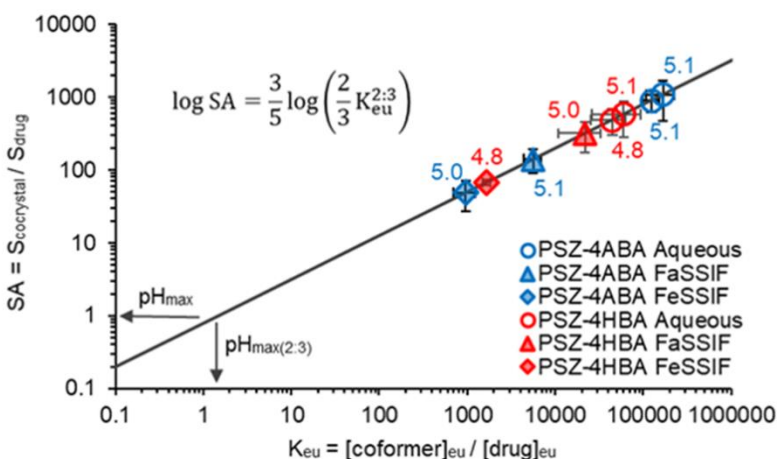


Figure 4.6. Predicted relationship between eutectic constant K_{eu} and cocystal solubility advantage (SA) for 2:3 posaconazole – 4-aminobenzoic acid (PSZ-4ABA) cocystal and 2:3 posaconazole – 4-hydroxybenzoic acid (PSZ-4HBA) cocystal. K_{eu} value of 1.5 indicates pH_{max} for a 2:3 cocystal. Symbols represent values calculated from experimental measurements. Numbers next to symbols represent equilibrium pH. Line predicted from Equation 4.4. Error bars represent standard deviations. PSZ-4ABA data courtesy of Dr. Gislaine Kuminek.

Eutectic concentrations can also be used to calculate cocystal solubility.²⁸ The general equation for this calculation is

$$S_{cocystal} = y \sqrt{\frac{[drug]_{eu}^y [coformer]_{eu}^z}{y^y z^z}} \quad (4.5)$$

which for the 2:3 PSZ cocystals is

$$S_{2:3 \text{ PSZ-CF}} = 2 \sqrt{\frac{[drug]_{eu}^2 [coformer]_{eu}^3}{108}} \quad (4.6)$$

Equations 4.5 and 4.6 describe cocystal solubility in terms of moles of drug for comparison to drug solubility.²⁹

The aqueous solubilities (Table 4.3) are shown to be similar for both cocystals, and solubility increased in biorelevant media. FeSSIF had a greater solubilization for the drug than FaSSIF, particularly for the 4-ABA cocystal. The cocystal solubility advantage over drug is also shown to decrease with drug solubilization in biorelevant media. This means that SA can be

modulated with solubilizing agents to reduce the risk of conversion during dissolution and to promote sustained supersaturation.¹⁷

Table 4.3. Cocrystal Solubility, Solubility Advantage (SA), and Dose/solubility Ratio (D_0) Values.

Cocrystal	Media	Final pH ^a	$S_{\text{cocrystal}}$ (mM) ^b	SA	$D_{0(\text{drug})}$ ^c	$D_{0(\text{cocrystal})}$ ^d
2:3 PSZ-4ABA	Blank FaSSIF	5.1 ± 0.1	0.11 ± 0.04	1069 ± 601	16496 ± 5880	16 ± 6
	Blank FeSSIF	5.1 ± 0.1	0.10 ± 0.02	892 ± 285	14630 ± 2955	16 ± 3
	FaSSIF	5.1 ± 0.1	0.50 ± 0.12	139 ± 49	476 ± 106	3.4 ± 0.8
	FeSSIF	5.0 ± 0.1	0.90 ± 0.25	48 ± 21	95 ± 26	1.9 ± 0.5
2:3 PSZ-4HBA	Blank FaSSIF	5.1 ± 0.1	0.13 ± 0.02	576 ± 294	7679 ± 4345	14 ± 2
	Blank FeSSIF	4.8 ± 0.1	0.11 ± 0.02	482 ± 188	7466 ± 3211	15 ± 3
	FaSSIF	5.0 ± 0.1	0.19 ± 0.04	315 ± 141	2817 ± 1401	9 ± 2
	FeSSIF	4.8 ± 0.1	0.51 ± 0.02	67 ± 6	227 ± 21	3.4 ± 0.1

^a Initial pH was 6.5 ± 0.1 for Blank FaSSIF and FaSSIF media, and 5.0 ± 0.1 for Blank FeSSIF and FeSSIF media.

^b Calculated according to Equation 4.6.

^c Calculated from $C_{\text{dose}} = 1.71$ mM (molar equivalent of 300 mg PSZ dose in 250 mL luminal volume) and values in Table 4.2 according to Equation 4.7.

^d Calculated from $C_{\text{dose}} = 1.71$ mM (molar equivalent of 300 mg PSZ dose in 250 mL luminal volume) and S_{CC} values according to Equation 4.8.

The drug and cocrystal dose/solubility ratios in Table 4.3 are given by

$$D_{0(\text{drug})} = \frac{C_{\text{dose}}}{S_{\text{drug}}} \quad (4.7)$$

and

$$D_{0(\text{cocrystal})} = \frac{C_{\text{dose}}}{S_{\text{cocrystal}}} \quad (4.8)$$

where C_{dose} is the dose concentration, based on a 300 mg PSZ dose and a volume of 250 mL (volume to dissolve the dose or luminal volume). $D_{0(\text{drug})}$ is a well-recognized unitless parameter that describes the extent to which the drug dose can dissolve.^{30, 31} In fact, the Quantitative Biopharmaceutics Classification System describes Category II drugs (low solubility, high permeability) as having $D_{0(\text{drug})} > 1$.³² The results in Table 4.5 show $D_{0(\text{drug})} \gg 1$ in all studied media, indicating that solubility would need to be increased 95 – 16496 times to be able to completely dissolve the dose. Because of the high cocrystal SA, $D_{0(\text{cocrystal})}$ values are orders of magnitude lower. In biorelevant media, both cocrystals were observed to have $D_{0(\text{cocrystal})}$ values of 2 – 9, meaning that with the dynamic process of absorption, a cocrystal formulation may be able to completely dissolve the dose.

Comparing SA and $D_{0(\text{drug})}$ is useful to assess cocrystal dissolution and supersaturation behavior as recently demonstrated.^{33, 34} One can assess whether: (1) the cocrystal solubility is adequate to fully dissolve the drug dose without precipitation, $D_{0(\text{drug})} < SA$ ($C_{\text{dose}} < S_{\text{cocrystal}}$), and (2) the drug supersaturation is limited by C_{dose} or by $S_{\text{cocrystal}}$. Under the studied conditions, $D_{0(\text{drug})} > SA$ and dose – limited supersaturation is not expected ($C_{\text{dose}} > S_{\text{cocrystal}}$).

Solubility Product K_{sp} and Cocrystal Solubility – pH Dependence

Solubility is a conditional constant and is dependent on pH, while the solubility product K_{sp} is not. K_{sp} governs the equilibrium between dissociation (dissolution) and association (precipitation) of the solid and solution phases. K_{sp} is calculated as

$$K_{sp} = [\text{drug}]^y [\text{coformer}]^z \quad (4.9)$$

where component concentrations are the product of only the species in the same molecular state as the cocrystal, i.e., neutral. For 2:3 PSZ cocrystals, K_{sp} was calculated as the stoichiometric product of the nonionized species at the eutectic point, according to

$$K_{sp(2:3 \text{ PSZ-CF})} = [\text{PSZ}]_{\text{eu,non}}^2 [\text{CF}]_{\text{eu,non}}^3 \quad (4.10)$$

K_{sp} values are reported in Table 4.4 and were evaluated from the nonionized species of the aqueous eutectic measurements. pK_{sp} values are also reported since K_{sp} values are very small, where $pK_{sp} = -\log K_{sp}$. K_{sp} is directly proportional to intrinsic cocrystal solubility, and higher K_{sp} values correspond to lower pK_{sp} . PSZ-4HBA was found to have a higher K_{sp} than PSZ-4ABA, which predicted slightly higher solubility in basic conditions as the effect of cofomer ionization decreases. Similar solubility – pH dependence is expected in this region given similar aqueous cofomer solubilities and ionization.^{9, 18-20} K_{sp} and pK_{sp} values have been published for several cocrystals and salts, but we are not currently aware of any reported values for other 2:3 cocrystals and salts for comparison.^{33, 35-37}

Table 4.4. K_{sp} , pK_{sp} , pH_{max} , and $S_{\text{cocrystal}}$ at pH_{max} Values for Posaconazole Cocrystals.

Cocrystal	K_{sp} (M^5) ^a	pK_{sp} ^b	pH_{max}	$S_{\text{cocrystal}(pH_{\text{max}})}$ (mM)
2:3 PSZ-4ABA	$(3.7 \pm 2.1) \times 10^{-22}$	21.4	1.3	41.3
2:3 PSZ-4HBA	$(1.3 \pm 0.9) \times 10^{-21}$	20.9	1.9	3.1

^a Calculated according to Equation 4.9.

^b Calculated according to $pK_{sp} = -\log K_{sp}$.

Figure 4.7 shows the predicted and experimental solubility – pH dependence of PSZ drug and cocrystals as a function of K_{sp} (Table 4.4) and component pK_a values (Table 4.1). While self-buffering of components prevented studying a wider range of equilibrium pH values, these predictions provide insights into the ability of PSZ cocrystals to alter the solubility – pH dependence of the parent drug and to generate supersaturation in different regions of the gastrointestinal tract. Predicted and experimental solubilities are in excellent agreement within

the studied pH, and these predictions have been experimentally validated for wider pH ranges for several other cocrystals.^{12, 15, 29, 33, 35-40}

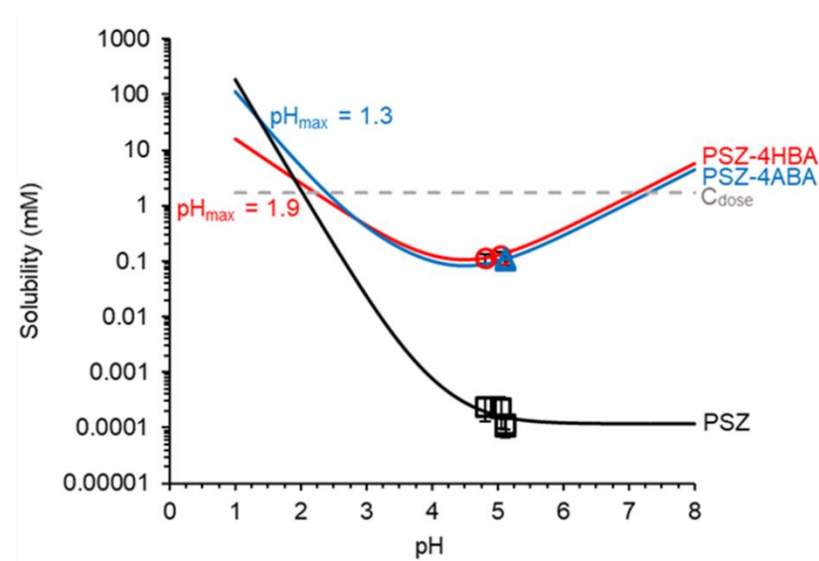


Figure 4.7. Solubility – pH dependence of basic drug posaconazole (PSZ), 2:3 posaconazole – 4-aminobenzoic acid cocrystal (PSZ-4ABA), and 2:3 posaconazole – 4-hydroxybenzoic acid cocrystal (PSZ-4HBA). Lines predicted according to Equations 4.12, 4.13, and 4.15, values in Tables 4.1 and 4.4, and $S_{PSZ,0} = 1.2 \times 10^{-4}$ mM. Experimental values are in Tables 4.2 and 4.3. Error bars represent standard deviations. PSZ-4ABA data courtesy of Dr. Gislaine Kuminek.

While drug solubility decreases exponentially with increasing pH, both cocrystals have U-shaped curves and much weaker solubility – pH dependence. Cocrystal solubilities are greater than C_{dose} at $pH < 2.2 - 2.4$ and $pH > 7.1 - 7.3$, but even at their lowest solubilities (pH 4.5) PSZ cocrystals are only 16.1 times lower than C_{dose} . In comparison, $S_{PSZ} > C_{dose}$ at $pH < 2.0$, but over 10,000 times lower than C_{dose} at $pH > 5.0$. This finding shows that PSZ cocrystal solubilities are less affected by differences in gastric (1-3) and intestinal (6-7) pH, and that the cocrystals have a greater potential to dissolve the dose. This behavior has important implications for improving the erratic bioavailability associated with current oral PSZ formulations.

Figure 4.7 also shows the transition point pH_{max} . PSZ-4ABA was more soluble in acidic conditions as a result of the basic pK_a 2.6 of the amphoteric cofomer, which resulted in a lower

$pH_{\max} = 1.3$ for PSZ-4ABA compared to $pH_{\max} = 1.9$ for PSZ-4HBA (Table 4.4). For both cocrystals, $S_{\text{cocrystal}} < S_{\text{drug}}$ at $pH < pH_{\max}$, $S_{\text{cocrystal}} = S_{\text{drug}}$ at $pH = pH_{\max}$, and $S_{\text{cocrystal}} > S_{\text{drug}}$ at $pH > pH_{\max}$, showing that relative cocrystal stability changes with pH.

The general equation that describes cocrystal solubility as a function of pH is

$$S_{\text{cocrystal}} = y^{y+z} \sqrt{\frac{K_{\text{sp}}}{(y^y z^z)}} \delta_{\text{drug,I}}^y \delta_{\text{coformer,I}}^z \quad (4.11)$$

where $\delta_{\text{drug,I}}$ and $\delta_{\text{coformer,I}}$ represent the respective contributions of drug and coformer ionization to cocrystal solubility.^{28, 41} $S_{\text{cocrystal}}$ is expressed as moles of drug in this form of the equation. This is useful as one is interested in the cocrystal to drug solubility ratios and supersaturation levels with respect to drug.

Table 4.5 shows the δ_I expressions in terms of pK_a and pH for dibasic, amphoteric, and monoprotic acidic components such as PSZ, 4ABA, and 4HBA. Stoichiometric coefficients and δ_I expressions in Table 4.5 are substituted into Equation 4.9 to give

Table 4.5. Ionization Terms (δ_I) for Posaconazole Drug and Coformers to Predict Cocrystal and Drug Solubilities according to Equations 4.12, 4.13, and 4.15.

Component	Ionization	$\delta_{\text{drug,I}}$ Or $\delta_{\text{coformer,I}}$
PSZ	Dibasic	$1 + 10^{pK_{a2,PSZ}-pH} + 10^{pK_{a1,PSZ}+pK_{a2,PSZ}-2pH}$
4ABA	Amphoteric	$1 + 10^{pH-pK_{a1,4ABA}} + 10^{pK_{a2,4ABA}-pH}$
4HBA	Acidic	$1 + 10^{pH-pK_{a,4HBA}}$

$$S_{2:3 \text{ PSZ-4ABA}} =$$

$$2 \sqrt[5]{\frac{K_{\text{sp}}}{108} (1 + 10^{pK_{a2,PSZ}-pH} + 10^{pK_{a1,PSZ}+pK_{a2,PSZ}-2pH})^2 (1 + 10^{pH-pK_{a1,4ABA}} + 10^{pK_{a2,4ABA}-pH})^3} \quad (4.12)$$

and

$$S_{2:3 \text{ PSZ-4HBA}} = 2 \sqrt[5]{\frac{K_{sp}}{108} (1 + 10^{pK_{a2,PSZ}-pH} + 10^{pK_{a1,PSZ}+pK_{a2,PSZ}-2pH})^2 (1 + 10^{pH-pK_{a,4HBA}})^3} \quad (4.13)$$

Equations 4.12 and 4.13 are used to predict cocrystal solubilities in Figure 4.7 with values in Tables 4.1 and 4.4. Derivations of Equations 4.12 and 4.13 are shown in Appendix 4B.

The general equation for drug solubility in terms of $\delta_{\text{drug,I}}$ is given by

$$S_{\text{drug}} = S_{\text{drug,0}} \delta_{\text{drug,I}} \quad (4.14)$$

where $S_{0,\text{drug}}$ is drug solubility under nonionized conditions. Substituting in $\delta_{\text{drug,I}}$ from Table 4.5 gives the solubility – pH dependence for PSZ as

$$S_{\text{PSZ}} = S_{\text{PSZ,0}} (1 + 10^{pK_{a2,PSZ}-pH} + 10^{pK_{a1,PSZ}+pK_{a2,PSZ}-2pH}) \quad (4.15)$$

Drug solubility is predicted in Figure 4.7 according to pK_a values in Table 4.1 and $S_{\text{PSZ,0}} = 1.2 \times 10^{-4}$ mM.

Cocrystal Solubility and Dissolution with Excess Coformer

We previously reported PSZ-4ABA and PSZ dissolution behavior in both FaSSIF and FeSSIF.⁶ The cocrystal sustained drug supersaturation ($\sigma = 2.8 - 3.1$) for the length of the experiment (180 minutes) in both media, reaching a $\sigma_{\text{max}} = [\text{PSZ}]_{\text{max}} / S_{\text{PSZ}} = 8.4$ at 5 minutes in FeSSIF and $\sigma_{\text{max}} = 16$ at 10 minutes in FaSSIF. While SA = 48 represented a theoretical thermodynamic limit to supersaturation in FeSSIF, $\sigma_{\text{max}} = 8.4$ is representative of the critical supersaturation for PSZ nucleation and a practical kinetic limit.

Previous values reported in this work represent stoichiometric cocrystal solubility and SA. However, in the presence of excess coformer, nonstoichiometric cocrystal solubility and SA are known to predictably decrease by definition of K_{sp} (Equation 4.9). Thus, the addition of

excess coformer during cocrystal dissolution may be used to fine-tune SA below critical supersaturation and thereby promote sustained supersaturation.

Figure 4.8 and Table 4.6 show the dissolution behavior of PSZ-4ABA in FeSSIF with and without excess coformer. 5.8 mM 4ABA was selected and pre-dissolved into the dissolution media to correspond to SA = 5.6, below the observed critical supersaturation 8.4 in FeSSIF studies but above the sustained supersaturation 2.8 – 3.1. The results in Figure 4.8a show that while cocrystal maintained $\sigma = 1.5 - 1.8$ from 10 – 180 minutes in the presence of 5.8 mM 4ABA and had superior dissolution performance compared to the drug in FeSSIF, it did not reach or maintain as high of supersaturation levels as in the absence of excess coformer. PSZ in other solid forms such as amorphous solid dispersions has been shown to maintain supersaturation levels of 1.5 – 3 up to 24 hours.⁴²⁻⁴⁴ These supersaturation levels appear to be within the metastable zone and below the threshold for nucleation to occur. Cocrystal dissolution at SA = 48 leads to an initial spike in supersaturation followed by precipitation and appears to have allowed the cocrystal to maintain a steady state at the higher level of the metastable zone, while modulating SA to 5.6 with excess coformer prevented a concentration spike and maintained a steady supersaturation level of 1.5 – 1.8 throughout the length of the experiment (180 minutes). Photomicrographs of dissolution aliquots are shown in Appendix 4C.

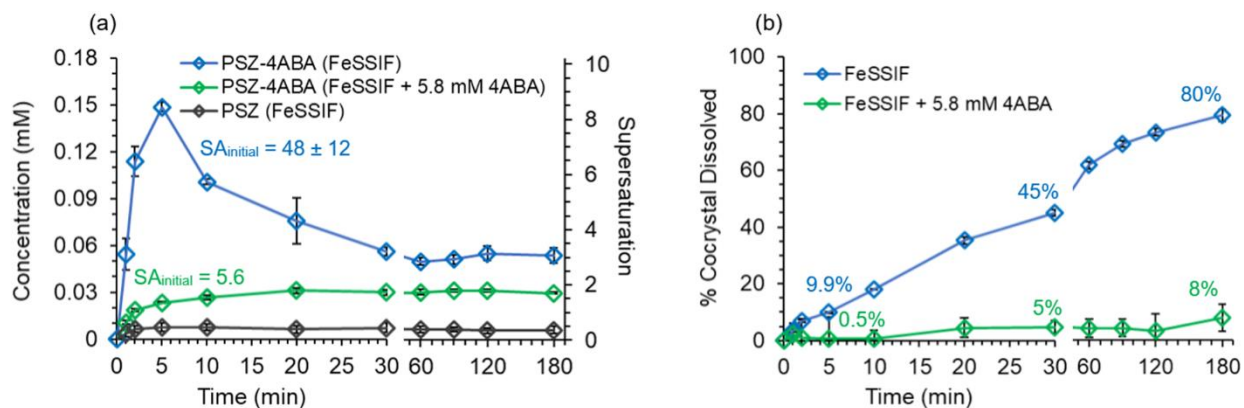


Figure 4.8. Cocrystral concentration – time and percentage cocrystral dissolved profiles in FeSSIF with and without excess cofomer. SA was predictably modulated from 48 to 5.6 with the addition of 5.8 mM 4ABA. Drug precipitation resulted in incongruent saturation, and the additional cofomer further decreased SA to 27.5 and 5.3 by 180 minutes. Cocrystral sustained supersaturation and performed better than the drug with and without excess cofomer, but lack of concentration spike and precipitation with excess cofomer at SA = 5.6 corresponded to a lower sustained supersaturation level and lower percentage cocrystral dissolved. Cocrystral and drug dissolution in FeSSIF have been previously reported and are included here for comparison.⁶ Error bars represent standard deviations.

Table 4.6. Cocrystal Dissolution Parameters with and without Excess Coformer.

Value	FeSSIF	FeSSIF + 5.8 mM 4ABA
SA_{initial}	48 ± 12	6
t_{max} (min)	5	120
C_{max} (mM)	0.148 ± 0.003	0.032 ± 0.001
σ_{max}	8.4 ± 0.2	1.79 ± 0.05
σ_{final} ^a	3.1 ± 0.3	1.71 ± 0.02
AUC (mM x min)	15.7 ± 4.6	5.4 ± 0.1
RAUC	13 ± 4	4.6 ± 0.4
Final [PSZ] (mM) ^a	$(5.4 \pm 0.5) \times 10^{-2}$	$(3.01 \pm 0.04) \times 10^{-2}$
Final [4ABA] (mM) ^a	2.1 ± 0.1	6.0 ± 0.1
Final $[\text{PSZ}]_{\text{non}}^2 [\text{4ABA}]_{\text{non}}^3$ ^a	9.7×10^{-24}	1.1×10^{-20}
Final % Cocrystal Dissolved ^a	80 ± 2	18.7 ± 0.9
Final pH ^a	5.01 ± 0.01	4.94 ± 0.01
Final Solid Phase(s) ^{ab}	PSZ-4ABA + PSZ	PSZ-4ABA

^a Final refers to 180 minute time point.

^b Characterized by DSC.

Furthermore, Figure 4.8b shows that 80% of cocrystal dissolved by 180 minutes without excess coformer, compared to only 8.1% with 5.8 mM 4ABA. Drug nucleation that occurred above the metastable zone in FeSSIF likely promoted further nucleation and growth even as the cocrystal maintained a steady state between cocrystal dissolution and drug precipitation within the metastable zone.

The influence of excess coformer on the dissolution of cocrystal components is shown in Figure 4.9. The 4ABA concentrations that would correspond to congruent dissolution are indicated according to a 2:3 stoichiometry. In FeSSIF, there is incongruent cocrystal dissolution after $t_{\text{max}} = 5$ minutes as a result of drug precipitation, coformer to drug molar ratio reaches a value of 38, and the final solid phase was characterized by DSC to be a mixture of PSZ-4ABA

and PSZ (Table 4.6). In contrast, cocrystal dissolution in media with excess coformer designed to generate supersaturations below the critical level, are shown to reduce the drug precipitation to undetectable levels per solid-state analysis results. In this case cocrystal dissolution is reduced by the proximity of solution conditions to cocrystal solubility so that more cocrystal cannot dissolve until drug precipitates. Therefore, driving forces for cocrystal dissolution and drug precipitation have been lowered while maintaining drug solution concentration levels about 1.7 times above drug solubility.

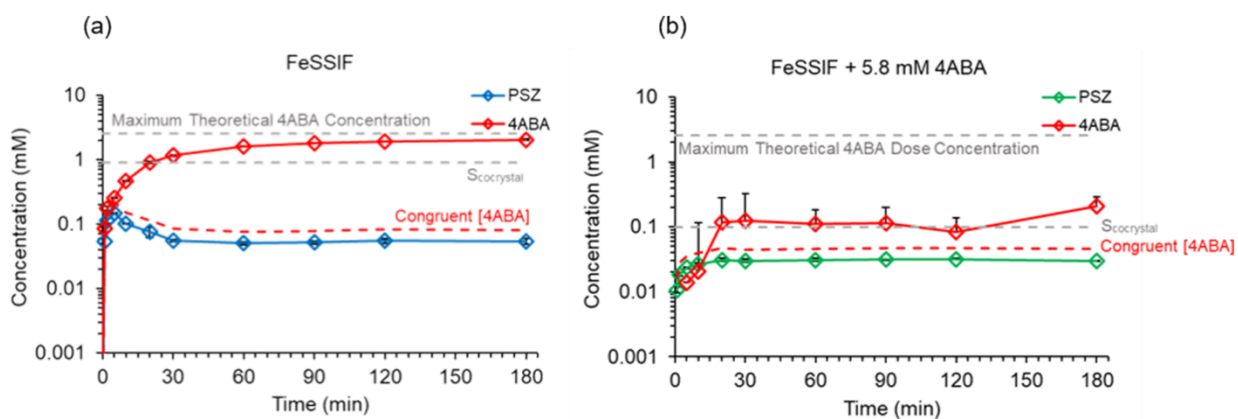


Figure 4.9. Component concentrations during PSZ-4ABA cocrystal dissolution in FeSSIF (a) with and (b) without 5.8 mM excess coformer. Incongruent dissolution was observed after 5 minutes in FeSSIF, but component dissolution was much closer to a stoichiometric ratio in FeSSIF + 5.8 mM 4ABA. Congruent [4ABA] line was calculated as $1.5 \times [\text{PSZ}]$. Error bars represent standard deviations (within points for [PSZ] and [4ABA] in FeSSIF).

The influence of coformer concentration on cocrystal dissolution behavior can be designed and analyzed by considering the phase solubility diagram in Figure 4.10. Cocrystal solubility is shown to decrease according to the K_{sp} from its stoichiometric solubility 0.9 mM (SA = 48) to nonstoichiometric solubility 0.1 mM (SA = 5.8). This analysis is useful for incongruent cocrystal dissolution as it will show how deviations from stoichiometric solution conditions as drug precipitates influences the driving force of these kinetic processes. As drug

precipitates the dissolution media becomes richer in coformer, decreasing the cocrystal solubility, possibly halting dissolution, and in some cases even reaching the eutectic point. In the system studied here, component concentrations from PSZ-4ABA dissolutions show that [PSZ] is above drug solubility indicating drug supersaturation. While [4ABA] in FeSSIF is observed to increase up to the coformer $C_{\text{dose}} = 2.6 \text{ mM}$, [4ABA] during dissolution with excess coformer was maintained at 5.8 – 6.0 mM (including excess 5.8 mM) over 180 minutes. The addition of 5.8 mM 4ABA also moved the dissolution concentrations much closer to the eutectic point, where drug solubility and nonstoichiometric cocrystal solubility are equal. This may have also contributed to stabilizing the cocrystal and allowing for the sustainment of supersaturation.

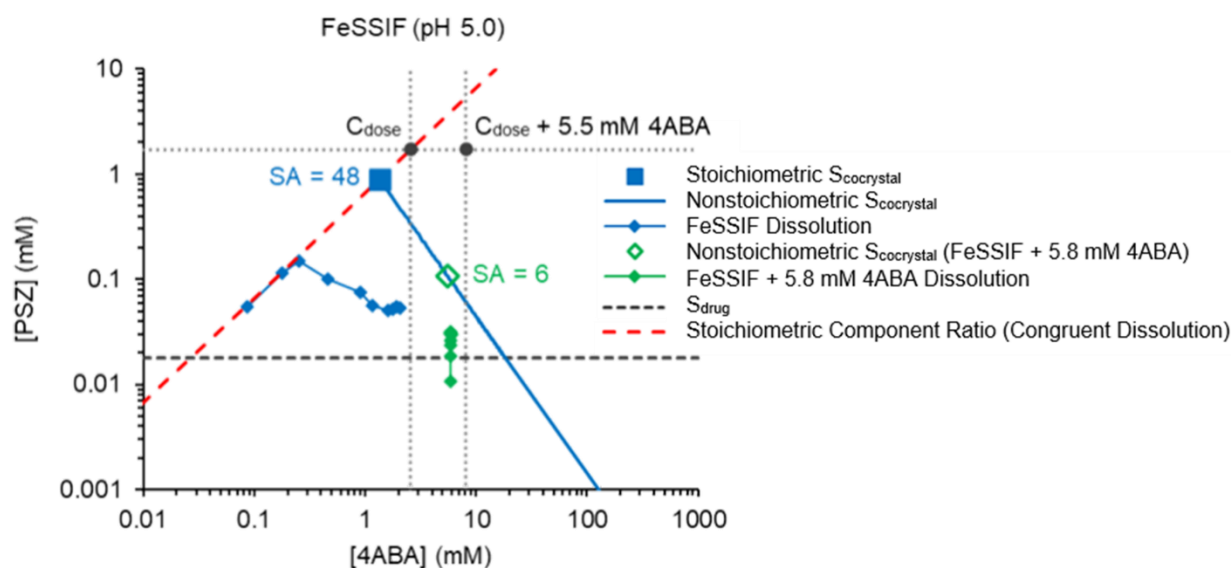


Figure 4.10. Phase solubility diagram for PSZ-4ABA in FeSSIF. Stoichiometric cocrystal solubility corresponds to SA = 48, and nonstoichiometric cocrystal solubility can be predictably modulated according to the K_{sp} (Equation 4.10). Excess of 5.5 mM 4ABA was predicted to correspond to SA = 6. Connected points show drug and coformer concentrations during dissolution with and without excess 4ABA.

Conclusions

This work shows the potential of cocrystals to solve the clinical challenges of poorly water-soluble drugs with erratic oral bioavailability such as PSZ. A second PSZ cocrystal was

discovered with coformer 4HBA and was characterized, but adequate single crystals were unable to be obtained to solve the crystal structure and definitively assess cocrystal stoichiometry or stoichiometries. Both PSZ-4HBA and PSZ-4ABA cocrystals were found to have softer solubility – pH dependence than PSZ, potentially mitigating the negative solubility and dissolution effects of increasing pH while moving in the gastrointestinal tract. Respective pH_{max} of 1.9 and 1.3 showed that the cocrystals have solubility advantage for a wide range of physiological pH, meaning that they will generate supersaturation and potentially enhance drug exposure at $\text{pH} > \text{pH}_{\text{max}}$. PSZ-4ABA sustained supersaturation in dissolution studies with excess coformer, which was selected to predictably modulate SA according to K_{sp} . Less cocrystal dissolution and drug precipitation were observed in the presence of excess coformer, suggesting that this strategy could be useful in designing delayed-release cocrystal formulations.

Acknowledgements

Research reported in this publication received financial support from the Upjohn Award from the College of Pharmacy, University of Michigan, and the National Institute of General Medical Sciences of the National Institutes of Health under Award Numbers R01GM107146. The content is solely the responsibility of the authors and does not necessarily represent the official views of the National Institutes of Health and other funding sources. We are grateful to Dr. Dongzhou Zhang and Prof. M. Fátima M. da Piedade for single crystal analysis, Prof. Matzger for X-ray analysis, Prof. Gustavo Rosania and Jennifer Diaz-Espinosa for Raman analysis and discussions, and Dr. Gislaine Kuminek for PSZ-4ABA solubility data collection.

References

1. Schiller, D. S.; Fung, H. B., Posaconazole: An Extended-Spectrum Triazole Antifungal Agent. *Clin Ther* **2007**, *29* (9), 1862-1886.
2. Walravens, J.; Brouwers, J.; Spriet, I.; Tack, J.; Annaert, P.; Augustijns, P., Effect of pH and Comedication on Gastrointestinal Absorption of Posaconazole: Monitoring of Intraluminal and Plasma Drug Concentrations. *Clin Pharmacokinet* **2011**, *50* (11), 725-34.
3. Hens, B.; Brouwers, J.; Corsetti, M.; Augustijns, P., Supersaturation and Precipitation of Posaconazole Upon Entry in the Upper Small Intestine in Humans. *J Pharm Sci* **2016**, *105* (9), 2677-2684.
4. Hens, B.; Corsetti, M.; Brouwers, J.; Augustijns, P., Gastrointestinal and Systemic Monitoring of Posaconazole in Humans After Fasted and Fed State Administration of a Solid Dispersion. *J Pharm Sci* **2016**, *105* (9), 2904-2912.
5. Dekkers, B. G. J.; Bakker, M.; van der Elst, K. C. M.; Sturkenboom, M. G. G.; Veringa, A.; Span, L. F. R.; Alffenaar, J.-W. C., Therapeutic Drug Monitoring of Posaconazole: an Update. *Curr Fungal Infect Rep* **2016**, *10* (2), 51-61.
6. Kuminek, G.; Cavanagh, K. L.; da Piedade, M. F. M.; Rodríguez-Hornedo, N., Posaconazole Cocrystal with Superior Solubility and Dissolution Behavior. *Cryst Growth Des* **2019**, *19* (11), 6592-6602.
7. Diakidou, A.; Vertzoni, M.; Dressman, J.; Reppas, C., Estimation of Intra-gastric Drug Solubility in the Fed State: Comparison of Various Media with Data in Aspirates. *Biopharm Drug Dispos* **2009**, *30* (6), 318-325.
8. Cristofolletti, R.; Patel, N.; Dressman, J. B., Differences in Food Effects for 2 Weak Bases With Similar BCS Drug-Related Properties: What Is Happening in the Intestinal Lumen? *J Pharm Sci* **2016**, *105* (9), 2712-2722.
9. Kuminek, G.; Cao, F.; Bahia de Oliveira da Rocha, A.; Goncalves Cardoso, S.; Rodríguez-Hornedo, N., Cocrystals to Facilitate Delivery of Poorly Soluble Compounds Beyond-Rule-of-5. *Adv Drug Deliv Rev* **2016**, *101*, 143-66.
10. Schultheiss, N.; Newman, A., Pharmaceutical Cocrystals and Their Physicochemical Properties. *Cryst Growth Des* **2009**, *9* (6), 2950-2967.
11. Shan, N.; Perry, M. L.; Weyna, D. R.; Zaworotko, M. J., Impact of Pharmaceutical Cocrystals: the Effects on Drug Pharmacokinetics. *Expert Opin Drug Met* **2014**, *10* (9), 1255-1271.
12. Chen, Y. M.; Rodríguez-Hornedo, N., Cocrystals Mitigate Negative Effects of High pH on Solubility and Dissolution of a Basic Drug. *Cryst Growth Des* **2018**, *18* (3), 1358-1366.

13. Maheshwari, C.; Andre, V.; Reddy, S.; Roy, L.; Duarte, T.; Rodríguez-Hornedo, N., Tailoring Aqueous Solubility of a Highly Soluble Compound via Cocrystallization: Effect of Coformer Ionization, pH(max) and Solute-solvent Interactions. *CrystEngComm* **2012**, *14* (14), 4801-4811.
14. Good, D. J.; Rodríguez-Hornedo, N., Solubility Advantage of Pharmaceutical Cocrystals. *Cryst Growth Des* **2009**, *9* (5), 2252-2264.
15. Bethune, S. J.; Huang, N.; Jayasankar, A.; Rodríguez-Hornedo, N., Understanding and Predicting the Effect of Cocrystal Components and pH on Cocrystal Solubility. *Cryst Growth Des* **2009**, *9* (9), 3976-3988.
16. Cao, F.; Amidon, G. L.; Rodríguez-Hornedo, N.; Amidon, G. E., Mechanistic Analysis of Cocrystal Dissolution as a Function of pH and Micellar Solubilization. *Mol Pharm* **2016**, *13* (3), 1030-1046.
17. Huang, Y.; Kuminek, G.; Roy, L.; Cavanagh, K. L.; Yin, Q.; Rodríguez-Hornedo, N., Cocrystal Solubility Advantage Diagrams as a Means to Control Dissolution, Supersaturation, and Precipitation. *Mol Pharm* **2019**, *16* (9), 3887-3895.
18. Courtney, R.; Wexler, D.; Radwanski, E.; Lim, J.; Laughlin, M., Effect of Food on the Relative Bioavailability of Two Oral Formulations of Posaconazole in Healthy Adults. *Brit J Clin Pharmacol* **2004**, *57* (2), 218-222.
19. Avdeef, A., pKa Determination. In *Absorption and Drug Development*, pp 31-173.
20. Gokel, G. E.; Gokel, G. W.; Dean, J. A., *Dean's Handbook of Organic Chemistry*. McGraw-Hill: 2004.
21. Rodríguez-Hornedo, N.; Nehm, S. J.; Seefeldt, K. F.; Pagán-Torres, Y.; Falkiewicz, C. J., Reaction Crystallization of Pharmaceutical Molecular Complexes. *Mol Pharm* **2006**, *3* (3), 362-367.
22. McQuiston, D. K.; Mucalo, M. R.; Saunders, G. C., The Structure of Posaconazole and its Solvates with Methanol, and Dioxane and Water: Difluorophenyl as a Hydrogen Bond Donor. *J Mol Struct* **2019**, *1179*, 477-486.
23. Woldemichael, T.; Keswani, R. K.; Rzczycki, P. M.; Murashov, M. D.; LaLone, V.; Gregorka, B.; Swanson, J. A.; Stringer, K. A.; Rosania, G. R., Reverse Engineering the Intracellular Self-Assembly of a Functional Mechanopharmaceutical Device. *Scientific Reports* **2018**, *8* (1), 2934.
24. Figueirêdo, C. B. M.; Nadvorny, D.; de Medeiros Vieira, A. C. Q.; Soares Sobrinho, J. L.; Rolim Neto, P. J.; Lee, P. I.; de La Roca Soares, M. F., Enhancement of Dissolution Rate through Eutectic Mixture and Solid Solution of Posaconazole and Benzimidazole. *Int J Pharm* **2017**, *525* (1), 32-42.
25. Chen, Y. J.; Wang, S. J.; Wang, S.; Liu, C. Y.; Su, C.; Hageman, M.; Hussain, M.; Haskell, R.; Stefanski, K.; Qian, F., Sodium Lauryl Sulfate Competitively Interacts with

- HPMC-AS and Consequently Reduces Oral Bioavailability of Posaconazole/HPMC-AS Amorphous Solid Dispersion. *Mol Pharm* **2016**, *13* (8), 2787-2795.
26. Lipert, M. P.; Roy, L.; Childs, S. L.; Rodríguez-Hornedo, N., Cocrystal Solubilization in Biorelevant Media and its Prediction from Drug Solubilization. *J Pharm Sci* **2015**, *104* (12), 4153-4163.
 27. Huang, N.; Rodríguez-Hornedo, N., Engineering Cocrystal Thermodynamic Stability and Eutectic Points by Micellar Solubilization and Ionization. *CrystEngComm* **2011**, *13* (17), 5409-5422.
 28. Good, D. J.; Rodríguez-Hornedo, N., Cocrystal Eutectic Constants and Prediction of Solubility Behavior. *Cryst Growth Des* **2010**, *10* (3), 1028-1032.
 29. Kuminek, G.; Rodríguez-Hornedo, N.; Siedler, S.; Rocha, H. V.; Cuffini, S. L.; Cardoso, S. G., How Cocrystals of Weakly Basic Drugs and Acidic Coformers Might Modulate Solubility and Stability. *ChemComm* **2016**, *52* (34), 5832-5.
 30. Oh, D.-M.; Curl, R. L.; Amidon, G. L., Estimating the Fraction Dose Absorbed from Suspensions of Poorly Soluble Compounds in Humans: A Mathematical Model. *Pharm Res* **1993**, *10* (2), 264-270.
 31. Amidon, G. L.; Lennernas, H.; Shah, V. P.; Crison, J. R., A Theoretical Basis for a Biopharmaceutic Drug Classification - the Correlation of in-Vitro Drug Product Dissolution and in-Vivo Bioavailability. *Pharm Res* **1995**, *12* (3), 413-420.
 32. Rinaki, E.; Valsami, G.; Macheras, P., Quantitative Biopharmaceutics Classification System: The Central Role of Dose/Solubility Ratio. *Pharm Res* **2003**, *20*, 1917-25.
 33. Machado, T. C.; Kuminek, G.; Cardoso, S. G.; Rodríguez-Hornedo, N., The Role of pH and Dose/solubility Ratio on Cocrystal Dissolution, Drug Supersaturation and Precipitation. *Eur J Pharm Sci* **2020**, 105422.
 34. Cavanagh, K. L.; Kuminek, G.; Rodríguez-Hornedo, N., Cocrystal Solubility Advantage and Dose/Solubility Ratio Diagrams: A Mechanistic Approach to Selecting Additives and Controlling Dissolution – Supersaturation – Precipitation Behavior. *Submitted to Molecular Pharmaceutics* **2020**.
 35. Cavanagh, K. L.; Maheshwari, C.; Rodríguez-Hornedo, N., Understanding the Differences Between Cocrystal and Salt Aqueous Solubilities. *J Pharm Sci* **2018**, *107* (1), 113-120.
 36. Shimpi, M. R.; Alhayali, A.; Cavanagh, K. L.; Rodríguez-Hornedo, N.; Velaga, S. P., Tadalafil–Malonic Acid Cocrystal: Physicochemical Characterization, pH-Solubility, and Supersaturation Studies. *Cryst Growth Des* **2018**, *18* (8), 4378-4387.
 37. Rosa, J.; Machado, T. C.; da Silva, A. K.; Kuminek, G.; Bortolluzzi, A. J.; Caon, T.; Cardoso, S. G., Isoniazid-Resveratrol Cocrystal: A Novel Alternative for Topical Treatment of Cutaneous Tuberculosis. *Cryst Growth Des* **2019**, *19* (9), 5029-5036.

38. Wei, Y.; Zhang, L.; Wang, N.; Shen, P.; Dou, H.; Ma, K.; Gao, Y.; Zhang, J.; Qian, S., Mechanistic Study on Complexation-Induced Spring and Hover Dissolution Behavior of Ibuprofen-Nicotinamide Cocrystal. *Cryst Growth Des* **2018**, *18* (12), 7343-7355.
39. Alhalaweh, A.; Roy, L.; Rodríguez-Hornedo, N.; Velaga, S. P., pH-Dependent Solubility of Indomethacin-Saccharin and Carbamazepine-Saccharin Cocrystals in Aqueous Media. *Mol Pharm* **2012**, *9* (9), 2605-2612.
40. Reddy, L. S.; Bethune, S. J.; Kampf, J. W.; Rodríguez-Hornedo, N., Cocrystals and Salts of Gabapentin: pH Dependent Cocrystal Stability and Solubility. *Cryst Growth Des* **2009**, *9* (1), 378-385.
41. Kuminek, G.; Cavanagh, K. L.; Rodríguez-Hornedo, N., Measurement and Mathematical Relationships of Cocrystal Thermodynamic Properties. In *Pharmaceutical Crystals*, Li, T.; Mattei, A., Eds. John Wiley & Sons, Inc.: 2019.
42. Schver, G. C. R. M.; Lee, P. I., Combined Effects of Supersaturation Rates and Doses on the Kinetic-Solubility Profiles of Amorphous Solid Dispersions Based on Water-Insoluble Poly(2-hydroxyethyl methacrylate) Hydrogels. *Mol Pharm* **2018**, *15* (5), 2017-2026.
43. Danda, L. J. d. A.; Batista, L. d. M.; Melo, V. C. S.; Soares Sobrinho, J. L.; Soares, M. F. d. L. R., Combining Amorphous Solid Dispersions for Improved Kinetic Solubility of Posaconazole Simultaneously Released from Soluble PVP/VA64 and an Insoluble Ammonio Methacrylate Copolymer. *Eur J Pharm Sci* **2019**, *133*, 79-85.
44. Figueirêdo, C. B. M.; Nadvorny, D.; Vieira, A. C. Q. d. M.; Schver, G. C. R. d. M.; Soares Sobrinho, J. L.; Rolim Neto, P. J.; Lee, P. I.; Soares, M. F. d. L. R., Enhanced Delivery of Fixed-dose Combination of Synergistic Antichagasic Agents Posaconazole-Benznidazole based on Amorphous Solid Dispersions. *Eur J Pharm Sci* **2018**, *119*, 208-218.

Appendix 4A

Single Crystals of PSZ-4HBA

Figure 4A.1 shows the crystal structure of PSZ-4HBA solved by SXRD, which reveals a 1:2 stoichiometry and an orthorhombic lattice of space group P 21 21 21. There is disorder in the PSZ molecule and specifically in the CH₃CHOH group. Orthorhombic unit cell dimensions are shown in Table 4A.1. R-factor was calculated as 9.15%.

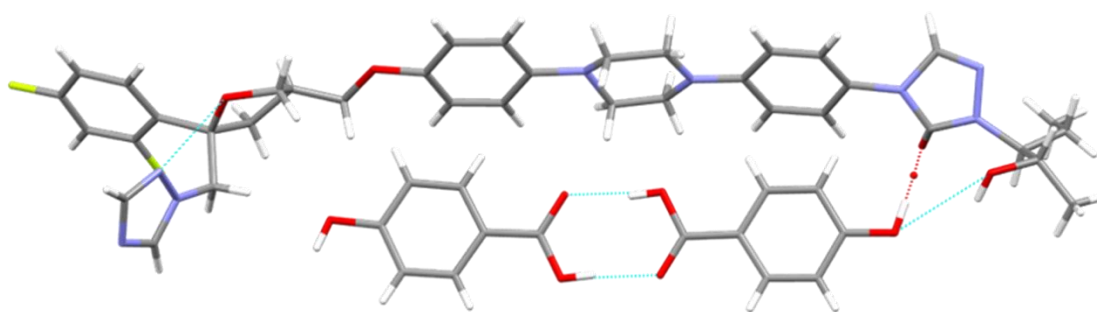


Figure 4A.1. Molecular interactions in the structure of PSZ-4HBA cocrystal. Figure was prepared using Mercury Version 4.3.1.

Table 4A.1. Unit cell dimensions of 1:2 PSZ-4HBA cocrystal.

$a = 5.8249(5) \text{ \AA}$	$\alpha = 90^\circ$	$Z = 4$
$b = 12.2592(8) \text{ \AA}$	$\beta = 90^\circ$	$Z' = 1$
$c = 69.415(5) \text{ \AA}$	$\gamma = 90^\circ$	$V = 4956.8(6)$

Figure 4A.2 shows photos and photomicrographs of single crystal growth. Figure 4A.2a shows the growth of large spherical particles during slow evaporation, and Figure 4A.2b shows the growth of needle-like rod crystals growing from a smaller spherical particle. A photomicrograph of an isolated needle-like single crystal in Figure 4A.2c shows suitable crystal length for single crystal X-ray diffraction, but crystal widths less than 40 μM are below the typical limit of quantification to solve crystal structures.

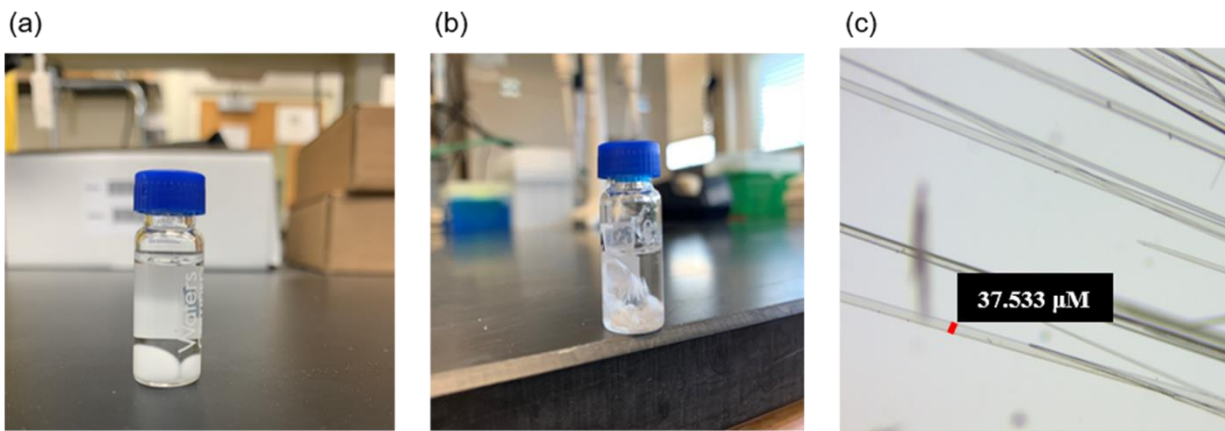


Figure 4A.2. Photos and photomicrograph of single crystal growth.

PSZ-4HBA Stoichiometry Determination by HPLC

Figure 4A.3 shows the coformer to drug ratio of pure PSZ-4HBA prepared by RCM. Cocystal samples from each batch were completely dissolved in 50:50 methanol : water with 0.1% trifluoroacetic acid, and component concentrations were quantified by HPLC. Component ratio suggests a 2:3 stoichiometry.

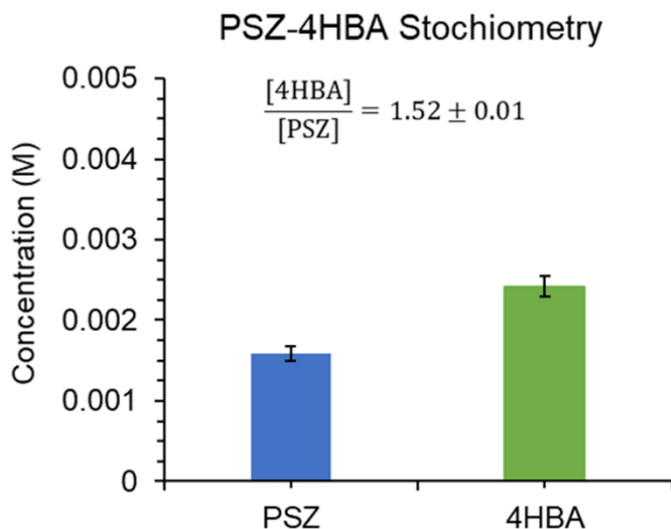


Figure 4A.3. 2:3 stoichiometry is indicated by completely dissolving pure PSZ-4HBA cocrystal synthesized by reaction crystallization method (RCM) and analyzing the concentration ratios by HPLC.

Appendix 4B

Derivation of 2:3 PSZ-4ABA Cocrystal Solubility as a Function of pH

The total posaconazole (PSZ) concentration in aqueous phase can be described by the sum of its ionized and nonionized species in solution as

$$[B]_T = [B]_{aq} + [BH^+]_{aq} + [BH_2^{2+}]_{aq} \quad (4B.1)$$

where B, BH⁺ and BH₂²⁺ represent PSZ nonionized, first protonated and second protonated species, respectively. Subscript T represents the concentrations of all species in solution and subscript aq represents the aqueous phase. The nonionized PSZ aqueous concentration [B]_{aq} is the intrinsic PSZ solubility, also expressed as S_{PSZ,0}.

The equilibrium expressions and constants of PSZ in solution are



$$K_{a1,B} = \frac{[H^+]_{aq} [BH^+]_{aq}}{[BH_2^{2+}]_{aq}} \quad (4B.3)$$



$$K_{\text{a2,B}} = \frac{[\text{H}^+]_{\text{aq}}[\text{B}]_{\text{aq}}}{[\text{BH}^+]_{\text{aq}}} \quad (4\text{B.5})$$

Substituting appropriate equilibrium constants into mass balance equation (Equation 4B.1), total drug concentration can be derived as

$$[\text{B}]_{\text{T}} = [\text{B}]_{\text{aq}} \left(1 + \frac{[\text{H}^+]_{\text{aq}}}{K_{\text{a2,B}}} + \frac{[\text{H}^+]_{\text{aq}}^2}{K_{\text{a1,B}}K_{\text{a2,B}}} \right) \quad (4\text{B.6})$$

Equation 4B.6 can also be expressed in terms of pH, pK_a and PSZ solubility as

$$S_{\text{PSZ,T}} = S_{\text{PSZ,0}} (1 + 10^{\text{p}K_{\text{a2,PSZ}} - \text{pH}} + 10^{\text{p}K_{\text{a1,PSZ}} + \text{p}K_{\text{a2,PSZ}} - 2\text{pH}}) \quad (4\text{B.7})$$

Similarly, 4-aminobenzoic acid (4ABA) total concentration in solution is the sum of its ionized and nonionized species

$$[\text{HAB}]_{\text{T}} = [\text{HAB}]_{\text{aq}} + [\text{HABH}^+]_{\text{aq}} + [\text{A}^-\text{B}]_{\text{aq}} \quad (4\text{B.8})$$

where HAB represent the nonionized 4ABA form, and HABH⁺ and A⁻B are the protonated and ionized species of the amphoteric cofomer, respectively. [HAB]_{aq}, represent the 4ABA intrinsic solubility, also referred to as S_{4ABA,0}.

The relevant solution equilibria and respective equilibrium constants of 4ABA are



$$K_{\text{a1,HAB}} = \frac{[\text{H}^+]_{\text{aq}}[\text{A}^-\text{B}]_{\text{aq}}}{[\text{HAB}]_{\text{aq}}} \quad (4\text{B.10})$$



$$K_{\text{a2,HAB}} = \frac{[\text{H}^+]_{\text{aq}}[\text{HAB}]_{\text{aq}}}{[\text{HABH}^+]_{\text{aq}}} \quad (4\text{B.12})$$

Substituting appropriate equilibrium constants into mass balance equation (Equation 4B.8), total 4ABA concentration can be derived as

$$[AB]_T = [HAB]_{aq} \left(1 + \frac{K_{a1,HAB}}{[H^+]_{aq}} + \frac{[H^+]_{aq}}{K_{a2,HAB}} \right) \quad (4B.13)$$

In terms of pH, pK_a and 4ABA solubility, Equation 4B.13 becomes

$$S_{4ABA,T} = S_{4ABA,0} (1 + 10^{pH-pK_{a1,4ABA}} + 10^{pK_{a2,4ABA}-pH}) \quad (4B.14)$$

A 2:3 cocrystal of a dibasic drug and an amphoteric coformer dissociates in solution according to its solubility product (K_{sp}), as



$$K_{sp} = [B]_{aq}^2 [HAB]_{aq}^3 \quad (4B.16)$$

where B and HAB represent the nonionized species of PSZ and 4ABA.

By combining Equations 4B.1 and 4B.8, and substituting appropriate equilibrium constants, an expression for total drug concentration as a function of total coformer concentration can be derived as

$$B_T^2 = \frac{K_{sp}}{[AB]_T^3} \left(1 + \frac{[H^+]_{aq}}{K_{a2,B}} + \frac{[H^+]_{aq}^2}{K_{a1,B}K_{a2,B}} \right)^2 \left(1 + \frac{K_{a1,HAB}}{[H^+]_{aq}} + \frac{[H^+]_{aq}}{K_{a2,HAB}} \right)^3 \quad (4B.17)$$

For a 2:3 cocrystal, the cocrystal solubility (S_{cocrystal}) under stoichiometric conditions is described as

$$S_{cocrystal,T} = \frac{1}{2}[B]_T = \frac{1}{3}[AB]_T \quad (4B.18)$$

Therefore, Equation 4B.17 can be rewritten as

$$S_{cocrystal,T} = \sqrt[5]{\frac{K_{sp}}{108} \left(1 + \frac{[H^+]_{aq}}{K_{a2,B}} + \frac{[H^+]_{aq}^2}{K_{a1,B}K_{a2,B}} \right)^2 \left(1 + \frac{K_{a1,HAB}}{[H^+]_{aq}} + \frac{[H^+]_{aq}}{K_{a2,HAB}} \right)^3} \quad (4B.19)$$

Which terms of pH and pK_a becomes

$$S_{\text{cocystal,T}} =$$

$$\sqrt[5]{\frac{K_{\text{sp}}}{108} (1 + 10^{\text{pK}_{\text{a}2,\text{PSZ}}-\text{pH}} + 10^{\text{pK}_{\text{a}1,\text{PSZ}}+\text{pK}_{\text{a}2,\text{PSZ}}-2\text{pH}})^2 (1 + 10^{\text{pH}-\text{pK}_{\text{a}1,4\text{ABA}}} + 10^{\text{pK}_{\text{a}2,4\text{ABA}}-\text{pH}})^3}$$

(4B.20)

Equation 4B.20 is expressed in terms of moles of cocystal. For comparison to drug solubility, cocystal solubility equation should be expressed in terms of moles of drug as

$$S_{\text{cocystal,T}} =$$

$$2 \sqrt[5]{\frac{K_{\text{sp}}}{108} (1 + 10^{\text{pK}_{\text{a}2,\text{PSZ}}-\text{pH}} + 10^{\text{pK}_{\text{a}1,\text{PSZ}}+\text{pK}_{\text{a}2,\text{PSZ}}-2\text{pH}})^2 (1 + 10^{\text{pH}-\text{pK}_{\text{a}1,4\text{ABA}}} + 10^{\text{pK}_{\text{a}2,4\text{ABA}}-\text{pH}})^3}$$

(4B.21)

Derivation of 2:3 and 1:2 PSZ-4HBA Cocystal Solubility as a Function of pH

Hydroxybenzoic acid (4HBA) mass balance

$$[\text{HA}]_{\text{T}} = [\text{HA}]_{\text{aq}} + [\text{A}^{-}]_{\text{aq}} \quad (4B.22)$$

Relevant solution equilibria and respective equilibrium constants of 4HBA



$$K_{\text{a,HA}} = \frac{[\text{H}^{+}]_{\text{aq}}[\text{A}^{-}]_{\text{aq}}}{[\text{HA}]_{\text{aq}}} \quad (4B.24)$$

Substituting appropriate equilibrium constants into mass balance equation, total 4HBA concentration can be derived as

$$[\text{A}]_{\text{T}} = [\text{HA}]_{\text{aq}} \left(1 + \frac{K_{\text{a,HA}}}{[\text{H}^{+}]_{\text{aq}}} \right) \quad (4B.25)$$

In terms of pH, pK_a and 4HBA solubility, Equation 4B.25 becomes

$$S_{4\text{HBA,T}} = S_{4\text{HBA,0}} (1 + 10^{\text{pH}-\text{pK}_{\text{a},4\text{HBA}}}) \quad (4B.26)$$

A 2:3 cocystal with dibasic drug and monoprotic acidic cofomer is described as



$$K_{sp} = [B]_{\text{aq}}^2 [HA]_{\text{aq}}^3 \quad (4B.28)$$

$$B_T^2 = \frac{K_{sp}}{[A]_T^3} \left(1 + \frac{[H^+]_{\text{aq}}}{K_{a2,B}} + \frac{[H^+]_{\text{aq}}^2}{K_{a1,B}K_{a2,B}} \right)^2 \left(1 + \frac{K_{a,HA}}{[H^+]_{\text{aq}}} \right)^3 \quad (4B.29)$$

For a 2:3 cocrystal, $S_{\text{cocrystal,T}}$ under stoichiometric conditions is described as

$$S_{\text{cocrystal,T}} = \frac{1}{2}[B]_T = \frac{1}{3}[A]_T \quad (4B.30)$$

$$S_{\text{cocrystal,T}} = \sqrt[5]{\frac{K_{sp}}{108} \left(1 + \frac{[H^+]_{\text{aq}}}{K_{a2,B}} + \frac{[H^+]_{\text{aq}}^2}{K_{a1,B}K_{a2,B}} \right)^2 \left(1 + \frac{K_{a,HA}}{[H^+]_{\text{aq}}} \right)^3} \quad (4B.31)$$

$S_{\text{cocrystal,T}}$ in terms of moles of drug:

$$S_{\text{cocrystal,T}} = 2 \sqrt[5]{\frac{K_{sp}}{108} \left(1 + \frac{[H^+]_{\text{aq}}}{K_{a2,B}} + \frac{[H^+]_{\text{aq}}^2}{K_{a1,B}K_{a2,B}} \right)^2 \left(1 + \frac{K_{a,HA}}{[H^+]_{\text{aq}}} \right)^3} \quad (4B.32)$$

A 1:2 cocrystal with dibasic drug and monoprotic acidic cofomer is described as



$$K_{sp} = [B]_{\text{aq}} [HA]_{\text{aq}}^2 \quad (4B.34)$$

$$B_T = \frac{K_{sp}}{[A]_T^2} \left(1 + \frac{[H^+]_{\text{aq}}}{K_{a2,B}} + \frac{[H^+]_{\text{aq}}^2}{K_{a1,B}K_{a2,B}} \right) \left(1 + \frac{K_{a,HA}}{[H^+]_{\text{aq}}} \right)^2 \quad (4B.35)$$

For a 1:2 cocrystal, $S_{\text{cocrystal,T}}$ under stoichiometric conditions is described as

$$S_{\text{cocrystal,T}} = [B]_T = \frac{1}{2}[A]_T \quad (4B.36)$$

$$S_{\text{cocrystal,T}} = \sqrt[3]{\frac{K_{sp}}{4} \left(1 + \frac{[H^+]_{\text{aq}}}{K_{a2,B}} + \frac{[H^+]_{\text{aq}}^2}{K_{a1,B}K_{a2,B}} \right) \left(1 + \frac{K_{a,HA}}{[H^+]_{\text{aq}}} \right)^2} \quad (4B.37)$$

In terms of pH and pK_a, Equation 4B.32 for 2:3 PSZ-4HBA becomes

$$S_{2:3 \text{ PSZ-4HBA}} = 2 \sqrt[5]{\frac{K_{sp}}{108} (1 + 10^{pK_{a2,PSZ}-pH} + 10^{pK_{a1,PSZ}+pK_{a2,PSZ}-2pH})^2 (1 + 10^{pH-pK_{a,4HBA}})^3}$$
(4B.38)

and Equation 4B.37 for 1:2 PSZ-4HBA becomes

$$S_{1:2 \text{ PSZ-4HBA}} = \sqrt[3]{\frac{K_{sp}}{4} (1 + 10^{pK_{a2,PSZ}-pH} + 10^{pK_{a1,PSZ}+pK_{a2,PSZ}-2pH})(1 + 10^{pH-pK_{a,4HBA}})^2}$$
(4B.39)

Solubility Calculations for 1:2 PSZ-4HBA versus 2:3 PSZ-4HBA

Cocrystal solubility is a function of relevant solution equilibria, solution conditions, and stoichiometry. Tables 4B.1 and 4B.2 shows cocrystal solubility, SA, and K_{sp} recalculated based on a 1:2 PSZ-4HBA stoichiometry. These values are compared to calculated values for a 2:3 PSZ-4HBA cocrystal, as presented in the main text. 1:2 cocrystal solubility in Table 4B.1 is calculated according to general Equation 4.5 as

$$S_{\text{cocrystal}} = \sqrt[3]{\frac{[\text{PSZ}]_{eu} [\text{4HBA}]_{eu}^2}{4}}$$
(4B.40)

Table 4B.1. Cocrystal Solubility and Solubility Advantage (SA) values calculated for 1:2 and 2:3 PSZ-4HBA.

Cocrystal	Media	Final pH ^a	S _{cocrystal} (mM) ^b	SA
1:2 PSZ-4HBA	Blank FaSSIF	5.1 ± 0.1	0.21 ± 0.03	962 ± 515
	Blank FeSSIF	5.1 ± 0.1	0.18 ± 0.03	790 ± 328
	FaSSIF	5.1 ± 0.1	0.29 ± 0.05	492 ± 247
	FeSSIF	5.0 ± 0.1	0.67 ± 0.02	88 ± 10
2:3 PSZ-4HBA	Blank FaSSIF	5.1 ± 0.1	0.13 ± 0.02	576 ± 294
	Blank FeSSIF	4.8 ± 0.1	0.11 ± 0.02	482 ± 188
	FaSSIF	5.0 ± 0.1	0.19 ± 0.04	315 ± 141
	FeSSIF	4.8 ± 0.1	0.51 ± 0.02	67 ± 6

^a Initial pH was 6.5 ± 0.1 for Blank FaSSIF and FaSSIF media, and 5.0 ± 0.1 for Blank FeSSIF and FeSSIF media.

^b Calculated according to Equation 4.5.

K_{sp} for 1:2 PSZ-4HBA in Table 4B.2 is calculated according to general Equation 4.9 as

$$K_{sp(1:2 \text{ PSZ-4HBA})} = [\text{PSZ}]_{\text{eu,non}} [\text{4HBA}]_{\text{eu,non}}^2 \quad (4B.41)$$

Table 4B.2. K_{sp}, pK_{sp}, pH_{max}, and S_{cocrystal} at pH_{max} Values for 1:2 and 2:3 PSZ-4HBA.

Cocrystal	K _{sp} ^a	pK _{sp} ^b	pH _{max}	S _{cocrystal(pHmax)} (mM)
1:2 PSZ-4HBA	(2.1 ± 0.7) × 10 ⁻¹² M ³	11.7	2.0	2.1
2:3 PSZ-4HBA	(1.3 ± 0.9) × 10 ⁻²¹ M ⁵	20.9	1.9	3.1

^a Calculated according to Equation 4.9.

^b Calculated according to pK_{sp} = - log K_{sp}.

Figure 4B.1 shows the predicted and experimental solubility – pH dependence for PSZ-4HBA cocrystal calculated as both 1:2 and a 2:3 cocrystal. The results show that a 1:2 cocrystal has a higher solubility and SA than the 2:3, but their pH – dependent behavior and pH_{max} are similar.

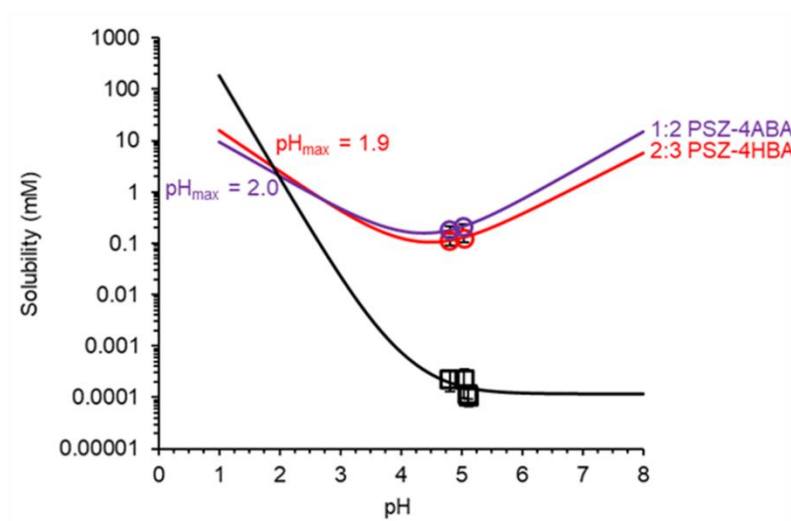


Figure 4B.1. PSZ-4HBA has similar solubility – pH dependence when calculated as a 1:2 and as a 2:3 cocrystal.

Appendix 4C

Photomicrographs of Cocrystal Dissolution

Figure 4C.1 shows photomicrographs of cocrystal dissolution aliquots with 5.8 mM 4ABA. Agglomeration and surface nucleation were not observed as previously shown during cocrystal dissolution in FaSSIF and FeSSIF (Figure 4C.2), and therefore were not the cause of dampened cocrystal dissolution in the presence of excess coformer. Increased drug precipitation during FeSSIF dissolution appears to have stimulated the particle agglomeration.

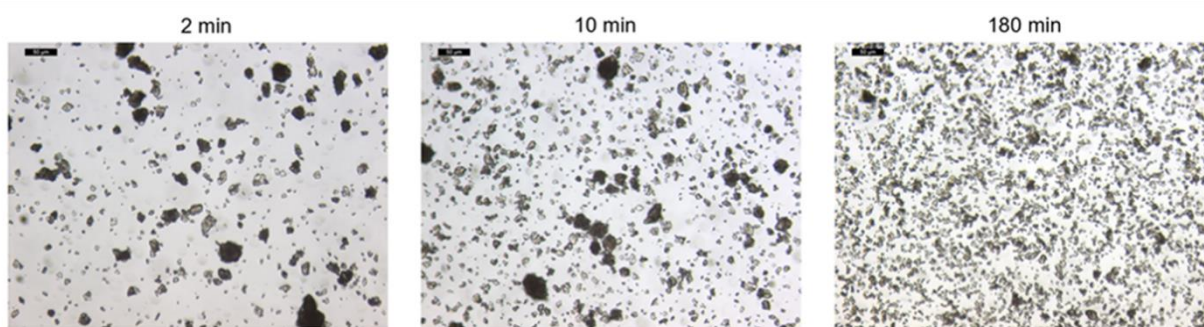
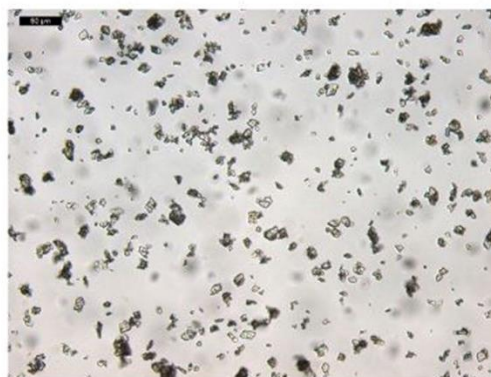
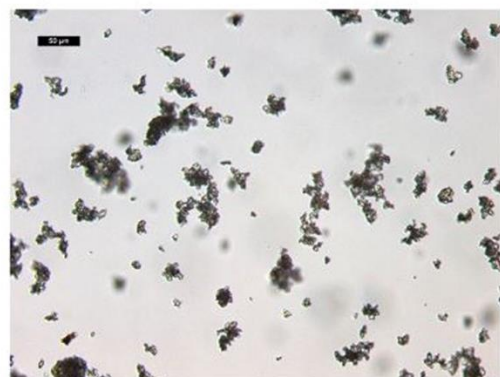
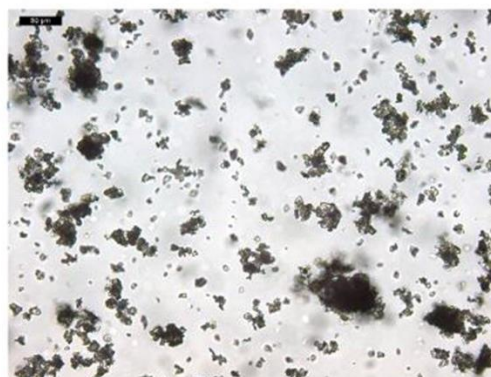
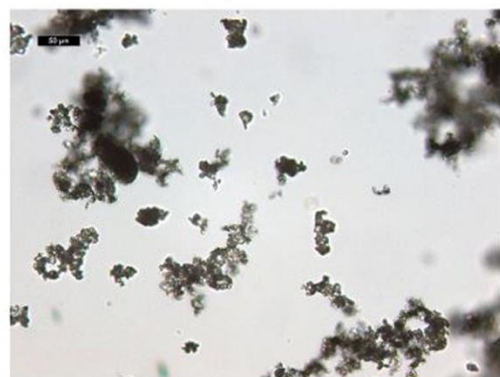


Figure 4C.1. Photomicrographs of cocrystal dissolution aliquots in FeSSIF + 5.8 mM 4ABA. With the addition of excess coformer, cocrystal did not form agglomerates as previously observed during dissolution in FeSSIF.

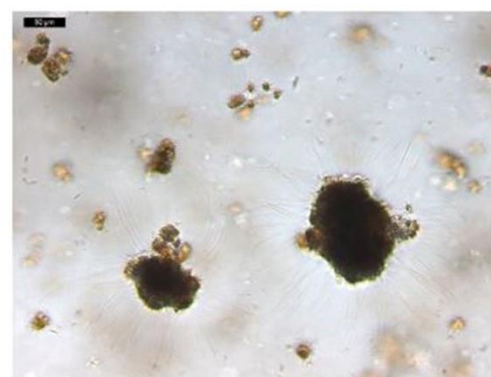
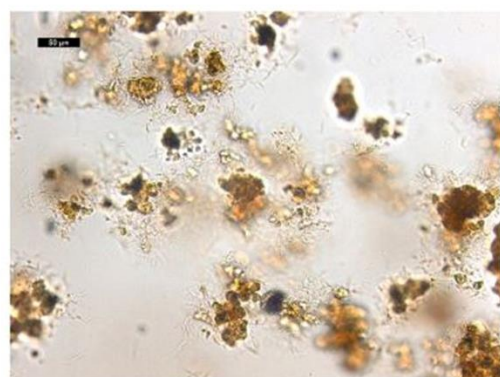
2 Minute
Aliquot



10 Minute
Aliquot



180 Minute
Aliquot



FaSSIF

FeSSIF

Figure 4C.2. Microscopy images of the transformation of PSZ-4ABA to PSZ during dissolution in FaSSIF and FeSSIF as reported by Kuminek et. al.¹

Reference

1. Kuminek, G.; Cavanagh, K. L.; da Piedade, M. F. M.; Rodríguez-Hornedo, N., Posaconazole Cocrystal with Superior Solubility and Dissolution Behavior. *Cryst Growth Des* **2019**, *19* (11), 6592-6602.

CHAPTER 5

Conclusions and Future Directions

The purpose of this research was to develop thermodynamic and mathematical relationships that can be used to predict and tailor cocrystal solubility and stability. The objectives of this research were to (1) to develop a quantitative, mechanistic-based approach through which known relationships between cocrystal solubility advantage (SA) and other key cocrystal solubility transition points can be used to fine-tune cocrystal inherent supersaturation, and (2) to assess and modulate the risk of conversion by rationally selecting additives that will exhibit thermodynamic and kinetic control over dissolution – supersaturation – precipitation (DSP) behavior given the drug dose. Overall, this work aims to provide a framework for rationally designing new cocrystals and for critically evaluating and optimizing DSP behavior.

This work focused on poorly water-soluble drugs cocrystallized with highly soluble cofomers. Cocrystal solubility – pH dependence was evaluated for basic drugs with acidic, amphoteric, and basic cofomers of varying stoichiometries. Equations were derived from relevant solution equilibria such as solubility product K_{sp} and component pK_a to predict cocrystal solubility across physiological pH. The predictions were validated with experimental solubility measurements, and excellent agreement was observed between predicted and experimental values. Accurate predictions importantly provide insights into potential experimentally inaccessible pH ranges and can save time, money, and materials by reducing the need for extensive experimentation.

The ionization of the cofomers altered the solubility – pH dependence of the studied cocrystals compared to parent drug. Posaconazole (PSZ) cocrystals with amphoteric 4-aminobenzoic acid (4ABA)¹ and newly discovered with acidic 4-hydroxybenzoic acid (4HBA) were found exhibit U-shaped solubility – pH profiles compared to the solubility of basic PSZ, which exponentially decreased with increasing pH. PSZ-4ABA and PSZ-4HBA were observed to have pH_{max} values of 1.3 and 1.9, respectively, which corresponded to $\text{SA} = 1$. Cocrystal SA values were increased to 596 – 6167 in pH 5.0 – 6.5, showing the ability of cocrystals to increase drug solubility by orders of magnitude.

Solubility – pH dependence was also studied for lamotrigine – nicotinamide cocrystal (LTG-NCT), lamotrigine – phenobarbital cocrystal (LTG – PB), and lamotrigine – saccharin salt (LTG-SAC). Within the literature, there is a commonly held notion that salts are inherently more soluble than cocrystals. However, the results of this work showed that cocrystals can be more soluble than salts or vice-versa, depending on the interplay between the chemistry of the solid and solution phases. K_{sp} is directly proportional to intrinsic cocrystal/salt solubility and followed the order $\text{LTG-NCT} > \text{LTG-SAC} > \text{LTG-PB}$. While LTG-NCT did not exhibit a pH_{max} and had solubility advantage across physiological pH, LTG-SAC was found to have solubility advantage above $\text{pH}_{\text{max}} = 5.0$ and LTG-PB was more stable than drug across physiological pH and only gained solubility advantage above $\text{pH}_{\text{max}} = 9.0$. These results allow for critical interpretation of previously reported LTG-NCT and LTG-SAC *in vitro* dissolution at pH 1.0 and pH 5.5.² LTG has been shown to only tolerate supersaturation levels of 2-3, so SA values much higher than this are likely to lead to rapid conversion. LTG-SAC salt had enhanced dissolution behavior compared to drug at pH 5.5, which was just above pH_{max} and corresponded to $\text{SA} = 2.5$, while LTG-NCT rapidly converted in solution and had no real dissolution advantage at $\text{SA} =$

11.3, which was above critical supersaturation. However, the opposite trend was observed at pH 1.0, where LTG-SAC was below pH_{max} and performed worse than LTG drug, while LTG-NCT had $SA = 1.3$ and sustained supersaturation. pH_{max} and SA are important parameters for both assessing cocrystal stability and for anticipating solution-mediated phase conversions.

Danazol – vanillin cocrystal (DNZ-VAN) is predominantly nonionized across physiological pH and was found to have aqueous $SA = 183$. This unnecessarily high SA left the cocrystal at high risk for rapid conversion during previously reported *in vitro* and *in vivo* experiments.³ Cocrystal solubility and SA have been shown to be tailorable as a function of solubilizing agent concentration,⁴⁻⁶ and here the relationship between SA and the drug solubilization power of surfactants (SP_D) was found to provide a mechanistic approach to rationally select additives and dial to a particular SA value to promote optimal DSP behavior. Tailoring SA below critical supersaturation promoted sustained supersaturation and increased drug exposure. A dual thermodynamic and kinetic approach of dialing SA with solubilizing additives and inhibiting precipitation with nucleation and growth inhibitors yielded the highest dissolution enhancement.

While SA decreases with increasing SP_D , $S_{cocrystal}$ and S_{drug} increase, and may even exceed the dose concentration (C_{dose}). Drug dose/solubility ratio ($D_{0(D)} = C_{dose} / S_{drug}$) was found to be an important parameter for assessing how much of the dose the cocrystal may dissolve, as well as the potential for dose-limited supersaturation or undersaturation (if $S_{cocrystal} > C_{dose}$). Inadvertently dose-limiting supersaturation can lead to incorrect interpretations of cocrystal DSP behavior and can limit the potential of cocrystals to enhance dissolution performance. In tandem, SA and $D_{0(D)}$ represent maximum theoretical supersaturation that can be tailored as a

function of SP_D , and knowledge of their values relative to critical supersaturation provide a holistic approach to interpreting, predicting, and optimizing cocrystal DSP behavior.

Finally, the addition of excess coformer was introduced as an additional strategy to predictably modulate SA by definition of K_{sp} . PSZ-4ABA stoichiometric SA = 48 in FeSSIF was tailored with excess coformer to nonstoichiometric SA = 6, which was below observed critical supersaturation of 8.4 and above sustained supersaturation of 2.8 – 3.1 during FeSSIF dissolution. While the cocrystal area under the curve with excess coformer was lower than without, the cocrystal did sustain supersaturation of 1.5 – 1.8 for the duration of the experiment (180 minutes). Furthermore, less cocrystal dissolution and drug precipitation were observed in the presence of excess coformer, as the cocrystal maintained quasi-equilibrium within the metastable zone. This finding suggests that excess coformer addition may be a useful strategy for designing delayed-release cocrystal formulations.

The findings of this work present a rational, streamlined approach for cocrystal development. Lack of critical understanding of cocrystal solution behavior and the underlying solution interactions that govern drug supersaturation and exposure have traditionally resulted in empirical, time-consuming, and oftentimes inadequate methods to control DSP behavior. Despite recent advancements in regulation, cocrystals remain in appearance as overly risky to develop and are a largely untapped drug development strategy.

Knowledge of cocrystal transition points is essential in order to effectively design cocrystal formulations that can generate both thermodynamically possible and kinetically sustainable supersaturation in the gastrointestinal tract. Thermodynamic relationships presented in this work allow for accurate predictions of cocrystal solubility and stability in many solution conditions from a single eutectic point measurement, which can be time, cost, and material

saving. These relationships and predictions allow for the optimization of SA, which has been shown to be effective in controlling cocrystal DSP behavior *in vitro*. However, while the few existing *in vivo* cocrystal studies retrospectively show promising utility of these relationships, further analysis of cocrystal *in vivo* DSP behavior is necessary.

Furthermore, many published *in vivo* studies have compared neat drug and cocrystal materials sans formulation. Given that unnecessarily high cocrystal SA and risk of conversion have been demonstrated to be mitigated in the presence of solubilizing agents or excess coformer, there is a need for more *in vivo* studies that incorporate formulation. Assessment of C_{dose} relative to $S_{\text{cocrystal}}$ is also critical in these studies, as dose-limiting supersaturation by modulating $D_{0(D)}$ may be a useful way to control DSP behavior for some cocrystals and required doses. Overall, direct *in vitro* and *in vivo* comparison of these different strategies for modulating SA and/or $D_{0(D)}$ will lead to increased understanding and control of cocrystal solution behavior and will result in the development of more effective cocrystal formulations.

References

1. Kuminek, G.; Cavanagh, K. L.; da Piedade, M. F. M.; Rodríguez-Hornedo, N., Posaconazole Cocrystal with Superior Solubility and Dissolution Behavior. *Cryst Growth Des* **2019**, *19* (11), 6592-6602.
2. Cheney, M. L.; Shan, N.; Healey, E. R.; Hanna, M.; Wojtas, L.; Zaworotko, M. J.; Sava, V.; Song, S. J.; Sanchez-Ramos, J. R., Effects of Crystal Form on Solubility and Pharmacokinetics: A Crystal Engineering Case Study of Lamotrigine. *Cryst Growth Des* **2010**, *10* (1), 394-405.
3. Childs, S. L.; Kandi, P.; Lingireddy, S. R., Formulation of a Danazol Cocrystal with Controlled Supersaturation Plays an Essential Role in Improving Bioavailability. *Mol Pharm* **2013**, *10* (8), 3112-27.
4. Huang, N.; Rodríguez-Hornedo, N., Engineering Cocrystal Solubility, Stability, and pH(max) by Micellar Solubilization. *J Pharm Sci* **2011**, *100* (12), 5219-34.
5. Huang, Y.; Kuminek, G.; Roy, L.; Cavanagh, K. L.; Yin, Q.; Rodríguez-Hornedo, N., Cocrystal Solubility Advantage Diagrams as a Means to Control Dissolution, Supersaturation, and Precipitation. *Mol Pharm* **2019**, *16* (9), 3887-3895.
6. Kuminek, G.; Cao, F.; Bahia de Oliveira da Rocha, A.; Goncalves Cardoso, S.; Rodríguez-Hornedo, N., Cocrystals to Facilitate Delivery of Poorly Soluble Compounds Beyond-Rule-of-5. *Adv Drug Deliv Rev* **2016**, *101*, 143-66.